

The Identification of a Meiosis-Specific
Phosphorylation of Exonuclease-I During
the Meiotic Recombination Pathway in
Saccharomyces cerevisiae

Hasan Fayiz Hasan Alnaser, MSc

**A thesis submitted for the degree of:
Doctor of Philosophy**

February 2019

The University of Sheffield

Department of Molecular Biology and Biotechnology

Summary

Meiosis is a cell division process specialised for the production of four genetically distinct haploid daughter cells from a single diploid parent cell. A meiosis-specific process of homologous recombination repairs Spo11 induced DNA double-strand breaks (DSBs) creating gene conversions and crossovers; a crucial pathway for genetic diversity and homologous chromosomes disjunction. An important step in this process is the resection of DSB sites to expose 3' single-stranded overhangs, which can then proceed to search for its homologous repair template. Exonuclease-1(Exo1) is a conserved nuclease with 5' → 3' DNA exonuclease activity and 5' flap endonuclease activity. Exo1 is required for progressive resection necessary for long tracts of 3' single-stranded DNA, critical for normal levels of recombination. The phosphorylation of Exo1 was first observed in response to DNA damage in *Saccharomyces cerevisiae* and this negatively regulates Exo1 nuclease activity. In this study, the phosphorylation of Exo1 during meiosis was investigated. After analysing Exo1 meiotic-phosphorylation by mass-spectrometry, additional residues were found to be phosphorylated in comparison to mitotically significant residues. The meiotic phosphorylation of Exo1 was found to be Tel1-dependent, and MRX complex dependent. Phosphorylated Exo1 may function during the bidirectional resection of Spo11 induced DSBs. The data presented in this thesis suggest a role of Tel1 kinase in initiating the resection process by regulating Sae2, Exo1, and the MRX complex.

Acknowledgments

To my greatest blessing, my family who supported me during my PhD journey. In the time of happiness and sorrow, they always gave the sustenance to my mind and kept me sane. To my siblings, Ahmed, Leen, and to our bride to be Lamis, there are no words that can describe the joy and happiness I feel in your company.


For my mother, for her love and warmth, you never stopped pushing me far and beyond, and the right path you always showed. For my father, for his unconditional support, a tough man yet the most loving. For my grandmother, the most resilient woman, and for you this PhD is dedicated.

To my love and my other half, my lovely fiancée Fidaa. You have supported me towards the end of this journey, and with great sacrifice accepted to start a new one with me. I love you with all of my life.

The journey has just started with continuing the work to discover and wonder. I would have not been able to start nor continue without the help of my supervisors Alastair and Bin. Both supported me during my time of need whether in Alastair's office or in the lab with Bin. The journey would have not been possible without Julia, and Laura, for their mental and lab support, the "pep" talks, and the motivation. To both of your faces I shall ever be grateful, especially to Julia for her flawless proofreading. Many thanks to Thane, for his help in the writing, the nonstop debates and discussion about anything, you will always be my "c'mon bro".

Many thanks to all of the students that worked under my supervision during my PhD: Claudio, Mathew, Stephen, and Annie. Special thanks and appreciation to Annuradha for her enthusiasm and Reem for her hard work in producing valuable data for this project.

Finally, many gratitude to the department of MBB for their financial support and covering the costs of my lab bench.

I love you all 

I finally did it!!

“Writing is like dancing with words...
but sometimes the words refuse.”

- *Karl Sharro*

Abbreviations

AE	Axial element
CE	Central element
ChIP	Chromatin-Immunoprecipitation
CO	Crossover
DAPI	4',6'-diamidino-2-phenylindole
dHJ	Double Holliday Junction
dH₂O	Deionised water
DNA	Deoxyribonucleic acid
DSB	Double strand break
DSBR	Double strand break repair
dsDNA	Double-stranded DNA
EDTA	Ethylene-diaminetetracetic acid
JM	Joint molecule
LE	Lateral elements
MI	Meiosis I
MII	Meiosis II
MMR	Mismatch repair
MRX	Mre11, Rad50, Xrs2
NCO	Non-crossover
NPF	nucleoprotein-filament
PCR	Polymerase chain reaction
PTM	Post-translational modification
RPA	Replication Protein A
SC	Synaptonemal complex
SPB	Spindle pole body
ssDNA	Single-stranded DNA
SMC	Structural maintenance of chromosome
SSE	structure-selective endonucleases
WCE	Whole-cell extract

Contents

<i>Summary</i>	i
<i>Acknowledgments</i>	ii
<i>Abbreviations</i>	iv
<i>Contents</i>	v
<i>List of Figures</i>	ix
<i>List of Tables</i>	xiii
Chapter 1. General Introduction	1
1.1 <i>Saccharomyces cerevisiae</i> as a model organism	1
1.2 The life cycle of <i>Saccharomyces cerevisiae</i>	2
1.3 Mitosis and Meiosis	7
1.4 Homologous chromosome pairing and synapsis	13
1.5 Programmed meiotic DNA double strand formation and processing	18
1.6 Recombination, crossover formation, and resolution	24
1.7 Meiosis regulation and the checkpoint network	29
1.8 Exonuclease 1 (Exo1)	32
1.9 Projects aims	34
Chapter 2. Materials and Methodology	35
2.1 Media and stock solutions:	35
2.1.1 Growth media:	35
2.1.2 Stock solutions:	37
2.2 Yeast Growth and Culturing Methods:	41
2.2.1 Yeast mating, diploid construction and strain storage	41
2.2.2 Yeast tetrad dissection	42
2.2.3 Genotyping and mating type testing	42
2.2.4 Yeast meiosis time coursing	43
2.2.5 DAPI staining of meiotic cells	43
2.3 Methods in molecular biology and biochemistry	44
2.3.1 DNA restriction digest	44
2.3.2 Phosphatase treatment of digested plasmid	44
2.3.3 DNA agarose gel electrophoresis	44
2.3.4 DNA purification kit from agarose gel (QIAquick Spin, Qiagen)	45
2.3.5 Ligation	45
2.3.6 Polymerase chain reaction (PCR)	46
2.3.7 Amplified DNA clean-up kit	46
2.3.8 Small scale plasmid isolation from <i>E. coli</i> (Mini-Prep) GeneJET Thermo	47
2.3.9 Transformation of <i>E. coli</i> competent cells	47

2.3.10	High efficiency yeast transformation	48
2.3.11	Yeast genomic DNA extraction	49
2.3.12	DNA sequencing sample preparation.....	49
2.3.13	Yeast protein extraction:	50
2.3.14	Protein concentration assay (Bradford assay)	51
2.3.15	Large-scale meiotic cells protein extraction by two-step purification	52
2.3.16	Lambda Phosphatase Assay	53
2.3.17	Sodium dodecyl sulphate polyacrylamide gel electrophoresis (SDS-PAGE).....	54
2.3.18	Western blotting and immunoprobing	55
2.4	Samples preparation for mass-spectrometry analysis	56
2.4.1	SDS-PAGE gel wash and dehydration:.....	56
2.4.2	Beads washing	56
2.4.3	Reduction and Alkylation:	57
2.4.4	Trypsin digestion.....	57
2.4.5	C18 desalting mini-columns	58
2.5	Yeast strains and plasmids	58
2.5.1	Haploid <i>S. cerevisiae</i> strains	58
2.5.2	Diploid <i>S. cerevisiae</i> strains.....	59
2.5.3	Plasmids	61
2.5.4	Primers	61
Chapter 3.	Phosphorylation of Exo1 during <i>S. cerevisiae</i> sporulation	62
	Introduction:.....	62
3.1	<i>Exo1-x9PK</i> analysis during yeast sporulation:.....	66
3.2	<i>EXO1-x9PK</i> and <i>exo1Δ</i> strains meiotic progression:.....	68
3.3	Epitope tagging of Exo1 with x5His- x6FLAG tag:	70
3.4	<i>Exo1-x5His-x6FLAG</i> is phosphorylated during meiosis:.....	74
3.5	Meiotic progression of the <i>Exo1-x5His-x6FLAG</i> strain:	76
3.6	<i>exo1-4S::A-x5His-x6FLAG</i> is phosphorylated during yeast meiosis:.....	79
3.7	Spore viability is not affected in the phosphorylation null mutant <i>exo1-4S::A</i> but reduced in <i>exo1Δ</i>	82
	Discussion:.....	84
Chapter 4.	Investigating the dependency of Exo1 phosphorylation during the meiotic recombination pathway	88
	Introduction:.....	88
4.1	Exo1 phosphorylation is Spo11-double-strand break dependent:.....	91
4.2	The phosphorylation of Exo1 is normal in pachytene arrested cells.....	94

4.3	Exo1 is over-phosphorylated during the meiosis of <i>dmc1Δ/rad51Δ</i> double-mutant	96
4.4	The phosphorylation event of Exo1 is inter-homologue repair dependent	98
4.5	Exo1 is not phosphorylated in the absence of Tel1 and Mec1 kinases:	101
4.6	The phosphorylation of Exo1 is Tel1 dependent in the absence of Sae2.....	111
4.7	Exo1 phosphorylation is MRX complex dependent:	120
	Discussion:.....	127
Chapter 5. Mass Spectrometry analysis of Exo1’s phosphorylation residues		131
	Introduction:.....	131
5.1	Large-Scale Two-Step Purification of <i>Exo1-x5His-x6FLAG</i> :	135
5.2	Mass-spectrometry of purified Exo1 and peptide generation by “in-gel” Trypsin treatment: 137	
5.3	Mass-spectrometry of purified Exo1 and peptide generation by “on-beads” Trypsin treatment:	146
5.3.1	Mass spectrometry for Exo1 purified sample from pre-meiotic synchronised cells... 147	
5.3.2	Mass spectrometry for purified Exo1 from meiotic cell culture after four-hours of meiosis induction	152
5.3.3	Mass spectrometry analysis for Exo1 sample purified from <i>sae2Δ</i> strain after four- hours of meiosis induction	156
	Discussion:.....	163
Chapter 6. General Discussion.....		167
6.1	Exo1 phosphorylation is Tel1 kinase dependent.....	168
6.2	Exo1 over-phosphorylation in the absence of <i>DMC1</i> and <i>RAD51</i>	170
6.3	Exo1 phosphorylation residues during meiosis.....	171
6.4	Future Directions:	174
Appendix:		177
A1:	Phosphatase assay for <i>Exo1-x9PK</i> and <i>exo1-4S::A-x9PK</i> by Strong, 2017.....	177
A2:	pBH368 plasmid map	178
A3:	Tagging of <i>EXO1-4S::A</i> allele with x5His-x6FLAG using the CRISPR-Cas9 system:	179
A4:	Western blot for large scal two-step purification for <i>EXO1</i> and <i>EXO1-x5His-x6FLAG</i> strains	180
A5:	The spectra of fragmented Exo1 phosphorylated peptides showing the relative intensity and the <i>m/z</i> of each fragment detected:.....	181
A5.1	MS spectra of Exo1 peptides detected in Exo1 purified sample from cells after four hours of meiosis induction: In-gel trypsin treatment and CID fragmentation	182
A5.2	MS spectra of Exo1 peptides detected in Exo1 purified sample from synchronised cells at the pre-sporulation stage: on-beads trypsin treatment and ETD fragmentation.....	185
A5.3	MS spectra of Exo1 peptides detected in Exo1 purified sample from cells after four hours of meiosis induction: on-beads trypsin treatment and ETD fragmentation	187

A5.4 MS spectra of Exo1 peptides detected in Exo1 purified sample from <i>sae2Δ</i> cells after four hours of meiosis induction: on-beads trypsin treatment and ETD fragmentation.....	197
A6 The cohesin subunit Scc3 is phosphorylated during meiosis and in response to Spo11-DSBs	215
A6.1 Scc3 is phosphorylated during meiosis:	218
A6.2 The phosphorylation of Scc3 is cohesin complex dependent:	221
A6.3 Scc3 phosphorylation is Spo11-DSB dependent and in the Tel1-mediated pathway	221
A6.4 The <i>scc3-9DQ</i> phosphorylation mimicking mutant is synthetically lethal:	223
A6.5 Scc3 is phosphorylation in response to DNA damage is mediated by Tel1 and Mec1 kinases:.....	226
A6.6 Discussion:	226
Bibliography:.....	230

List of Figures

Figure 1.1	The cell cycle of <i>S. cerevisiae</i>	4
Figure 1.2	The life-cycle of <i>S. cerevisiae</i>	6
Figure 1.3	The mitotic cell division	8
Figure 1.4	Meiosis	9
Figure 1.5	The cohesin complex	14
Figure 1.6	The synaptonemal complex	16
Figure 1.7	The bidirectional resection model	21
Figure 1.8	Crossover formation and Double-Holliday junction resolution by DSBR pathway and non-crossover formation via synthesis-dependent strand annealing pathway	24
Figure 1.9	Model for Dmc1 mediated strand-invasion during meiosis	26
Figure 1.10	The known motifs, domains, and phosphorylation sites of <i>S. cerevisiae</i> Exonuclease 1 (Exo1)	32
Figure 3.1	Western blot bands quantification using GeneTools software	65
Figure 3.2	<i>Exo1-x9PK</i> western blot analysis during meiosis	67
Figure 3.3	Meiotic progression of Exo1 strains during meiosis	69
Figure 3.4	Western blot analysis of TCA protein extracts from <i>Exo1-x9PK</i> meiotic samples	71
Figure 3.5	Western blot analysis of Ni-NTA affinity-purified <i>Exo1-x5His-x6FLAG</i> after four hours of meiosis induction	73
Figure 3.6	<i>Exo1-x5His-x6FLAG</i> is phosphorylated during meiosis	75
Figure 3.7	Western blot analysis of <i>Exo1-x5His-x6FLAG</i> strain's meiosis	77
Figure 3.8	Meiotic progression analysis of the <i>Exo1-x5His-x6FLAG</i> strain.	78
Figure 3.9	Western blot analysis of the <i>exo1-4S::A-x5His-x6FLAG</i> strain's meiosis	80
Figure 3.10	Meiotic progression analysis of <i>exo1-4S::A-x5His-x6FLAG</i> .	81
Figure 3.11	Spore viability of different Exo1 mutants	83
Figure 4.1	Analysis of Exo1 phosphorylation during <i>spo11-Y135F</i> sporulation	92
Figure 4.2	Analysis of <i>spo11-Y135F</i> meiosis progression	93
Figure 4.3	Exo1 phosphorylation was relatively normal in the pachytene arrested mutant <i>ndt80Δ</i>	95
Figure 4.4	Exo1 phosphorylation persisted during the meiosis of the double-mutant <i>dmc1Δ rad51Δ</i>	97
Figure 4.5	Phosphorylation analysis of Exo1 during <i>mek1-as</i> meiosis. <i>mek1-as</i> was inhibited at the third-hour of sporulation induction	99
Figure 4.6	Nuclear division analysis for <i>mek1-as</i> during meiosis showing MI and MII progression when <i>mek1-as</i> was inhibited and non-inhibited	100
Figure 4.7	Analysis of Exo1 phosphorylation during the meiosis of <i>tell1Δ</i> mutant and <i>TEL1</i>	103
Figure 4.8	Nuclear division analysis of <i>tell1Δ</i> strain	104
Figure 4.9	Analysis of Exo1 phosphorylation during the meiosis of <i>mecl1Δ sml1Δ</i> strain	106
Figure 4.10	Nuclear division analysis of <i>mecl1Δ sml1Δ</i> meiotic progression	107
Figure 4.11	Analysis of Exo1 phosphorylation in the absence of <i>TEL1</i> and <i>MEC1</i> during meiosis	109

Figure 4.12	Analysis of the meiotic progression in the absence of Tel1 and Mec1 kinases	110
Figure 4.13	Analysis of Exo1 phosphorylation during the meiosis <i>sae2Δ</i> mutant	112
Figure 4.14	Analysis of the meiotic progression of the <i>sae2Δ</i> mutant	113
Figure 4.15	Analysis of Exo1 phosphorylation during the meiosis of <i>sae2Δ tell1Δ</i> strain	115
Figure 4.16	Meiotic progression analysis of <i>sae2Δ tell1Δ</i> strain	116
Figure 4.17	Analysis of Exo1 phosphorylation during the meiosis of <i>sae2Δ mec1Δ sml1Δ</i> strain	118
Figure 4.18	Analysis of the meiotic progression of <i>sae2Δ mec1Δ sml1Δ</i> and <i>sae2Δ</i> strains	119
Figure 4.19	Analysis of Exo1 phosphorylation during the meiosis <i>mre11-H125N</i> mutant strain	122
Figure 4.20	Analysis of the meiotic nuclear division of <i>mre11-H125N</i>	123
Figure 4.21	Analysis of Exo1 phosphorylation during the meiosis of <i>mre11-58S</i> mutant	125
Figure 4.22	Analysis of the meiotic nuclear division of <i>mre11-58S</i>	126
Figure 5.1	An example of peptide showing the peptide-backbone cleavage sites of CID and ETD methods	133
Figure 5.2	Testing <i>Exo1-x5His-x6FLAG</i> elution from Ni-NTA beads	136
Figure 5.3	Immunoprecipitation of eluted <i>Exo1-x5His-x6FLAG</i> sample	138
Figure 5.4	SDS-PAGE gel of <i>Exo1-x5His-x6FLAG</i> purified by two-step purification method	139
Figure 5.5	Exo1 amino-acid sequence with the peptides sequences analysed by MS	142
Figure 5.6	P-label software showing the fragment ion spectra of the phosphorylated peptide SFNSSPILHEESK	145
Figure 5.7	Exo1 amino-acid sequence with the peptides sequences analysed by MS in the Exo1 purified sample from pre-sporulation culture	149
Figure 5.8	Exo1 amino-acid sequence with the peptides sequences analysed by MS in Exo1 purified sample from cells after four-hours of meiosis induction	154
Figure 5.9	Exo1 amino acid sequence showing the coverage of the MS analysis carried for Exo1 purified from meiotic cell that lack Sae2	160
Figure A1	<i>Exo1-X9PK</i> and the phosphorylation mutant <i>exo1-4S::A-X9PK</i> are phosphorylated during meiosis.	177
Figure A2	pBH368, <i>x6FLAG::KanMX</i> plasmid map	178
Figure A4	Western blot for Ni-NTA purified sample for <i>EXO1</i> and <i>Exo1-x5His-x6FLAG</i> meiotic samples followed by anti-FLAG immunoprecipitation.	180
Figure A5.1	MS spectra for KLS ^P NANVVQETLK with S431 phosphorylation	182
Figure A5.2	MS spectra for KLS ^P NANVVQETLKDTR with S431 phosphorylation	182
Figure A5.3	MS spectra for KLS ^P NANVVQETLKDTR with S431 phosphorylation	183
Figure A5.4	MS spectra for SFNSS ^P PILHEESK with S664 phosphorylation	183

Figure A5.5	MS spectra for SFNS ^{S^P?} ^{S^P?} PILHEESK where S663 and S663 residues where both had the same probability of being phosphorylated	184
Figure A5.6	MS spectra for SIS ^P LLSQVYK with S692 phosphorylation	184
Figure A5.7	MS spectra for KLS ^P NANVVQETLK with S431 phosphorylation	185
Figure A5.8	MS spectra for KLS ^P NANVVQETLKDTR with S431 phosphorylation	185
Figure A5.9	MS spectra for SVDERKS ^P FNSSPILHEESK with S660 phosphorylation	186
Figure A5.10	MS spectra for SVDERKS ^P FNSS ^P PILHEESK with S660 and S663 phosphorylation	186
Figure A5.11	MS spectra for LQLASK ^{S^P} NIEGK with S372 phosphorylation	187
Figure A5.12	MS spectra for KLS ^P NANVVQETLK with S431 phosphorylation	187
Figure A5.13	MS spectra for KLS ^P NANVVQETLKDTR with S431 phosphorylation	188
Figure A5.14	MS spectra for KLS ^P NANVVQETLKDTR with S431 phosphorylation	188
Figure A5.15	MS spectra for KLS ^P NANVVQET ^{T^P} LKDTR with S431 and T439 phosphorylation	189
Figure A5.16	MS spectra for LSNANVVQET ^{T^P} LKDTR with T439 phosphorylation	189
Figure A5.17	MS spectra for FRY ^{S^P} SSFSGV ^{NANRQPLFPR} with S585 phosphorylation	190
Figure A5.18	MS spectra for FRY ^{S^P} ^{SS^P} FSGV ^{NANRQPLFPR} with S585 and S587 phosphorylation	190
Figure A5.19	MS spectra for FRYSS ^{S^P} FSGV ^{NANR} with S587 phosphorylation	191
Figure A5.20	MS spectra for FRYSS ^{S^P} FSGV ^{NANRQPLFPR} with S587 phosphorylation	191
Figure A5.21	MS spectra for IVIDMK ^{S^P} VSER with S654 phosphorylation	192
Figure A5.22	MS spectra for SVDERKS ^{S^P} FNSSPILHEESK with S660 phosphorylation	192
Figure A5.23	MS spectra for SVDERKS ^{S^P} FNSS ^{S^P} PILHEESK with S660 and S664 or S663 phosphorylation	193
Figure A5.24	MS spectra for SFNS ^{S^P} ^{S^P} PILHEESK with S663 and S664 phosphorylation	193
Figure A5.25	MS spectra for SFNS ^{S^P} ^{S^P} PILHEESK with S663 and S664 phosphorylation	194
Figure A5.26	MS spectra for KSFNS ^{S^P} PILHEESK with S664 phosphorylation	194
Figure A5.27	MS spectra for DIETTK ^{S^P} SQARPAVR with S681 showing low phosphorylation probability	195
Figure A5.28	MS spectra for DIETTK ^{S^P} SQARPAVR with S682 phosphorylation	195
Figure A5.29	MS spectra for SIS ^P LLSQFVYK with S692 phosphorylation	196
Figure A5.30	MS spectra for SIS ^P LLS ^P QFVYK with S692 and S695 phosphorylation	196
Figure A5.31	MS spectra for LQLASK ^{S^P} NIEGK with S372 phosphorylation	197
Figure A5.32	MS spectra for KLS ^P NANVVQETLK with S431 phosphorylation	197

Figure A5.33	MS spectra for KLS ^P NANVVQETLKDTR with S431 phosphorylation	198
Figure A5.34	MS spectra for RKLS ^P NANVVQETLK with S431 phosphorylation	198
Figure A5.35	MS spectra for RKLS ^P NANVVQET ^P LK with S431 and S439 phosphorylation	199
Figure A5.36	MS spectra for RKLSNANVVQET ^P LK with S439 phosphorylation	199
Figure A5.37	MS spectra for FRYSS ^P SS ^P FSGVNANRQPLFPR with S585 and S587 phosphorylation	200
Figure A5.38	MS spectra for FRYSS ^P FSGVNANRQPLFPR with S587 phosphorylation	200
Figure A5.39	MS spectra for YSS ^P FSGVNANR with S587 phosphorylation	201
Figure A5.40	MS spectra for IVIDMK ^S ^P VDER with S654 phosphorylation. The methionine residue was oxidised	201
Figure A5.41	MS spectra for IVIDMK ^S ^P VDER with S654 phosphorylation	202
Figure A5.42	MS spectra for IVIDMK ^S ^P VDER with S654 phosphorylation	202
Figure A5.43	MS spectra for IVIDMK ^S ^P VDERK with S654 phosphorylation. The methionine residue was oxidised.	203
Figure A5.44	MS spectra for IVIDMK ^S ^P VDERK with S654 phosphorylation	203
Figure A5.45	MS spectra for SVDERK ^S ^P FNSSPILHEESK with S660 phosphorylation	204
Figure A5.46	MS spectra for SVDERKSFNS ^S ^P ^S ^P PILHEESK with S663 and S664 phosphorylation.	204
Figure A5.47	MS spectra for KSFNS ^S ^P ^S ^P PILHEESK with S663 and S664 phosphorylation	205
Figure A5.48	MS spectra for KSFNS ^S ^P ^S ^P PILHEESK with S663 and S664 phosphorylation	205
Figure A5.49	MS spectra for KSFNS ^S ^P ^S ^P PILHEESK with S663 and S664 phosphorylation.	206
Figure A5.50	MS spectra for KSFNS ^S ^P PILHEESK with S664 phosphorylation	206
Figure A5.51	MS spectra for KSFNS ^S ^P PILHEESK with S664 phosphorylation	207
Figure A5.52	MS spectra for KSFNS ^S ^P PILHEESKK with S664 phosphorylation	207
Figure A5.53	MS spectra for KSFNS ^S ^P PILHEESKK with S664 phosphorylation	208
Figure A5.54	MS spectra for SFNS ^S ^P PILHEESK with S663 and S664 phosphorylation	208
Figure A5.55	MS spectra for SFNS ^S ^P PILHEESK with S664 phosphorylation	209
Figure A5.56	MS spectra for SFNS ^S ^P PILHEESK with S664 phosphorylation	209
Figure A5.57	MS spectra for SFNS ^S ^P PILHEESKK with S664 phosphorylation	210
Figure A5.58	MS spectra for DIETTK ^S ^P ^S ^P QARPAVR with S681 and S682 phosphorylation	210
Figure A5.59	MS spectra for DIETTK ^S ^P ^S ^P QARPAVR with S681 and S682 phosphorylation	211
Figure A5.60	MS spectra for DIETTK ^S ^P QARPAVR with S682 phosphorylation	211
Figure A5.61	MS spectra for ^S ^P ISLLSQFVYKGK with S690 phosphorylation	212
Figure A5.62	MS spectra for ^S ^P [?] I ^S ^P [?] LL ^S ^P QFVYK with S690 or S692, and S695 phosphorylation.	212
Figure A5.63	MS spectra for SIS ^P LL ^S ^P QFVYKGK with S692 and S695 phosphorylation	213
Figure A5.64	MS spectra for SIS ^P LLSQFVYK with S692 phosphorylation	213
Figure A5.65	MS spectra for SIS ^P LLSQFVYKGK with S692 phosphorylation	214

Figure A6.1	Scc3 is phosphorylated during meiosis	220
Figure A6.2	Phosphatase treatment for <i>Scc3-PK</i> purified after four-hours of meiosis induction	220
Figure A6.3	Scc3 phosphorylation is Rec8 dependent	222
Figure A6.4	Scc3 phosphorylation is Spo11-DSB dependent and Scc3 phosphorylation persisted in <i>sae2Δ</i> strain meiosis	222
Figure A6.5	The phosphorylation mutant <i>Scc3-9S/T::A-PK</i> is not phosphorylated during meiosis	224
Figure A6.6	The phosphorylation mimicking mutant <i>Scc3-9S/T::D-PK</i> (<i>Scc3-9DQ</i>) is synthetically lethal	224
Figure A6.7	The <i>scc3-3DQ</i> mutant (T264D, T306D, T348D) is synthetically lethal	225
Figure A6.8	Scc3 is phosphorylated in response to DNA damaging agent MMS	227

List of tables

Table 2.1	Amino acid stock solution and the final concentration of amino acids used in sporulation media for supplementation	38
Table 2.2	List of haploid yeast strains used in this study	58
Table 2.3	List of diploid yeast strains used in this study	59-60
Table 2.4	List of plasmids used in this study	61
Table 2.5	List of primers used in this study	61
Table 5.1	The ten most abundant proteins in Exo1 purified sample by “in-gel” preparation	141
Table 5.2	Table showing Exo1 phosphorylated peptides detected by MS for in-gel treated <i>Exo1-x5His-x6FLAG</i>	143
Table 5.3	The ten most abundant proteins detected by MS in the Exo1 purified sample from pre-sporulation culture	148
Table 5.4	Exo1 phosphorylated peptides detected in Exo1 purified sample from pre-sporulation culture	150
Table 5.5	The frequency of each detected phosphorylated site in Exo1 purified sample from pre-sporulation culture	151
Table 5.6	The intensity of the most abundant proteins detected in Exo1 purified sample from cells after four-hours of meiosis induction	153
Table 5.7	The twenty phosphorylated peptides detected by MS in Exo1 purified sample from a meiotic cell culture at fourth-hour time-point	155
Table 5.8	The phosphorylation site frequency for the MS carried out for Exo1 purified from cells after four-hours of sporulation	157
Table 5.9	The ten most intense proteins in the MS sample for Exo1 purified from <i>sae2Δ</i> cells	159
Table 5.10	The 35 phosphorylated peptides detected by MS with 14 unique phosphorylation sites for Exo1 purified from meiotic cell that lack Sae2	161
Table 5.11	Phosphorylation site frequency of Exo1 phosphorylated residues in meiotic cells that lack Sae2	162

Chapter 1. General Introduction

1.1 *Saccharomyces cerevisiae* as a model organism

Unicellular fungi usually referred to as yeast, are eukaryotic microorganisms classified in the fungus kingdom. One of the most common and widely used yeast is *Saccharomyces cerevisiae*, which is a member of the Ascomycota phylum, known as budding yeast, brewer's yeast, or baker's yeast. "*Saccharomyces*" etymologically derives from Greek origins, meaning sugar-fungus; "*Saccharo-*" derives from "*saccharon*" (Greek - σάκχαρον) which means sugar and "*myces*" (Greek - μύκης) meaning fungus. The word "*cerevisiae*" comes from Latin which means beer. From its name *Saccharomyces cerevisiae* means "sugar-fungus beer" in Latinised-Greek, referring to its use in producing alcohol from sugars by anaerobic fermentation.

S. cerevisiae is widely used as a eukaryotic model organism, suitable for molecular biology and genetic research. The suitability of *S. cerevisiae* as a eukaryotic model organism stems from its ability to grow fast, its fully sequenced genome, and its well characterised cell cycle. In addition, the fundamentals of the molecular pathways such as chromosome segregation, transcription, and DNA replication are highly conserved between eukaryotes. Therefore, understanding the molecular pathways that govern the cell cycle in yeast could be easily translated to human-based molecular biology research. This paves the way in understanding how our cells conduct their everyday life, allowing for drug discovery and characterising diseases. Additionally, yeast meiosis is strikingly similar to human meiosis with many conserved proteins between both organisms that participate in similar functions. The meiotic cycle in yeast has been extensively studied which truly helped in understanding meiosis in humans.

Several yeast backgrounds have been developed and employed for biochemical and genetic studies. Most notably S288C, as it is the first yeast background to have its genome sequenced. Other yeast backgrounds are also used such as W303 which is easily transformable. In this study, the SK1 yeast background was used as a model organism to analyse the biochemistry of an exonuclease protein during meiosis. SK1 is primarily used in meiosis studies as it has the ability to be induced and synchronised into meiotic cell division by starvation. Concisely, *S. cerevisiae* is well suited as a model organism in meiotic studies, as it is easy to manipulate, grows fast, and is well-studied.

1.2 The life cycle of *Saccharomyces cerevisiae*

S. cerevisiae exists in two states, a haploid state (n), and a diploid state (2n). The *S. cerevisiae* haploid nucleus contains one copy of each of its 16 chromosomes (n=16), while the diploid state contains two copies of each chromosome, where each set of chromosomes is inherited from each parent i.e. homologous chromosomes. Both states, whether diploid or haploid, are maintained when cells divide by mitotic cellular division producing two genetically identical daughter cells.

The typical eukaryotic cell cycle is morphologically divided into two basic parts, interphase and mitosis. During interphase, the nucleus appears uniform as chromosomes are decondensed and distributed in the nucleus. Subsequently, during mitosis, chromosomes are condensed and segregate, usually ending with cell division producing two identical daughter cells. As the cell goes through the interphase stage towards mitosis, the DNA in the nucleus is synthesised and replicated. The timing of the DNA replication divides the interphase stage into three discrete phases, gap one (G1), DNA synthesis (S), and gap two (G2). The G1-phase, or sometimes called first growth, corresponds to the gap between mitosis and DNA synthesis. The G2-phase which is also known as second growth, corresponds to the gap between the completion of DNA

synthesis and mitosis. Therefore, the phases of the cell cycle can be divided into four subsequent phases, G1, S, G2, and finally mitosis (M) as shown in Figure 1.1.

The duration of the cell cycle varies between different kinds of cells and organisms. *S. cerevisiae* can progress through the four stages of the cell cycle in about 90 minutes. Furthermore, the *S. cerevisiae* cell cycle is primarily regulated at a point in late G1-phase called START (Hartwell, 1974). The passage through “START” is controlled mainly by three different factors; the availability of nutrients, mating factors, and cell size. After passing through “START”, a bud starts to emerge and continue to grow until it separates as a daughter cell after the M-phase.

S. cerevisiae cell cycle phases

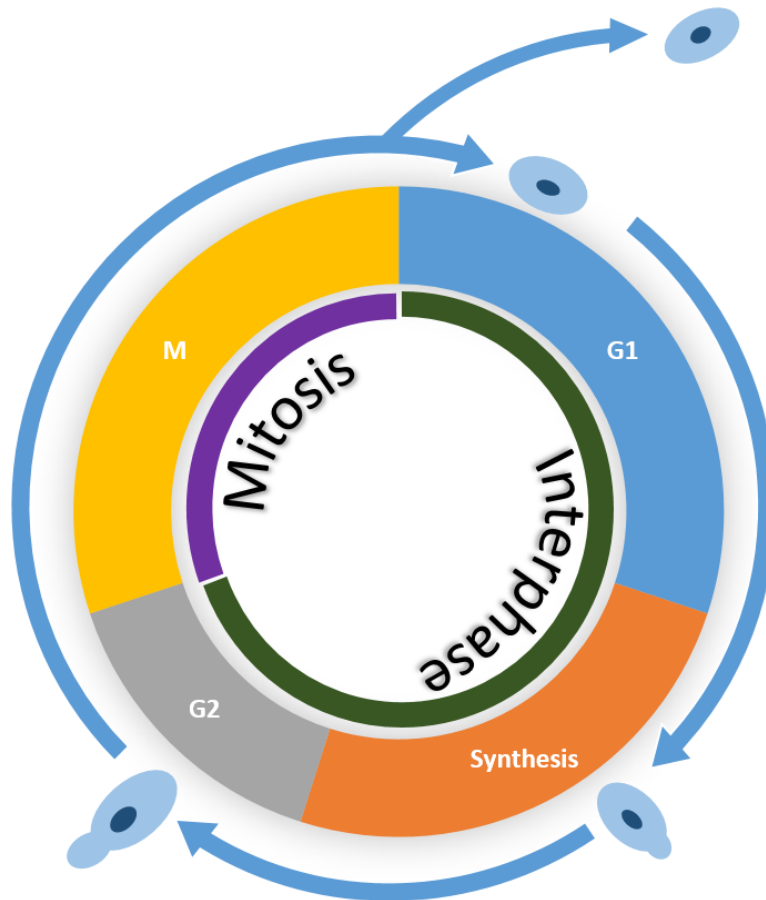


Figure 1.1 The cell cycle of *S. cerevisiae*

The yeast cell cycle is divided into two stages, mitosis (cell division), and interphase. The interphase stage is divided into three sub-stages, gap-1 (G1), DNA replication (Synthesis), and gap-2 (G2). A bud starts to emerge during the S-phase, preparing for cell division. The mitosis phase (M), is where the cells divide after making sure DNA replication had occurred. In mitotically dividing *S. cerevisiae* cells, chromosomes segregation occurs during cell division (M-phase) by budding hence the name “budding yeast”.

As *S. cerevisiae* can exist in a diploid state, the production of diploids is achieved by mating two haploids of opposite mating types, *MAT α* , and *MAT a* . Each mating type, *MAT a* and *MAT α* , produces pheromones called **a**- and **α** -factors respectively. Both mating types have receptors for their opposite pseudo-gender pheromones projecting a “*shmoo*” towards the source of the mating type pheromone (Merlini et al., 2013). Ultimately, opposite mating types fuse together forming a zygote which starts producing diploid cells. The produced diploid cells proliferate in the same way as haploid cells through mitotic cellular division. However, when diploids are starved of carbon and nitrogen sources, they go through a non-proliferative form of cell division where they go through two rounds of cell divisions called meiosis I and meiosis II. This produces four genetically distinct haploid spores from a single parent, where all are protected by a thick membrane called ascus. When the conditions allow for cell growth, spores germinate producing haploids, Figure 1.2.

S. cerevisiae isolated from the environment, especially from fruit skins, usually have the ability to change their mating type. However, common laboratory strain backgrounds are unable to do so due to the deletion of the HO endonuclease gene, which is required for gene conversion at the *MAT* locus by generating a DNA double-strand break (DSB). This ultimately prevents haploid colonies from changing their mating type, avoiding the production of unwanted diploids by mating.

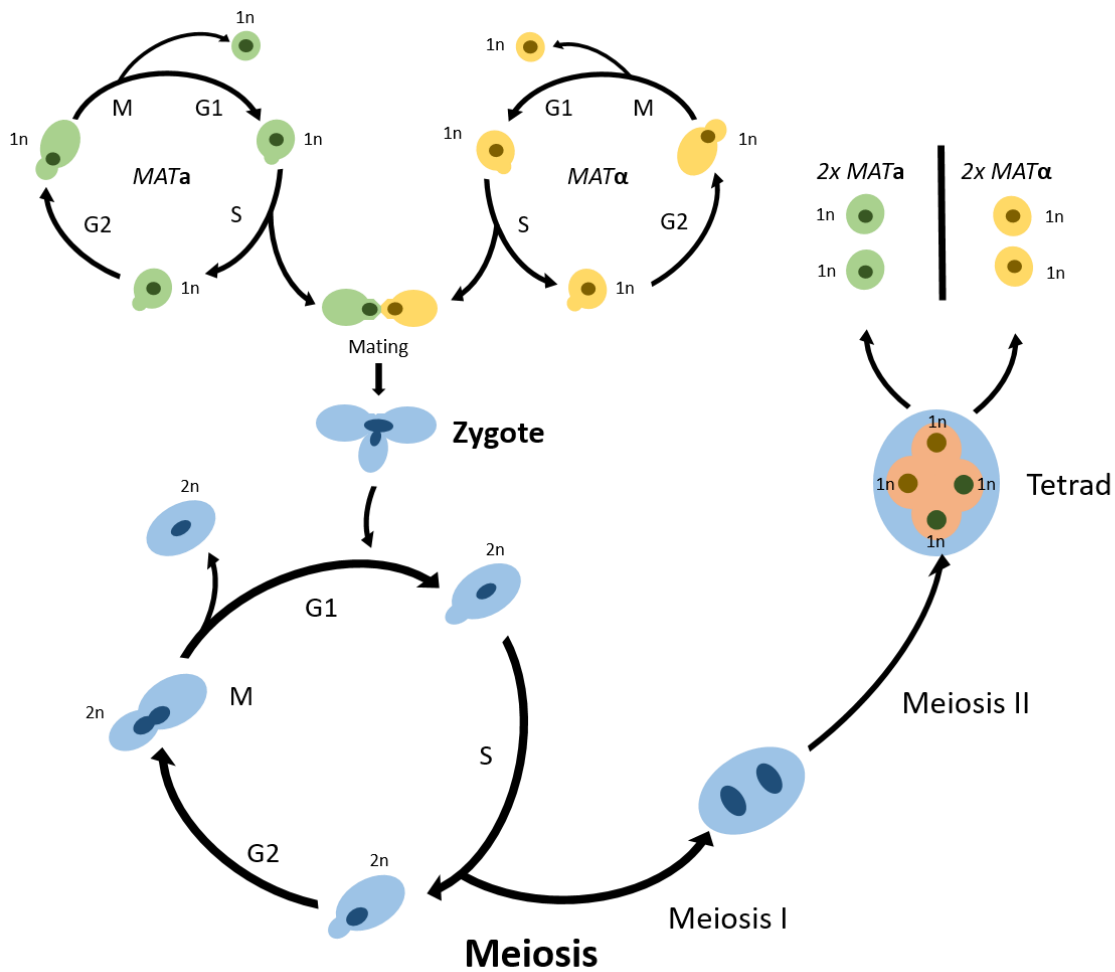


Figure 1.2 The life-cycle of *S. cerevisiae*

Budding yeast can exist in two states, a haploid state (n), and a diploid state ($2n$). Both states proliferate by cell division creating identical daughter cells. Haploids can exist in two forms, $MATa$ and $MAT\alpha$, these pseudo-genders are called mating types as they can fuse and mate to create a zygote. The “binocular” shaped zygotes start to produce diploids after the fusion of both mating types nuclei. To produce haploids, diploid cells go through meiosis when starved. This type of cell division is characterised with two subsequent nuclear divisions, producing four distinct daughter cells from a parental origin. These daughter cells are actually spores that germinate to haploids when growth conditions are met.

1.3 **Mitosis and Meiosis**

The proliferation of haploid and diploid yeast depends on mitotic cell division, which is a form of asexual reproduction. Each mitotic cell division yields two genetically identical daughter cells from a parental origin. This occurs after each chromosome is copied by DNA replication during S-phase, generating two identical sister chromatids. Once the cell ensures the completion of DNA replication, chromosomes condense and migrate to the equator of the cell. As illustrated in Figure 1.3, sister chromatids segregate to opposite poles of the cell ensuring that both daughter cells receive two copies of each homologue if the parent is a diploid and a single copy if the parent is a haploid. Furthermore, in order to produce haploids from a diploid parental cell, a different type of cell division occurs called meiosis.

Meiosis is characterised by two rounds of chromosome segregation events, first by reductional division and then by equational division. During reductional division, also called meiosis I (MI), homologous chromosomes segregate to opposite poles of the cell. This is followed by equational division, meiosis II (MII), where sister chromatids segregate. By the end of the second segregation step, four distinct daughter cells are produced from a single parent where each cell has one set of chromosomes i.e. haploids, Figure 1.4. The production of haploids is not the only outcome of meiosis as gene shuffling occurs between homologous chromosomes as illustrated in Figure 1.4. This is achieved by repairing the parental DNA by homologous recombination caused by programmed DNA damage (Sun et al., 1989; de Massy et al., 1995). This is important for the survival of the species as producing more genetic variants allows for adaptation to the environment and evolution. Most importantly, the recombination of homologous chromosomes during meiosis tether both homologues. This provides the resistance to pulling forces exerted by microtubules during chromosomes segregation that is vital for faithful homologous chromosome segregation.

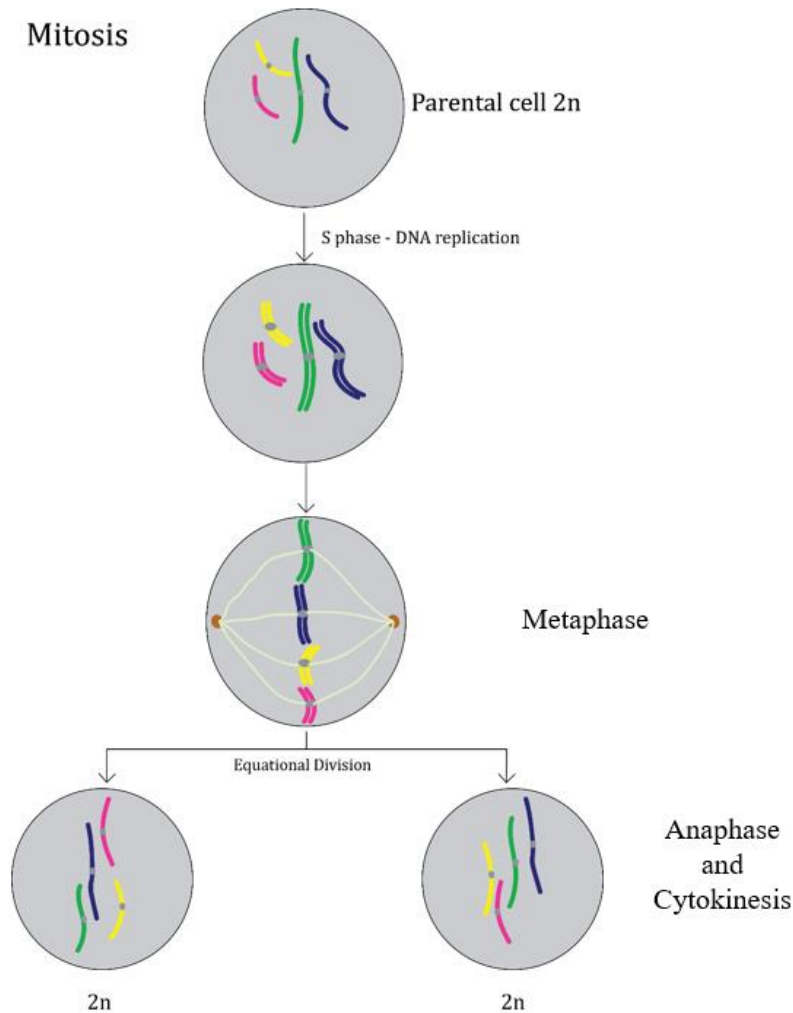


Figure 1.3 The mitotic cell division

Mitosis is a proliferative form of cell division that is observed in somatic cells in higher eukaryotes. After DNA replication, chromatids are replicated producing sister-chromatids that are held together by sister chromatid cohesion. After the subsequent G₂ phase, the cell enters the mitotic stages. During metaphase, the chromosomes condense and are aligned at the equator of the cell, also called the metaphase plate. Spindles that are attached to the kinetochore of each chromosome pull each sister chromatid to opposite poles of the cell, separating each chromatid to each pole. After cytokinesis two identical daughter cells are produced with same number of chromosomes. In the case of this figure it is a diploid cell, hence $2n$.

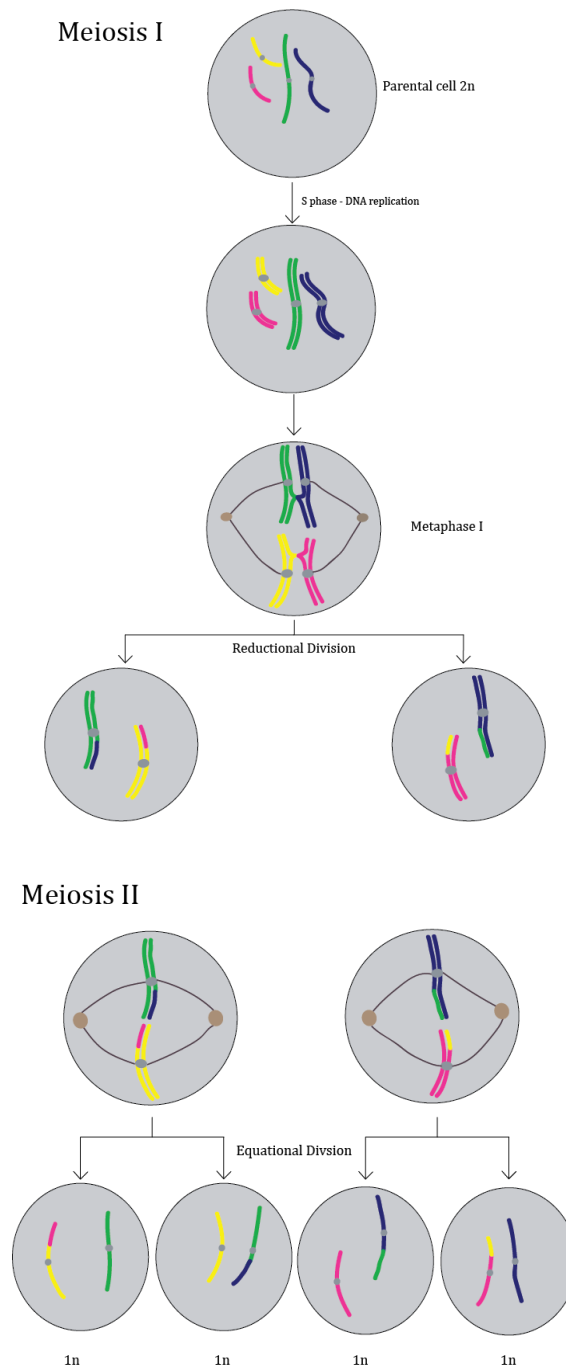


Figure 1.4 Meiosis

Meiotic cell division is characterised by two rounds of nuclear division, the reductional division (also called meiosis I), and the equational division (also known as meiosis II). This produces four distinct daughter cells with half of the number of the parental chromosomes, $2n \rightarrow n$. In contrast to mitotic cell division, homologous chromosomes align and pair where reciprocal DNA exchange occurs. This tethers both homologues by creating a crossover, after which the chromosomes are aligned at the metaphase plate in metaphase-I. The dissolution of cohesion between the chromosome arms, and the forces of meiotic spindles pull each homologue to opposite poles of the cell marking the end of meiosis I. In the next stage of cell division, sister chromatids are segregated in a similar way to mitotic cell division.

During cell division and chromosome segregation, the cell goes through stages that were characterised by cytological features. These subsequent stages are: interphase, prophase, metaphase, anaphase, and finally telophase. Interphase is when the DNA is decondensed, and the nucleus appears uniform. The subsequent prophase stage is characterised with condensed chromosomes followed by metaphase which is when chromosomes are assembled at the equator of the cell also known as the metaphase plate. During anaphase, the chromosomes segregate, and appear to be pulled to opposite poles of the cell. Finally, telophase is when the chromosomes are observed at each pole of the cell, followed shortly by cytokinesis. Both mitosis and meiosis go through each of these stages. The mitotic cellular division go through these stages once per division, while meiotic cell division enter these stages twice, as two rounds of chromosome segregation occur of a single round of DNA replication i.e. MI and MII.

The *S. cerevisiae* meiotic cell division is triggered by starvation due to a lack of nutrients such as glucose and nitrogen. The cells then exit from the mitotic cycle in G1 stage and enter into the pre-meiotic S-phase (Mitchell, 1994). This occurs by the phosphorylation of a meiosis specific transcription activator *IME1* (Kassir et al., 1988; Rubin-Bejerano et al., 2004) and the activation of a meiosis specific kinase *IME2* (Foiani et al., 1996). After the DNA is replicated, the cell is committed to go through meiotic cell division. Following this, the cell enters prophase-I where homologous chromosomes pair and synapse, which is facilitated by homologous recombination and the formation of the synaptonemal complex (SC). The SC is a conserved proteinaceous structure that forms a tight association between homologous chromosomes, synapsing homologous chromosomes together (Zickler and Kleckner, 1999). Synapsed homologous chromosomes are then physically linked by the process of homologous recombination which creates crossovers. The prophase-I stage is the longest stage in meiotic cell division, taking about 90% of the total time of meiosis. Hence, the phase is divided into sub-stages each with a cytological feature, these stages are: leptotene, zygotene, pachytene, and

diplotene/diakinesis. During leptotene, the chromosomes assume a “bouquet” conformation as the telomeres become tethered to the nuclear envelope (Zickler and Kleckner, 1998). Subsequently, at zygotene homologous chromosomes begin to come closer together, and appear to be shorter and fatter (Zickler and Kleckner, 1998). By pachytene, the full length of the homologous chromosomes are tightly associated; fully synapsed. At the diplotene/diakinesis stage, homologous chromosomes are separated but remain held together at the chiasmata where cross-overs and the exchange of genetic material occur (Zickler and Kleckner, 1998).

After all of the Prophase-I stages are completed, the cell then enters metaphase-I, where homologous chromosomes are aligned at the metaphase plate. This occurs as tubulin spindles are attached at the centromere of each homologue, where pulling forces act between them and protein structures at each pole of the cell called the spindle pole bodies (SPB). The progression of cells to anaphase-I is triggered by the dissolution of the cohesion between sister-chromatid arms. This stage is featured by the segregation of homologous chromosomes to opposite poles of the cells which marks the end of MI. As the cells progress to the second chromosome segregation step (MII), the same cell stages are repeated. The chromosomes are aligned at the metaphase plate during metaphase-II. After that the cells go into anaphase-II which is characterised by sister-chromatid segregation via the dissolution of the centromeric cohesion between sister-chromatids.

To ensure that each haploid receives the correct sets of chromosomes. Homologous chromosomes synapse, and are physically linked by crossovers. Failure to do so would result in non-disjunction leading to the formation of aneuploid haploids. In sexually reproducing organisms, non-disjunction leads to the production of aneuploid gametes. Aneuploidy in humans is the leading genetic cause of congenital birth defects and spontaneous abortions. Most aneuploidies are the result of MI non-disjunction, most notably chromosome trisomy;

where three copies of a chromosome are present after fertilisation (Hassold and Hunt, 2001). The most common trisomy in humans is trisomy 21 (Down's syndrome) which is mostly caused by maternal MI non-disjunction (Lamb et al., 2005). MII non-disjunction can also lead to trisomies, but it is observed less frequently for most chromosomes. There are, however, some exceptions, for example trisomy 18 (Edward's syndrome) in humans is typically caused by MII non-disjunction (Hassold et al., 2007). In humans, most trisomies are of maternal origin, where increased maternal age is proportional to trisomy cases (Hassold et al., 2007). Female mammalian meiosis (oogenesis) commences in the foetal ovaries where oocytes differentiate from sexually dimorphic primordial germ cells (Kocer et al., 2009). Around the time of birth, the meiotic cell cycle in oocytes are arrested in a late-prophase stage called dictyate where homologous chromosomes have finished the recombination step with chiasmata formation. The dictyate arrest can last for decades in humans where sister-chromatid cohesion deteriorate with time which significantly contributes to age-dependent aneuploidy of maternal cause (Jessberger, 2012).

1.4 **Homologous chromosome pairing and synapsis**

The pairing of homologous chromosomes starts at the early leptotene stage eventually associating each homologous pair tightly together (Zickler and Kleckner, 1998). This is done by a process called synapsis, which is when the SC is formed and homologous recombination between non-sister chromatids form crossovers. To achieve this, one or both chromosome ends bind to a shared region of the nuclear envelope after chromosome condensation in early-leptotene (Chikashige et al., 1997). This causes the chromosomes to fold upon themselves, restricting them to a particular area of the nuclear envelope forming a bouquet like morphology (Zeng et al., 2018). This formation is thought to increase the frequency of chromosome collisions, possibly promoting homologue interactions (Harper et al., 2004). Eventually, homologous chromosomes synapse and produce crossovers holding both homologues together. The tethering of homologous chromosomes as a product of homologous recombination is important for chromosome segregation during MI.

Sister chromatids are held together by cohesin, a protein complex that localises along the length of chromatid fibres. The main structural components of cohesin complex in *S. cerevisiae* are composed of two structural maintenance of chromosomes (SMCs) proteins: Smc1, and Smc3. The other two proteins are Rec8, and Scc3. Rec8 is a meiotic specific cohesin subunit but in mitotically cycling cells, Scc1 is the paralogue in place of Rec8. Smc1, Smc3, and Rec8 all form a tripartite ring structure, while Scc3 is bound to Rec8 or Scc1, Figure 1.5. The cohesin complex is loaded onto chromatin fibres before DNA replication. This is done by a conserved protein loading complex composed of two proteins Scc2, and Scc4, by loading the cohesin complex at the kinetochore (Hinshaw et al., 2017). Consequently, loaded cohesin complexes are translocated along chromatin fibres towards the pericentromeric region driven by ATP hydrolysis (Hu et al., 2011). Cohesin complexes on chromatin fibres are established after DNA replication, where sister chromatids are held tightly. The cohesin subunit Rec8 plays a vital

role in the formation of the SC, as it functions in the recruitment of the SC lateral element protein Red1 (Klein et al., 1999; Brar et al., 2009). After the formation of crossovers and the dissolution of SC at the on-set of diplotene (Jordan et al., 2009), the only thing that is holding both homologous chromosomes together is the cohesin complex. The release of cohesin from chromosome arms commences the first chromosome segregation step. This is done by the action of a protein called separase; which cleaves Rec8, dissociating sister chromatid cohesion (Buonomo et al., 2000). However, Rec8 subunits at the centromeric region are protected from cleavage by Sgo1 (shugoshin) during anaphase-I (Watanabe et al., 2005). Later at anaphase-II, centromeric Rec8 subunits are cleaved by separase followed by sister chromatid segregation (Terret and Jallepalli, 2006).

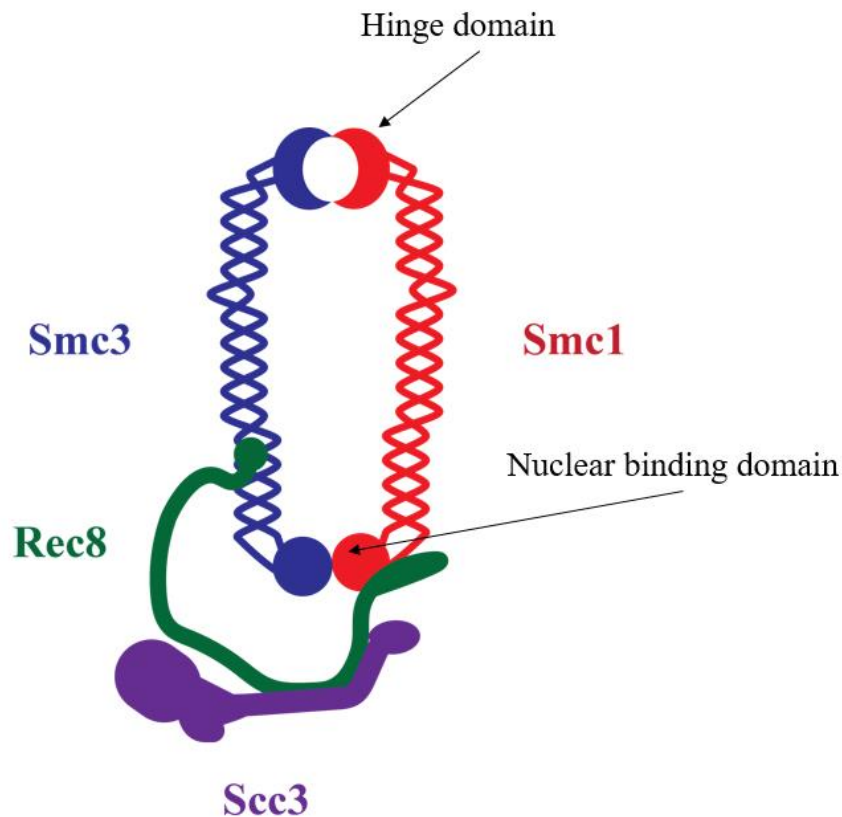


Figure 1.5 The cohesin complex

The cohesin complex is one of the most studied protein complexes. The full structure of the complex and the way it interacts with the DNA remains an interesting field of research. The putative model of the complex is as shown with two SMC proteins, Smc1 (red) and Smc3 (blue). Both proteins are paralogues with almost identical structures. At the apex of the complex is where Smc1 and Smc3 meet which is called the hinge-domain. At the other end of each protein where they meet again is called the nuclear binding domain. The hinge-domain and the nuclear binding domain is separated with a coiled-coil region. Smc3 is the cohesin complex subunit that does the ATPase activity which is believed to be important for cohesin distribution on the chromosomes. Rec8 protein (green) links both Smc1 and Smc3 proteins where its cleavage dissociates the complex from the DNA. The dissociation of cohesin marks meiosis I for arm cohesin or meiosis II for centromeric cohesin. Rec8 has a crucial role in recombination, and facilitates the formation of the synaptonemal complex. Scc3 is important for the complex stability on the DNA, binds to Rec8, and its full function remains unknown.

The alignment of homologous chromosomes, their stability, and the environment needed to facilitate homologous recombination is maintained by the SC. The SC is first formed by structures consisting of Red1 and Hop1 called the axial elements (AE) on sister chromatids organising the chromatid fibres, eventually forming the lateral elements of the SC (Hollingsworth et al., 1990; Smith and Roeder, 1997). When the SC matures it forms a zip-like proteinaceous structure, consisting of a central element (CE) and a lateral element (LE) connecting paired homologous chromosomes together, Figure 1.6 (Schmekel et al., 1993). The assembly of the SC begins during mid-leptotene due to the interaction of programmed meiotic DNA double strand breaks (DSBs) with homologous sequences, facilitating the formation of inter-axis bridges between homologues (Padmore et al., 1991; McKee, 2004). Cohesin subunit Rec8 mediates the recruitment of axis protein Red1 which forms the AE (Klein et al., 1999). During zygotene and after the AE assembly, Zip1 (a ZMM protein) arranges itself perpendicular to the AE forming the backbone of the transverse filaments (Sym et al., 1993). Zip1 association and its assembly is facilitated by other factors, such as Zip3 and Hop2 (Henry et al., 2006; Serrentino et al., 2013). After the initiation of synapsis, CE proteins Ecm11 and Gmc2 facilitate the interlocking of AE joining homologues in a zip-like fashion (Humphryes et al., 2013). The interlocking of the AE forms the LE of the SC, where the formation and maturation of SC elements are finished by the pachytene stage.

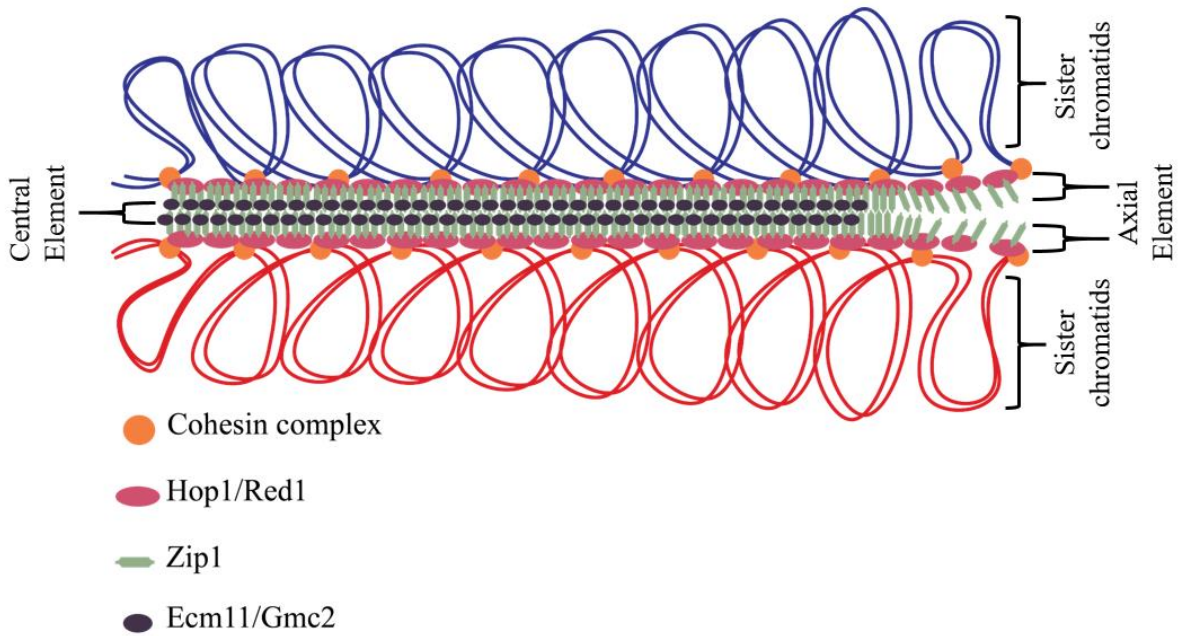


Figure 1.6 The synaptonemal complex

The synaptonemal complex (SC) is formed between homologues during meiosis where it facilitates synapsis and recombination. The complex is first formed by axial elements Hop1-Red1, facilitated by the cohesin complex. Once homology is found, Zip1 is recruited where it forms the transversal filament. Finally, Ecm11/Gmc2 forms the central elements after the complex is polymerised in such a way that resembles a zipper. Ultimately, both homologues are juxtaposed where they continue with the homologous recombination pathway creating crossovers linking both of them together.

1.5 **Programmed meiotic DNA double strand formation and processing**

The physical links between homologous chromosomes by crossover formation is promoted by the formation of programmed DSBs and their repair by homologous recombination. Meiotic DSBs formed during leptotene are created by Spo11; a meiosis specific topoisomerase-like protein (Keeney et al., 1997). Two Spo11 monomers catalyse the transesterification of the DNA phosphodiester backbone, generating a pair of single stranded nicks which forms a DNA-DSB (Keeney et al., 1997). The Tyr-135 residue in Spo11 is directly involved in this reaction, as mutating the tyrosine residue to phenylalanine prevents the formation of Spo11-DSBs (Bergerat et al., 1997; Diaz et al., 2002). Spo11 induced DNA-DSBs occurs at specific loci in a non-random fashion, and are distributed across the genome of *S. cerevisiae*, producing about 150 to 200 DSBs (Keeney, 2001). These areas are termed recombination hotspots where DSBs are likely to occur but are not guaranteed. Recombination hotspots are commonly found in promoter regions (Wu and Lichten, 1994), and in the presence of certain histone modifications (Petes, 2001), possibly due to the open configuration of the chromatin fibres at these loci. On the other hand, coldspots are likely to be found at the telomeres or proximal to centromeric regions (Baudat and Nicolas, 1997).

Spo11 by itself is not sufficient to generate DSBs as other factors and proteins are also required. Although these factors and proteins have been characterised, the full mechanism is not well understood. Nine proteins are vital for the formation of Spo11-DSBs: Ski8, Rec102, Rec104, Rec114, Mei4, Mer2, Mre11, Rad50, and Xrs2, as reviewed by Keeney, 2008. During S-phase, Spo11 is co-localised with Rec8 at pericentromeric regions, and is distributed along the axes of replicated chromatids through Spo11-Ski8 association with Rec102-Rec104 (Sasanuma et al., 2007; Kugou et al., 2009). To prepare for Spo11-DSBs, AE proteins Hop1 and Red1 recruit Mer2 to the chromatin axis, which is dependent on Mer2 phosphorylation by Cdc28

(Henderson et al., 2006; Panizza et al., 2011; Murakami and Keeney, 2014). The phosphorylation of Mer2, facilitates the recruitment of other pre-DSB recombinosome factors such as Rec114, Mei4, and Xrs2 at chromatin axes (Panizza et al., 2011). Mre11 co-localises with Spo11 and is thought to be associated with the pre-DSB recombinosome factors via Xrs2 interaction with phosphorylated Mer2 (Borde et al., 2004; Panizza et al., 2011). Mre11 forms a complex with Rad50, and Xrs2 called the MRX complex, and is implicated in the initial processing of Spo11-DSBs. Spo11-DSBs normally occur at looped regions of the chromatin away from the chromatin axis while the pre-DSB complex is at the axial region of the chromatin. To bring pre-DSB recombinosome factors closer to looped chromatin regions, the Spp1 subunit of the Set1 complex promotes the tri-methylation of histone 3, lysine 4 (H3K4) histone subunit (Kirmizis et al., 2007; Acquaviva et al., 2013). Spp1 was found to interact with phosphorylated Mer2, and it has been proposed that this interaction could potentially bring the axis and loop regions together in order to induce Spo11-DSB formation (Acquaviva et al., 2013). The full mechanism of Spo11-DSB production remains an interesting area to study, especially when it comes to how Spo11-DSBs are signalled. Recent unpublished biochemical studies by Scott Keeney's group showed that Spo11 pre-DSB complex composed of Spo11, Rec102, Rec104, and Ski8 has a monomeric (1:1:1:1) stoichiometry. This was concluded by using a combination of structural modelling, mutagenesis, and crosslinking couple to mass spectrometry. Since two Spo11 molecules are needed for DSB formation, this observation suggests that the dimerisation of Spo11 maybe a control mechanism to catalyse DSB formation.

After the formation of the Spo11-DSB forming complex, DSBs are possibly formed by the dimerisation of Spo11. Each monomer of Spo11 is covalently bound to 5' ends of the DNA duplex (Keeney et al., 1997). In order to begin with DNA-DSB end processing, covalently bound Spo11 must be liberated from DSB ends. This is an important step for the subsequent resection process which then expose long tracts of 3'ssDNA capable of efficient homologous

recombination. The removal of Spo11 possibly occurs by asymmetrical nicking of the DNA by single-stranded endonucleolytic cleavage, releasing Spo11 with a short oligonucleotide still covalently bound to it (Neale et al., 2005; Garcia et al., 2011). The release of Spo11 dimers from DSBs relies on the MRX complex and the Sae2 endonuclease (Moreau et al., 1999; Farmer et al., 2012). During meiosis in *mre11-H125N* and *mre11-58S* (nuclease deficient) cells, Spo11-DSBs are accumulated and not repaired (Tsubouchi and Ogawa, 1998). Furthermore, cells that lack *SAE2* during meiosis accumulate Spo11-DSBs that are not repaired and DNA end resection is not detected (McKee and Kleckner, 1997a; Prinz et al., 1997).

MRX is a highly conserved protein complex, composed of three subunits: Mre11, Rad50, and Xrs2. Mre11 is a DNA binding protein with dual nuclease activities that are manganese-dependent; a DNA endonuclease activity, and a 3' → 5' DNA exonuclease activity (Paull and Gellert, 1998; Usui et al., 1998). The Rad50 subunit of the MRX complex is composed of two heptad repeats that form a coiled-coil region. The coiled-coil heptad repeats bring both ATPase motifs, Walker A and Walker B in close proximity from its N- and C-terminals respectively, as reviewed by Borde, 2007. The apex of the coiled-coil region contains a zinc-hook domain, which facilitates the interactions between Rad50 molecules (Hopfner et al., 2001). This interaction between Rad50 molecules allows for the tethering of DNA-DSB ends by two MRX complexes at each DNA end. The ATP binding promotes Rad50 dimerisation and DNA binding, which is vital for MRX complex nuclease functions (Alani et al., 1990). The *rad50S* hypomorphic mutant, with several point mutations at the ATP binding domain, showed an accumulation of unrepaired Spo11-DSBs (Alani et al., 1990). The Xrs2 subunit functions in the nuclear localisation of Mre11, MRX complex integrity, recruits the complex to Spo11 pre-DSB complex (Borde et al., 2004; Tsukamoto et al., 2005), and functions in Tel1 association to DNA DSBs (Nakada et al., 2003). All of the complex components are crucial for the formation of Spo11-DSBs. Several separation of function alleles permits DSB formation, but

prohibit resection such as *mre11-58S*, which is thought to also prohibit MRX complex formation (Alani et al., 1990; Borde, 2007).

Sae2 promotes the double-stranded DNA endonuclease activity of Mre11, which generate nicks in the DNA at the 5' end of the strand (Cannavo and Cejka, 2014). An *in vitro* study of Sae2 showed a endonuclease activity on ssDNA and ssDNA/dsDNA junctions, stimulated by the MRX complex (Lengsfeld et al., 2007). It was also shown that the interaction between both proteins Mre11 and Sae2 facilitates the recruitment of MRX complex to the DNA (Cannavo and Cejka, 2014). Moreover, the MRX complex and Sae2 functions were shown to be implicated in removing covalently bound proteins from DSBs in mitotically dividing cells (Lengsfeld et al., 2007).

The 5' ends of DNA-DSBs are further processed in a two-step process following the removal of the Spo11-oligonucleotide complexes; first the DNA is resected by Mre11 nuclease function (Neale et al., 2005), then by 5' → 3' DNA resection by another nuclease, exposing long 3'ssDNA fragments (Hodgson et al., 2011; Garcia et al., 2011). The formation of long tracts of 3'ssDNA is important for efficient and normal levels of crossovers (Zakharyevich et al., 2010). This is because the minimum length homology required for efficient DSB repair in mitotically dividing cells has been estimated at 250bp (Jinks-Robertson et al., 1993; Inbar et al., 2000). Exo1, Sgs1, and Dna2 were reported to be the nucleases that function in the 5' → 3' long resection during the repair of mitotic DSBs (Mimitou and Symington, 2009; Hodgson et al., 2011). However, it was shown that Sgs1; partner of Dna2, does not function in DNA resection during meiosis (Zakharyevich et al., 2010). The average resection length of Spo11-DSBs is around 800 nucleotides (nt), whereas in the absence of Exo1 the resection length was dramatically reduced to around 270nt (Zakharyevich et al., 2010). The resection observed during meiosis in *exo1Δ* cells could be a product of Mre11's initial processing, as Mre11 can resect 5' DNA ends (Hodgson et al., 2011). These observations concluded that meiotic DSB

ends are processed with bidirectional resection by MRX and Exo1, Figure 1.7. The Mre11 3' → 5' exonuclease is responsible for the initial resection process towards DSB ends from the single-stranded nick created by Mre11 endonuclease (Garcia et al., 2011). The 5' → 3' resection is done by the exonuclease activity of Exo1, which resects away from Spo11-DSBs creating a long 3' ssDNA fragment.

Exo1 (exonuclease 1) has a 5' → 3' exonuclease activity and a 5' flap endonuclease activity (Lieber, 1997). Post-translational modifications (PTM) of Exo1 were observed in mitotically dividing cells, in response to DNA damaging agents (Morin et al., 2008; Bologna et al., 2015). Exo1 is regulated by two types of PTMs, phosphorylation which has been proposed to negatively regulate Exo1's nuclease activity (Morin et al., 2008), and sumoylation which limits pathological resection (Bologna et al., 2015). Furthermore, differential phosphorylation of Exo1 in human cell-lines was shown to be important for Exo1 recruitment to the DNA, and to negatively regulate its nuclease function (Tomimatsu et al., 2014).

As 3' ssDNA are being exposed, RPA (Replication Protein A) is associated to resected ssDNA preventing the formation of DNA secondary structures, and from nucleolytic degradation (Chen et al., 2013). This generates RPA-ssDNA nucleoprotein filaments that facilitates the binding for recombinases, which is important for homology search and recombination (Bishop et al., 1992; Chen et al., 2013). With the help of recombinases and other factors, 3' ssDNA overhangs search for a repair template at the homologue region which is a key step in crossover formation.

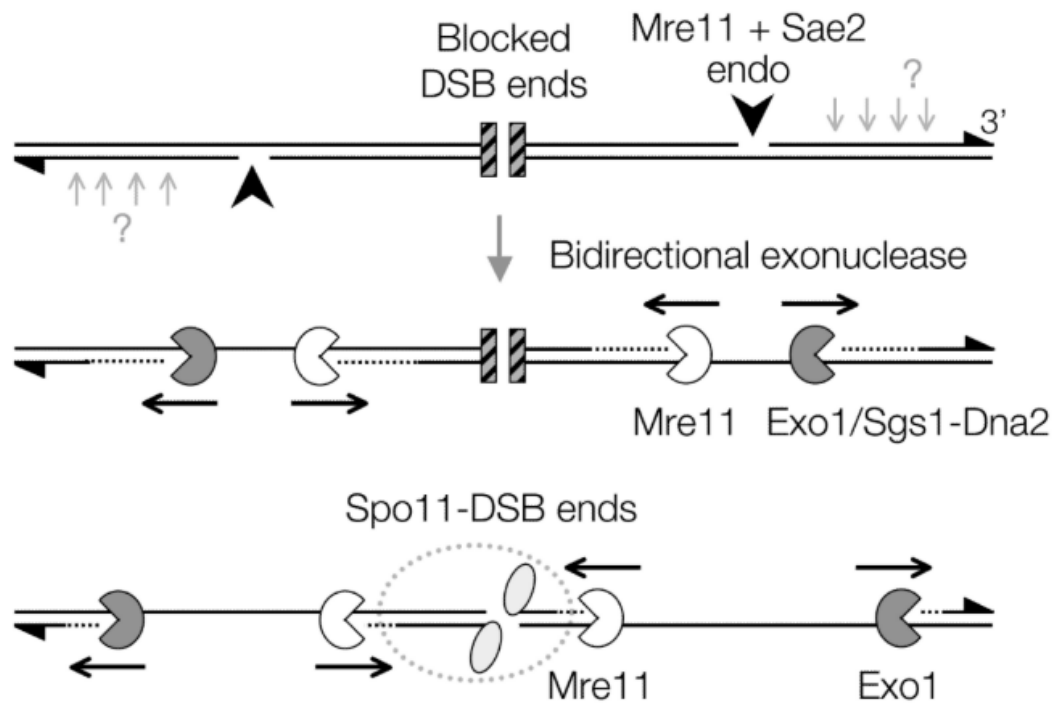


Figure 1.7 The bidirectional resection model

This model was proposed by Neale et al. 2005 and Garcia et al. 2011. After the formation of Spo11-DSBs, Spo11 is covalently bound to DNA ends blocking any further processing. With the help of Sae2 and Mre11, the DNA is nicked by endonucleolytic cleavage exposing a small fragment of ssDNA. Mre11 and Exo1/Sgs1 commence the bidirectional resection where Mre11 does the 3' → 5' exonuclease activity towards the DSB end, while Exo1/Sgs1 is responsible for the 5' → 3' exonuclease activity away from the DSB end. This eventually liberates Spo11-oligonucleotide molecules, exposing long tracts of 3' ssDNA.

Image from (Garcia et al., 2011)

1.6 **Recombination, crossover formation, and resolution**

After the resection of DSB ends and the production of RPA coated 3' ssDNA, proteins called recombinases bind to ssDNA tails and form tracts of protein coated DNA called nucleoprotein-filaments (NPFs) (Chen et al., 2013). NPFs with the help of other accessory proteins search for the homologous duplex DNA. Once a homologous region is found, NPFs invade the homologous duplex displacing the complementary strand forming a D-loop. The displaced complementary strand is used as a template for DNA synthesis, where the newly synthesised short strand is ligated to the other 5' end of the processed DSB. As one of the DNA strands has been repaired, the invader ssDNA is repaired by DNA synthesis, eventually ligating it to the opposite 5' end of the DSB. This pathway known as the double-strand break repair (DSBR) which forms two junctions known as a double-Holliday junction (dHJ), producing a four-stranded branched intermediate called a joint molecule (JM) (Stahl, 1996). Ultimately, dHJs are resolved creating a crossover (CO) that is essential for homologous chromosomes tethering, Figure 1.8. COs are produced as a result of the exchange of genetic material between homologous chromosome arms, and eventually tether both homologues together. Chiasma is the cytological manifestation of a CO, and at least one per chromosome is needed for normal disjunction (Fleidel-Alon et al., 2009). Occasionally, homologous recombination can yield a NCO which does not tether both homologues, and this depends on stable joint molecule formation (Allers and Lichten, 2001).

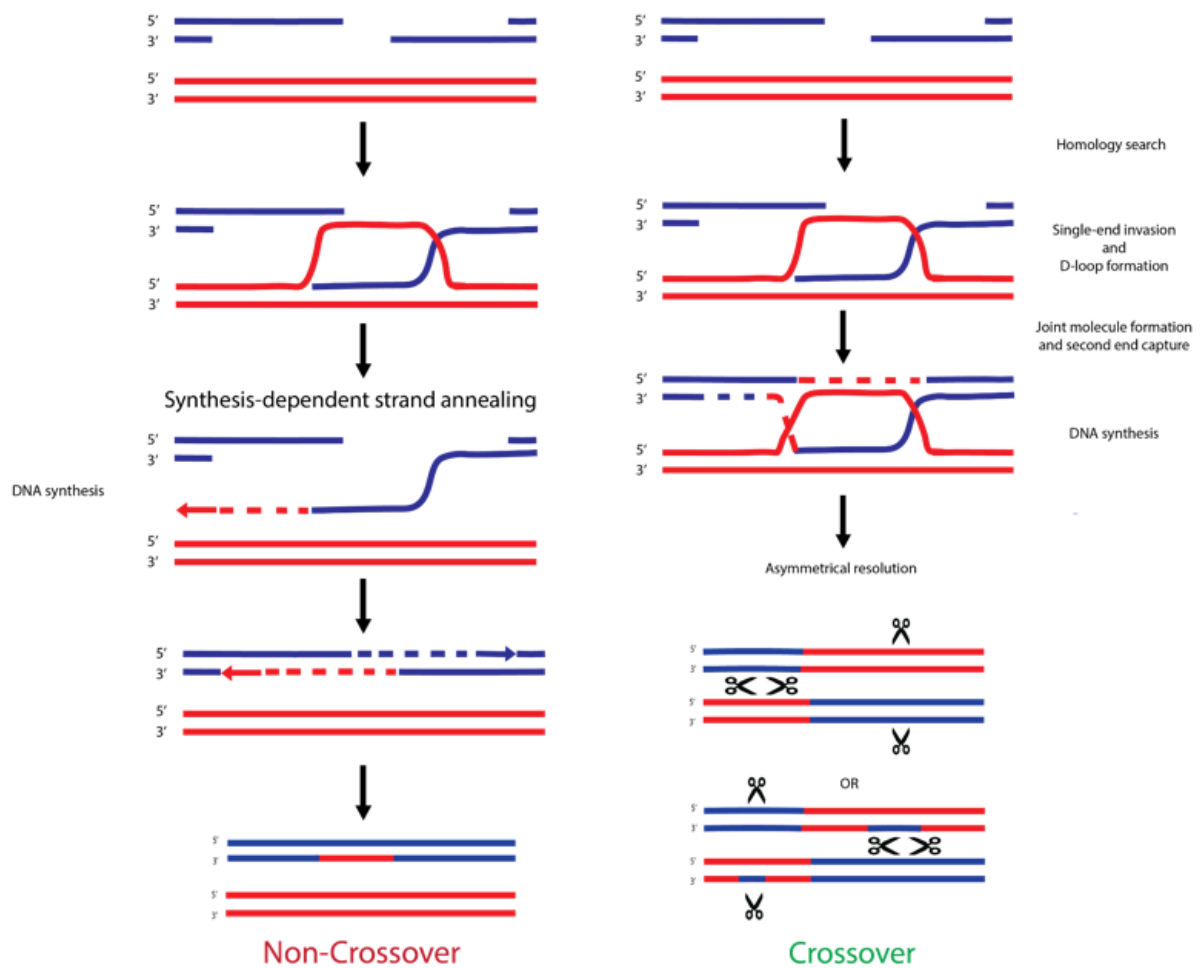


Figure 1.8 Crossover formation and Double-Holliday junction resolution by DSBR pathway and non-crossover formation via synthesis-dependent strand annealing pathway.

After the processing of DSBs and the subsequent steps of the production of long 3' ssDNA fragments. The protein coated ssDNA strand invades the complementary DNA sequence at the homologue. After DNA synthesis and ligation, a joint molecule is formed with two Holliday junctions (right). The asymmetrical resolution by resolvases act on these dhJs and crossover is produced that tether both. Unstable joint molecules cannot form crossovers (left), where the DSB break is repaired via synthesis-dependent strand annealing, and homologous chromosomes are not tethered.

The two recombinases that function during meiosis in *S. cerevisiae*, are homologues of the prokaryotic recombinase RecA, called Rad51 and the meiosis specific Dmc1 (Bishop et al., 1992; Shinohara et al., 1992). Both recombinases can bind to ssDNA forming a contiguous helical NPFs which promotes the search for homologous dsDNA and DNA strand exchange between nearly identical DNA strands (Masson and West, 2001). Rad51 predominantly functions in the homologous recombination pathway that repairs DSBs during mitotically cycling cells (Baumann and West, 1998). However, during meiosis repair occurs between homologous chromosomes where a meiosis specific recombinase Dmc1 is required for repair (Bishop et al., 1992; Cloud et al., 2012). Rad51 activity is required for efficient homologous recombination during meiosis, since in the absence of *RAD51*, meiotic homologous recombination is impaired (Krejci et al., 2012). While in the absence of *DMC1* during meiosis, 3' ssDNA is accumulated due to over-resection resulting in cell-cycle arrest in late prophase (Schwacha and Kleckner, 1997; Hunter and Kleckner, 2001). Furthermore, a protein complex composed of Mei5 and Sae3 is required for the loading of Dmc1 onto ssDNA (McKee and Kleckner, 1997b; Hayase et al., 2004). In the absence of either proteins during meiosis, the cells arrest at the prophase stage, and similar phenotypes were observed to *dmc1Δ* meiosis (McKee and Kleckner, 1997b; Hayase et al., 2004). Additionally, Hop2-Mnd1 complex stabilises Dmc1-NPFs, and facilitates the duplex DNA capture for homology search, Figure 1.9 (Sansam and Pezza, 2015). The Rad54 and Tid1 (also known as Rdh54) proteins, both enhance Rad51 and Dmc1 mediated DSB repair (Shinohara et al., 2000). Although Tid1 is not meiosis specific, it interacts with Dmc1 where this interaction promotes CO formation, and facilitates Dmc1-mediated JMs (Nimonkar et al., 2012). On the other hand, Rad54 promotes Rad51-mediated inter-sister DNA strand exchange (Nimonkar et al., 2012). Because of this, Hed1 a meiosis specific protein which inhibits the formation of Rad51-Rad54 complexes, possibly to promote inter-homologue repair rather than sister repair (Busygina et al., 2008).

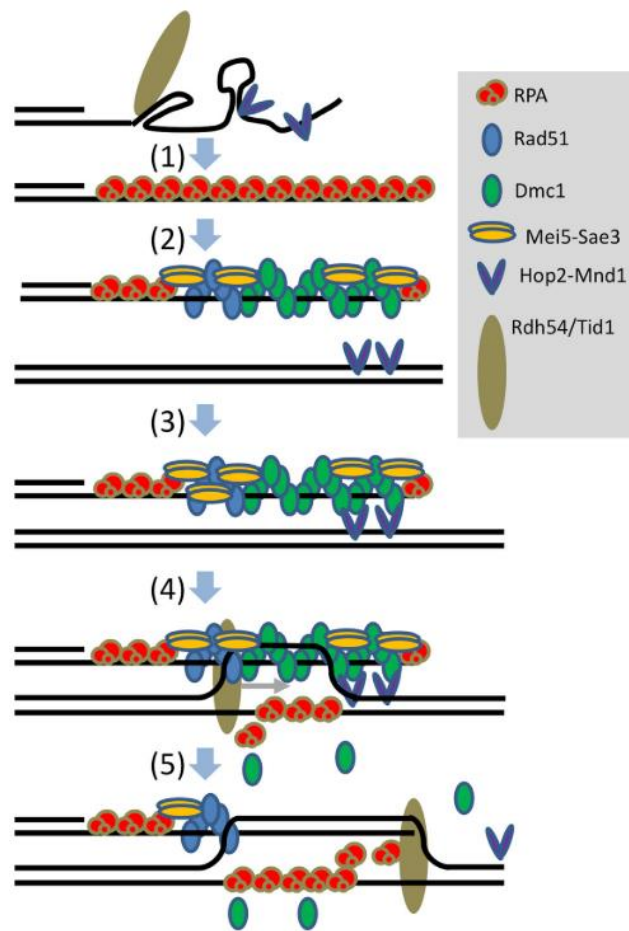


Figure 1.9 Model for Dmc1 mediated strand-invasion during meiosis

(1) RPA binds to ssDNA stabilising it and eliminating any secondary structures preventing other proteins from interacting with ssDNA fragments. (2) RPA then facilitates the binding of Dmc1 to ssDNA with the help of Mei5-Sae3 and Tid1. (3) Hop2-Mnd1 that is bound to dsDNA captures Dmc1-NPFs. (4) This allows for homology search and recognition, forming a D-loop structure that is stabilised by RPA binding to the complementary exposed strand. (5) Tid1 elongates the D-loop and stabilises the loop structure by the removal of Dmc1.

Image from (Chan et al., 2018)

The meiosis specific kinase Mek1 phosphorylates Hed1 which activates its inhibition of Rad51-Rad54 complexes (Suhandynata et al., 2016). Mek1 is implicated in controlling many components required for inter-homologue bias (Niu et al., 2007). Moreover, Srs2 a DNA helicase, was observed to promote inter-homologue repair by removing Rad51 from NPFs (Sasanuma et al., 2013). However, not all meiotic DSBs are repaired by inter-homologue bias as some are repaired by inter-sister repair, especially in highly-polymorphic regions between homologues (Goldfarb and Lichten, 2010).

In *S. cerevisiae*, the majority of COs are distributed along the chromosomes in a non-random fashion. This type of COs known as Type I COs tend to be evenly spaced and widely distributed by a phenomenon known as crossover interference as reviewed by Zickler and Kleckner, 2016. This pattern is thought to be a product of positive selection and stabilisation of some nascent JMs in a process called CO designation. The designation of COs is facilitated by ZMM proteins promoting the maturation of recombination intermediates into dHJs (Lynn et al., 2007). The ZMM protein group includes seven proteins that facilitate recombination and SC assembly. Zip1 is part of the transverse filament of the SC and its function is facilitated by Zip2, Zip3, and Zip4 (Lynn et al., 2007). The other proteins from this group, Mer3, Msh4, and Msh5 are required for CO formation (Nakagawa and Ogawa, 1999; Snowden et al., 2004).

Type I COs that arose from ZMM-stabilised JMs are resolved by the MutL γ nuclease complex (Mlh1-Mlh3), Sgs1-Top3-Rmi1, and exonuclease-independent functions of Exo1 (Zakharyevich et al., 2012; Rogacheva et al., 2014). Furthermore, the MutL γ dHJ resolution pathway is dependent on mismatch repair (MMR) proteins Msh4 and Msh5 (Argueso et al., 2004). This pathway produces the majority of COs (Zakharyevich et al., 2012) and its resolution activity can only produce a CO product (Zakharyevich et al., 2012).

Type II COs that are produced by the resolution of ZMM-independent JMs are resolved by three structure-selective endonucleases (SSEs): Mus81-Mms4, Yen1, and Slx1-Slx4 (De los Santos et al., 2003; Zakharyevich et al., 2012). Type II COs do not display CO interference and their resolution is thought to be SSE-dependent (De los Santos et al., 2003). In contrast to the MuLγ resolution pathway, the resolution of JMs by SSE-dependent pathways does not guarantee a CO formation (Zakharyevich et al., 2012).

The resolution of mature JMs into COs by nucleolytic cleavage is associated with the expression of *NDT80* (Allers and Lichten, 2001), and the subsequent expression of *CDC5* (Sourirajan and Lichten, 2008). The resolution of JMs by SSEs Mus81-Mms4, and Yen1 are controlled by Cdc5 kinase (Matos et al., 2011), while the regulation of MuLγ-dependent resolution i.e. Type I COs, remains unknown.

1.7 Meiosis regulation and the checkpoint network

Meiosis is remarkable, as different independent mechanisms work together in a timely and concerted manner to achieve faithful cell division. This is controlled by surveillance mechanisms that signal normal progression and is triggered in the event of an abnormal progression. These checkpoints create dependent relationships between independent processes, in a network that ensures correct conditions for each stage. For example, in mutants that lack the ability to process DSBs during meiosis i.e. *dmc1Δ* and *sae2Δ*, the cell cycle arrests and the production of aneuploid gametes is prevented. Hence, any defects in major events during meiosis would arrest or delay the cell progression due to either; failure to complete vital processes, or failure to trigger key signalling checkpoints.

In *S. cerevisiae*, the expression of the *IME1* transcription factor and its regulation by different factors such as mating type, nitrogen source, and carbon source leads to the transcription of early meiotic proteins (Kassir et al., 1988; Mitchell, 1994). These early meiotic proteins are required for the entry into pre-meiotic S-phase, chromosome recombination, and pairing (Primig et al., 2000). One of the significant targets of Ime1 is *IME2*, which transcribes Ime2 kinase (Mitchell et al., 1990). The Ime2 kinase activity is required for initiation of the meiotic DNA replication (Foiani et al., 1996) by the activation of Cdc28 associated with the b-cyclins Clb5 and Clb6 (Dirick et al., 1998). Cdc28 is required for the exit from pachytene (Shuster and Byers, 1989) and directly regulates Spo11-DSBs initiation (Henderson et al., 2006). Subsequently, *NDT80* expression is induced which is a transcription factor that is required for the exit from pachytene, and for the activation of middle-sporulation genes (Hepworth et al., 1998). Ndt80 activates the transcription of itself, *CDC5* (Sourirajan and Lichten, 2008), *CLB1*, and *CLB3* (Carlile and Amon, 2008). Clb1 and Clb3 are required for the exit from MI, and MII respectively. In the absence of *NDT80* during meiosis, cells arrest at the Pachytene stage, with fully synapsed chromosomes, and unresolved HJs (Allers and Lichten, 2001). The transcription of *NDT80* occurs in two stages during meiosis, first by Ime1, and then by itself as Ndt80 binds to specific DNA sequence on its own promoter (Montano et al., 2002).

In the presence of unrepaired DSBs, the meiotic recombination checkpoint is triggered (Lydall et al., 1996), which is an altered version of the DNA damage checkpoint in mitotically dividing cells. Both Tel1 and Mec1 checkpoint kinases play a redundant role in regulating DSB processing during meiosis and mitotically dividing cells as reviewed by Subramanian and Hochwagen, 2014. Tel1 and Mec1 are serine/threonine kinases (Mallory and Petes, 2000), where they preferentially phosphorylate their substrates on serine or threonine residues that precede glutamate residues, also known as SQ/TQ (Traven and Heierhorst, 2005). The MRX complex and Sae2 are both involved in checkpoint activation via Tel1 activity in mitotic cells

but the activation mechanism in meiosis is not fully characterised (Nakada et al., 2003; Borde, 2007; Cartagena-Lirola et al., 2006). Both kinases Tel1 and Mec1 have been shown to phosphorylate components of the MRX complex (Usui et al., 2001) and Sae2 (Cartagena-Lirola et al., 2006). The phosphorylation of Sae2 was thought to be one of the mechanisms by which Mec1 and Tel1 kinases contribute to meiotic DSB processing. Additionally, Cdc28 was found to phosphorylate Sae2 (Huertas et al., 2008), where this modification is important in regulating Sae2 endonuclease function (Manfrini et al., 2010), and the physical interaction of Sae2 to Rad50 promoting MRX endonuclease function (Cannavo et al., 2018). These observations suggest that Tel1, Mec1, and Cdc28 kinase activities are important in regulating Spo11-DSB processing. Furthermore, a complex composed of Rad17-Ddc1-Mec3, recruits Mec1 to resected DSBs where Hop1 is phosphorylated (Carballo et al., 2008). Subsequently, the meiosis specific kinase Mek1 binds to phosphorylated Hop1 resulting in activation of Mek1 (Carballo et al., 2008). Mek1 activation and activity is very crucial for inter-homologue bias during meiosis, preventing DSB repair between sister chromatids (Niu et al., 2007; Suhandynata et al., 2016). The elimination of Mek1 activity requires the transcription of *CDC5* by Ndt80 which may play a role in controlling the meiotic progression of the cell (Prugar et al., 2017).

In addition to the pachytene checkpoint and the meiotic recombination checkpoint, the completion of faithful DNA replication before meiosis may act as a checkpoint by itself. This is because partial pre-meiotic DNA replication impairs Spo11-DSB formation and DNA recombination (Blitzblau and Hochwagen, 2013). Additionally, when pre-meiotic DNA replication is delayed, Mec1 inhibits the expression of Spo11 (Blitzblau and Hochwagen, 2013), and Dbf4 inhibits Mer2 phosphorylation (Blitzblau and Hochwagen, 2013). The failure to synapse homologues also arrests the cell cycle progression, and in the absence of DSBs, SC formation is delayed via Zip3 activity (MacQueen and Roeder, 2009). The full meiotic

checkpoint network is intricate and not fully understood. Efforts are now being made to map the full network.

1.8 **Exonuclease 1 (Exo1)**

Exo1 is a member of the Rad2/XPG nuclease family, and functions in multiple DNA repair pathways such as homologous recombination, mismatch repair (MMR), and telomere maintenance, Figure 1.10. It was initially identified as a 5' → 3' dsDNA exonuclease during the meiotic division of *Schizosaccharomyces pombe* (Szankasi and Smith, 1992). Afterwards, Exo1 was identified to function in the MMR pathway (Szankasi and Smith, 1995), by possessing a 5' flap-endonuclease activity (Tran et al., 2002). As discussed earlier, Exo1 and MMR proteins are implicated in CO formation during meiosis (Khazanehdari and Borts, 2000), and Exo1 was found to interact with MMR proteins (Nielsen et al., 2004; Tran et al., 2007). Based on this, Exo1 was thought to be the nuclease required for producing 3' ssDNA which is an important step in homologous recombination. However, in the absence of *EXO1* during meiosis, homologous recombination still occurs but at lower efficiency, with delayed meiotic progression (Tsubouchi and Ogawa, 2000). Additionally, the hyper-resection process observed during the meiosis of *dmc1Δ* cells was reduced in the absence of *EXO1* but was not eliminated (Tsubouchi and Ogawa, 2000). Later experiments showed that the hyper-resection observed in the absence of *DMC1* during meiosis is caused by Exo1 and Sgs1 (Manfrini et al., 2010), but in *DMC1* meiosis Exo1 does the long-resection process (Zakharyevich et al., 2010). The MRX complex can still carry out resection by utilising the nuclease activity of Mre11, this is because in absence of *EXO1* and *SGS1*, resection length is dramatically reduced but not lost (Zakharyevich et al., 2010). Furthermore, Exo1 has been shown to facilitate type I COs by the interaction with Mlh1 protein of the MuLγ complex (Zakharyevich et al., 2010, 2012).

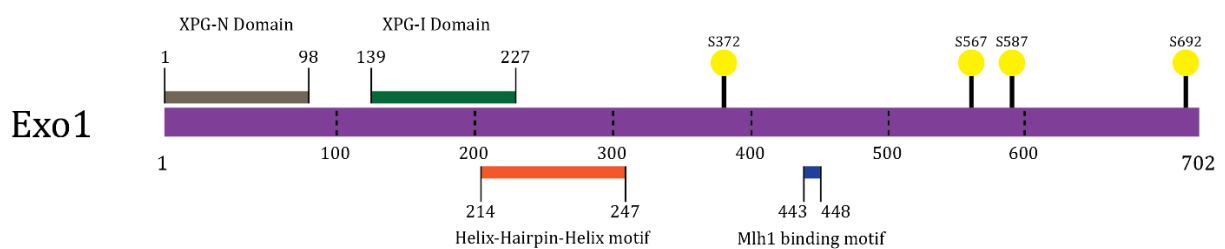


Figure 1.10 The known motifs, domains, and phosphorylation sites of *S. cerevisiae* Exonuclease 1 (Exo1)

S. cerevisiae EXO1 transcribes a 702 amino acid protein with two known nuclease domains XPG-N and XPG-I. XPG-N is on towards the N-terminal of Exo1, and the XPG-I is an internal domain in Exo1. At the centre of Exo1 a motif called Helix-Hairpin-Helix was characterised which is a DNA binding motif. The Mlh1 binding site shown in blue is in the middle of Exo1 sequence. The C-terminal has been proposed to bind to other mismatch repair proteins. The phosphorylation of Exo1 during mitotically dividing cells occurs at four serine residues that are mostly close to the C-terminal of Exo1 (yellow circles). This phosphorylation event was identified in response to DNA damaging agents and has been proposed to negatively regulate the nuclease activity of Exo1.

The activity of Exo1 is regulated by post-translational modifications (PTMs) in response to DNA damaging agents such as camptothecin (Morin et al., 2008; Bologna et al., 2015), bleomycin (Strong, 2017), and gamma-ray irradiation (Tomimatsu et al., 2014). The phosphorylation of Exo1 in response to DNA damage is proposed to negatively regulate its nuclease function (Morin et al., 2008). However, hEXO1 phosphorylation is proposed to promote the resection activity (Tomimatsu et al., 2014). hEXO1 is sumoylated possibly to control the resection level in the cell preventing pathological DNA resection (Bologna et al., 2015). The phosphorylation of Exo1 during *S. cerevisiae* meiosis was previously reported by Strong, 2017, where the phosphorylation of Exo1 was suggested to be in different residues than the phosphorylation observed in response to DNA damaging agents. The regulation of Exo1 during meiosis still remain unknown, and the function of the meiotic phosphorylation is an interesting area to explore.

1.9 **Projects aims**

The regulation of Spo11-DSB processing and DNA ends resection activity is not well understood. Thus far the initial Spo11-DSB processing activity is known to be mediated by Sae2 phosphorylation by Cdc28 (Huertas et al., 2008), and the long DNA resection activity is regulated by Tel1 kinase (Mimitou et al., 2017). The aim of this study was to explore the functionality and the dependency of the phosphorylation of Exo1 during *S. cerevisiae* meiosis. This was done by analysing the phosphorylation of Exo1 in different mutant backgrounds in the meiotic homologous recombination pathway and the checkpoint network. Finally, the meiotic specific phosphorylation residues of Exo1 were characterised by mass-spectrometry analysis. This was done after developing a novel technique to purify proteins from meiotic samples for the purpose of mass-spectrometry analysis. This study suggests a role of Tel1 mediated phosphorylation of Exo1 which potentially regulate the long-resection process during meiosis, and could explain the short DNA resection activity observed in the absence of Tel1.

Chapter 2. Materials and Methodology

2.1 Media and stock solutions:

2.1.1 Growth media:

All types of media and solutions were made with dH₂O and if necessary sterilized by autoclaving, 110 °C for 15 minutes. In some cases, solutions were filter-sterilised using 0.22µm filters (Sartorius Stedim Biotech). Percentage concentrations used in this thesis are v/v for liquids and w/v for solid chemicals.

YPAD:

Standard yeast growth media containing: 1% yeast extract (BD biosciences), 2% peptone (BD biosciences), 40mg/L adenine (Sigma), and 2% D-glucose (Fisher). 2% agar (BD biosciences) was added for solid media. Yeast strains with *HphMX*, *NatMX*, or *KanMX* genes were selected on YPAD plates containing 200µg/ml of Hygromycin B (Formedium), 50µg/ml of Nourseothricin (Werner BioAgents), and 100µg/ml of G418-disulphide (Melford Labs) respectively. The antibiotic compounds were added to autoclaved molten YPAD agar at 55 °C.

YPG:

Solid media used for selecting out cells with weak mitochondria “petite cells”. It is composed of 1% yeast extract (BD biosciences), 2% peptone (BD biosciences), 3% glycerol (Fisher scientific), and 2% agar (BD biosciences).

Minimal Media:

Minimal media plates were prepared as: 0.67% yeast nitrogen base free of amino acids (BD biosciences), 2% D-glucose (Fisher scientific), 2% agar (BD biosciences).

Amino Acid dropout:

Made similarly to minimal media plates but with the addition of 0.85g/L of amino acid dropout mixture. The complete-mix contains: 0.8g adenine, 0.8g arginine, 0.8g histidine, 0.8g uracil, 0.8g tryptophan, 1.2g lysine, 1.2g tyrosine, 2.4g leucine, 4.0g histidine, and 8.0g threonine. The dropout mix contains same amount as the complete but excluding one or two amino acid(s).

YPA:

A pre-sporulation media for meiotic synchronisation. The media is composed of 1% yeast extract (BD biosciences), 2% peptone (BD biosciences), and 1% potassium acetate (Sigma/Fluka)

Potassium Acetate for Sporulation:

Liquid media (Sporulation Media – SPM) is composed of 0.3% potassium acetate (Sigma), 0.02% Raffinose (Sigma), plus the appropriate amino acid supplements, see Amino acids stock in section 2.1.2.

Solid media is composed of 1% potassium acetate, 0.1% yeast extract (BD biosciences), 0.67% yeast nitrogen base free of amino acids (BD biosciences), and 2% agar (BD biosciences).

LB (Luria-Bertani Broth):

Standard medium used for the growth of *Escherichia coli*. The medium contains 1% Tryptone (BD biosciences), 0.5% yeast extract (BD biosciences), and 1% NaCl (Fisher scientific). For selection of *E. coli* with replicating plasmids expressing Ampicillin resistance gene, Ampicillin 50µg/ml (Sigma) was added.

2xYT (2x Yeast extract and Tryptone):

This medium was used as a solid media for the purpose of selecting transformed replicating plasmids expressing Ampicillin resistance gene. The media is made of: 1.6% Tryptone (BD biosciences), 1% yeast extract (BD biosciences), 0.5% NaCl (Fisher scientific), and 2% agar (BD biosciences). 50µg/ml of Ampicillin (Sigma) was added to autoclaved molten 2xYT agar.

2.1.2 Stock solutions:

Amino acid stocks:

Stock solutions of amino acids (Sigma) were made up as g/100ml in dH₂O and filter sterilised to concentrations specified in Table 2.1. The stock amino acid solutions were stored at room temperature, while the light sensitive histidine and tryptophan were stored away from light.

Blocking buffer:

5% w/v skimmed milk powder (Sigma), dissolved in PBS-T

Buffer-D:

1.85M NaOH (Fisher scientific) and 7.5% v/v 2-mercaptoethanol (Sigma)

Buffer-G:

6M guanidine hydrochloride (Sigma), 100mM sodium phosphate buffer pH8.0 (Fisher), 10mM tris-HCl pH8.0 (Sigma), 10mM Imidazole (Sigma), and 0.1% v/v Triton X-100 (Sigma). Triton is added for small-scale extraction only, and the buffer is filtered to remove the silica (anti-caking agent) in the guanidine hydrochloride.

Buffer-U:

8M urea PlusOne™ (Fisher scientific), 100mM sodium phosphate buffer pH6.8 (Fisher), 10mM tris-HCl pH6.8 (Sigma), 10mM Imidazole (Sigma) and 0.1% v/v Triton X-100 (Sigma). The buffer is filtered to remove any particulates.

Table 2.1 Amino acid stock solution and the final concentration of amino acids used in sporulation media for supplementation

<i>Amino acid</i>	<i>Stock concentration w/v</i>	<i>Final concentration per 1L of sporulation media (mg/L)</i>
Adenine	0.2	5
Arginine	1	5
Aspartic acid	1	25
Glutamic acid	1	25
Histidine	1	5
Isoleucine	1	7.5
Leucine	1	25
Lysine	1	7.5
Methionine	1	5
Phenylalanine	1	12.5
Serine	8	100
Threonine	4	50
Tryptophan	1	5
Tyrosine	0.2	7.5
Uracil	0.2	5
Valine	3	37.5

Native Wash Buffer:

10mM Tris pH8.0 (Sigma), 500mM NaCl (Fisher scientific), 20mM Na-Pyrophosphate (Sigma), 30mM NaF (Sigma), 0.1% v/v Triton X-100 (Sigma), one phosphatase inhibitor table per 100ml (Roche) and one protease inhibitor tablet per 100ml (Roche)

Native Elution Buffer:

Same as Native Wash buffer but with 5mM EDTA and 150mM imidazole.

10mM Tris pH8.0 (Sigma), 500mM NaCl (Fisher scientific), 5mM EDTA (Fisher scientific), 150mM Imidazole (Sigma), 20mM Na-Pyrophosphate (Sigma), 30mM NaF (Sigma), 0.1% v/v Triton X-100 (Sigma), one phosphatase inhibitor table per 100ml (Roche) and one protease inhibitor tablet per 100ml (Roche).

Native Lysis Buffer:

50mM Tris pH8.0 (Sigma), 150mM NaCl (Fisher scientific), 5mM EDTA (Fisher scientific), 0.5% v/v NP-40 (Sigma), 1mM phenylmethane sulfonyl fluoride – PMSF (Acros), 20mM Na-Pyrophosphate (Sigma), 30mM NaF (Sigma), one phosphatase inhibitor table per 50ml (Roche) and one protease inhibitor tablet per 50ml (Roche).

PBS-T (Phosphate-buffered saline with 0.1% tween):

Phosphate-buffer tablets were used (Sigma), one tablet per 200ml of dH₂O. The solution was mixed and 0.1% v/v of Tween (Sigma) was added.

2x Protein loading buffer (Laemmli buffer):

250mM tris-HCl pH 6.8 (Sigma), 4% w/v SDS (Fisher scientific), 20% Glycerol (Fisher scientific), 10% v/v 2-Mercaptoethanol, and 0.25% v/v super-concentrated bromophenol blue solution (Fisher scientific).

50x TAE buffer:

DNA gel electrophoresis running buffer containing 2M Tris-acetate (Sigma), 50mM EDTA pH 8.0 (Fisher scientific).

SDS-PAGE:

For 6% resolving gel, 6ml for one 1mm Novex gel (Invitrogen). The resolving gel mix is made of: 1.2ml 30% 37.5:1 acrylamide:bis solution (National Diagnostics), 3.12ml dH₂O, 1.56ml 1.5M Tris pH8.0 (Sigma), 0.06ml 10% w/v SDS (Fisher scientific), 0.06ml 10% w/v ammonium persulfate (Fisher scientific), and 0.005ml of TEMED (Sigma).

For 4% stacking gel, 2ml for one 1mm Novex gel (Invitrogen). The stacking gel mix is made of: 0.33ml 30% 37.5:1 acrylamide:bis solution (National Diagnostics), 1.4ml dH₂O, 0.25ml 1.0M Tris pH6.8 (Sigma), 0.02ml 10% w/v SDS (Fisher scientific), 0.02ml 10% w/v ammonium persulfate (Fisher scientific), and 0.002ml of TEMED (Sigma).

10x running buffer:

For SDS-PAGE running containing 3% w/v Tris-base (Sigma), 14.4% v/v glycine (Sigma), and 1% w/v SDS (Fisher scientific). The solution was diluted to 1x using dH₂O.

10x transfer buffer:

After SDS-PAGE running, proteins are transferred to nitrocellulose membrane (Amersham). The stock buffer for the transfer buffer contains 3% Tris-base (Sigma), and 14.4% glycine (Sigma). The solution is diluted to 1x using 200ml Methanol (Fisher scientific) and 700ml of dH₂O to make 1L.

2.2 Yeast Growth and Culturing Methods:

The SK1 yeast background was used in this study. In comparison to other yeast backgrounds, the SK1 diploid strains can be easily synchronised for sporulation after nitrogen starvation and in the presence of non-fermentable carbon source, such as potassium acetate (Kane and Roth, 1974). The rapid growth of SK1 and synchronisation into meiosis makes it an ideal model organism to study meiosis and yeast sporulation. S288C yeast background was only used to test for SK1 haploid strains mating-type.

2.2.1 Yeast mating, diploid construction and strain storage

To produce diploid cells, two freshly grown haploid strains of opposite mating type were mixed together on a YPAD agar plate and incubated at 30°C for 3 to 4 hours. Using a yeast tetrad micro-manipulator (MSM 400, Sanger Instruments) ten zygotes were picked and grown for two overnights at 30°C. The colonies were then checked using a light microscope and tested for mating type (see 2.2.3) to ensure that they are diploids. This method was used to make new strains with the desired genotype where multiple matings were done to produce the desirable haploid strain. To add a new strain to the strain collection, a colony was inoculated into 10ml of YPAD and left to grow at 30°C. On the next day the cells are harvested by centrifugation (2,000g, 1min), the cell pellet was resuspended in 1ml of 50% glycerol and stored in a cryogenic vial (Thermo) at -80°C. To recover yeast strains from the strain collection, 1µl of cells were picked using an inoculation loop and patched on YPAD agar plates and incubated at 30°C.

2.2.2 Yeast tetrad dissection

Diploid strains were patched to YPG and left to grow for 16-18 hours at 30°C. The patch was then inoculated to YPAD plate and incubated for an overnight at 30°C. The patch was then inoculated on a potassium acetate plate and left to sporulate at 30°C for one to two overnights. To break the ascus a digestion solution was prepared containing 9µl of 1.2M sorbitol, and 1µl 10mg/ml Zymolyase T20. Using a 20µl pipette tip, a minuscule amount of sporulated tetrads were picked from the patch and re-suspended in the digestion solution and incubated at 30°C for 15 minutes. 5µl of the solution was then transferred into a YPAD plate where tetrads are then dissected to single spores using a micro-manipulator (MSM 400, Sanger Instruments). The spores were incubated at 30°C for two overnights or when haploid colonies grow to 2mm in diameter.

2.2.3 Genotyping and mating type testing

To determine the mating type of a haploid strain, the unknown mating type haploid was mated with both mating type testers. Two haploid S288C strains of different mating type (a/α), deficient in *his1*, BM216 (*MATa*) and BM217 (*MAT α*) were used. To test for the mating type, the haploid colony is replicated into two MM plates each containing either BM216 or BM217. The MM plates are then incubated in 30°C for one to two overnights. If growth is observed in one of the mating type tester MM plate, then the haploid is the opposite mating type of the mating type tester. If no growth was observed, then the strain in question could be a diploid.

2.2.4 Yeast meiosis time coursing

Strains were patched on YPG and incubate at 30°C for 16-18 hours. The strains were then streaked to single colonies on a YPAD plate and left to grow for 40-48 hours at 30°C. A single colony was picked and grown in 20ml of YPAD at 30°C with shaking. The next day, the cells were inoculated into YPA at 0.3 OD₆₀₀ and left to grow for sixteen hours. Cells were then harvested by centrifugation (2,000g, 2 minutes) and washed with 200ml of 1% potassium acetate solution. The cells were then inoculated to SPM at 1.9 OD₆₀₀ with the addition of the appropriate amino acid solution. The cell culture was then incubated with shaking at 30°C for 24hrs where 15mls cells were taken from 0 to 8hrs at two-hours intervals. Cells were harvested at each time point by centrifugation (13,000g, 1 minute) and washed with 1ml ice-cold dH₂O. The pellets were then stored at -80°C for protein extraction on the next day.

2.2.5 DAPI staining of meiotic cells

DAPI is a fluorescent stain that binds to adenine-thymine rich regions in the DNA. When DAPI is bound to the DNA, it emits blue light when excited with ultraviolet light. To stain meiotic cells, 750µl of meiotic culture was added to 500µl of ethanol (Fisher) and mixed. After that 1µl of 1mg/ml of DAPI was added and vortexed well. Following this the cells were harvested by centrifugation (16,000g, 2 minutes) and the supernatant was discarded. The cells were then resuspended with 200µl of 50% glycerol (Fisher), and 5µl was spread on a microscopy slide. Finally, the cell nuclei were visualised and counted using a fluorescent microscope (DMLB Leica). 100 cells were scored for each time-point and the meiotic progression of the cells was assessed by the number of nuclei each cell possess at each time-point.

2.3 Methods in molecular biology and biochemistry

2.3.1 DNA restriction digest

To analyse recombinant plasmids. A small-scale digest was prepared by incubating 0.5µg of recombinant DNA for 30 minutes at 37°C, with 0.5µl of restriction enzyme(s) (Thermo), and 1x FastDigest™ buffer (Thermo) in a total volume of 10µl.

To construct recombinants by plasmid vector digest, 0.9µg-1.5µg of plasmid DNA was incubated for 30 minutes at 37°C, with 1µl of restriction enzyme(s) (Thermo), and 1x FastDigest™ buffer (Thermo) in a total volume of 30µl.

2.3.2 Phosphatase treatment of digested plasmid

To prevent self-ligation of digested vectors during the subsequent ligation step, the 5'-terminal phosphate residue is removed. This was done by adding 1U of shrimp alkaline-phosphatase (NEB) to digested vectors and incubated for 20 minutes at 37°C.

2.3.3 DNA agarose gel electrophoresis

This method is used to test for the length of a DNA fragment, whether it is a PCR product or restriction enzyme digestion product. Agarose (Biogene) was dissolved in 1x TAE buffer to make 0.8% agarose gel. After cooling down the mixture, 0.5 µg/ml of ethidium bromide (Sigma) was added and mixed well. After pouring the mixture on a cast with the combs in place and allowing to cool, the gel was then fully submerged in an electrophoresis tank (BioRad) containing 1xTAE buffer. DNA samples with 6x loading dye (NEB) and the appropriate DNA ladder (GeneRuler™ 1kb, NEB) were then loaded into the gel and ran at 130V for 30 minutes. The gel was then subjected to UV light to visualize DNA bands and analyse the fragment(s) size.

2.3.4 DNA purification kit from agarose gel (QIAquick Spin, Qaigen)

To isolate DNA fragments after restriction digest, the digest products were separated by running the digestion mixture on a 0.8% agarose gel. The DNA to be isolated was determined by comparing the DNA fragment bands with the standard size DNA ladder (GeneRuler™ 1kb, NEB). The desired fragment was visualised on a UV visualiser, and excised out of the gel using a clean square cover-slip (Academy). The gel slice was then weighed and three volumes of Buffer QG was added and incubated at 50°C for 10 minutes with shaking. After the gel slice was dissolved completely, 1 gel volume of isopropanol (Fisher) was added and mixed. The sample was then added to a QIAquick spin column placed in a 2ml collection tube. The column was centrifuged (16,000g, 1 minute) and the flow-through was discarded. The column was washed with 500µl of Buffer QG, centrifuged (16,000g, 1 minute) and the flow-through was discarded. The column was washed again by adding 750µl of Buffer PE, followed by centrifugation (16,000g, 1 minute) and discarding the flow-through. An additional centrifugation step was done to eliminate residual ethanol. Finally, the DNA was eluted by 10µl of MilliQ water to the column's filter and centrifuging (16,000g, 1 minute).

2.3.5 Ligation

Ligation was carried out by co-purifying the insert and vector from agarose gel in the same column (See 2.3.4). After eluting the DNA with 10µl MilliQ water, 5µl of Ligation Solution I (Takara, Clontech) was added and incubated at 16°C for 30 minutes. The ligated product was then transformed to *E. coli* competent cells.

2.3.6 Polymerase chain reaction (PCR)

For DNA fragment amplification PCR BIO HiFi polymerase (PCRBiosystems) was used. The following mixture was used for a 50µl reaction: 1µl of template DNA, 10µl of 5x PCR BIO reaction buffer (containing 5mM dNTPs), 2µl of each 10µM forward and reverse primers, 0.5µl of HiFi polymerase, and 34.5µl of MilliQ dH₂O. The PCR thermocycler (PCR ProFlex) is programmed to start the initial denaturation at 98°C for 2 minutes. This is followed by 25-35 cycles of: denaturation at 98°C for 30 seconds, annealing at 55°C for 30 seconds, and extension at 72°C for 30 seconds per 1kb of template DNA. After the cycles are done, the last step in the program is the final extension at 72°C for 10 minutes. Finally, PCR products are then stored at 4°C for further processing.

2.3.7 Amplified DNA clean-up kit

PCR purification was done using GeneJET PCR purification kit (ThermoFisher), all centrifugation steps were done at 16,000g. After the PCR is done, 1:1 volume of binding buffer is added to the PCR product, making sure the solution colour is yellow. The solution was then transferred to a spin column on a collection tube and centrifuged for 1 minute, the flow-through was then discarded. 700µl of wash buffer was added to the column and centrifuged for 1min, the flow-through was discarded. Another centrifugation step was done to completely remove any remaining wash buffer. The column was then transferred to a microfuge tube and 50µl of dH₂O was added to the column's filter and centrifuged for 1 minute to collect the purified PCR product.

2.3.8 Small scale plasmid isolation from *E. coli* (Mini-Prep) GeneJET Thermo

Plasmid extraction from *E. coli* was made by using GeneJET mini-prep kit (Thermo). Overnight *E. coli* cultures were made by inoculation into 5ml of LB/Ampicillin media at 37°C. The bacterial culture was then harvested by centrifugation (6,000g, 2 minutes). After that, the cell pellet was then resuspended using 250µl of resuspension solution and vortexed for 10 seconds. Subsequently, 250µl of lysis solution was added and the tube was inverted 6 times to mix. After mixing, 350µl of neutralisation solution was added, mixed by inverting the tube 6 times and centrifuged (12,000g, 5 minutes). The supernatant was then moved to a GeneJET spin column and centrifuged (12,000g, 1 minute). Afterwards the column was washed by adding 500µl of wash solution and centrifuged (12,000g, 1 minute), the wash step was repeated. In order to ensure that no ethanol is left in the column after washing, the column was centrifuged empty (12,000g, 1 minutes) and then left to dry in a 65°C oven for 5 minutes. Finally, the purified plasmid was eluted by adding 50µl of MilliQ dH₂O and collected in a new tube by centrifugation (12,000g, 1 minute).

2.3.9 Transformation of *E. coli* competent cells

Rubidium chloride competent cells (BL21) were made by Dr. Bin Hu and 100µl aliquots were stored at -80°C. For plasmids amplification including cloned plasmids. The ligation mix or 1ng of plasmid DNA was added to 100µl of competent cells, mixed by pipetting, and incubated on ice for 40 minutes. Subsequently the cells were heat-shocked at 42°C for 90 seconds and then allowed to rest on ice for 5 minutes. In order to recover the cells, 1ml of LB was added and the cells were incubated at 37°C for 1 hour with mixing. After that the cells were harvested by centrifugation (10,000g, 1 minute), washed with 1ml dH₂O and centrifuged again. The cells were then resuspended with 100µl of dH₂O and 90µl were spread on LB plates with Ampicillin. The rest of the cells were diluted with 90µl of dH₂O followed by spreading on LB plates with Ampicillin. Finally, the plates were incubated for an overnight at 37°C.

2.3.10 High efficiency yeast transformation

A single colony was grown in 10ml of YPAD at 30°C with shaking for an overnight. The cell culture was then harvested by centrifugation (1,000g; 3 minutes), the supernatant was discarded and the pellet was washed with 1ml of 100mM lithium acetate and centrifuged again. The wash step was repeated and the culture was transferred into a microfuge tube and centrifuged (1,000g; 1 minute). The cell pellet was re-suspended in 100mM lithium acetate with 2 volumes of the cell pellet. 50µl aliquots were transferred to microfuge tubes and incubated at 30°C for 30 minutes. Meanwhile, sonicated salmon sperm DNA was boiled at 95°C for 5 minutes then left to cool on ice for 5 minutes. After that 240µl of 50% Polyethylene Glycol was added, then 36µl of 1.0M lithium acetate followed by 25µl of sonicated salmon sperm single strand DNA. 50µl of purified PCR product was added to the transformation sample while 50µl of dH₂O was added to the control. The mixture was gently mixed by pipetting and then incubated at 30°C for 30 minutes. The cells were then heat shocked at 42°C for 20 minutes, and then harvested by centrifugation (1,000g; 3 minutes). The supernatant was discarded and the cells were gently resuspended in 1ml of YPAD and incubated at 30°C for 90 minutes with gentle shaking. The cells were then harvested by centrifugation (1,000g; 1 minute) and washed with 1ml of dH₂O. Finally, the cells were spread on the appropriate selection plate e.g. G418 and incubated at 30°C for two overnights.

2.3.11 Yeast genomic DNA extraction

DNA extraction was performed to sequence or PCR transformed genes, making sure that the gene was correctly incorporated into the genome. For yeast DNA extraction, MasterPure™ purification kit (Epicentre) was used. DNA purification was done from a single yeast colony grown on solid YPAD. The colony was scraped and transferred to 300µl of yeast lysis buffer. The cells were vortexed well and incubated at 65°C for 15 minutes. The lysed cells were then placed on ice for 5 minutes then 150µl of protein precipitation solution was added and the sample was vortexed for 10 seconds. Cell debris were then pelleted by centrifugation (16,000g, 10 minutes) and the supernatant was transferred to another microfuge tube. Consequently, 500µl of isopropanol was added to precipitate the genomic DNA and the tube was mixed by inversion. The precipitated DNA was pelleted by centrifugation (16,000g, 10 minutes), the supernatant was discarded and the pellet was washed with 70% ethanol. The sample was briefly centrifuged (16,000g, 15 seconds) and the ethanol was aspirated out to remove all of the remaining ethanol. Finally, the DNA pellet was dissolved in 35µl of dH₂O at 37°C.

2.3.12 DNA sequencing sample preparation

DNA sequencing was carried out using Mix2Seq service by Eurofins Genomics. Templates consisted of 15µl of purified DNA, for plasmid DNA the concentration was 100ng/µl. For purified PCR products, the concentration was 5ng/µl for 300-1,000bp template, and 10ng/µl for >1,000bp. In order to sequence the region of interest, sequencing primers were designed upstream of this region, 2µl of sequencing primer 10µM was added to the template and mixed. The Mix2Seq tubes were then sent for sequencing.

2.3.13 Yeast protein extraction:

a. Trichloroacetic acid (TCA) for whole cell extract

For TCA extraction, frozen pellets were re-suspended in 1ml of ice-cold dH₂O followed by the addition of 150µl Buffer-D and incubated on ice for 15 minutes. 150µl of 55% TCA solution was added, mixed by vortex, and incubated on ice for further 10 minutes. The samples were then centrifuged (16,000g, 10 minutes) and the supernatant was discarded. The pellet was then re-suspended in 200µl of 2x protein loading buffer and incubated at 95°C for 5 minutes. To neutralise the samples, 50µl of 1.0M Tris pH8.8 was added and mixed. To run the samples in SDS-PAGE, they were centrifuged (16,000g, 10 minutes) and 10µl of the supernatant was used for analysis on SDS-PAGE.

b. Guanidine Hydrochloride protein extraction and His-tag purification

Frozen meiotic cell pellets were re-suspended in 300µl of Buffer-G. An equal amount of acid-washed beads (BioSpec) were added. The cells were then lysed using a bead beater (mini-Beadbeater 16, BioSpec) for 6 minutes. In order to separate the lysate from the glass beads, a hole was punctured at the bottom of the tube, the tube was then placed on a 5ml Eppendorf tube, and centrifuged (2,000g, 1 minute). The lysates were then transferred to a new microfuge tube and centrifuged (16,000g, 30 minutes) to remove cell debris. The supernatant was then transferred to a new tube and topped up with Buffer-G to 1ml. To purify His-tagged proteins, 30µl of equilibrated Nickel-NTA agarose beads (Qiagen) were added to each cell extract and incubated at room temperature with rolling for 2 hours. The beads were then washed three times with 1ml of Buffer-U, each time for 5 minutes at room temperature with rolling. The washed beads were then collected by centrifugation (300g, 2 minutes), and the proteins were eluted by adding 50µl of protein loading buffer and incubating at 95 °C for 5 minutes.

c. Native extraction and Immuno-precipitation of proteins

Frozen cell pellets were re-suspended in ice cold Native Lysis Buffer. Equal volume of acid-washed beads (BioSpec) were added. To lyse the cells a bead beater (mini-Beadbeater 16, BioSpec) was used for 1 minute for three times with 5 minutes on ice between each beat. In order to separate the lysate from the glass beads, a hole was punctured at the bottom of the tube, the tube was then placed on a 5ml Eppendorf tube, and centrifuged at 4°C (2,000g, 1 minute). The lysate was then harvested by centrifugation at 4°C (16,000g, 30 minutes). After that, the supernatant was added to a new LoBind 1.5ml Eppendorf tube (Eppendorf), and the protein concentration was measured using BioRad Bradford Assay (BioRad), see 2.3.14. To purify FLAG-tagged proteins, 30µl of washed Anti-FLAG M2 magnetic beads (Sigma) were added to 2mg of lysate and incubated for an over-night at 4°C with rolling. On the next day, the beads were washed three times with 1ml of ice-cold Native Lysis Buffer, followed by another three times of 1ml of the same buffer and each for 5 minutes at 4°C with rolling. The proteins were then eluted with 50µl of protein loading buffer, were 5µl was used for analysis on SDS-PAGE.

2.3.14 Protein concentration assay (Bradford assay)

Protein concentration was determined using Bradford reagent from BioRad Protein Assay Kit. The Bradford reagent was diluted 1:5 with dH₂O mixed and 1ml aliquots were made. In order to determine the protein concentration in a sample, the OD₅₉₅ of each reading must be compared to a protein standard calibration curve. The protein standard is made by diluting bovine-serum albumin – BSA (NEB) to 1mg/ml with the appropriate lysis buffer. After mixing the BSA solution, the BSA is diluted again with 1ml of 1x Bradford reagent to 2mg/µl, 4mg/µl, 6mg/µl, 8mg/µl, 10mg/µl, and 15mg/µl. Each of the solutions' OD₅₉₅ was measured and plotted on a graph. After that 1µl of sample was added to 1ml of Bradford reagent and OD₅₉₅ was

measured. The protein concentration was determined by comparing the OD595 reading to the BSA standard graph.

2.3.15 Large-scale meiotic cells protein extraction by two-step purification

Meiotic cell cultures were made as described in 2.2.4, six flasks were used of the same strain each was 500ml of meiotic culture. At the desirable time-point all of the 3L of cells were collected by centrifugation at 4°C (9,000g, 20 minutes). The cell pellet was weighed and for each 100mg of cells, 1ml of Buffer-G (without triton) was added. The cells were then lysed using a cell disruptor (Constant Systems ltd) at 30psi, up to three rounds were done. Afterwards, 0.1% of Triton X-100 (Sigma) was added and the lysate was vortexed for 10 seconds. The cell debris were then pelleted by centrifugation (16,000g, 20 minutes) and the supernatant was filtered using a 0.2µm PES filter (Rapid-flow, Nalgene-Thermo). For each 10ml of lysates, 0.1ml of Nickel-NTA agarose resin (Qiagen) were used. The Ni-NTA resin were added and incubated at room temperature for an overnight with rolling. On the next day the Ni-NTA resin were collected by centrifugation (300g, 2 minutes) and washed with 5ml of Buffer-U. The wash step was done three times each for 5 minutes at room temperature with rolling. The Ni-NTA resin were collected (300g, 2 minutes) the supernatant was discarded and 5ml of native wash buffer was added. The tubes were incubated at room temperature for 5 minutes with rolling. Meanwhile, Poly-Prep columns (BioRad) were equilibrated with 1ml of native wash buffer. After the wash is done the nickel beads were transferred to the Poly-prep columns, one column for every 0.2-0.5ml of nickel beads. To further wash out any remaining urea or guanidine hydrochloride, 10ml of native wash buffer was added to each column and left to flow. Subsequently, the nickel beads were eluted with a total volume of 1ml of native elution buffer. The elution was carried out by mixing the nickel beads and incubating at room temperature for 30-45 minutes. After the eluent was collected the elution step was repeated. For each eluent, 40µl of washed M2 Anti-FLAG beads (Sigma) were added and incubated at

4°C for an overnight with rolling. On the next day the anti-FLAG beads were washed three times with 1ml of native wash buffer. This was followed by three 1ml washes, each wash was done for 5 minutes at 4°C with rolling. Finally, the anti-FLAG beads were either sent for mass-spectrometry or eluted with 50µl of protein loading buffer and loaded into SDS-PAGE.

2.3.16 Lambda Phosphatase Assay

Meiotic cell samples were taken after four hours of meiosis induction. Three samples were taken at 30 OD600 worth of cells, these samples were from the same cell culture. Protein extraction was done as described in 2.3.13b. Subsequently, the Ni-NTA beads were washed with Native Wash buffer, where one sample was washed with the same buffer without the addition of any phosphatase inhibitors. After the Native Wash was done, three reactions were prepared. All reactions contained X1 PMP buffer (NEB), and 1mM of MnCl₂ (NEB) with a total reaction volume of 50µl. The first reaction contained phosphatase inhibitors without the addition of Lambda phosphatase (NEB). The second reaction contained 200U of Lambda phosphatase (NEB) without phosphatase inhibitors. Finally, the third reaction contained 200U of Lambda phosphatase (NEB) with phosphatase inhibitors. All of the reactions were incubated at 30C° for 1 hour. After the reaction time was done X1 of PLB was added and boiled at 95C° for 5 minutes. Finally the samples were run on SDS-PAGE as described and 2.3.17 and then run on a Western Blot as described in 2.3.18.

2.3.17 Sodium dodecyl sulphate polyacrylamide gel electrophoresis (SDS-PAGE)

SDS-PAGE is used to separate proteins on the basis of size. SDS is an anionic detergent, it coats around the polypeptide backbone giving the same charge:mass ratio to all of the different sized polypeptides. These polypeptides run through the acrylamide matrix by applying an electrical field across the gel. The acrylamide matrix retards proteins, as longer heavier polypeptide fragments take more time to travel through the matrix than shorter lighter fragments.

The empty 1mm thick gel cassette was mounted straight up. The 6ml of resolving mix (see 2.1.2) was poured first after commencing the polymerisation process. This was done by adding 60µl of 10% ammonium persulfate which act as a linker, followed by adding 6µl of TEMED which is the catalyst. After pouring the resolving gel, 1ml of isopropanol (Fisher scientific) was layered to remove any bubbles on the surface of the gel. Afterwards, the gel solidified and the isopropanol was washed away using dH₂O. The stacking gel is then poured on top, this was done after the addition of 20µl of 10% ammonium persulfate, and 2µl of TEMED to the stacking mix (see 2.1.2). A 12-well comb was then inserted into the cassette and the stacking gel was allowed to set. Once stacking gel was fully solidified, the comb was removed, and the gel was mounted into the electrophoresis tank (Novex Mini-Gel Tank, Thermo). The tank chamber was filled with 400ml of 1x SDS running buffer, and protein samples were loaded. The samples were prepared by adding an equal volume of 2X protein loading buffer, and boiled at 95°C for 5 minutes. The samples were centrifuged (16,000g, 1 minute) prior to loading. After loading and securing the gel inside the tank, an electric field was subjected using a powerpack (Bio-Rad) at 30mA per gel. The gel running was stopped once the visible bromophenol blue front had reached the end of the gel. After that the stacking gel was discarded and the resolving gel was left for Coomassie blue staining (Instant Blue™, Expedeon), or further analysis using Western blot method.

2.3.18 Western blotting and immunoprobng

The Western blot was carried out by making a Western blot sandwich as instructed by the manufacturer (Bio-Rad). The sandwich cassette consisted of a sponge, three layers of 3MM Whatman paper, an SDS-PAGE gel, a nitrocellulose membrane (Amersham), another three layers of 3MM Whatman paper, and another sponge. As the direction of protein transfer is from the cathode to the anode, the gel is placed on the side of the cathode, whereas the membrane is placed towards the side of the anode. This assembly is done in ice-cold 1x transfer buffer, and started by applying an electrical field through the sandwich for 1 hour at 0.4A.

After the proteins were transferred to the nitrocellulose membrane, the membrane was moved to a tray containing 25ml of blocking buffer and incubated with shaking for 30 minutes. Afterwards, the blocking buffer was removed and the membrane was transferred to a falcon tube containing 5ml of blocking buffer with the appropriate primary antibody diluted to 1:3,000. The membrane was then incubated for 1 hour at room temperature or for an overnight at 4°C with mixing. The membrane was then washed with 25ml of PBS-T for three times each for 5 minutes at room temperature with mixing. The membrane was then incubated with the secondary antibody (1:3,000) for 30 minutes at room temperature with mixing. Afterwards, the membrane was washed again as described above. To visualise probed proteins, an equal volume of Luminol reagent and Peroxide solution was mixed (Immobilon Western Chemiluminescent HRP substrate solutions, MilliPore). The membrane was placed on a glass plate and 1ml of the Luminol and Peroxide mix was added on top. Finally, a picture of the membrane was taken using the gel documentation system (G:Box XX9, Syngene).

2.4 Samples preparation for mass-spectrometry analysis

Samples preparation were carried out in the biOMICS Biological Mass-Spectrometry facility sample preparation laboratory. The water used in the subsequent methods was Mass-Spectrometry grade dH₂O. Eppendorf tubes used were all Lo-Bind tubes for more efficient treatment.

2.4.1 SDS-PAGE gel wash and dehydration:

The protein bands of interest were excised out of a stained SDS-PAGE gel and carefully minced to small cubes. To wash away any SDS or staining, the gel pieces were transferred to a new tube, then 1ml of 50mM ammonium bicarbonate/ 50% acetonitrile (AB/ACN) was added and incubated with shaking at room temperature for an overnight. After making sure no staining was left in the gel, the supernatant was discarded and 400µl of 100mM ammonium carbonate was added. The gel pieces were then incubated at room temperature with shaking for 10 minutes, and the step was repeated. After the gel pieces were completely swollen, the supernatant was discarded and 400µl of AB/ACN was added and incubated at room temperature with shaking for 10 minutes, this step was repeated. Finally, the gel pieces were dehydrated with 500µl of 100% acetonitrile. This step will completely dehydrate the gel releasing any remaining salts or staining.

2.4.2 Beads washing

Magnetic beads were washed with 1ml PBS twice, one of which was for 5 minutes with rolling at 4°C. After discarding the PBS, the beads were then resuspended in 100µl of 6M guanidine hydrochloride.

2.4.3 Reduction and Alkylation:

To reduce cysteine-cysteine disulphide bonds, 300µl of TCEP was added to the gel pieces and incubated at 70°C for 20 minutes. After cooling down the gel pieces at room temperature, 200µl of 50mM iodoacetamide was added and the tubes were covered with aluminium foil since iodoacetamide is light sensitive. The tube was then incubated at room temperature with shaking for 30 minutes. Afterwards, the gel pieces were washed and dehydrated as mentioned above. For on-beads reduction and alkylation, 2µl of TCEP was added to anti-FLAG beads and incubated for 10 minutes at 70°C. After cooling down the beads to room temperature, 20µl of 50mM iodoacetamide was added and incubated at room temperature with shaking for 30 minutes. The solution was then diluted with 800µl of 100mM ammonium bicarbonate.

2.4.4 Trypsin digestion

To digest polypeptides “in-gel”, the gel pieces were resuspended in 200µl of 100mM ammonium bicarbonate solution and 2µg of Trypsin (NEB) was added. The tubes were left on ice until the gel pieces were fully hydrated, after that the tubes were incubated for an overnight at 37°C. To release the digested peptides from the gel, 100µl of acetonitrile was added and incubated at 37°C for 15 minutes, then the supernatant was transferred to a new tube. Subsequently, 150µl of 0.5% formic acid was added to gel pieces and incubated at room temperature for 15 minutes with shaking. Following this, 300µl of acetonitrile was added and incubated at room temperature for 15 minutes with shaking. The supernatant was then collected and the previous two steps were repeated to release most of the peptides. Finally, the gel pieces were completely dehydrated by adding 100µl of acetonitrile and incubated at room temperature for 15 minutes with shaking. The supernatant was then pooled with previous collections. Finally, the peptides were dried using a vacuum centrifuge at 45°C for 2 hours. The digested and dried peptides samples were then given to the mass spectrometry facility for analysis.

To digest proteins from “on-beads” sample, 20µl of 0.1µg/µl (2µg) of Trypsin (NEB) was added, then the beads were then incubated at 37°C for four hours. The supernatant was then transferred to a new tube and 20µl of 10% formic acid was added. The pH of the solution must be ~3pH and was tested using a pH indicator strip.

2.4.5 C18 desalting mini-columns

This method is used for “on-beads” digested proteins, and is used to remove any remainder salt that can hinder the mass spectrometry analysis. All of the subsequent centrifugation steps were carried out at 1,500g for 1 minute. The C18 columns (Peirce™, Thermo) were first conditioned with 200µl of 50% acetonitrile and centrifuged, the flow-through was discarded, and the step was repeated. The column was then equilibrated with 200µl of 0.5% formic acid and centrifuged, the flow-through was discarded, and the step was repeated. Afterwards, 150µl of digested peptide were added and centrifuged. The flow-through was recovered and loaded again into the column and centrifuged again. The second flow through was discarded and the step was repeated until all of the protein sample went through the column. To wash the peptides, 200µl of 0.5% formic acid was added, the flow-through was discarded, and the wash step was repeated. To elute the digested peptides from the C18 column, the column was placed on a new tube and 20µl of 70% acetonitrile was added and centrifuged. The flow-through was collected and the step was repeated to elute more peptides. Finally, the eluted peptides were then dried using a vacuum centrifuge at 45°C for 2 hours.

2.5 Yeast strains and plasmids

2.5.1 Haploid *S. cerevisiae* strains

Table 2.2 List of haploid yeast strains used in this study

Name	Genotype	Source
BM216	<i>MATa</i> his1 (S288C background)	B. Hu
BM210	<i>MATα</i> his1(S288C background)	B. Hu

2.5.2 Diploid *S. cerevisiae* strains

Table 2.3 List of diploid yeast strains used in this study

All of the deleted genes were introduced into a strain by mating to a strain that lacks the gene of interest.

Name	Genotype	Source
dAG1713	<i>MATa/a ho::LYS2, lys2 ura3::hisG trp1::hisG</i> <i>Exo1-x6PK::KanMX / Exo1-x6PK::KanMX</i>	E. Strong
BM3	<i>MATa/a ho::LYS2, lys2, ura3::hisG, leu2::hisG, his3::hisG, trp1::hisG</i>	K. Nasmyth Lab
BM9	<i>MATa/a ho::LYS2, lys2, ura3::hisG, leu2::hisG, his3::hisG, trp1::hisG</i> <i>Exo1-5xHis-6xFLAG::KanMX / Exo1-6xHis-6xFLAG::KanMX</i>	This study By A. Mukherjee
BM10	<i>MATa/a ho::LYS2, lys2, ura3::hisG, leu2::hisG, his3::hisG, trp1::hisG</i> <i>Exo1-5xHis-6xFLAG::KanMX / Exo1-6xHis-6xFLAG::KanMX</i> <i>rad51Δ::caURA3 / rad51Δ::caURA3</i> <i>dmc1Δ::KanMX / dmc1Δ::KanMX</i>	This study By A. Mukherjee
BM142	<i>MATa/a ho::LYS2, lys2, ura3::hisG, leu2::hisG, his3::hisG, trp1::hisG</i> <i>Exo1-5xHis-6xFLAG::KanMX / Exo1-6xHis-6xFLAG::KanMX</i> <i>sae2Δ::HphMX / sae2Δ::HphMX</i>	This study
BM145	<i>MATa/a ho::LYS2, lys2, ura3::hisG, leu2::hisG, his3::hisG, trp1::hisG</i> <i>Exo1-5xHis-6xFLAG::KanMX / Exo1-6xHis-6xFLAG::KanMX</i> <i>tell1Δ::caURA3 / tell1Δ::caURA3</i>	This study
BM148	<i>MATa/a ho::LYS2, lys2, ura3::hisG, leu2::hisG, his3::hisG, trp1::hisG</i> <i>Exo1-5xHis-6xFLAG::KanMX / Exo1-6xHis-6xFLAG::KanMX</i> <i>mec1Δ::NatMX / mec1Δ::NatMX</i> <i>sml1Δ::HphMX / sml1Δ::HphMX</i>	This study
BM169	<i>MATa/a ho::LYS2, lys2, ura3::hisG, leu2::hisG, his3::hisG, trp1::hisG</i> <i>Exo1-5xHis-6xFLAG::KanMX / Exo1-6xHis-6xFLAG::KanMX</i> <i>mec1Δ::NatMX / pCLB2-Mec1-3HA::KanMX</i> <i>sml1Δ::HphMX / sml1Δ::HphMX</i> <i>tell1Δ::caURA3 / tell1Δ::caURA3</i>	This study
BM172	<i>MATa/a ho::LYS2, lys2, ura3::hisG, leu2::hisG, his3::hisG, trp1::hisG</i>	This study

	<i>Exo1-5xHis-6xFLAG::KanMX / Exo1-6xHis-6xFLAG::KanMX</i> <i>spo11-Y135F::KanMX / spo11-Y135F::KanMX</i>	
BM179	<i>MATa/a ho::LYS2, lys2, ura3::hisG, leu2::hisG, his3::hisG,</i> <i>trp1::hisG</i> <i>Exo1-5xHis-6xFLAG::KanMX / Exo1-6xHis-6xFLAG::KanMX</i> <i>mre11-H125N / mre11-H125N</i>	This study
BM182	<i>MATa/a ho::LYS2, lys2, ura3::hisG, leu2::hisG, his3::hisG,</i> <i>trp1::hisG</i> <i>Exo1-5xHis-6xFLAG::KanMX / Exo1-6xHis-6xFLAG::KanMX</i> <i>mre11-58S / mre11-58S</i>	This study
BM192	<i>MATa/a ho::LYS2, lys2, ura3::hisG, leu2::hisG, his3::hisG,</i> <i>trp1::hisG</i> <i>Exo1-5xHis-6xFLAG::KanMX / Exo1-6xHis-6xFLAG::KanMX</i> <i>sae2Δ::HphMX / sae2Δ::HphMX</i> <i>tell1Δ::caURA3 / tell1Δ::caURA3</i>	This study
BM199	<i>MATa/a ho::LYS2 lys2 ura3 leu2 arg4-nsp,bgl ade2D trp1::hisG</i> <i>Exo1-5xHis-6xFLAG::KanMX / Exo1-6xHis-6xFLAG::KanMX</i> <i>ndt80Δ::ADE2 / ndt80Δ::ADE2</i>	This study
BM212	<i>MATa/a ho::LYS2 lys2 ura3 leu2 arg4-nsp,bgl ade2D trp1::hisG</i> <i>Exo1-4S/A-6xHis-6xFLAG::NatMx</i>	This study
BM215	<i>MATa/a ho::LYS2, lys2, ura3::hisG, leu2::hisG, his3::hisG,</i> <i>trp1::hisG</i> <i>Exo1-5xHis-6xFLAG::KanMX / Exo1-6xHis-6xFLAG::KanMX</i> <i>mec1Δ::NatMX / mec1Δ::NatMX</i> <i>sml1Δ::HphMX / sml1Δ::HphMX</i> <i>sae2Δ::HphMX / sae2Δ::HphMX</i>	This study
BM221	<i>MATa/a ho::LYS2, lys2, ura3::hisG, leu2::hisG, his3::hisG,</i> <i>trp1::hisG ade2D</i> <i>Exo1-5xHis-6xFLAG::KanMX / Exo1-6xHis-6xFLAG::KanMX</i> <i>ADE2::pLW21mek1as / ADE2::pLW21mek1as</i> <i>Δmek1::LEU2 / Δmek1::LEU2</i>	This study

2.5.3 Plasmids

Table 2.4 List of plasmids used in this study

Name	Genotype, <i>E. coli</i> marker = Amp	Source
pBH173	<i>NatMX</i>	B. Hu
pBH259	<i>Exo1-6xPK::KanMX</i>	B. Hu
pBH261	<i>Cas9-KanMX::Leu2</i>	B. Hu
pBH368	<i>5xHis-6xFLAG::KanMX</i>	K. Shirahige
pBH951	<i>5xHis-6xFLAG::NatMX</i>	This study

2.5.4 Primers

Table 2.5 List of primers used in this study

All primers used were from Integrated DNA Technologies (IDT)

Name	Sequence	Product size
Exo1ChromFLAG_F	CGG CAG TCA GAT CTA TCT CCT TGC TTT CCC AAT TTG TTT ATA AAG GTA AAC TGA AGC TTC GTA CGG GAT C (75bp)	1,844bp for pBH368
Exo1ChromFLAG_R	CGA GAT TTT CAT TTG AAA AAT ATA CCT CCG ATA TGA AAC GTG CAG TAC TTA ACT TGG CCA CTA GTG GAT CTG AT (74bp)	
Exo1-FLAG-F	AAG CCT TAT TGG TGC CAG GTC A (22bp)	1,800bp for <i>EXO1-x5His-x6FLAG</i> in gDNA extracts
Tef1TerR	ACT GGA TGG CGG CGT TAG TAT CG (23bp)	
Exo1SACHromFLAG_F	CGG CAG TCA GAT CTA TCG CCT TGC TTT CCC AAT TTG TTT ATA AAG GTA AAC TGA AGC TTC GTA CGG GAT C (70bp)	1,499bp for pBH951 (Annealing temperature was set at 60°C)
Exo1SACHromFLAG_R	TTT TCA TTT GAA AAA TAT ACC TCC GAT ATG AAA CGT GCA GTA CTT AAC TTG CTG CAG GAA TTC GAG CTC G (70bp)	

Chapter 3. Phosphorylation of Exo1 during *S. cerevisiae* sporulation

Introduction:

Exo1 is a conserved nuclease with 5' → 3' DNA exonuclease activity and 5' endonuclease activity (Tran et al., 2004). Exo1's nuclease activity was previously described during mitosis and meiosis (Mimitou and Symington, 2009). This nuclease function of Exo1 was characterised during the homologous recombination repair pathway exposing long tracts of 3' ssDNA. The production of long 3' ssDNA overhangs are essential for efficient DNA repair by homologous recombination. In the absence of *EXO1* in *S. cerevisiae*, cells are more sensitive to DNA damaging agents (Morin et al., 2008). During meiosis, Exo1 functions in the 5' → 3' DNA resection process in the homologous recombination pathway, producing a long 3' ssDNA tail capable of efficient strand invasion (Zakharyevich et al., 2010). Additionally, Exo1 showed nuclease-independent functions in HJ resolution (Zakharyevich et al., 2010; Keelagher et al., 2011). In the absence of *EXO1* during meiosis, phenotypes such as hypo-resection, reduced, and delayed crossovers were observed (Keelagher et al., 2011). Mitotic specific post-translational modifications (PTMs) of yeast Exo1 such as phosphorylation (Morin et al., 2008) and sumoylation of human EXO1 (Bologna et al., 2015) regulate the stability of the protein and the processing of DNA lesions. Thus far, in the published literature, Exo1 PTMs have been characterised only in mitotically dividing cells and in response to DNA damaging agents but little is known about the meiosis-specific regulation of Exo1 (Morin et al., 2008; Tomimatsu et al., 2014, 2017). For instance, the phosphorylation of four serine residues (S372, S567, S587, S692) in Exo1 were characterised in response to uncapped telomeres (Morin et al., 2008). In yeast, telomere uncapping is induced in Cdc13-defective mutant where the DNA damage checkpoint is activated (Garvik et al., 1995), leading to long tracts of 3' ssDNA mediated by Exo1 (Maringele and Lydall, 2002). In a mutant with uncapped telomeres, Morin et al. showed

that upon mutating the phosphorylated serine residues to alanine; a non-phosphorylatable residue, the phosphorylation of Exo1 was abolished. Additionally, the non-phosphorylatable mutant *exo1-4S::A* was slightly less sensitive to DNA damage than *EXO1* (Morin et al., 2008). This phosphorylation event is believed to negatively regulate Exo1 nuclease activity and prevent pathological over-resection (Morin et al., 2008).

During meiosis, Spo11-DSBs are processed and resected to produce long tracts of 3'ssDNA, section 1.5. Since Exo1 was shown to be phosphorylated in response to uncapped telomeres when 3'ssDNA is in abundance, the same phosphorylation event could occur during meiosis, specifically during DNA resection. Strong's PhD thesis showed that the phosphorylation mutant *exo1-4S::A* can be phosphorylated during meiosis by utilising a phosphatase assay Figure A1 (Appendix I), this suggested that different residues are phosphorylated during meiosis. The control Exo1 functions during meiosis remain uncharacterised and Exo1's phosphorylation during meiosis might be how Exo1's functions are regulated.

The x9PK tagged Exo1 was previously used by Strong, the same tagged protein was first used to expand this study. However, the epitope tagged protein did not produce reliable results to assess the phosphorylation of Exo1 during meiosis. Therefore, an alternative strategy was used. The tag was changed to x5His-x6FLAG and the protein was extracted under denaturing conditions followed by Nickel-NTA agarose affinity-purification. This method showed more reliable results, and proved to be an effective way to analyse the phosphorylation of Exo1 during meiosis.

The phosphorylation of Exo1 was assessed by analysing the electrophoretic mobility shift of Exo1 during meiosis. The electrophoretic mobility-shift of Exo1 and the non-modified band were quantified using GeneTools by SynGene. All of the quantified bands were blanked against the background signal of the band's lane, Figure 3.1. After the quantification and blanking of the modified and non-modified band intensities, the proportion of each blanked-band intensity for each time-point was calculated as shown below and plotted against time, post-meiosis induction.

$$(\textit{Phosphorylation proportion} = \frac{\textit{modified band}}{\textit{modified} + \textit{nonmodified}})$$

The aim of this chapter is to demonstrate the assay developed to analyse Exo1 phosphorylation during meiosis. The assay developed would be later used to analyse Exo1 phosphorylation during the meiosis of different and significant mutant strains. Additionally, the meiotic progression and the spore viability of *EXO1*, *exo1Δ*, and *exo1-4S::A* were analysed to understand the meiotic functions of Exo1.

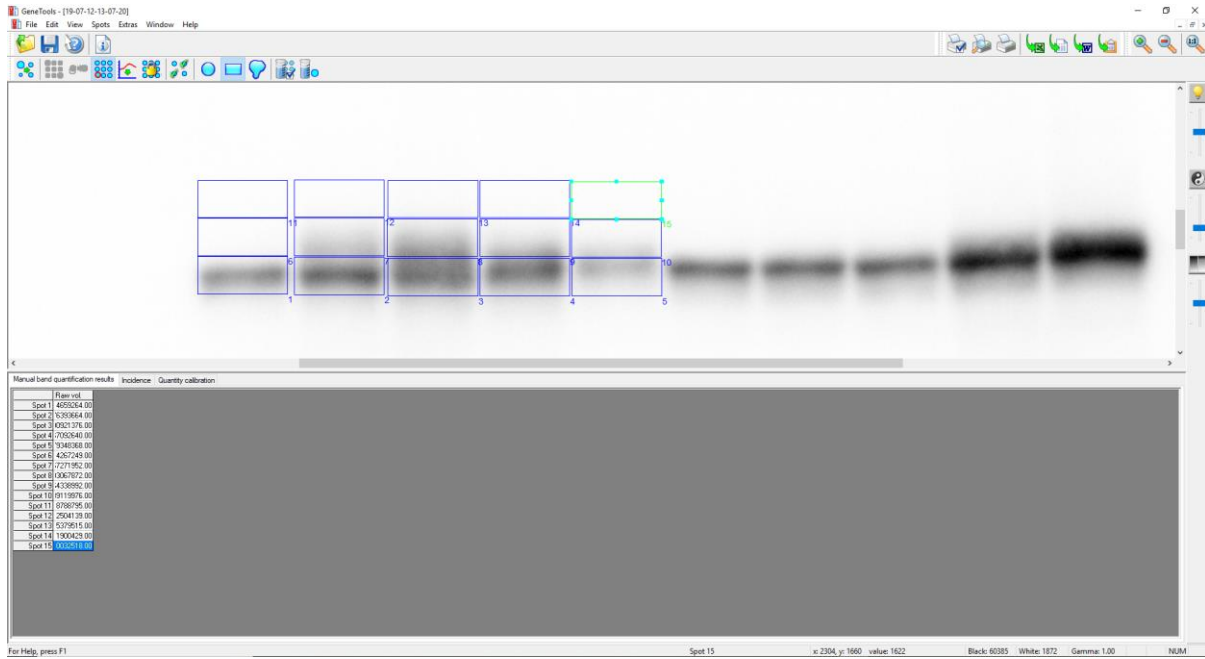


Figure 3.1 Western blot bands quantification using GeneTools software

An example of how phosphorylation proportions have been quantified. The bottom blue rectangles are where the non-modified bands were quantified. The middle blue rectangles are where the modified bands were quantified. Each quantified band was blanked by the top area of the band's respective lane, top rectangles.

Results:

3.1 *Exo1-x9PK* analysis during yeast sporulation:

To investigate *Exo1* phosphorylation during meiosis, a non-tagged wild-type control strain and a *Exo1-x9PK* tagged strain were induced into meiosis and sampled at hourly intervals. Whole cell protein extraction was done using the TCA protein extraction method and subsequently analysed by western blot, Figure 3.2a. A uniform non-specific 135kDa protein band was visible across all samples. 100kDa protein bands were only detected in the x9PK epitope tagged *Exo1* strain and not in wild-type, suggesting that the bands corresponds to *Exo1-x9PK*. At the beginning of meiosis induction, *Exo1-x9PK* expression was low as a very faint band was observed. The faint band increased in intensity after two hours of meiosis induction and gradually increased further in intensity peaking after five hours of sporulation induction. The band's intensity then decreased at the seventh time-point. Two hours following the induction of meiosis, the *Exo1-x9PK* band was preceded by a faint smear, annotated with a red asterisk on Figure 3.2a. The faint smear is possibly caused by the reduced motility of *Exo1-x9PK* entailed by the increase of its molecular weight, possibly due to a post-translational modification such as phosphorylation. By the third and fourth hour time-points, two faint yet distinct bands were observed. By the fifth hour, the two bands were indistinguishable, forming a thick and intense *Exo1-x9PK* band. At the seventh hour time-point, little to no smear was detected above the non-modified *Exo1-x9PK* band. Figure 3.2b shows the phosphorylation proportion of *Exo1-x9PK* during meiosis plotted against time post-meiosis induction. This was done after the bands were quantified as described earlier. The phosphorylation of *Exo1-x9PK* peaked at 25% after four hours. The phosphorylation proportion then decreased after five hours of meiosis and decreased further as the cells progress through meiosis.

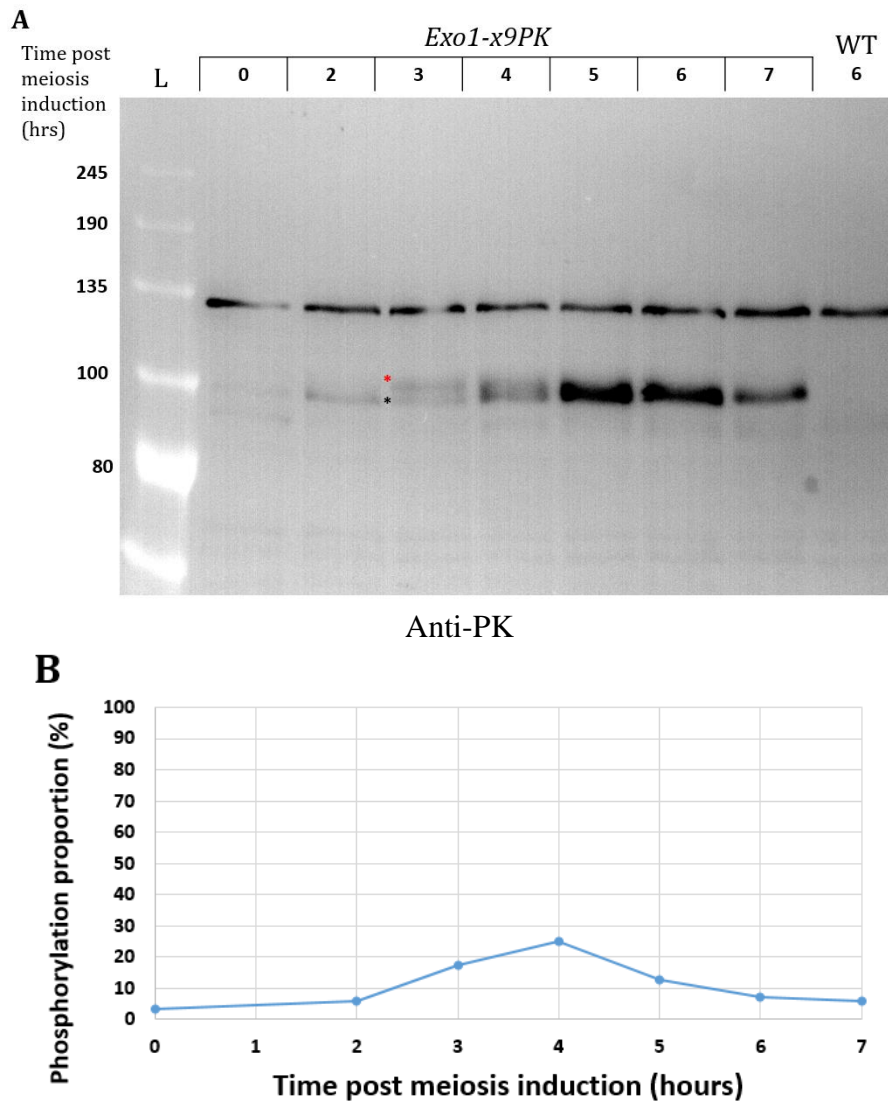


Figure 3.2 *Exo1-x9PK* western blot analysis during meiosis

- A) Western blot analysis of *Exo1-x9PK* during meiosis. Protein samples were taken at 0, 2, 3, 4, 5, 6, and 7 hours during the sporulation of *Exo1-x9PK*. A sixth hour sample was taken from wild-type *EXO1* sporulation. The PK antibody (anti-PK) exhibited a non-specific uniform band of 135kDa across all samples, even in the *EXO1* sample. This suggests that the band seen around 100kDa is of *Exo1-x9PK* as it corresponds to the size of the tagged protein. The band intensity increased as meiosis progressed and then gradually decreased until the 7th-hour sample. A smear can be observed emerging at the third hour and peaking in signal at the fourth hour. The smear was then reduced as meiosis progressed.
- B) The intensity of each phosphorylation band/smear (red asterisk on Figure 3.1a) and the non-modified band (black asterisk on Figure 3.1a) were measured and the proportion of the phosphorylated/non-modified band was calculated and plotted against time post-meiosis induction. The phosphorylation proportion is represented by percentage. After three hours of meiosis induction, the phosphorylation proportion was 17% and peaked at 25% after four hours of sporulation. At the subsequent time-points; five and six hours, the phosphorylation proportion reduced steadily to 12%, and then to 7% respectively. After seven-hours of sporulation, the phosphorylation signal was very low, with phosphorylation proportion at 6%.

3.2 **EXO1-x9PK and exo1Δ strains meiotic progression:**

Meiotic nuclear division was monitored during the sporulation of *EXO1-x9PK*, *EXO1*, and *exo1Δ* strains in order to study the meiotic progression by counting the DAPI stained nuclear spots at each time-point. Examining the meiotic progression of these strains is crucial in order to make sure that the tag does not interfere with the protein function, as well as to study the meiotic progression in the absence of *EXO1*. Any delay or disruption of the progression is a sign of a defective cell checkpoint or stage. For instance, Exo1 functions in two different stages of meiotic recombination; during the long-resection of DSBs, and the resolution of dHJs. Disruption of either process could have implications on the meiotic progression of the cells. To examine if the epitope tag affects Exo1 functions during meiosis, the *EXO1-x9PK* strain was induced into meiosis and samples were taken at hourly intervals. The meiotic progression of *EXO1-x9PK* strain was tested once, while *EXO1* and *exo1Δ* strains were tested thrice. The meiotic progression of the tagged Exo1 strain was relatively normal, in comparison to the meiotic progression of *EXO1*, Figure 3.3a, b, and d. The meiotic progression of *exo1Δ* strain was slightly delayed but exhibited normal levels of sporulation of 96%, Figure 3.3c. This shows that *EXO1* is required for punctual meiosis timing and early progression, but it does not affect spore production. By contrast, the *EXO1-x9PK* strain produced divided nuclei with similar timing to *EXO1*, Figure 3.3c, suggesting the *Exo1-x9PK* protein is probably fully functional.

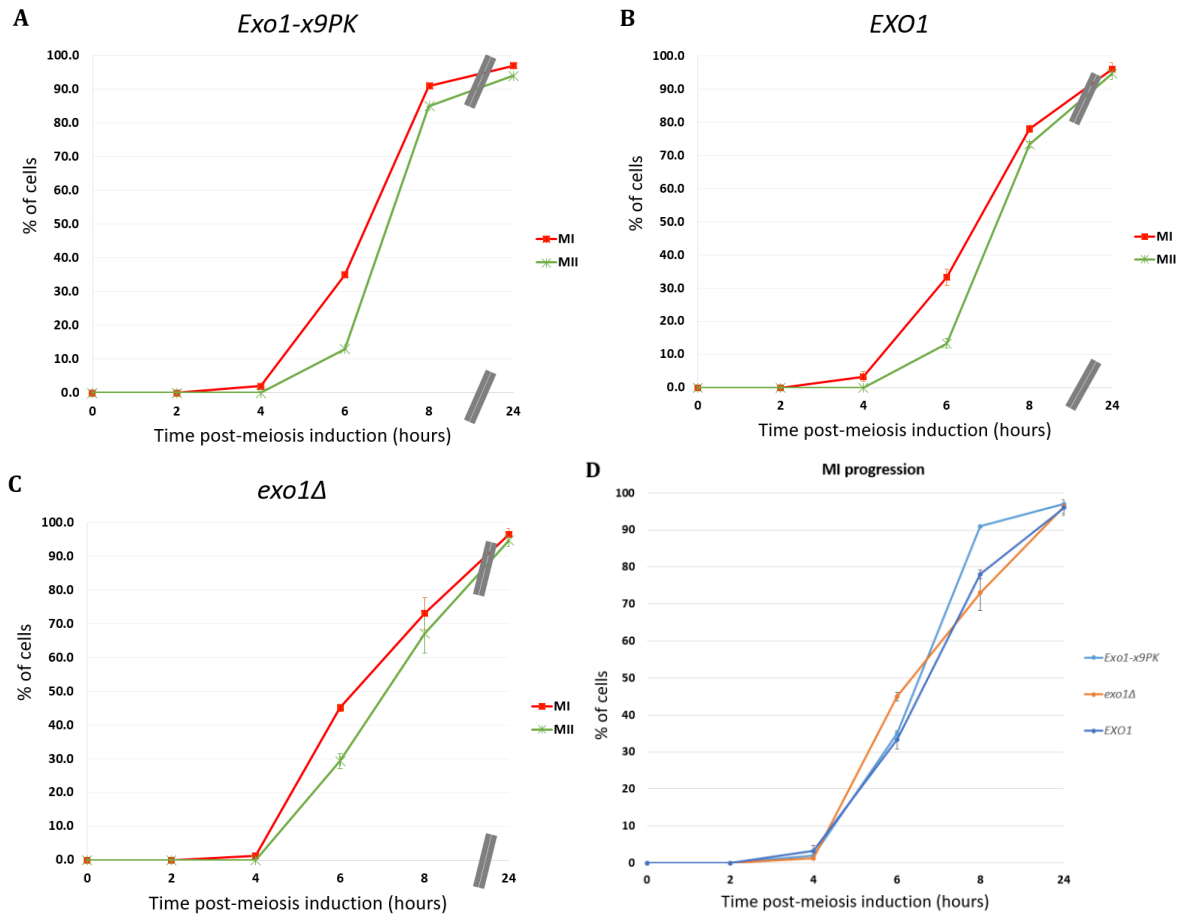


Figure 3.3 Meiotic progression of Exo1 strains during meiosis.

- A.** Nuclear division analysis of the *Exo1-x9PK* strain meiosis showing no significant defects in meiotic progression. The strain went through MI and MII at the appropriate time.
- B.** Wild-type *EXO1* meiotic nuclear division analysis. Meiosis was normal indicating that the cells were successfully synchronised into meiosis. ($n = 3$, error bars represent the standard deviation from the mean)
- C.** The meiotic progression of *exo1Δ* revealed a slightly delayed meiosis program. ($n = 3$, error bars represent the standard deviation from the mean)
- D.** Comparing meiosis I progression of all strains, the meiotic progression of *exo1Δ* was slightly delayed. Even with this delayed meiosis program, the strain was still able to produce tetrads at normal levels after 24 hours of meiosis induction.

3.3 Epitope tagging of Exo1 with x5His- x6FLAG tag:

Multiple TCA protein extractions were prepared for meiotic *Exo1-x9PK* samples to investigate the phosphorylation of Exo1. This method proved to be unreliable, resulting in production of inconsistent data. As shown in Figure 3.4, meiotic samples of the *Exo1-x9PK* TCA extraction showed a smear below the 100kDa *Exo1-x9PK* band, and occasionally no band was detected. This is possibly due to a new batch of anti-PK antibody that might not be compatible to *Exo1-x9PK*. Troubleshooting the methods of TCA protein extraction, SDS-PAGE, and western blot were not successful. Therefore, the epitope tag was changed to the x5Hisx6FLAG tag which consist of a penta-histidine sequence (5xHis) followed by six copies of the FLAG sequence (6xFLAG) as described by Hopp and Prickett, 1988. The use of the x5His-x6FLAG tag would allow for affinity-purification after protein extraction under denaturing conditions, followed by western blot using the linear x6FLAG tag.

In order to tag Exo1 with x5His-x6FLAG, the tag sequence with its selection marker, *KanMX* was amplified by PCR. This was done by using the Exo1ChromFLAG forward and reverse primers to amplify the tagging cassette from pBH368, plasmid map Figure A2 (Appendix II). The PCR product from pBH368 was then transformed into the *EXO1* strain using the method described in section 2.3.10. The integration of the newly tagged *EXO1* was checked by PCR, and western blot (data not shown).

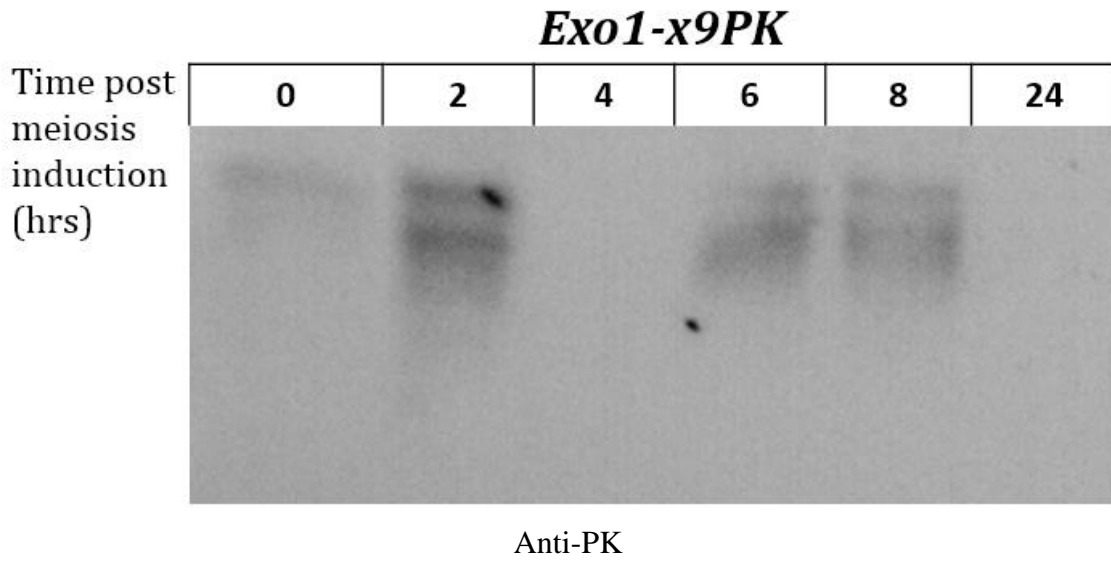


Figure 3.4 A representation of a western blot analysis of TCA protein extracts from *Exo1-x9PK* meiotic samples. Many replicates yielded the same result of a smear around the Exo1 expected size. A top band can be seen with a smear below it and occasionally no signal was observed in the sample such as the 4-hour and 24-hour timepoints.

Guanidinium hydrochloride protein extraction was used for the newly tagged strain as described in section 2.3.13b. Guanidinium hydrochloride at 6M is a strong denaturing agent, eliminating any protease or phosphatase activity. To purify Exo1 under denaturing conditions, charged Ni-NTA affinity resin was used. The charged nickel ions on the NTA-agarose resin can bind to polyhistidine sequences such as the penta-histidine sequence at the C-terminal of the tagged Exo1, ultimately purifying Exo1 along with histidine rich proteins. The tagged Exo1 can then be visualised by western blot using the FLAG antibody that can bind specifically to the linear epitope FLAG tag. The Exo1 tagged diploid strain and the parental wild-type strain were induced into meiosis and a sample was taken from each after four hours of sporulation induction. This was done because at the fourth hour, Exo1's signal was the highest, and electrophoretic mobility shift was more pronounced. *Exo1-x5His-x6FLAG* was purified using Ni-NTA from 30OD of cells, and 20µl of whole cell extract (WCE) was loaded after washing out the salts using StrataClean resin (Agilent). As shown in Figure 3.5, Exo1 was successfully purified and a 100kDa band that corresponds to Exo1 can be observed in the Ni-NTA affinity-purified *Exo1-x5His-x6FLAG* sample. In the WCE extract samples, a band can be observed in the wild type and *Exo1-x5His-x6FLAG* samples which is believed to be an anti-FLAG non-specific band, suggesting that this band could be for a protein that anti-FLAG antibody can bind to. The non-specific band was not observed in the wild type Ni-NTA affinity-purification sample, meaning that this protein was not eliminated from the sample upon Ni-NTA purification. This means that Exo1 can be purified using this method, eliminating any antibody non-specific binding. Interestingly, a faint but distinct band can be observed above the brighter 100kDa Exo1 band in the Ni-NTA *Exo1-x5His-x6FLAG* sample. This band could be a manifestation of Exo1 phosphorylation, similar to the phosphorylation observed in *Exo1-x9PK*. However, in order to confirm that the electrophoretic mobility shift (smear) is phosphorylation, phosphatase assay must be done.

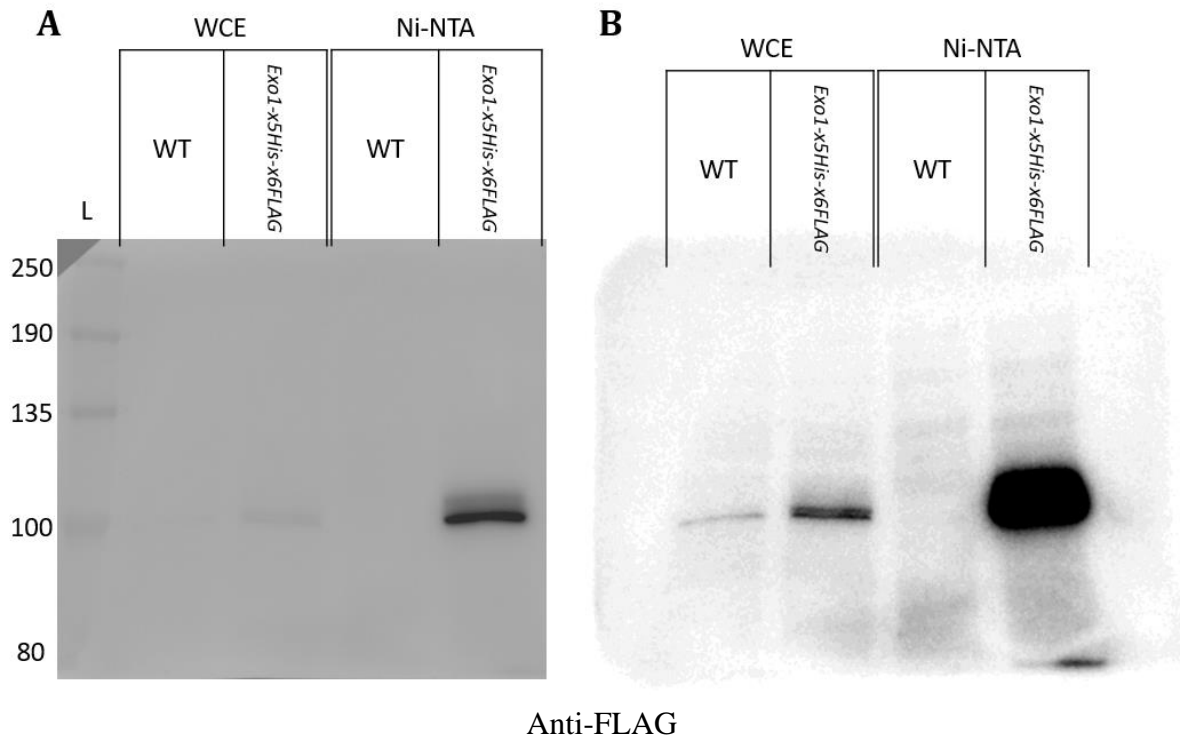


Figure 3.5 Western blot analysis of Ni-NTA affinity-purified *Exo1-x5His-x6FLAG* after four hours of meiosis induction. **A** and **B** are both the same western blot but with different contrast levels done to show the faint bands of the whole-cell extracts (WCEs). WCEs were from 30OD of cells. The FLAG antibody non-specific binding band can be detected in both WCEs. However, an extra band can be seen above it in the *Exo1-x5His-x6FLAG*. These two bands are separated by a thin area where the bottom band is believed to be *Exo1-x5His-x6FLAG*. Ni-NTA affinity purification for the wild-type (WT) sample did not produce the FLAG non-specific band. A thick band with a fainter band above it can be observed for the Ni-NTA purified *Exo1-x5His-x6FLAG*.

3.4 **Exo1-x5His-x6FLAG is phosphorylated during meiosis:**

Treatment of purified *Exo1-x5His-x6FLAG* with phosphatase was carried out to confirm whether the electrophoretic mobility shift seen earlier is due to phosphorylation. The protein was extracted and purified from cells after four hours of meiosis induction. This is because at the fourth hour, the electrophoretic mobility shift had the highest level of signal compared to other time-points. The protein purification and treatment with phosphatase was carried out as described in 2.3.16. This protein purification method preserves the phosphorylation of Exo1, but it was done in high-salt denaturing conditions. As Lambda phosphatase cannot function in these conditions, the salts were carefully washed before phosphatase treatment. The purified protein extracts were treated with three combinations of phosphatase and phosphatase inhibitors.

The second lane of Figure 3.6 western blot shows the Ni-NTA purified sample treated with phosphatase inhibitors without the addition of phosphatase. The third lane is the purified protein sample treated with phosphatase in the absence of inhibitors. The fourth lane is the purified sample treated with both, phosphatase and phosphatase inhibitors. *Exo1-x5His-x6FLAG* electrophoretic mobility shift can be observed in the second and fourth lane. The electrophoretic mobility shift was absent when the sample was treated with phosphatase only, as shown in the third lane. This suggests that the presence of the higher molecular weight smear depends upon treatment with phosphatase. This concludes that the higher electrophoretic mobility species of *Exo1-x5His-x6FLAG* seen as a smear on western blot is a manifestation of the phosphorylated species of *Exo1-x5His-x6FLAG*.

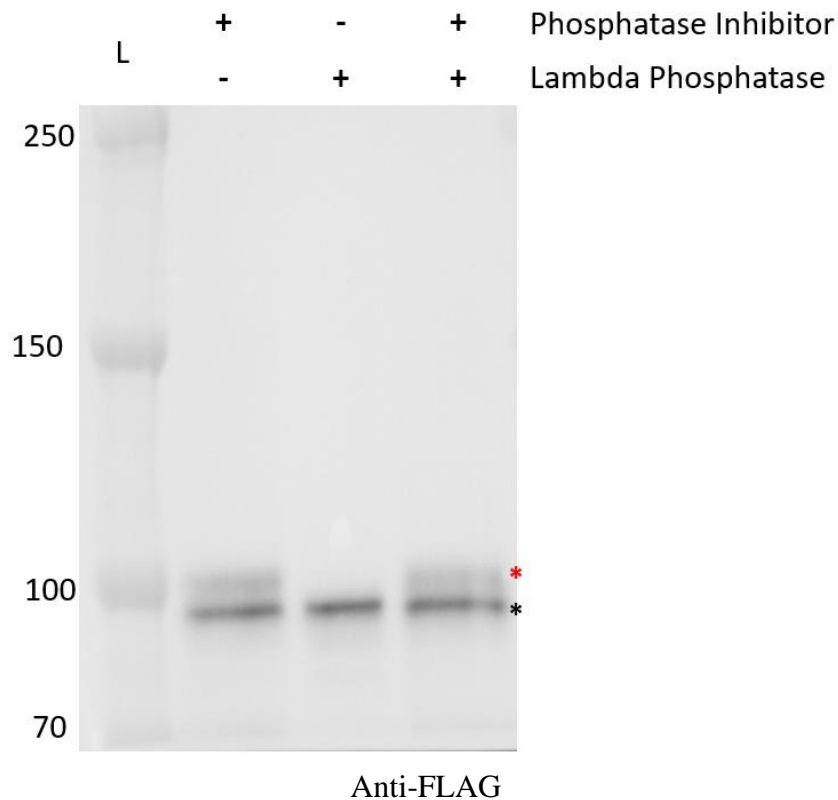


Figure 3.6 *Exo1-x5His-x6FLAG* is phosphorylated during meiosis.

The samples were extracted from cells at four hours of meiosis, each at 30OD₆₀₀. Ni-NTA purification was done at denaturing conditions and then the salts were washed out. The purified samples have been treated with various combinations of Lambda phosphatase and phosphatase inhibitors indicated by + or -. A band can be seen across all samples around 100 kDa which is the expected size of *Exo1-x5His-x6FLAG* (black asterisk). The second and fourth lane show an electrophoretic mobility shift (red asterisk), which suggests that *Exo1* is phosphorylated. The smear is absent in the third lane, in which the purified protein samples has been treated with phosphatase in the absence of inhibitors, suggestive of a removal of phosphorylation. This confirms that the higher molecular weight band is the phosphorylated form of *Exo1-x5His-x6FLAG*.

3.5 **Meiotic progression of the *Exo1-x5His-x6FLAG* strain:**

To demonstrate that the new tag did not affect the function of Exo1, and to analyse the phosphorylation of Exo1 during meiosis, the FLAG tagged Exo1 strain was induced into meiosis along with the *EXO1* strain, where samples were taken at two-hour intervals until the eighth hour. Samples were taken to monitor the meiotic nuclear division by DAPI staining, and for protein extraction under denaturing conditions. Upon western blotting, no bands were detected in *EXO1* meiosis, and bands that corresponds to *Exo1-x5His-x6FLAG* was observed across the sample of the tagged strain, Figure 3.7a. In the tagged strain fourth-hour sample, a pronounced electrophoretic mobility shift can be observed and appeared as a distinct band. The up-shifted band was then reduced to a smear as meiosis progress. The phosphorylation proportion was quantified for each time-point and plotted against time, post-meiosis induction. As shown in Figure 3.7b, the up-shifted band proportion compared to the non-modified band peaked at $51\% \pm 5.3$ after four hours of meiosis induction, after which it decreased to $21.2\% \pm 2.8$ at the sixth time-point. After eight hours of meiosis induction, the phosphorylation signal proportion decreased further to $12.9\% \pm 3.3$ and was not totally abolished. Furthermore, the meiotic progression of *EXO1-x5His-x6FLAG* was slightly earlier compared to *EXO1* and did not exhibit any meiotic progression defects, Figure 3.8. This data shows that the newly used tag (x5His-x6FLAG) is an effective tag to study Exo1 PTM during meiosis.

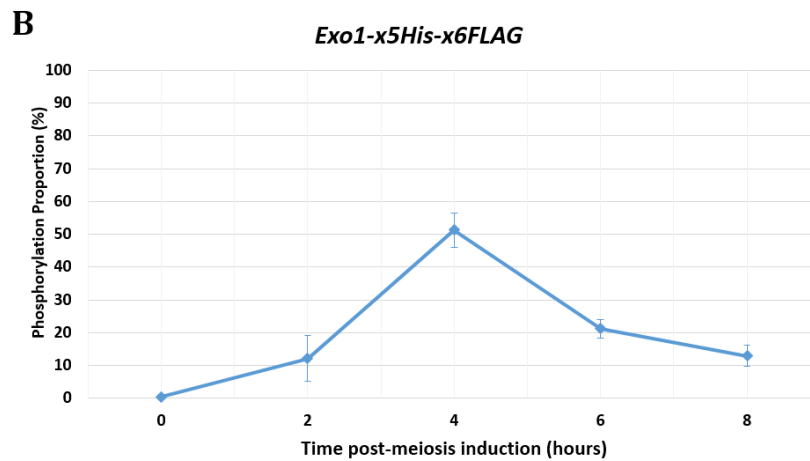
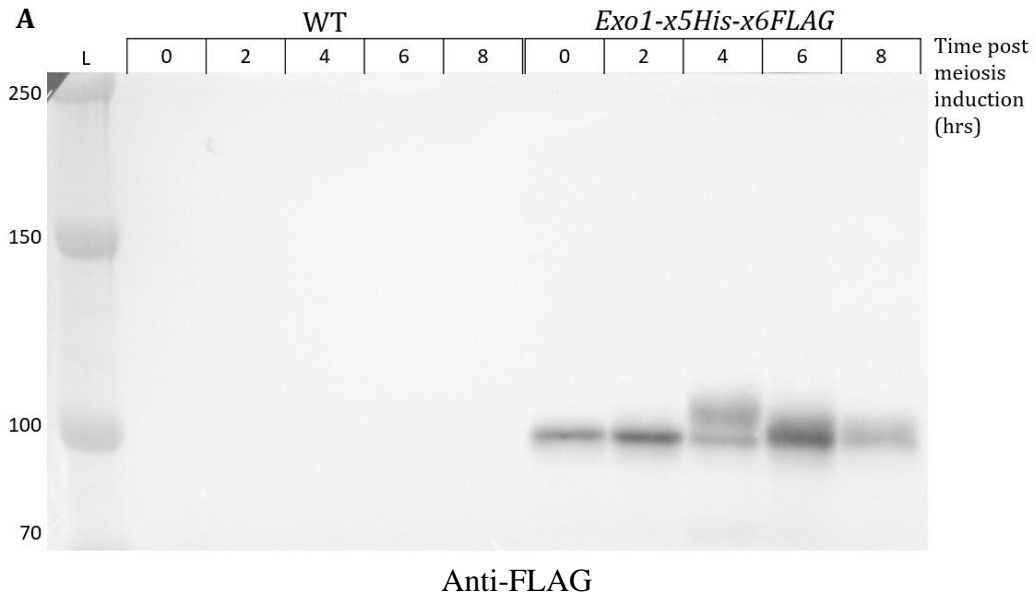


Figure 3.7 Western blot analysis of *Exo1-x5His-x6FLAG* strain's meiosis

- A)** Western blot for *Exo1-x5His-x6FLAG* during meiosis. Samples were taken at 0, 2, 4, 6, and 8 hours, post meiosis induction. Samples from wild-type meiosis were also taken at the same time-points. No bands were detected in the wild-type samples. *Exo1-x5His-x6FLAG* bands at 100kDa can be observed across all time-points. After 4 hours of meiosis induction, two bands be observed, one is from modified and non-modified species of Exo1. The top modified band was then reduced to a smear as meiosis progress.
- B)** Phosphorylation proportion analysis for *Exo1-x5His-x6FLAG* phosphorylation. ($n = 3$, error bars represent the standard deviation from the mean). After two hours of meiosis induction, the proportion value was at $12.1\% \pm 7.1$. The proportion value peaked at $51.2\% \pm 5.3$ after four hours of sporulation and then decreased to $21.2\% \pm 2.8$ after six hours of meiosis induction. At the eighth hour time-point, the phosphorylation proportion reduced further to $12.9\% \pm 3.3$.

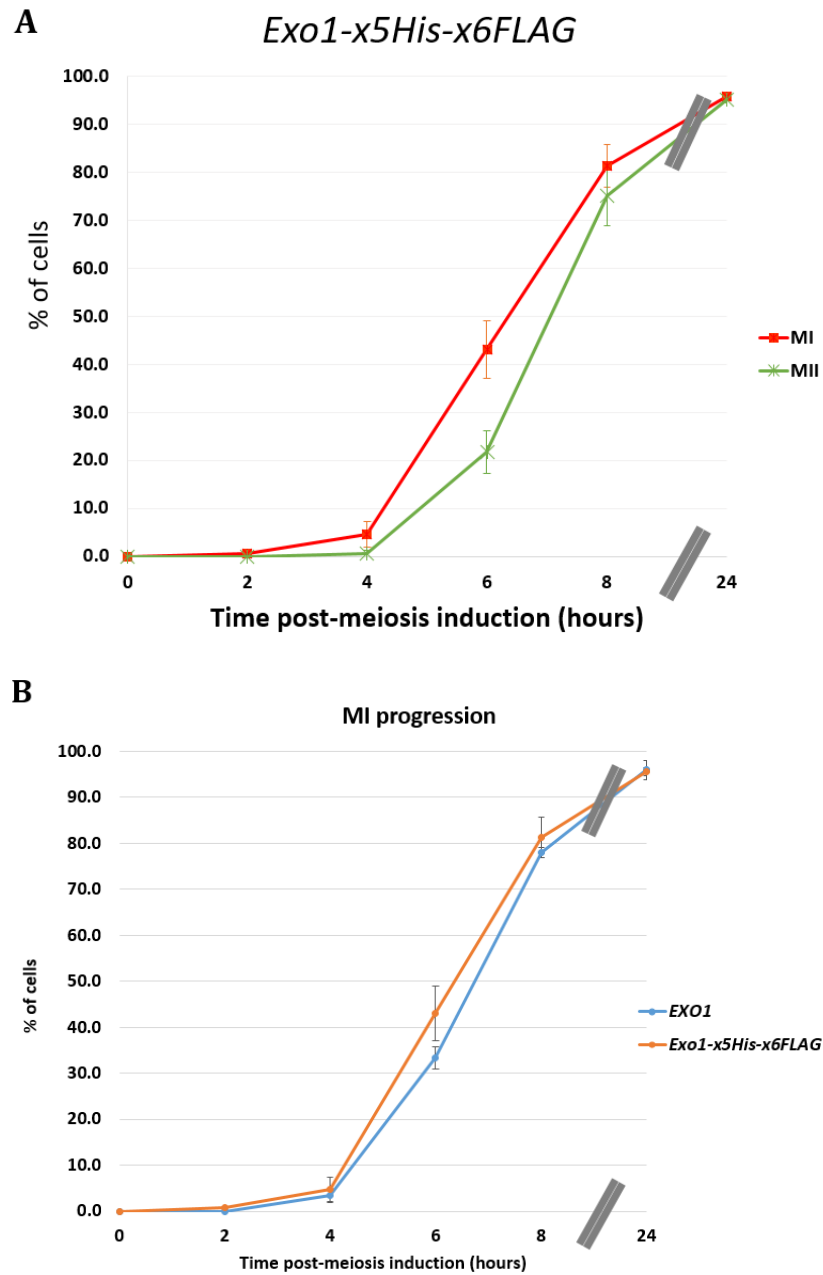


Figure 3.8 Meiotic progression analysis of the *Exo1-x5His-x6FLAG* strain.

($n = 3$, error bars represent the standard deviation from the mean)

A) After six hours of meiosis induction, $43\% \pm 6.0$ of cells went through MI and 22% went through MII ± 4.5 . At the subsequent time-point, $81\% \pm 4.4$ went through MI, and $75\% \pm 6.2$ went through MII. After 24 hours of meiosis induction, $95\% \pm 0.6$ of cells went through all stages of meiosis, indicating a relatively normal meiosis.

B) *EXO1* and *Exo1-x5His-x6FLAG* MI progression side by side. The data shows that *Exo1-x5His-x6FLAG* is slightly earlier than *EXO1* but with no drastic differences.

3.6 ***exo1-4S::A-x5His-x6FLAG* is phosphorylated during yeast meiosis:**

As previously reported by Strong's PhD thesis, *exo1-4S::A* is phosphorylated during meiosis, demonstrated by a phosphatase assay, Figure A1 (Appendix I). To confirm this result, *exo1-4S::A* was tagged with x5His-x6FLAG using the CRISPR-Cas9 system (see appendix III) and the homozygous diploid was induced into meiosis alongside with wild-type tagged strain. Samples were taken at two-hour intervals until the eighth hour for DAPI staining and protein extraction. Proteins were extracted using the guanidinium hydrochloride extraction method, followed by Ni-NTA affinity purification. The purified protein samples were analysed by western blot. At the fourth hour time point sample of both strains, two distinct bands can be seen with equal signal. The top band was then reduced to a smear after six hours of meiosis induction for both strains, Figure 3.9a. As shown in Figure 3.9b, the phosphorylation proportion of the phosphorylation mutant strain peaked at $55\% \pm 3.7$ after four hours of sporulation. Subsequently the phosphorylation proportion declined to $25.9\% \pm 1.8$ at the sixth hour time-point and decreased further to $23.5\% \pm 8.8$ after eight hours of sporulation. The phosphorylation proportion of the *exo1-4S::A* was slightly higher than wild type at the fourth, and sixth hour samples, but was significantly higher at the eighth hour sample. Upon DAPI staining of the cells during meiosis, the meiotic progression of the mutant was normal, Figure 3.10a. The meiosis progression of *exo1-4S::A-x5His-x6FLAG* was slightly earlier than *Exo1-x5His-x6FLAG* and *EXO1*, Figure 3.10b, which can be considered normal with no apparent meiotic defects.

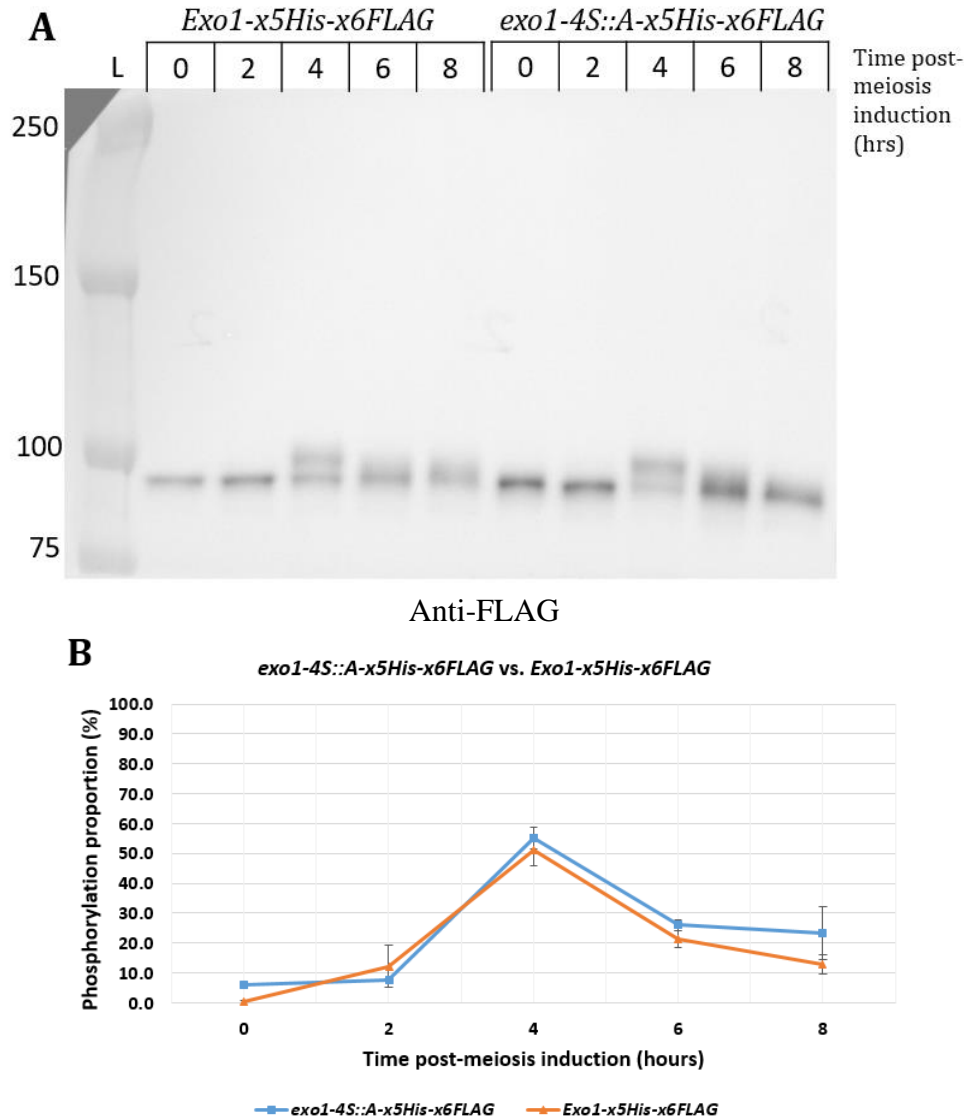


Figure 3.9 Western blot analysis of the *exo1-4S::A-x5His-x6FLAG* strain's meiosis

- A) Western blot analysis of *exo1-4S::A-x5His-x6FLAG* and *Exo1-x5His-x6FLAG* during meiosis. Samples were taken after 0, 2, 4, 6, and 8 hours, post-meiosis induction. After four hours, a thick band can be observed in both strains which comprised of two different forms of Exo1, modified and non-modified. The electrophoretic mobility shift was reduced to a smear as meiosis progressed to the eighth hour. The electrophoretic mobility shift of both strains profile looks similar.
- B) Phosphorylation proportion analysis of *exo1-4S::A-x5His-x6FLAG* compared with *Exo1-x5His-x6FLAG*. $n = 3$, error bars represent the standard deviation from the mean. The phosphorylation proportion of *exo1-4S::A-x5His-x6FLAG* was at $7.6\% \pm 0.5$ after two hours of sporulation induction. After four hours of sporulation, the phosphorylation proportion peaked at $55.0\% \pm 3.7$. Subsequently, the phosphorylation proportion decreased to $25.9\% \pm 1.8$ after six hours of meiosis induction, and decreased further to $23.5\% \pm 8.8$ after eight hours. Both phosphorylation proportion profile are similar, except for the eight hour time-point where *exo1-4S::A-x5His-x6FLAG* showed a higher proportion.

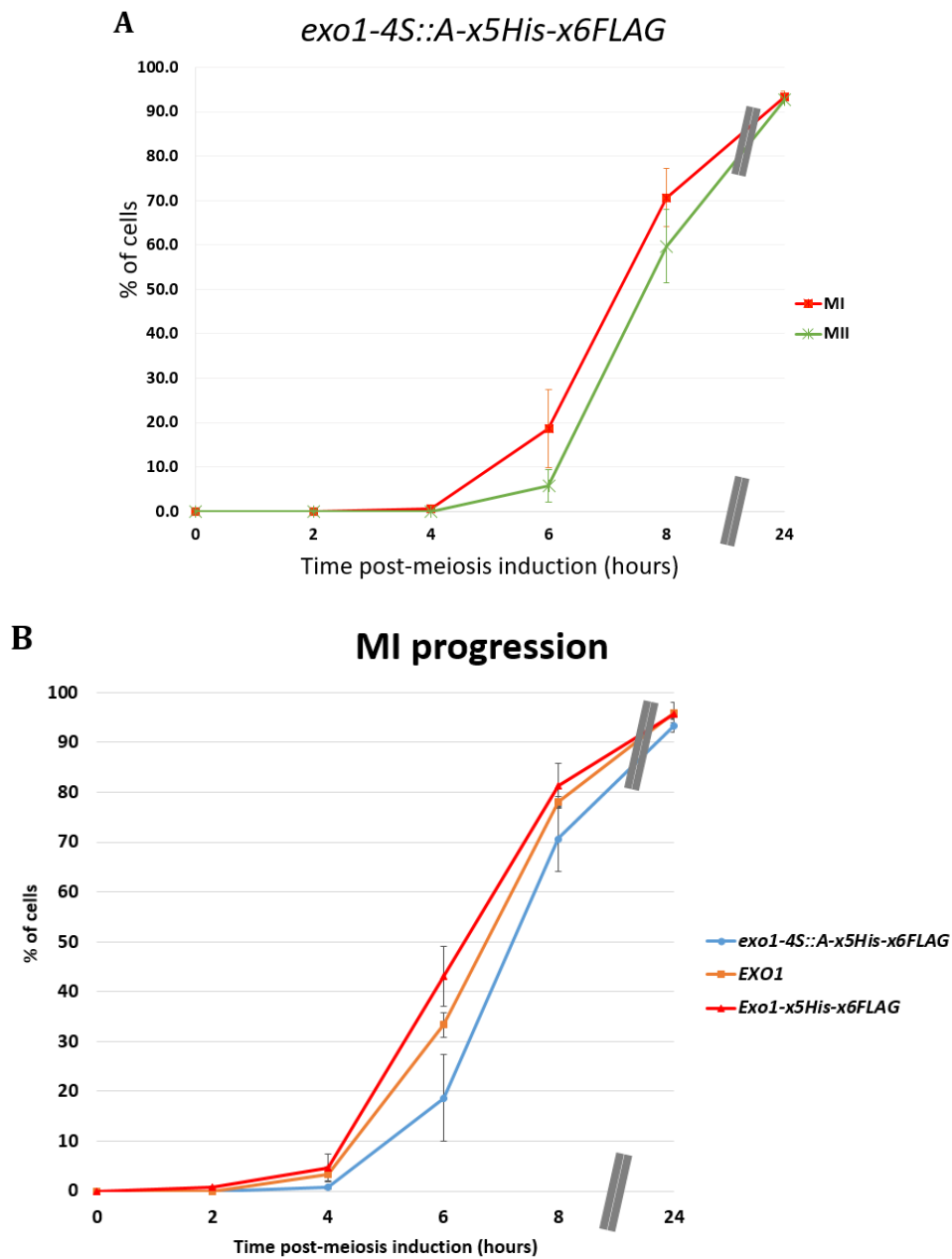


Figure 3.10 Meiotic progression analysis of *exo1-4S::A-x5His-x6FLAG*.

($n = 3$, error bars represent the standard deviation from the mean)

A) After six hours of meiosis induction, $19\% \pm 8.7$ of the cells went through MI, and $6\% \pm 3.7$ went through MII. As meiosis progressed to the eighth hour, $71\% \pm 6.5$ of cells went through MI, and $60\% \pm 8.3$ of cells went through MII. After 24 hours of meiosis induction $93\% \pm 0.88$ of cells went through all stages of meiosis.

B) MI progression comparison between *exo1-4S::A-x5His-x6FLAG*, *EXO1*, and *Exo1-x5His-x6FLAG*. The meiotic progression of the phosphorylation mutant tagged strain was earlier than WT and WT-tagged strain.

3.7 **Spore viability is not affected in the phosphorylation null mutant *exo1-4S::A* but reduced in *exo1Δ***

Spores are the product of yeast meiosis. A good indication of faithful chromosome segregation is the ability of these spores to germinate into healthy haploids. For instance, chromosome aberrations and aneuploidy are caused by errors in chromosome segregation during meiosis. Such aberrations are mostly caused by a defective pathway or a cell-cycle checkpoint during meiosis. If chromosome segregation in MI is defective, then all four daughter cells produced will most probably have chromosomal aberrations. On the other hand, malfunctions in MII would mostly produce two healthy daughter cells, with the other two with potential chromosomal aneuploidies. Yeast tetrad dissection was performed for four different strains: *EXO1*, *EXO1-x5His-x6FLAG*, the phosphorylation mutant *exo1-4S::A-x5His-x6FLAG*, and *exo1Δ*. This was done to test the spore viability and viability pattern of each strain. The *EXO1-x5His-x6FLAG* strain showed a spore viability of $95\% \pm 1.0$, while the phosphorylation mutant *exo1-4S::A-x5His-x6FLAG* strain had a spore viability of $96.3\% \pm 1.0$, Figure 3.11. *EXO1* cells have an average spore viability of $98.8\% \pm 1.0$. The *exo1Δ* strain had only $70.4\% \pm 1.6$ viability, with random viability patterns. This is a sign of a defective meiosis program, consistent with the published literature. Interestingly, the inability to phosphorylate mitotically significant residues did not affect the spore viability. Suggesting that other residues are phosphorylated or the mitotic significant phosphorylation sites do not function during meiosis.

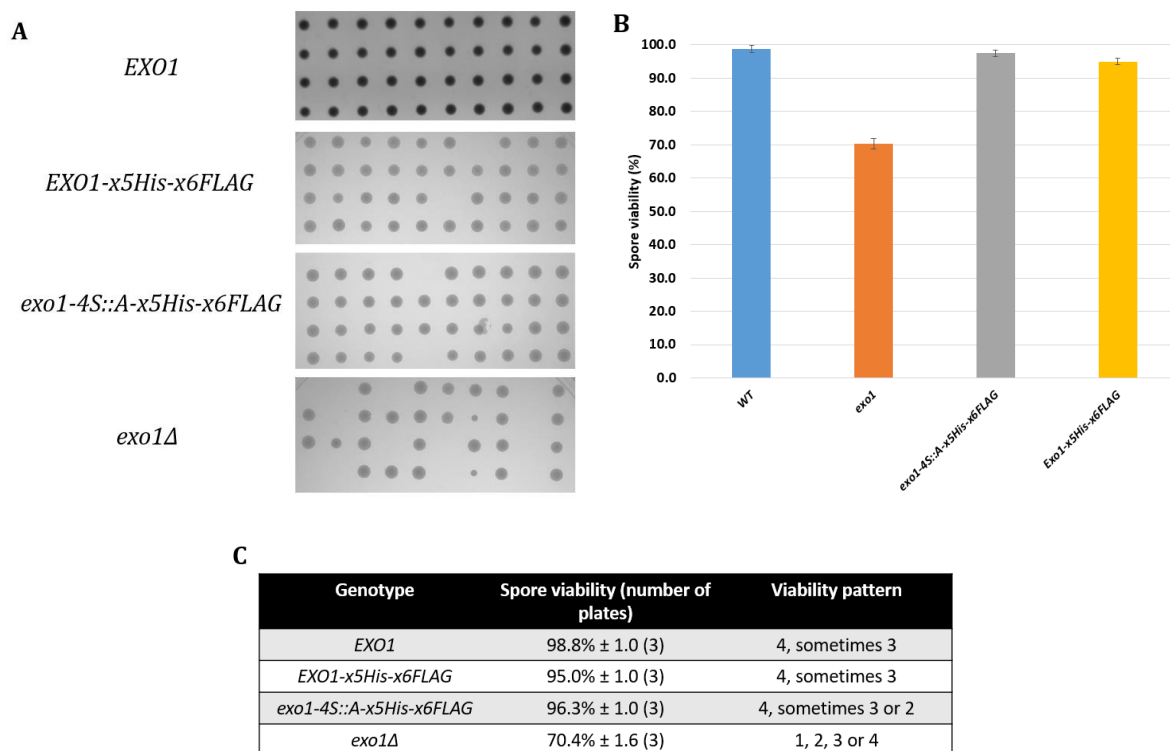


Figure 3.11 Spore viability of different Exo1 mutants

($n = 3$, error bars represent the standard deviation from the mean)

- A)** Examples of the spore viability patterns observed of tetrad dissected onto YPD plate. The *exo1Δ* strain had a random viability pattern.
- B)** Graph comparing the spore viability of each strain.
- C)** Table summarising the mean spore viability of each strain. Three plates were dissected for each strain (240 spores each) to produce a standard deviation from the mean. Viability pattern can indicate whether non-disjunction has occurred during MI (2 spore viable) or MII (combinations 1, 2, 3 and 4 spores viable).

Discussion:

The phosphorylation of Exo1 during mitosis and in response to DNA damage has been previously reported by Morin et al., 2008. However, the function of Exo1 phosphorylation during meiosis still remains uncharacterised. Studying Exo1 proved challenging; epitope tagging or any modifications to the *EXO1* genomic locus usually failed. When Exo1 was eventually tagged with x9PK, it paved the way to further understand Exo1 functions and its phosphorylation.

The expression of *Exo1-x9PK* was examined during meiosis as whole-cell extraction was done using TCA method. As shown in Figure 3.2, the expression of *Exo1-x9PK* was barely detectable before meiosis induction of the synchronised cells. At this stage (0-hour time-point), the cells were synchronised by starvation and were no longer undergoing DNA replication. As Exo1 has been implicated in the repair and stability of stalled DNA-replication forks (Cotta-Ramusino et al., 2005), the low level of *Exo1-x9PK* expression observed at 0-hour time-point might account for the lack of DNA replication in these cells. After two hours of meiosis induction the level of Exo1 expression was increased, at this stage most cells were undergoing DNA replication. The level of *Exo1-x9PK* expression peaked at the fourth-hour time-point. At this time-point, DNA-DSBs levels reach their peak and their subsequent need for repair and crossover resolution correlate with the highest level of *Exo1-x9PK* expression. By the eighth-hour time-point, the level of *Exo1-x9PK* expression was decreased. The activity of Exo1 might not be needed at this stage as the vast majority of breaks are repaired, and crossovers resolved.

The meiotic progression of *Exo1-x9PK* was normal when compared to *EXO1*, Figure 3.2. This suggests that the x9PK tag did not interfere to Exo1 meiotic function. When *exo1Δ* and *EXO1* meiotic progressions were compared, *exo1Δ* showed a delayed meiosis programme, showing that Exo1 is required for punctual meiosis. This correlates to the published literature as Exo1 functions in DSB repair and crossover resolution (Garcia et al., 2011; Zakharyevich et al., 2010).

Unfortunately, subsequent experiments have failed to study *Exo1-x9PK* during meiosis. This was because of either: failure to properly execute the TCA protein extraction method, or possibly a faulty batch of PK antibody. As shown in Figure 3.4, the *Exo1-x9PK* TCA protein extraction showed a smear when analysed by western blot. The smear and the band on top are around 100kDa, which is the expected size of Exo1. This issue was solved simply by changing the epitope x9PK tag to x5His-x6FLAG. The tag can be used for affinity purification by utilising the penta-histidine sequence, as well as immunoprecipitation by using the epitope six FLAG repeat. The expression of the newly made fusion protein was tested by the guanidinium hydrochloride protein extraction method followed by western blot analysis. As demonstrated earlier, the FLAG antibody binds to a non-specific protein of just lighter than Exo1, however the non-specific protein was eliminated when Ni-NTA affinity-purification method was done. This technique is very effective and consistent as no proteolytic or phosphatase activity can occur. Using this technique has two disadvantages, other histidine rich proteins could be purified and Exo1 expression cannot be analysed. Nevertheless, none of these proposed histidine rich proteins were detected by the FLAG antibody when western blot for the non-tagged *EXO1* strain was done, as shown in Figure 3.5.

In this western blot done to test for the Ni-NTA purification of *Exo1-x5His-x6FLAG*, Figure 3.5. The tagged protein was purified from cells induced into meiosis, after four-hours of meiotic induction. The signal that corresponds to *Exo1-x5His-x6FLAG* showed an electrophoretic mobility shift, which suggests a post-translation modification. Since *Exo1-x9PK* has been shown to be phosphorylated, the *Exo1-x5His-x6FLAG* could be phosphorylated as well. To confirm this phosphorylation event, a phosphatase assay done. After immunoblotting a western with anti-FLAG antibody, the sample treated with phosphatase only did not exhibit an electrophoretic mobility shift, Figure 3.6. On the other hand, an electrophoretic mobility shift was observed in the protein samples that were treated with phosphatase inhibitors with or without phosphatase. This suggests that *Exo1-x5His-x6FLAG* is phosphorylated during meiosis, and confirms previous experiments.

The x5His-x6FLAG tag on Exo1 did not affect the meiotic progression of the cells. The meiotic progression of *Exo1-x5His-x6FLAG* and *EXO1* were both very similar, Figure 3.8. Furthermore, the phosphorylation proportion of *Exo1-x5His-x6FLAG* during meiosis peaked at 51.2% after four-hours of meiosis induction, Figure 3.7. At this time-point DNA-DSBs levels are high, where they are being repaired, and crossovers are being resolved. Since Exo1 has been shown to function in DNA-DSB resection and crossover resolution. The phosphorylation of Exo1 at this time-point can be correlated to both functions. The phosphorylation proportion was then reduced as meiosis progress but it was not abolished. This needs to be investigated further whether the band shift seen at the eighth-hour time-point is phosphorylation. The PK tagged Exo1 strain showed lower phosphorylation proportions than the x5His-x6FLAG. This is because the gel running of both samples was different; the PK tagged proteins were previously run on 7.5% acrylamide gel, while the x5His-x6FLAG was run on 6% acrylamide gel. The lower percentage gel allow for higher resolution for proteins at the range of 100-kDa molecular weight.

The *exo1-4S::A* mutant was reported to be phosphorylated during *S. cerevisiae* meiosis in Strong's 2017 PhD thesis. Strong's thesis demonstrated the mutant phosphorylation by carrying out a phosphatase treatment assay for immunoprecipitated *exo1-4S::A-x9PK*, purified from cells at the fourth-hour time-point. Additionally, *exo1-4S::A-x9PK* was analysed during meiosis by using TCA protein extraction followed by western blot. The technique of TCA protein extraction and western blot for x9PK was not consistent enough to produce reliable results. Therefore, the x9PK tag in *EXO1-4S::A* was changed to x5His-x6FLAG. This allowed the utilisation of the guanidinium hydrochloride protein extraction and the Ni-NTA affinity-purification method. The tag change was done by using the CRISPR/Cas9 system which yielded the desired strain. The phosphorylation of *exo1-4S::A-x5His-x6FLAG* during meiosis showed similar proportions and profile as the wild-type tagged Exo1. As shown in Figure 3.9b, the phosphorylation peaked after four hours of meiosis induction. Hence, the phosphorylation mutant *exo1-4S::A-x5His-x6FLAG* was phosphorylated during meiosis at the expected time, confirming previous experiments by Strong, 2017.

The inability to phosphorylate Exo1 residues that are significant in mitosis did not affect the meiotic progression of the cell. Additionally, almost all of the spores produced from *exo1-4S::A-x5His-x6FLAG* sporulation were viable, compared *Exo1-x5His-x6FLAG* and *EXO1* sporulation. In conclusion, the inability to phosphorylate mitotically significant serine residues in Exo1 did not affect Exo1 function during meiosis. In the absence of *EXO1*, the viability pattern was random and only 70.5% of the spores produced were viable, a significant reduction compared to wild-type sporulation. Hence, Exo1 is required for faithful meiosis.

Chapter 4. Investigating the dependency of Exo1 phosphorylation during the meiotic recombination pathway

Introduction:

The post-translational modification of proteins such as phosphorylation can regulate a protein's biochemical processes and it is important in cell-cycle checkpoint signalling. During meiosis the homologous recombination pathway is triggered in the presence of Spo11-DSBs. The meiotic homologous recombination pathway is similar to the homologous recombination pathway during mitosis with some differences. Whether in mitosis or meiosis, two redundant kinases Tel1 and Mec1 phosphorylate many components of the homologous recombination pathway. In addition, both kinases function in the signalling pathway triggering a cell-cycle checkpoint event (Lydall et al., 1996; Usui et al., 2001). To know whether Exo1 phosphorylation is caused by the homologous recombination kinases Tel1 and Mec1, the phosphorylation of Exo1 was examined in the presence of either or both and when they are hyper-active. The kinases are hyperactive due to the presence of unrepaired Spo11-DSBs. For example, Hop1 which is a protein required for inter-homologue repair during meiosis, is hyper-phosphorylated when DSBs are processed but not repaired (Carballo et al., 2008). There are other examples of proteins that are phosphorylated during the meiotic homologous recombination pathway such as Mre11 (Simoneau et al., 2014), Xrs2 (Simoneau et al., 2014), Rec8 (Katis et al., 2010), and Sae2 (Manfrini et al., 2010).

Exo1 phosphorylation event during mitotic cell-division was shown to inhibit Exo1 nuclease function (Morin et al., 2008). In another study, Exo1 was shown to be phosphorylated during meiosis, independent of the mitotic phosphorylation event (Strong, 2017). Several studies have showed that during yeast sporulation Exo1 had temporally and biochemically distinct

activities; a nuclease activity which required to produce long tracts of 3' ssDNA (Zakharyevich et al., 2010; Garcia et al., 2011), and a dHJs resolution activity (Tsubouchi and Ogawa, 2000; Zakharyevich et al., 2010; Keelagher et al., 2011). Therefore, the phosphorylation of Exo1 could regulate its meiotic activities. To explore the phosphorylation event further, the dependency of the phosphorylation needs to be identified during the meiotic homologous recombination pathway. This was done by analysing Exo1 phosphorylation in different mutants in the homologous recombination pathway. For instance, Exo1 was hyper-phosphorylated during the meiosis of the double mutant *dmc1Δ rad51Δ* (Strong, 2017), where DSBs were over-resected (Hunter and Kleckner, 2001). Therefore, the hyper-phosphorylation of Exo1 and the over-resection could be correlated. To understand this phosphorylation event further, Exo1 will be analysed during the meiosis of cells that are defected in Spo11-DSB processing such as *sae2Δ* and *mre11* mutants. In these mutants the inability to repair Spo11-DSBs trigger a cell-cycle checkpoint, which has been proposed to hyper-activate the Tel1-mediated cell cycle checkpoint as reviewed by Longhese et al., 2009. Both of these mutants would exaggerate the cell-cycle checkpoint response, which has been implicating in hyper-phosphorylating DSB-processing proteins.

The kinase responsible of phosphorylating Exo1 during meiosis also needs to be characterised. There are three key kinases that control the homologous recombination pathway during meiosis, Cdc28, Mek1, Tel1, and Mec1. The cyclin-dependent kinase Cdc28 directly regulates DNA DSBs that initiate recombination (Henderson et al., 2006), and controls DNA-end resection via Sae2 (Huertas et al., 2008). Mek1 is a master regulator of meiosis, it controls the entry to meiosis, and have a major function in inter-homologue recombination bias (Hollingsworth, 2016). Tel1 and Mec1 both regulate the meiotic recombination pathway, specifically in the formation and processing of Spo11-DSBs. Thus, Exo1 phosphorylation will be tested in strains that are deficient in Tel1 and/or Mec1 during meiosis. Finally, as Exo1 has

two temporal and distinct functions during meiosis, the phosphorylation event needs to be tested if it is DSB end processing dependent or dHJs resolution dependent. This was done by examining the phosphorylation of Exo1 in the absence of *NDT80* as joint-molecules are not resolved and stay intact in this mutant (Allers and Lichten, 2001).

In this chapter, three repeats were done for each experiment to confirm the reproducibility of the results. The aim of this chapter is to investigate the phosphorylation of Exo1 during the sporulation of different meiotic mutants. This will help in understanding the underlying function and the dependency of Exo1 phosphorylation during meiosis.

Results:

4.1 Exo1 phosphorylation is Spo11-double-strand break dependent:

Spo11 is a topoisomerase-like protein that initiates meiotic recombination by the formation of DNA-DSBs (Keeney et al., 1997). As demonstrated in chapter 3, the phosphorylation of Exo1 peaked after four hours of meiosis induction which coincides when most of Spo11-DSBs are formed. Therefore, it is logical to consider that Exo1 phosphorylation is correlated to DNA-DSB ends processing. To test whether this phosphorylation event is dependent on meiotic recombination processing, the phosphorylation event was tested in a nuclease mutant *spo11-Y135F*. In this mutant, the tyrosine-135 residue is mutated to phenylalanine which lacks the catalytic –OH group preventing DSB formation (Bergerat et al., 1997). A diploid homozygous strain that expresses *Exo1-x5His-x6FLAG* and *spo11-Y135F* was induced into meiosis. Samples were taken every two hours and protein extraction was performed followed by Ni-NTA affinity-purification. Upon western blot analysis, the electrophoretic mobility shift of Exo1 could not be observed, Figure 4.1a. However, a smear was observed at the sixth and eighth hour time-points. The phosphorylation/smear signal was barely detected when the bands were quantified for the first three time-points, Figure 4.1b. A phosphorylation proportion of around 9% was detected after six and eight hours of meiotic induction, $8.8\% \pm 1.2$ and 8.7 ± 2.2 respectively. The lack of Exo1 upshift band at the fourth hour time-point suggests that Exo1 phosphorylation was dramatically reduced in the absence of Spo11-DSBs. This also suggests that this phosphorylation event dependence on the formation of Spo11-DSBs. The meiotic progression of the strain was tested, as shown in Figure 4.2, the meiotic progression of *spo11-Y135F* strain was earlier than wild-type, consistent with published data (Cha et al., 2000). This is because the activation of the cell cycle checkpoint is dependent on DSB induction, and the cell cycle checkpoint is not activated in this mutant, thus the cells meiotic progression was not disrupted by the DNA damage cell-cycle checkpoint.

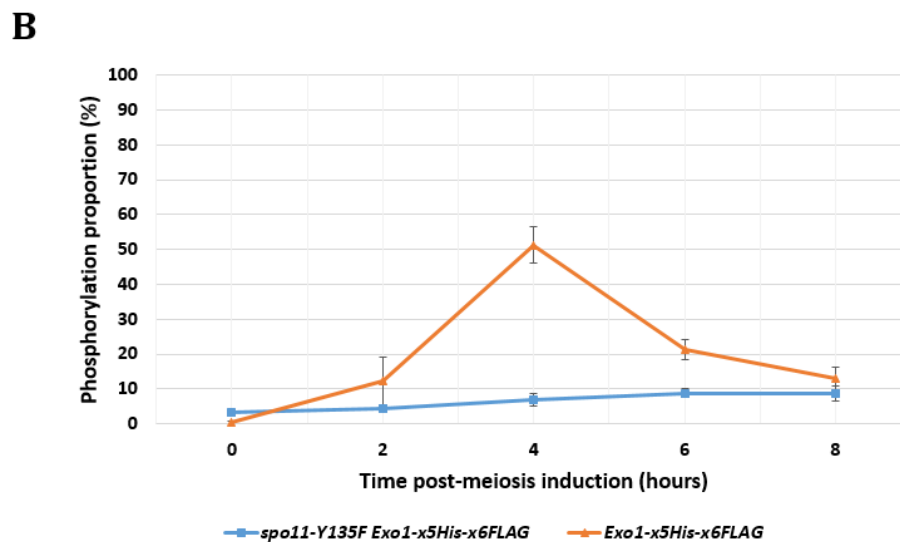
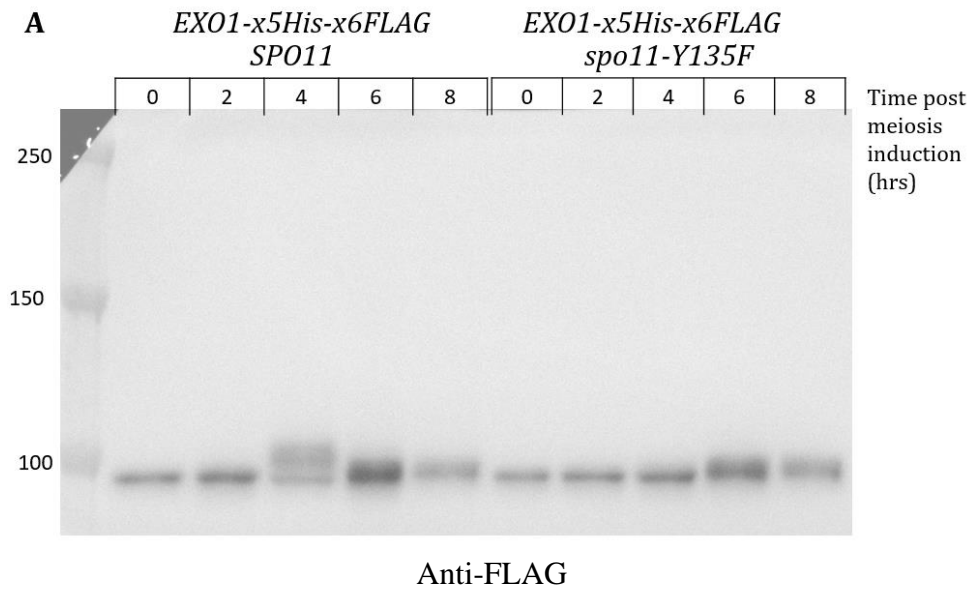


Figure 4.1 Analysis of Exo1 phosphorylation during *spo11-Y135F* sporulation

A) Western blot analysis of Exo1 during the meiosis of *spo11-Y135F* mutant. In the mutant sample, Exo1 did not show an electrophoretic mobility shift at the fourth-hour time-point. A smear can be observed at the sixth and eighth-hour time-points, similar to the smear observed in *SPO11* strain at the same time-points.

B) Phosphorylation proportion analysis of Exo1 showed a very weak phosphorylation signal at the fourth-hour time-point ($7.1\% \pm 1.8$). $n = 3$, error bars represent the standard deviation from the mean. The phosphorylation proportion increased to $8.8\% \pm 1.2$ and $8.7\% \pm 2.2$ at six and eight hour time-points respectively. This correlates to the smear seen in the western blot.

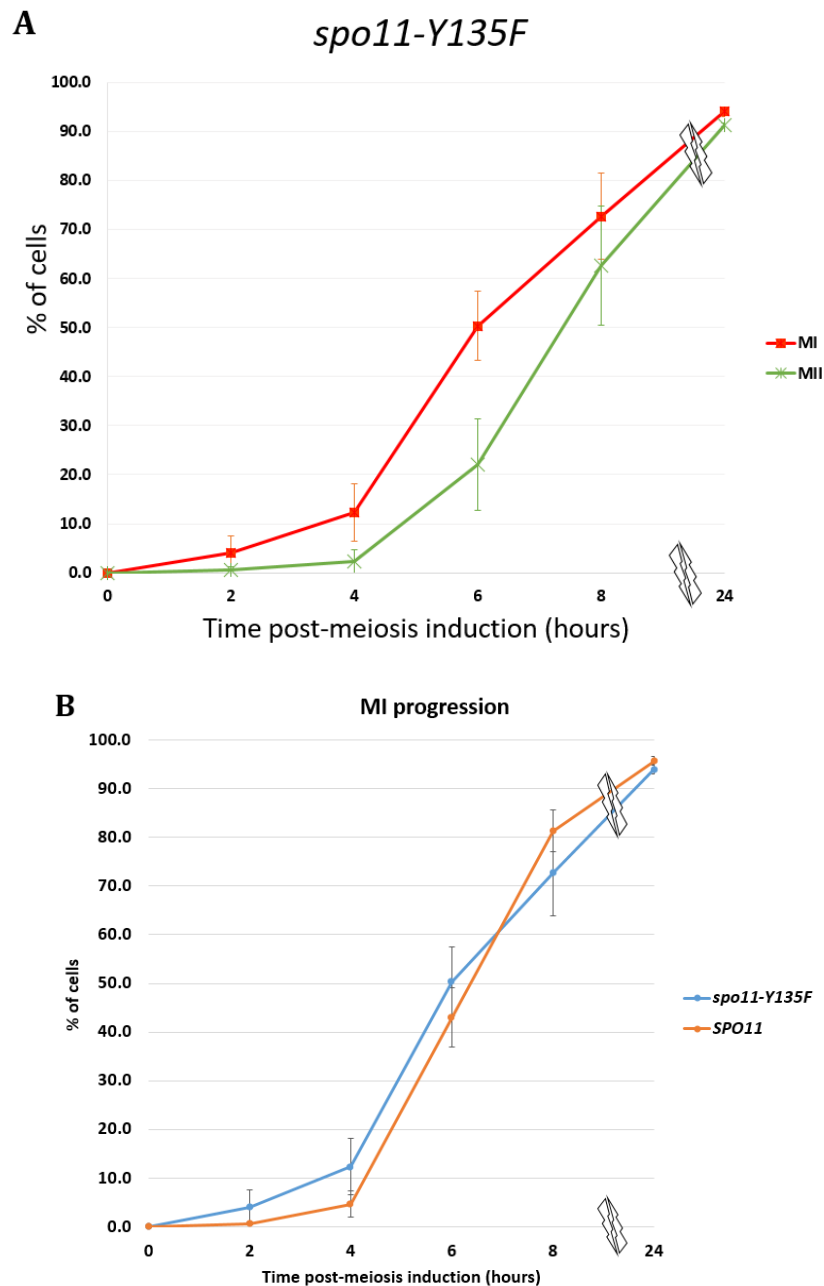


Figure 4.2 Analysis of *spo11-Y135F* meiosis progression

- A) *spo11-Y135F* nuclear division analysis showed an early meiosis. $n = 3$, error bars represent the standard deviation from the mean. After four-hours of meiosis induction $12.3\% \pm 5.8$ of cells went through MI which is higher than expected. At the sixth hour time-point, $50.3\% \pm 7.0$ of cells went through MI and $22.0\% \pm 9.3$ of cells went through MII. After eight hours of meiosis induction the majority of cells went through all stages of meiosis, $72.7\% \pm 8.8$ of cells went through MI and $62.7\% \pm 12.2$ went through MII. Eventually after 24-hours of meiosis induction, $91.3\% \pm 0.3$ of cells went through all stages of meiosis.
- B) MI progression comparison between *spo11-Y135F* and *Exo1-x5His-x6FLAG*. *spo11-Y135F* showed early MI progression at 2, 4, and 6 hour time-points.

4.2 The phosphorylation of Exo1 is normal in pachytene arrested cells

The meiotic prophase pathway act as a checkpoint ensuring that homologous chromosomes had formed bivalents, and JMs are produced. *NDT80* is a meiotic specific transcription factor that is responsible for the exit from pachytene (Xu et al. 1995). In the absence of *NDT80* during meiosis, cells are arrested at the pachytene stage where the SC remains intact with unresolved JMs (Allers and Lichten 2001). To test whether Exo1 phosphorylation is dependent on dHJ resolution, the phosphorylation event was studied during the meiosis induction of *ndt80Δ* mutant that expresses *Exo1-x5His-x6FLAG* protein. Samples were taken every two hours, post-meiosis induction until the eighth hour for protein purification followed by western blot analysis. As shown in Figure 4.3a, the electrophoretic mobility shift of Exo1 in the absence of *NDT80* appeared to be similar to the upshift observed in wild type samples. The upshift increased in signal followed by a decrease at similar time-points to wild type. The phosphorylation proportion in *ndt80Δ* samples peaked at $49.5\% \pm 4.7$ after four hours of meiosis induction, Figure 4.3b. This is similar to the wild type meiosis phosphorylation proportion, which peaked at $51.2\% \pm 5.2$ at the same time-point. However, in this mutant the phosphorylation proportion at the sixth-hour time-point was higher than wild type, $35.0\% \pm 2.0$ and $21.3\% \pm 2.8$ respectively. When the meiotic progression of *ndt80Δ* strain was analysed, all cells were mono-nucleated at all tested time-points. This confirms the pachytene arrest phenotype of *ndt80Δ*. Since Exo1 was phosphorylated and dephosphorylated in this mutant. This result suggest that Exo1 phosphorylation occur at the early stages of DNA DSB processing and is independent to JMs resolution.

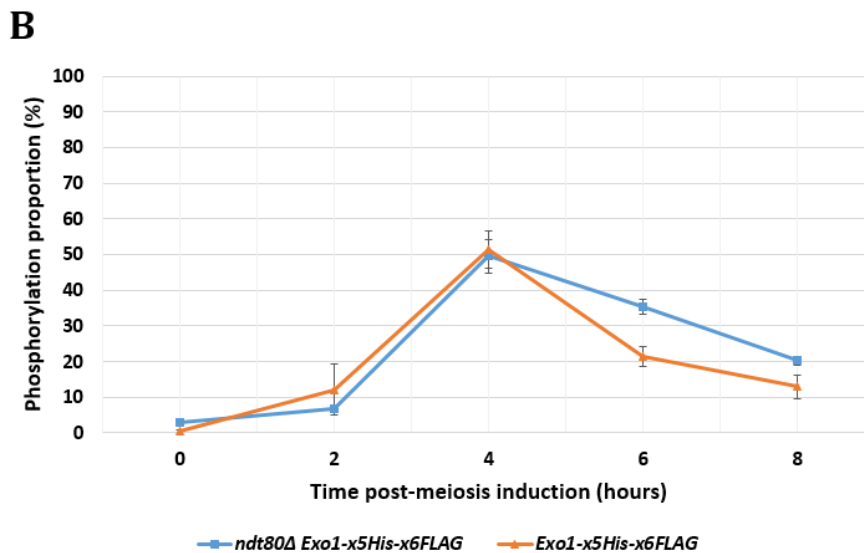
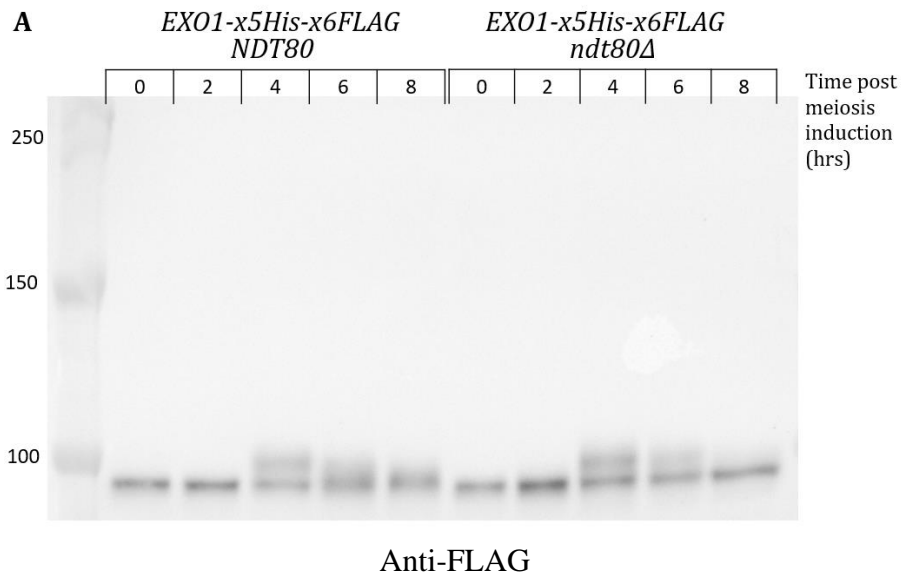


Figure 4.3 Exo1 phosphorylation was relatively normal in pachytene arrested mutant *ndt80Δ*

- A)** Western blot analysis of Exo1 during the meiosis of *ndt80Δ* strain. Exo1 electrophoretic mobility shift can be observed after four hours of meiosis induction. The upshifted band was then reduced at the subsequent time-points similar to *NDT80* strain.
- B)** Exo1 meiotic phosphorylation proportion in the absence of *NDT80*. $n = 3$, error bars represent the standard deviation from the mean. The phosphorylation proportion peaked at $49.5\% \pm 4.7$ after four hours of sporulation and was then reduced to $35.3\% \pm 2.0$, and to $20.2\% \pm 1.3$ after six and eight hours of meiosis induction respectively.

4.3 **Exo1 is over-phosphorylated during the meiosis of *dmc1Δ/rad51Δ* double-mutant**

Exo1 is involved in two temporal and biochemical distinct activities during meiosis which are DNA resection and procrossover functions (Zakharyevich et al., 2010). To isolate the function of Exo1 to DSB resection, a strain that lacks the nucleofilament proteins formation was used to analyse Exo1 phosphorylation; *dmc1Δ/rad51Δ*. Dmc1 is a meiotic specific RecA homologue that can bind to RPA 3' ssDNA creating a Dmc1-DNA nucleofilament that is crucial for homologue strand invasion (Bishop et al., 1992). Rad51 is also a RecA homologue with multifunctional properties, it catalyses recombination directly in mitosis (Shinohara et al., 1992) and indirectly, via Dmc1, during meiosis (Cloud et al., 2012). In the absence of both proteins, the strand invasion step cannot occur, with over-resected 3' ssDNA, and no dHJs are formed (Schwacha and Kleckner, 1997; Hunter and Kleckner, 2001). The double-mutant *dmc1Δ rad51Δ* strain expressing *Exo1-x5His-x6FLAG* was induced into meiosis and samples were taken every two hours. Ni-NTA purification was performed, and Exo1 was analysed by western blot. As shown in Figure 4.4a, Exo1 electrophoretic mobility shift appeared after four-hours of meiosis induction and was apparent after six hours of sporulation where it persisted until the eight-hour time-point. In contrast, the upshifted band in *DMC1* strain can be only observed at the four-hour time-point, and earlier than the phosphorylation observed in *dmc1Δ rad51Δ* samples. As shown in Figure 4.4b, the phosphorylation proportion was at $37.4\% \pm 9.1$ after four hours of sporulation followed by a steady increase to $52.1\% \pm 5.9$, and then to $53.4\% \pm 5.8$, after six hours and eight hours of sporulation respectively. Since DNA repair cannot be completed in this mutant and strand-invasion cannot occur. This result suggests that Exo1 is phosphorylated prior to strand invasion. Additionally, the hyper-phosphorylation event might be correlated to the over-resection process, since Exo1 has been implicated in the over-resection process in the absence of *DMC1* (Manfrini et al., 2010),

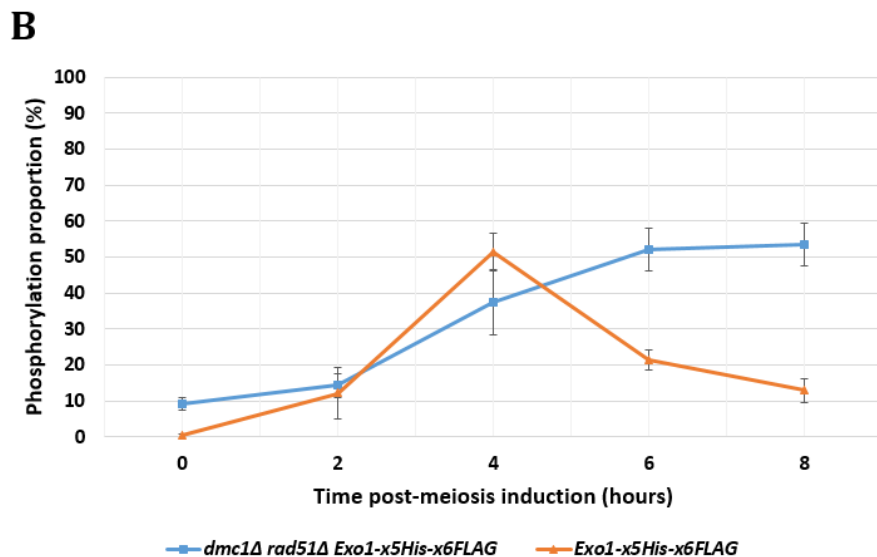
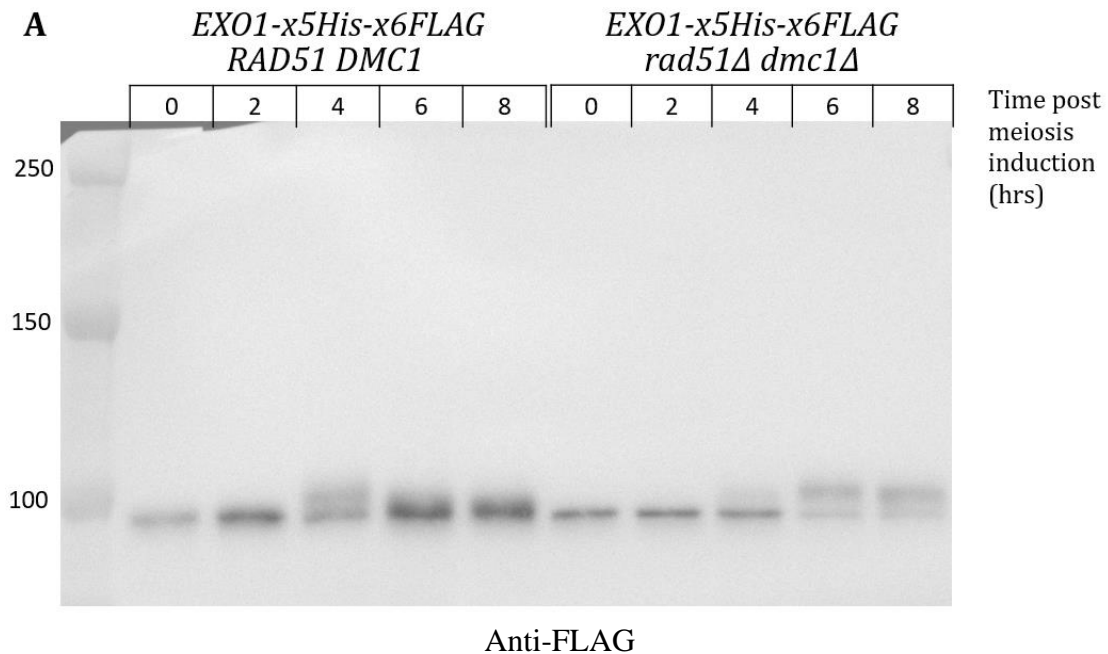


Figure 4.4 Exo1 phosphorylation persisted during the meiosis of the double-mutant *dmc1Δ rad51Δ*

- A) Western blot analysis of Exo1 during the meiosis of *dmc1Δ rad51Δ* strain. In the double-mutant samples, Exo1 electrophoretic mobility shift can be observed after four hours of meiosis induction and persisted until the eighth hour of meiosis. At the fourth hour time-point the double-mutant upshifted band had a lower intensity when compared to the *DMC1 RAD51* sample.
- B) Exo1 phosphorylation proportion analysis of *dmc1Δ rad51Δ* strain, and wild-type strain. $n = 3$, error bars represent the standard deviation from the mean. Across the double-mutant samples, the phosphorylation proportion increased to $37.4\% \pm 9.1$ after four hours of sporulation and increased further to $52.1\% \pm 5.9$ and $53.4\% \pm 5.8$ after six and eight hours of meiosis induction. The wild type strain showed lower phosphorylation proportions at six and eight hours, $21.3\% \pm 2.8$ and $12.9\% \pm 3.3$ respectively.

4.4 **The phosphorylation event of Exo1 is inter-homologue repair dependent**

To create crossovers that are essential for homologous chromosomes segregation, the repair mechanism must be biased towards inter-homologue recombination instead of sister-chromatids repair. However, during meiosis inter-sister repair could occur, specifically in highly polymorphic regions where Spo11-DSBs are induced (Goldfarb and Lichten, 2010). The meiosis specific kinase Mek1 has shown to control many of the components required for inter-homologue bias (Niu et al., 2007). To test whether Exo1 phosphorylation is dependent on Mek1 function, a *mek1-as* mutant with an increased size of the ATP binding pocket was used. The ATP binding pocket of *mek1-as* can be inhibited by the addition of a small molecule inhibitor 1-NM-PP1 (Wan et al., 2004). When *mek1-as* is inhibited, DSBs are repaired by Dmc1-independent pathways possibly by inter-sister repair (Wan et al., 2004). To test if Exo1 phosphorylation is dependent on Mek1 function, a *mek1-as* strain that also expresses *Exo1-5xHis-6xFLAG* was induced into meiosis. After three hours of meiosis induction the meiosis culture was split into two, one added with DMSO as control while the other with 2 μ M of 1-NM-PP1. The inhibition of *mek1-as* after three hours of sporulation induction was done as it is the hour before the peak of Spo11-DSBs formation and Exo1 phosphorylation. After analysing Exo1 by western blot, in the four hour time-points of both samples, the electrophoretic mobility shift of Exo1 was not observed when *mek1-as* was inhibited but was observed when *mek1-as* was not inhibited, Figure 4.5a. As shown in Figure 4.5b, the phosphorylation proportion of *mek1-as* with DMSO peaked at 41.3% \pm 2.8 after four hours of sporulation and then subsequently reduced. The phosphorylation proportion signal was drastically reduced when *mek1-as* was inhibited with phosphorylation proportion below 10% across all time-points. The meiotic progression of *mek1-as* was relatively similar to inhibited *mek1-as*, as MI progression was similar, Figure 4.6. The progression through MII was also similar for *mek1-as* and inhibited *mek1-as*.

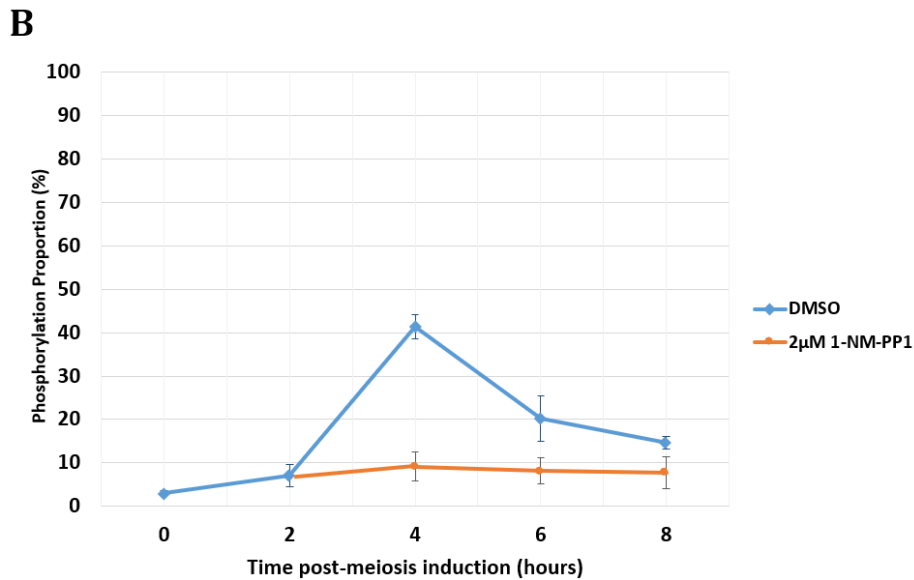
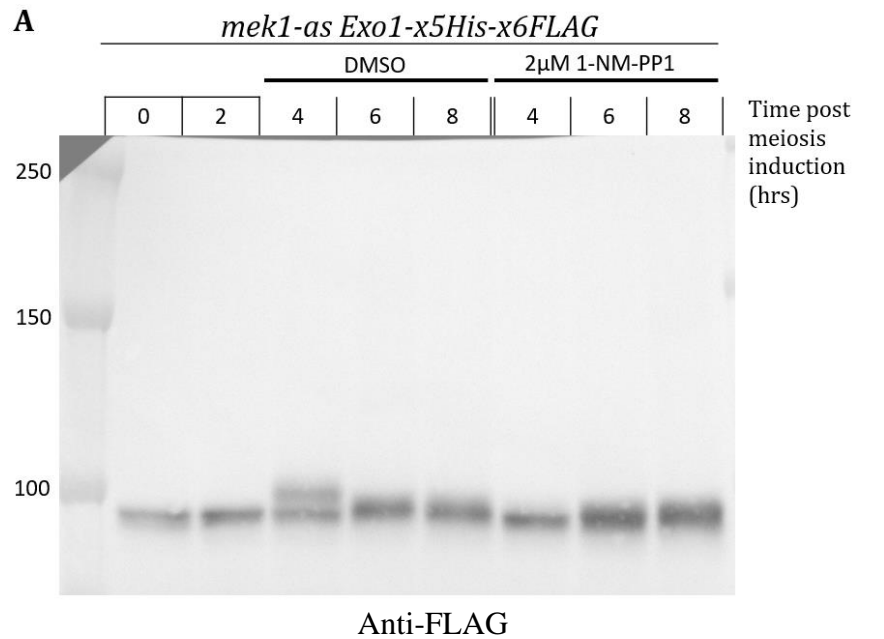


Figure 4.5 Phosphorylation analysis of Exo1 during *mek1-as* meiosis. *mek1-as* was inhibited at the third-hour of sporulation induction.

- A)** Western blot analysis of Exo1 during the meiosis of *mek1-as* strain. The cell culture was split into two after three-hours of meiosis induction. Promptly DMSO was added for one culture as control, and 2 μ M of 1-NM-PP1 was added to the second culture. At the fourth-hour time-point, only the sample taken from the DMSO culture showed an Exo1 electrophoretic mobility shift and no upshift band was observed when *mek1-as* was inhibited.
- B)** The phosphorylation proportion of the control sample (DMSO) peaked at 41.3% \pm 2.8 after four hours of sporulation, this was followed by a steady decrease to 20.2% \pm 5.2 and 14.6% \pm 1.5 at the subsequent time-points. $n = 3$, error bars represent the standard deviation from the mean. The phosphorylation was barely detected after the inhibition of *mek1-as* with values below 10% across all time-points (9.2% \pm 3.3, 8.1% \pm 3.0, 7.7 \pm 3.7 for four, six, and eight hours respectively).

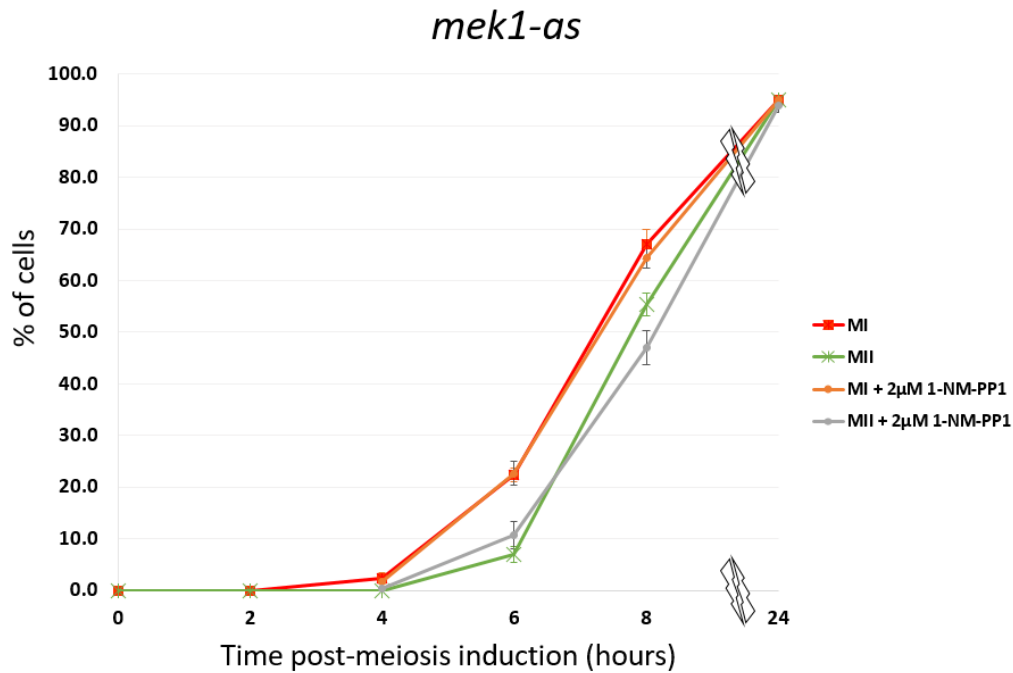


Figure 4.6 Nuclear division analysis for *mek1-as* during meiosis showing MI and MII progression when *mek1-as* was inhibited and non-inhibited.

MI progression was very similar between both cultures. $n = 3$, error bars represent the standard deviation from the mean. After six hours of meiosis induction, $22.3\% \pm 1.3$ of cells from *mek1-as* culture went through MI. At the same time-point, $22.7\% \pm 2.6$ of cells from the inhibited *mek1-as* culture went through MI. At the subsequent time-point $67.0\% \pm 2.9$ and $64.3\% \pm 3.2$ of cells went through MI, from *mek1-as* and inhibited *mek1-as* respectively. The MII progression of both cultures were very similar. After eight hours of meiosis induction, $55.3\% \pm 2.9$ and $47.0\% \pm 3.2$ of cells went through MII, from *mek1-as* and inhibited *mek1-as* respectively.

This result suggests that the phosphorylation of Exo1 is dependent on Mek1 kinase function, as Exo1 electrophoretic mobility shift was absent when *mek1-as* was inhibited. In the absence of Mek1 kinase function, most of the DSBs are transiently repaired by inter-sister repair (Wan et al., 2004; Terentyev et al., 2010). This means that the exaggerated electrophoretic mobility shift of Exo1 observed during wild-type meiosis can be correlated to inter-homolog repair. This however does not rule out the possibility of Exo1 phosphorylation during inter-sister repair in meiosis.

4.5 Exo1 is not phosphorylated in the absence of Tel1 and Mec1 kinases:

As Spo11-DSBs are formed, Tel1 and Mec1 kinases become active, controlling major components of the homologous repair pathway (Lydall et al., 1996; Usui et al., 2001; Cheng et al., 2013). Both Tel1 and Mec1 kinases are serine/threonine kinases (Mallory and Petes, 2000). They preferentially phosphorylate their substrates on serine or threonine residues that precede glutamate residues, that is known as SQ/TQ (Traven and Heierhorst, 2005). The Tel1 kinase phosphorylates the MRX complex and Sae2 in the presence of DSBs (Usui et al., 2001; Terasawa et al., 2008). This phosphorylation event promotes the processing and the repair of DSB ends. Resected DNA ends lead to the activation of Mec1 in a positive feedback loop, leading to a cell cycle arrest via the inhibition of Ndt80 (Gray et al., 2013). For instance in absence of Dmc1 and Mec1 functions, cells proceed through meiosis without repairing DSBs, bypassing a cell cycle checkpoint (Lydall et al., 1996). Therefore, the activity of both kinases ensures that DSBs are completely repaired before proceeding in meiosis. There are other functions that both kinases take part on, for example Tel1 also functions in preventing clusters of Spo11-DSBs forming at a local site, which is theorised to help in dispersing DSBs along the chromosomes (Garcia et al., 2015). Also both kinases are implicated in inter-homolog repair

bias, via phosphorylation of Hop1 and the subsequent activation of Mek1 (Carballo et al., 2008).

To test whether the phosphorylation of Exo1 is influenced by Tel1 and Mec1 the phosphorylation was analysed in the absence of one of the kinases or both. A *tel1Δ* strain and a *TEL1* strain expressing *Exo1-x5His-x6FLAG* were induced into meiosis and sampled every two hours. Upon western blot analysis, the electrophoretic mobility shift of Exo1 showed after four hours of meiosis induction for both strains, Figure 4.7a. Exo1 upshift appeared at similar time-points in both *TEL1* and *tel1Δ* samples. The phosphorylation proportion of Exo1 in the absence of Tel1 peaked at $39.6\% \pm 4.8$ after four hours of meiosis induction, Figure 4.7b. A slight reduction to the phosphorylation peak observed in *TEL1* meiosis ($51.2\% \pm 5.3$). At six and eight hour time-points the phosphorylation proportion in *tel1Δ* sample was slightly higher than *TEL1*, $26.7\% \pm 3.5$, and $17.5\% \pm 2.8$ respectively. This result suggest that Exo1 phosphorylation might not be dependent on Tel1 function. The meiotic progression of this strain was drastically delayed, as shown by the MI and MII progressions in Figure 4.8a and Figure 4.8b. This might be because in the absence of Tel1, Spo11-DSBs rates are higher than normal requiring more time for their repair. The delay in meiosis progression observed here could influence the reduced phosphorylation proportion observed in this mutant.

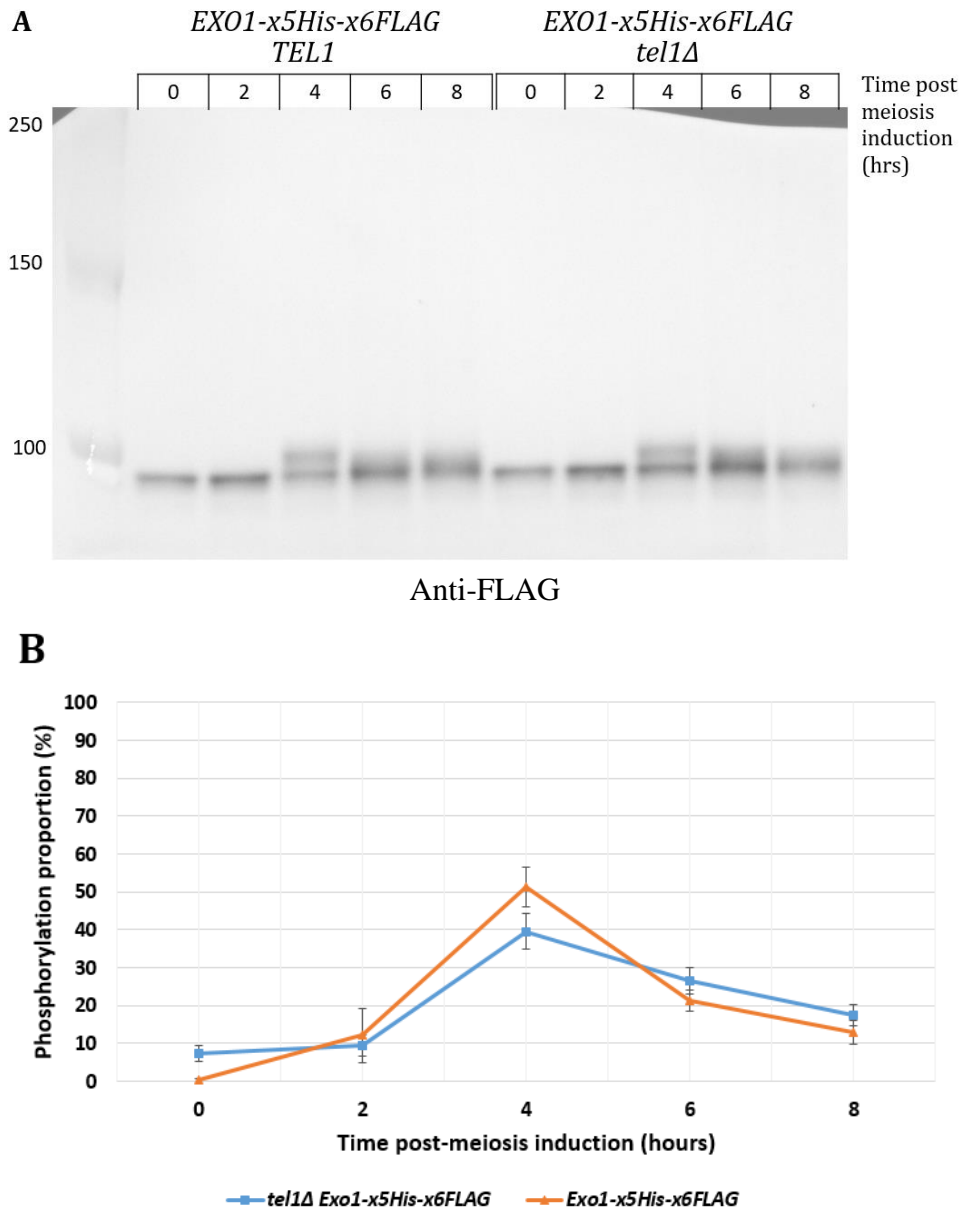


Figure 4.7 Analysis of Exo1 phosphorylation during the meiosis of *tel1Δ* mutant and *TEL1*

- A) Western blot analysis of Exo1 during the meiosis of *tel1Δ* strain. Exo1 mobility shift was similar in both strains. The upshifted band appeared after four hours of meiosis induction and was then reduced to a smear after six and eight hours of meiosis.
- B) Phosphorylation proportion analysis for Exo1 during *tel1Δ* meiosis. $n = 3$, error bars represent the standard deviation from the mean. The phosphorylation proportion peaked at $39.6\% \pm 4.8$ at the four-hour time-point, and then decreased to $26.7\% \pm 3.5$, and $17.5\% \pm 2.8$ at the next time-points. The phosphorylation of Exo1 in *TEL1* strain peaked at a higher point and at the same time-point as in *tel1Δ* strain.

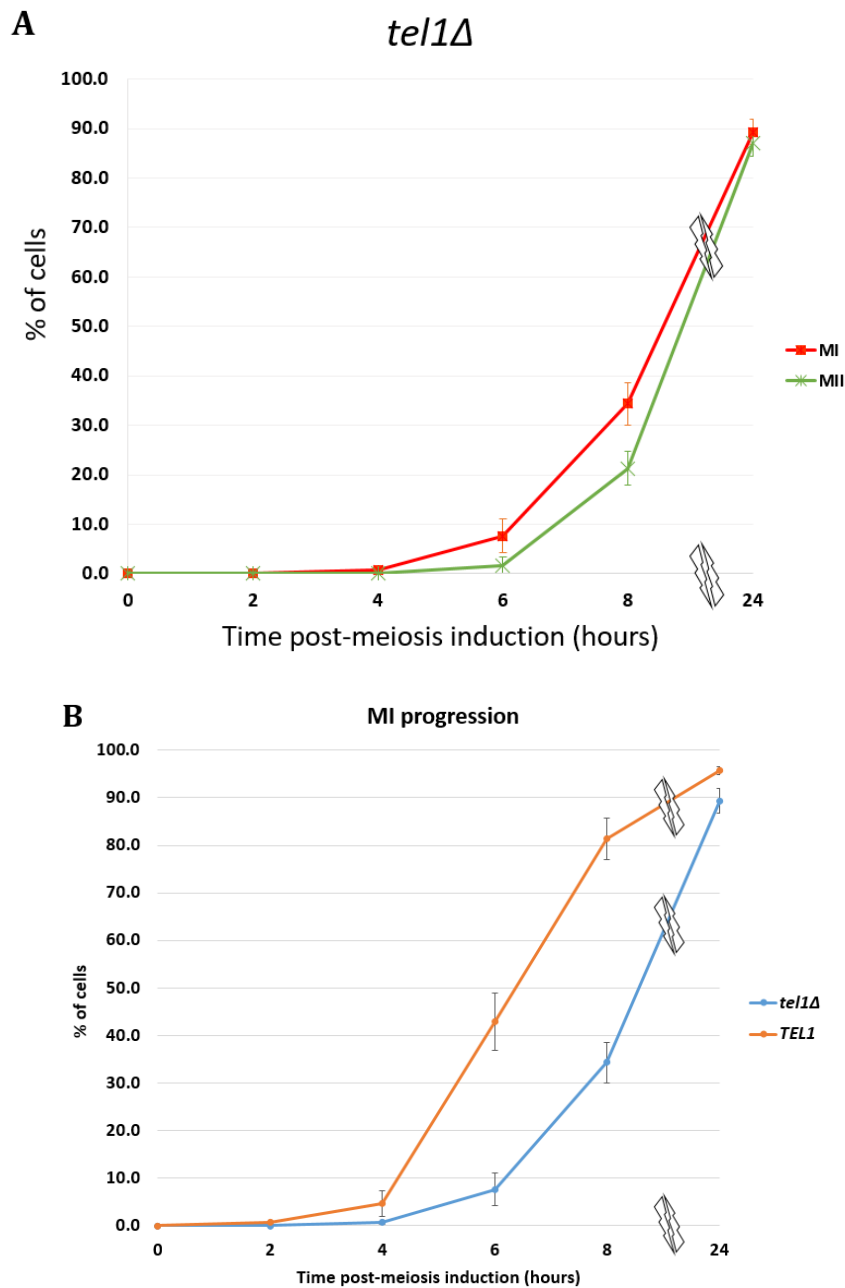


Figure 4.8 Nuclear division analysis of *tel1Δ* strain

- A) MI and MII progression for *tel1Δ* strain. $n = 3$, error bars represent the standard deviation from the mean. The meiotic progression of the strain was delayed as after six hours of meiosis induction only $7.7\% \pm 3.5$ of cells went through MI and $1.7\% \pm 1.7$ of cells went through MII. After eight hours of meiosis induction, $34.3\% \pm 4.3$ of cells went through MI and $21.3\% \pm 3.5$ went through MII. Eventually, $87.0\% \pm 2.5$ of cells went through MII after 24-hours of meiosis induction.
- B) MI progression of *tel1Δ* and *TEL1* strain when both strains express *Exo1-x5His-x6FLAG*. The *tel1Δ* showed a very delayed MI progression.

Mec1 is an essential kinase during the cell cycle, deleting the gene causes cell death. This is due the essential function of Mec1 during DNA replication as it controls Sml1 which regulates deoxyribonucleotide pools (Zhao et al., 2001). However, deleting both genes *MEC1* and *SML1* does not affect cell growth. To test whether Mec1 influence the phosphorylation of Exo1, a double-delete mutant was made; *mec1Δ sml1Δ*, which expresses *Exo1-x5His-x6FLAG*. The strain was induced into meiosis with *MEC1 SML1* strain and samples were taken every two hours of sporulation. Upon western blot analysis, the electrophoretic mobility shift of Exo1 across *mec1Δ sml1Δ* samples was significantly reduced when compared to *MEC1 SML1* samples, Figure 4.9a. In *mec1Δ sml1Δ* six- and eight-hours samples, a smear can be observed that is preceding Exo1 non-modified band. The phosphorylation proportion of Exo1 was significantly reduced across *mec1Δ sml1Δ* samples, Figure 4.9b. At the fourth hour time-point, Exo1 phosphorylation proportion was at $20.7\% \pm 3.0$ in *mec1Δ sml1Δ* sample, compared to $51.2\% \pm 5.3$ for *MEC1 SML1*. Since the electrophoretic mobility of Exo1 was reduced in this mutant, this result suggest that Exo1 phosphorylation might be dependent on Mec1 function. The meiotic progression of *mec1Δ sml1Δ* strain was late as shown in Figure 4.10a. When compared to *MEC1 SML1*, the meiotic progression of the strain showed a significant delay, and spore production was defected, Figure 4.10b. The reduced electrophoretic mobility shift observed could be because of defective meiotic progression of the cell, which may have affected the synchronisation of the cells.

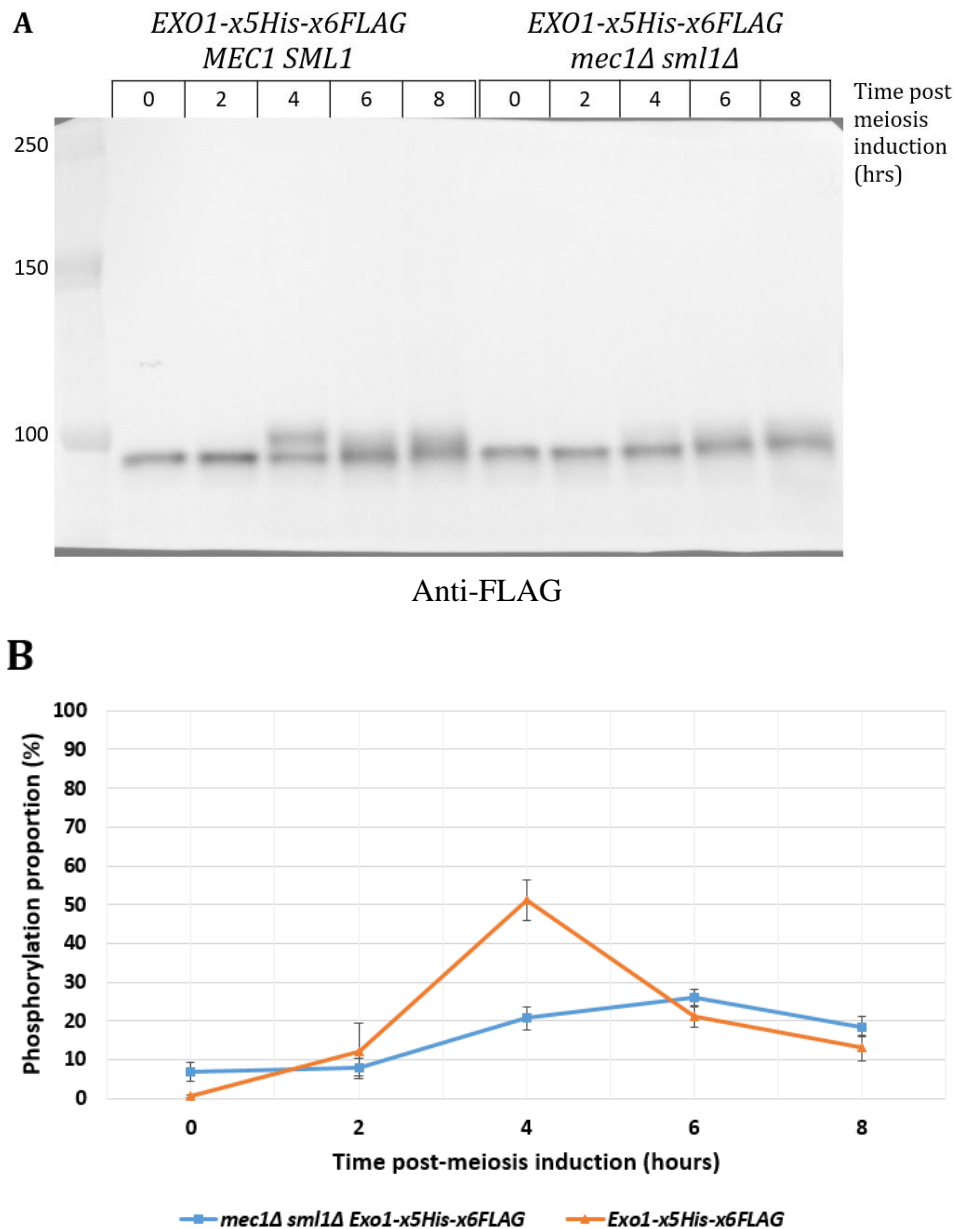


Figure 4.9 Analysis of Exo1 phosphorylation during the meiosis of *mec1Δ sml1Δ* strain

A) The western blot of Exo1 did not show an electrophoretic mobility shift in *mec1Δ sml1Δ* samples. A smear was observed at the four-hour time-point and increased in intensity at the six-hour time-point, this was followed by a slight decrease in signal. In *MEC1 SML1* samples, Exo1 electrophoretic mobility shift was shown as a distinctive band at the four-hour time-point and was reduced to a smear in the subsequent time-points.

B) Exo1 phosphorylation proportion analysis in *mec1Δ sml1Δ* samples. $n = 3$, error bars represent the standard deviation from the mean. In the double-deleted strain, the phosphorylation proportion was at $20.7\% \pm 3.0$ after four hours of meiotic induction. The phosphorylation proportion slightly increased at the six-hour time-point $26.0\% \pm 2.3$ and was followed by a decrease to $18.5\% \pm 2.6$ at the eight-hour time-point. In *MEC1 SML1* samples, the phosphorylation proportion peaked at $51.2\% \pm 5.3$, significantly higher than the phosphorylation proportion of the double mutant at the same time-point.

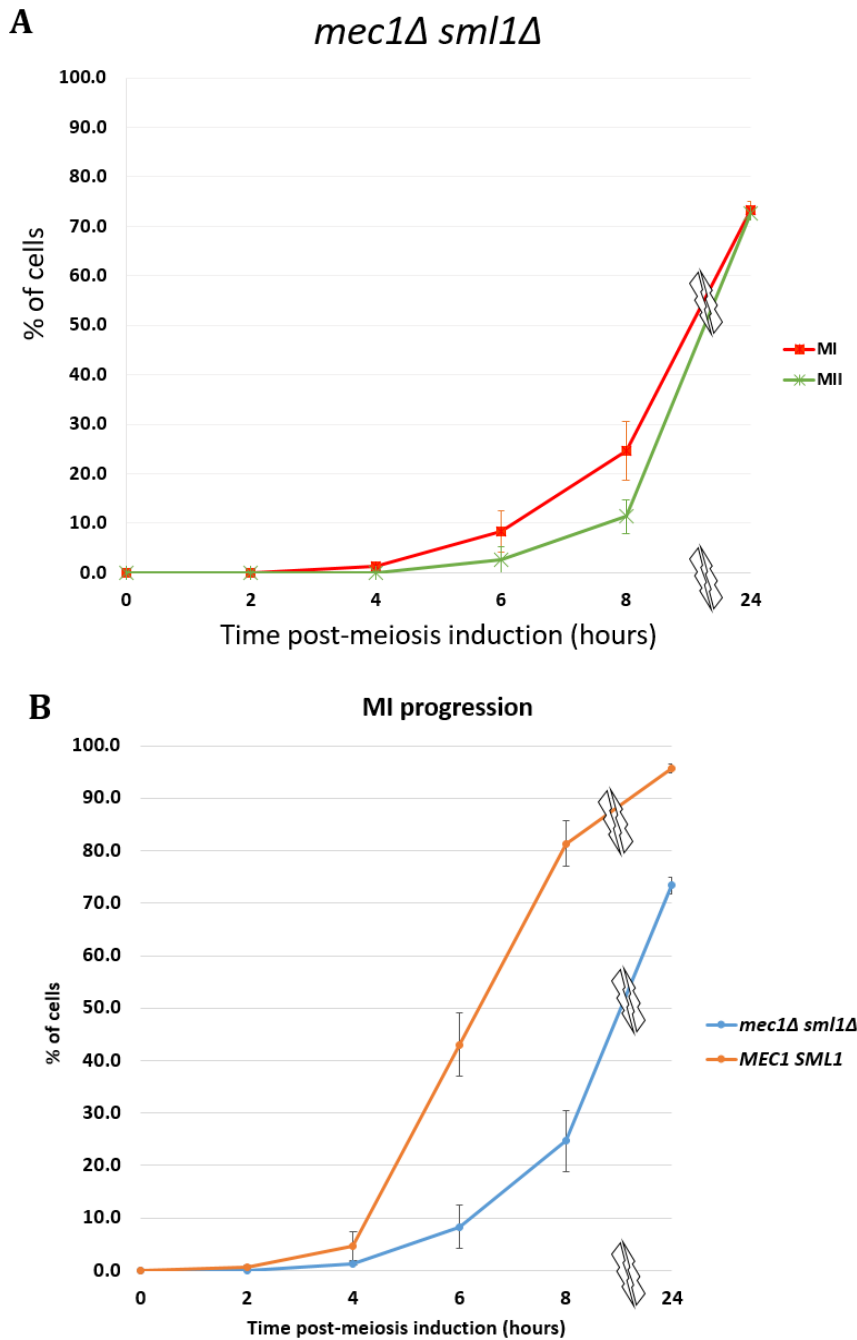


Figure 4.10 Nuclear division analysis of *mec1Δ sml1Δ* meiotic progression

- A)** The meiotic progression of *mec1Δ sml1Δ* was drastically delayed. After six hours of meiosis induction, $8.3\% \pm 4.1$ of cells went through MI and $2.7\% \pm 2.7$ went through MII. After eight hours of meiosis induction, $24.3\% \pm 5.9$ of cells went through MI and $11.3\% \pm 3.5$ of cells went through MII. After 24-hours of meiosis induction only $72.7\% \pm 1.5$ of cells managed to go through all stages of meiosis.
- B)** MI progression comparison between *mec1Δ sml1Δ* and *MEC1 SML1* strains. $n = 3$, error bars represent the standard deviation from the mean. The mutant strain showed a significant delayed and defective meiotic progression. The production of spores was reduced, and only $73.3\% \pm 1.7$ of cells managed to go through MI after 24-hours of meiosis induction.

As Exo1 phosphorylation is still observed in the absence of either Tel1 or Mec1 during meiosis. The phosphorylation event needs to be tested during meiosis and in the absence of both Tel1 and Mec1 kinases. In the absence of Tel1 and Mec1, DSBs persist throughout the meiotic program and nuclear division occur (Cartagena-Lirola et al., 2006). To reduce the mitotic effect of losing both kinase functions at the same time. A heterozygous diploid strain was made at the *MEC1* locus where one copy of *MEC1* was deleted while the other was expressed using the *CLB2* mitotic specific promoter (strain genotype in section 2.5.2, strain name: BM169). The heterozygous diploid strain was induced into meiosis, and samples were taken for western blot and nuclear division analysis. Upon western blot analysis, Exo1 electrophoretic mobility shift was not detected in absence of Tel1 and Mec1 functions, Figure 4.11a. A slight smear appeared at the sixth- and eighth-hour time-points, similar to the smear observed in wild type at the same time-points. The phosphorylation proportion of Exo1 at the fourth hour time-point was significantly lower than wild type, Figure 4.11b. However, the phosphorylation proportions at six- and eight-hours samples were similar to wild type levels in the same time points. The meiotic progression of the cells was very impaired, and it was difficult to synchronise into meiosis, Figure 4.12a. When comparing MI progression of the mutant strain and wild type, the mutant strain exhibited early meiosis progression at the initial time-points, Figure 4.12b. However, the mutant strain showed delay and defective MI progression after eight and 24-hours of meiosis induction. These results suggest that Tel1 and Mec1 function are required for normal meiotic progression and Exo1 phosphorylation is dependent on Tel1 and Mec1 kinases.

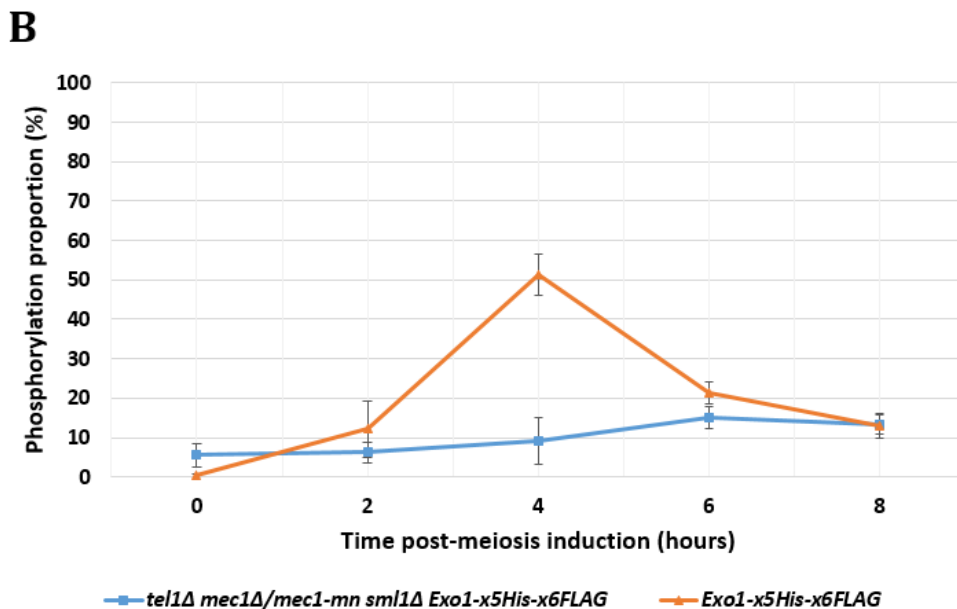
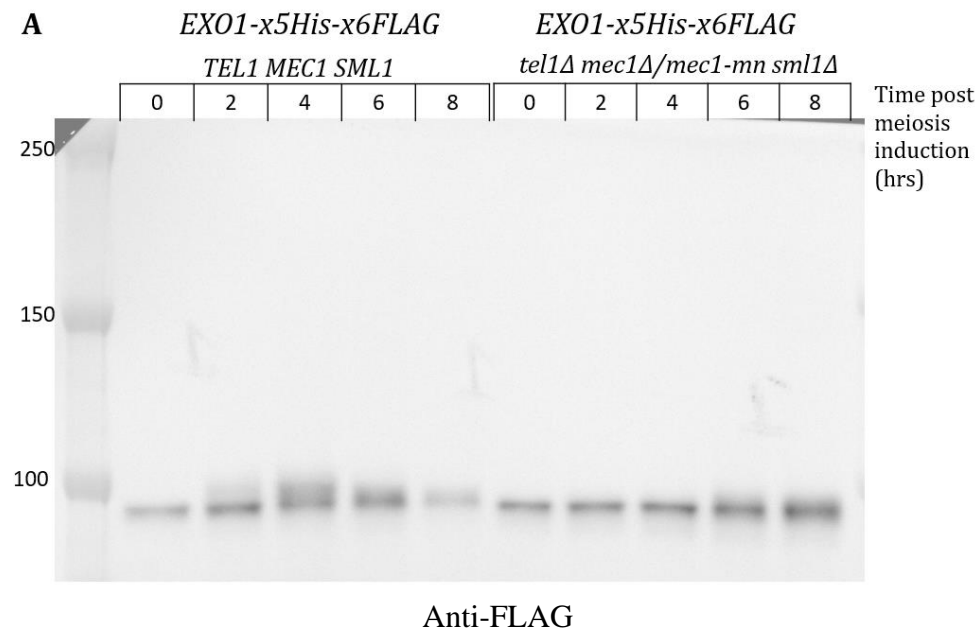


Figure 4.11 Analysis of Exo1 phosphorylation in the absence of *TEL1* and *MEC1* during meiosis

- A)** Western blot analysis of Exo1 showed no apparent electrophoretic mobility shift across all time-points. A smear can be observed across the sixth and eighth-hour time-points.
- B)** The phosphorylation proportion of Exo1 in the mutant strain samples was lower than wild-type samples. $n = 3$, error bars represent the standard deviation from the mean. At the four-hour time-point, the mutant strain showed a phosphorylation proportion of $9.2\% \pm 5.9$. After six hour and eight hours of meiosis induction the phosphorylation proportion was at $15.1\% \pm 2.8$ and $13.3\% \pm 2.3$ respectively. This increase correlates to the smear observed in the western blot.

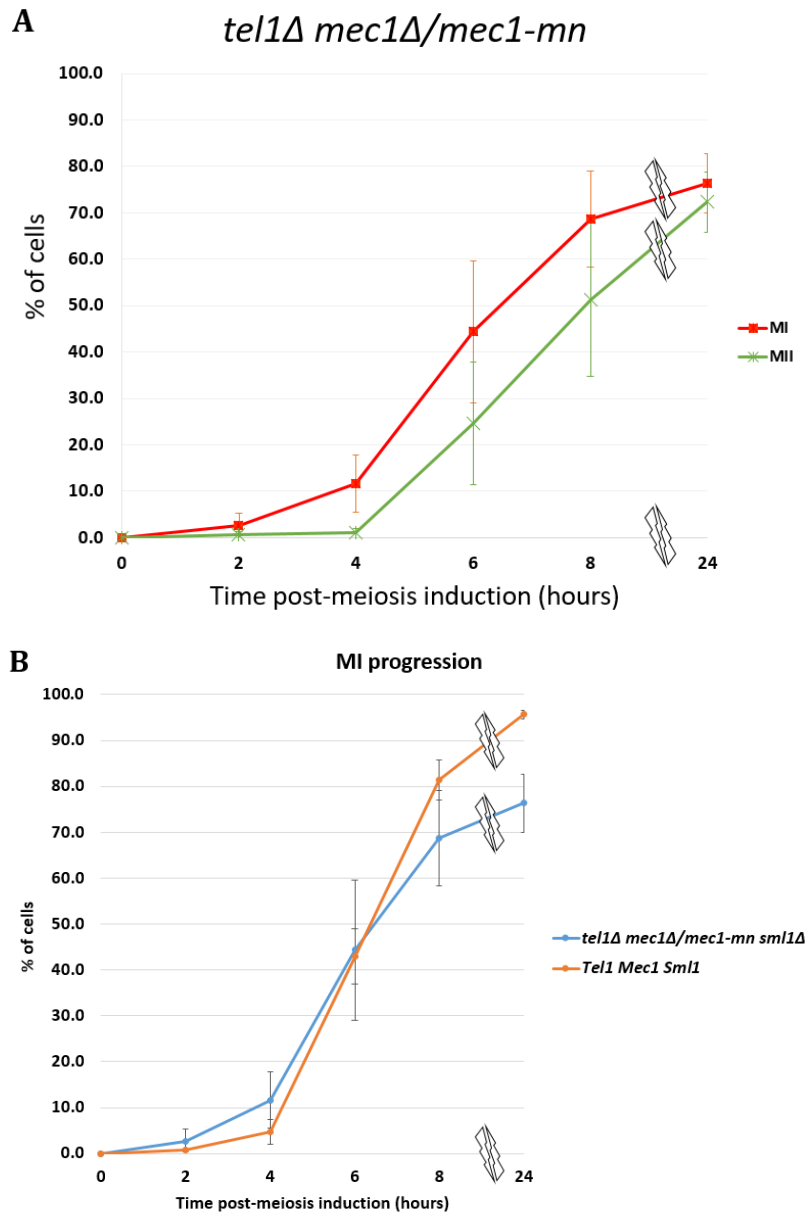


Figure 4.12 Analysis of the meiotic progression in the absence of Tel1 and Mec1 kinases

- A) MI and MII progression of the mutant strain showed an abnormal meiotic program. $n = 3$, error bars represent the standard deviation from the mean. The standard deviation of each time-point was very high, this might be because of abnormal synchronisation of the cells. After four hours of meiosis induction, $11.7\% \pm 6.2$ of cells went through MI, and $1.0\% \pm 6.2$ of cells went through MII. After six hours of meiosis induction, $44.3\% \pm 15.3$ of cells went through MI and $24.7\% \pm 13.2$ of cells went through MII. At the next time-point, $68.7\% \pm 10.4$ of cells went through MI, and $51.3\% \pm 16.5$ went through MII. Eventually after 24-hours of meiosis induction only $72.3\% \pm 6.5$ of cells managed to go through all stages of meiosis.
- B) MI progression of the double mutant and wild-type strain. The double mutant showed a slightly earlier meiosis progression at zero, two, four, and six-hour time-points. However, the double mutant showed slower MI progression after eight hours of meiosis induction. After 24-hours of meiosis induction, the mutant showed a pronounced reduction in MI progression compared to wild-type meiosis.

4.6 **The phosphorylation of Exo1 is Tel1 dependent in the absence of Sae2**

Sae2 is an endonuclease that is required for Spo11-DSB processing by regulating the Mre11 complex (Lengsfeld et al., 2007; Cannavo and Cejka, 2014). In the absence of *SAE2*, meiotic division is delayed and spore formation is reduced (Prinz et al., 1997). Additionally, Sae2 has been implicated in DSB ends processing, as Spo11 stay covalently bound to DSB ends in *sae2Δ* strain meiosis (Keeney and Kleckner, 1995; Neale et al., 2005). The lack of Sae2 has been shown to trigger the activation of Tel1 (Usui et al., 2001), possibly because the MRX complex keeps recruiting Tel1 to unrepaired DSB sites (Nakada et al., 2003). The continuous recruitment of Tel1 to unrepaired DSB sites causes the over-phosphorylation of Tel1 targets such as Hop1 (Carballo et al., 2008), Mre11, and Xrs2 (Usui et al., 2001). To test if Exo1 is a target of Tel1, the phosphorylation was examined in the absence of Sae2. Mutant *sae2Δ* strain was made that expresses *Exo1-x5His-x6FLAG* and was induced into sporulation, where samples were taken for protein and nuclear division analysis. The western blot showed an electrophoretic mobility shift for Exo1 in both strains, Figure 4.13a. Exo1 upshifted band was pronounced at four- and six-hour time-points in *sae2Δ* samples. At the eighth-hour time-point Exo1 upshifted band was closer to the non-modified band but with equal intensity. The phosphorylation proportion of Exo1 across *sae2Δ* samples was higher than wild type, especially at the sixth and eighth hour time-points, Figure 4.13b. The meiotic progression of the strain was severely impaired, and the majority of cells did not go through MII, Figure 4.14a. When the progression of MI is compared to *SAE2*, an extreme delay can be observed, Figure 4.14b, consistent with the published literature (Prinz et al., 1997). The persistence of Exo1 electrophoretic shift observed in this mutant could be correlated to Tel1 continuous activation, suggesting a role of Tel1 in Exo1 phosphorylation.

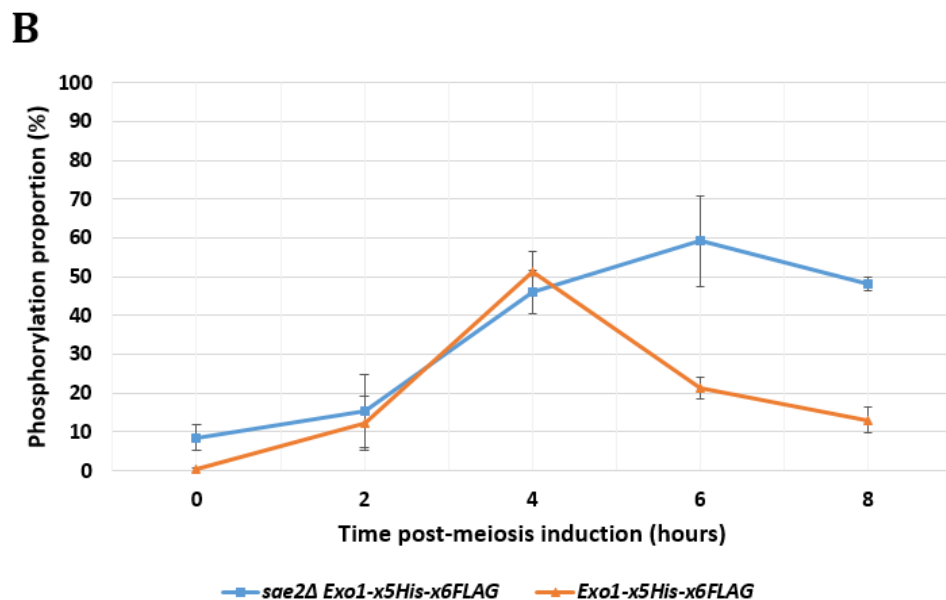
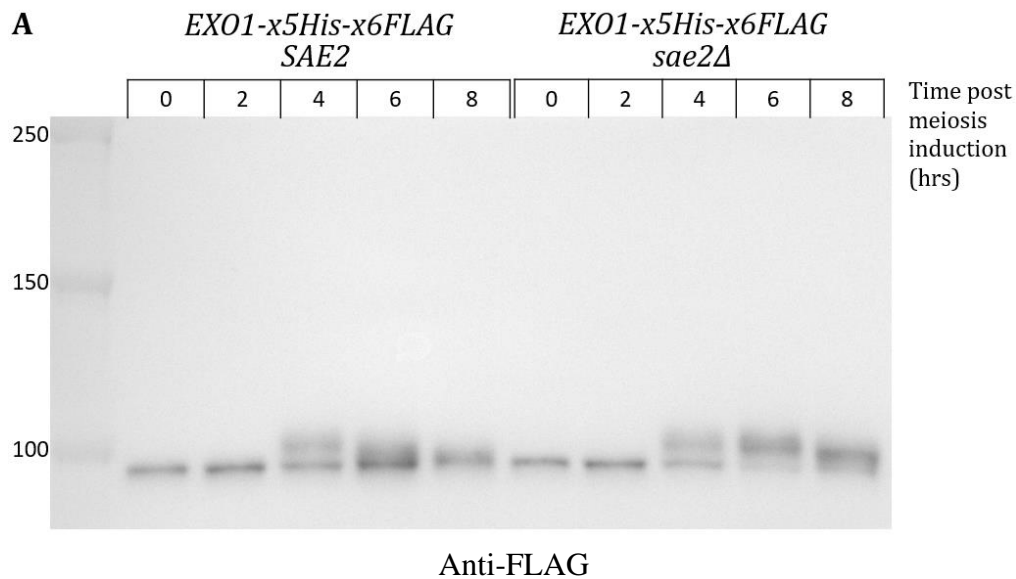


Figure 4.13 Analysis of Exo1 phosphorylation during the meiosis *sae2Δ* mutant

- A) In both mutant and wild type samples, Exo1 electrophoretic mobility shift was observed after four hours of meiosis induction. The upshifted band persisted in the mutant where it can be observed at the six-hour time-point. Exo1's mobility-shift was then slightly reduced at the eight-hour time-point, but can still be observed as two distinct bands.
- B) The phosphorylation proportion of Exo1 in *sae2Δ* samples showed a value of $45.9\% \pm 5.6$ at the four-hour time-point. $n = 3$, error bars represent the standard deviation from the mean. At the six-hour time-point the phosphorylation proportion increased further to $59.2\% \pm 11.7$, and was followed by a slight decrease to $48.1\% \pm 1.8$.

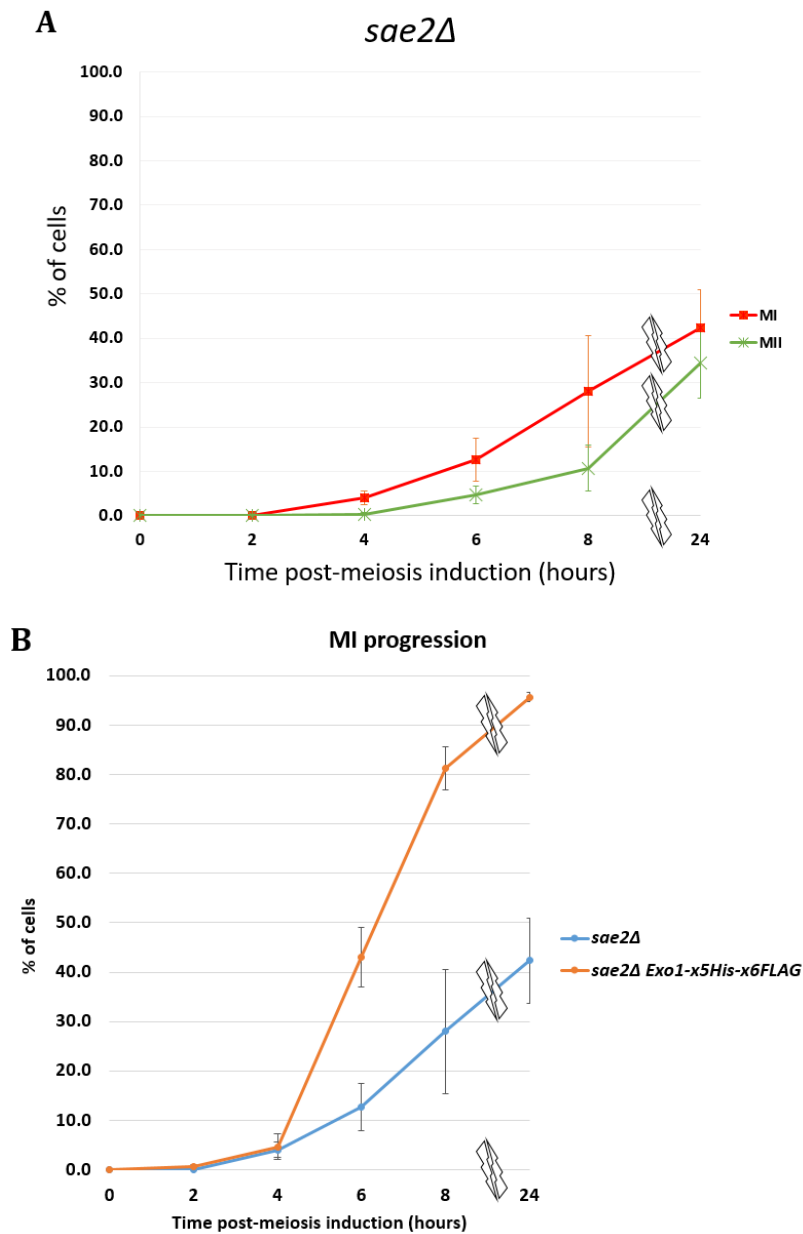


Figure 4.14 Analysis of the meiotic progression of the *sae2Δ* mutant

- A)** The meiotic progression of the cells was extremely impaired. $n = 3$, error bars represent the standard deviation from the mean. After six hours of meiosis induction $12.7\% \pm 4.9$ of cells went through MI, and $4.7\% \pm 2.03$ went through MII. After eight hours, $28.0\% \pm 12.5$ of cells went through MI, and $10.7\% \pm 5.2$ went through MII. Eventually, after 24-hours of meiosis induction only $34.3\% \pm 7.9$ of cells managed to go MII
- B)** MI progression of *sae2Δ* and *SAE2* strain. The mutant strain showed an extremely delayed and impaired meiosis. After 24-hours of meiosis induction only $42.3\% \pm 8.7$ of the mutant cells managed to go through MI.

The hyper-phosphorylation of Exo1 observed in *sae2Δ* meiosis could be caused by the continuous kinase activity of Tel1. To test this, a double deleted strain *sae2Δ tel1Δ* and a *sae2Δ* strains that express *Exo1-x5His-x6FLAG* were induced into sporulation and samples were taken every two hours. Upon western blot analysis, Exo1 electrophoretic mobility shift was not observed across all of the double mutant time-points, Figure 4.15a. However, at six and eight hour time-points, a smear can be observed on top of Exo1 band. As shown in Figure 4.15b, the phosphorylation proportion of the double mutant was significantly lower than the phosphorylation proportion observed across *sae2Δ* time-points. The meiotic progression of the double mutant was impaired and delayed, Figure 4.16a. When compared to *sae2Δ* meiotic progression, the double mutant, *sae2Δ tel1Δ*, showed more efficient meiotic progression, Figure 4.16b. This is because the deletion of *TEL1* causes the cells to bypass a cell cycle checkpoint, continuing nuclear division even when DSBs are not repaired (Gray et al., 2013). The very low phosphorylation proportion of the double mutant's samples suggests that the phosphorylation of Exo1 is dependent on Tel1, especially when Spo11 cannot be removed from DNA DSB ends.

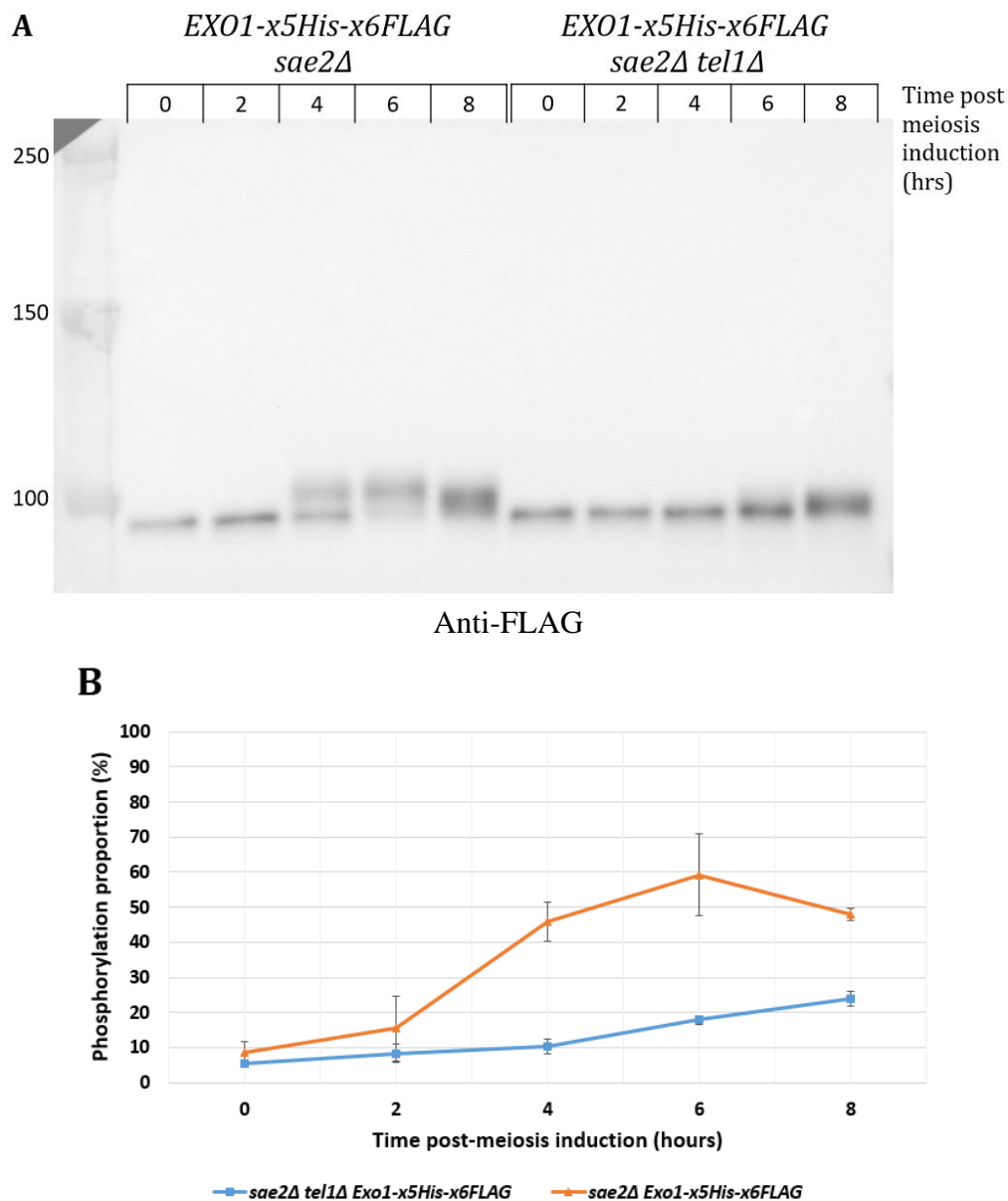


Figure 4.15 Analysis of Exo1 phosphorylation during the meiosis of *sae2Δ tel1Δ* strain

- A) The western blot did not show an electrophoretic mobility shift of Exo1 across *sae2Δ tel1Δ* samples. However, a smear can be observed in the double mutant's six and eight hour samples.
- B) The phosphorylation proportion of the double mutant was significantly lower than *sae2Δ*. $n = 3$, error bars represent the standard deviation from the mean. At the fourth hour time-point the phosphorylation proportion of the double mutant was at $10.3\% \pm 2.0$ and increased to $17.8\% \pm 1.2$, and $23.8\% \pm 2.2$ at six and eight hour time-points.
- C) The meiotic progression was abnormal. After six hours of sporulation 28% of cells were bi-nucleates and 6% were tri/tetra-nucleates. After eight hours of meiotic induction, 14% of cells were bi-nucleates, and 43% were tri/tetra-nucleates. Eventually after 24 hours, 66% of cells were tri/tetra-nucleates, most of which did not form spores.

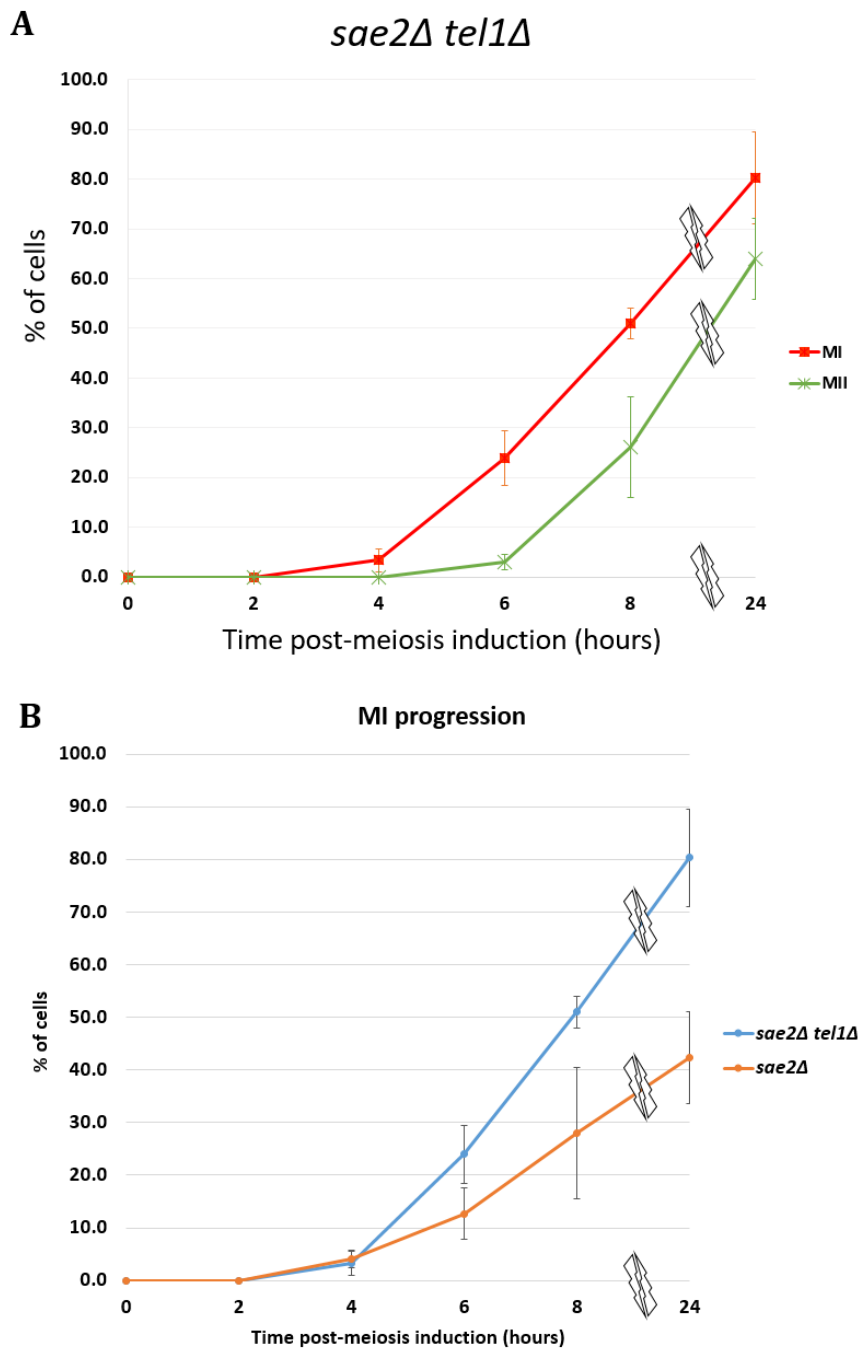


Figure 4.16 Meiotic progression analysis of *sae2Δ tel1Δ* strain

- A) The meiotic progression was abnormal. $n = 3$, error bars represent the standard deviation from the mean. After six hours of meiosis induction, $24.0\% \pm 5.5$ of cells went through MI, and $3.0\% \pm 1.5$ went through MII. At the subsequent time-point, $51.0\% \pm 3.0$ of cells went through MI and $26.0\% \pm 10.1$ of cells went through MII. Eventually after 24-hours of meiosis induction, only $64.0\% \pm 8.14$ of cells went through all stages of meiosis, and $80.3\% \pm 9.3$ of cells went through MI.
- B) MI progression of *sae2Δ tel1Δ* and *sae2Δ*. The double mutant was delayed but most of the cells ($80.3\% \pm 9.3$) managed to go through MI after 24-hours of meiosis induction. The single mutant *sae2Δ* was more delayed and lower number of cells ($42.3\% \pm 8.7$) managed to go through MI after 24-hours of meiosis induction.

As Tel1 and Mec1 have redundant role during the meiotic homologous recombination pathway. The phosphorylation of Exo1 observed in *sae2Δ* was tested in *sae2Δ mec1Δ* to know if it is due to Mec1 kinase activity. This was done to investigate if the phosphorylation observed earlier was solely dependent on Tel1 activity. A strain lacking *SAE2*, *MEC1*, and *SML1* was induced into meiosis, with *sae2Δ* strain as control. As shown in Figure 4.17a, an electrophoretic mobility shift can be observed in both strains. However, the upshift observed in the triple mutant strain was slightly reduced at the eight-hour time-point. In the triple mutant samples, the proportion of Exo1 phosphorylation peaked at $46.9\% \pm 0.4$ after four hours of meiosis induction and was reduced at the subsequent time-points, Figure 4.17b. The meiotic progression of *sae2Δ mec1Δ sml1Δ* strain was delayed and showed a meiotic progression defect, Figure 4.18a. However, the majority of cells ($77.7\% \pm 1.8$) went through all stages of meiosis after 24-hours of meiosis induction. The MI progression of the triple mutant strain was earlier than *sae2Δ*, Figure 4.18b. This is because, Ndt80 is not inhibited at appropriate levels, allowing for the cells to bypass the arrest in pachytene (Xu et al., 1995; Gray et al., 2013). The phosphorylation proportion result demonstrated here suggests that the persistent phosphorylation of Exo1 observed in *sae2Δ* requires the function of Mec1.

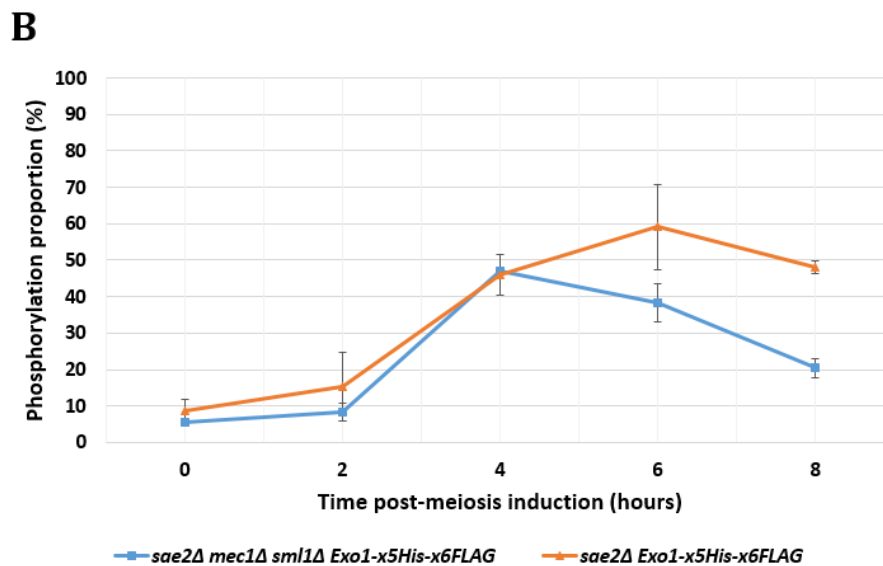
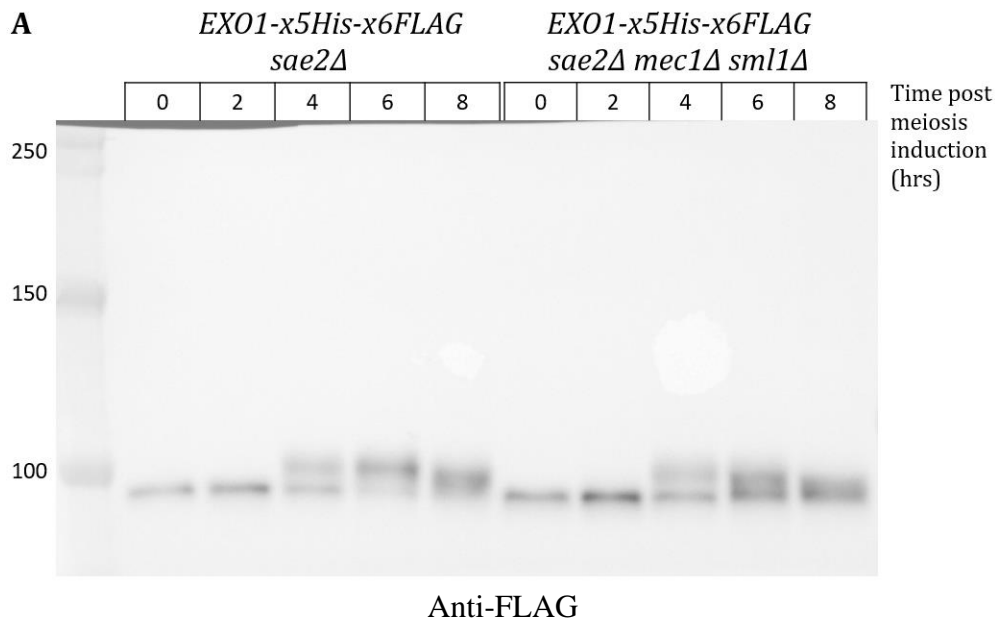


Figure 4.17 Analysis of Exo1 phosphorylation during the meiosis of *sae2Δ mec1Δ sml1Δ* strain

- A) Western blot analysis of Exo1 in *sae2Δ mec1Δ sml1Δ* samples showed an electrophoretic mobility shift band after four hours of meiosis induction. The upshifted band intensity decreased as meiosis progress to six and eight hours.
- B) The phosphorylation proportion of the double mutant peaked at $46.9\% \pm 0.4$ at the fourth hour time-point. $n = 3$, error bars represent the standard deviation from the mean. The phosphorylation proportion of Exo1 was then decreased to $38.3\% \pm 5.3$, and then to $20.4\% \pm 2.5$ at six and eight hour time-points respectively. This is significantly lower than Exo1's phosphorylation proportion observed in *sae2Δ* samples.
- C) The meiotic progression was abnormal, after six hours of meiosis induction 28% of cells were bi-nucleates, and 1% were tri/tetra-nucleates. At the next time-point, 22% of cells bi-nucleates, and 49% were tri/tetra-nucleates. Eventually after 24 hours of meiosis induction, 4% were bi-nucleates, and 75% were tri/tetra-nucleates with spore formation.

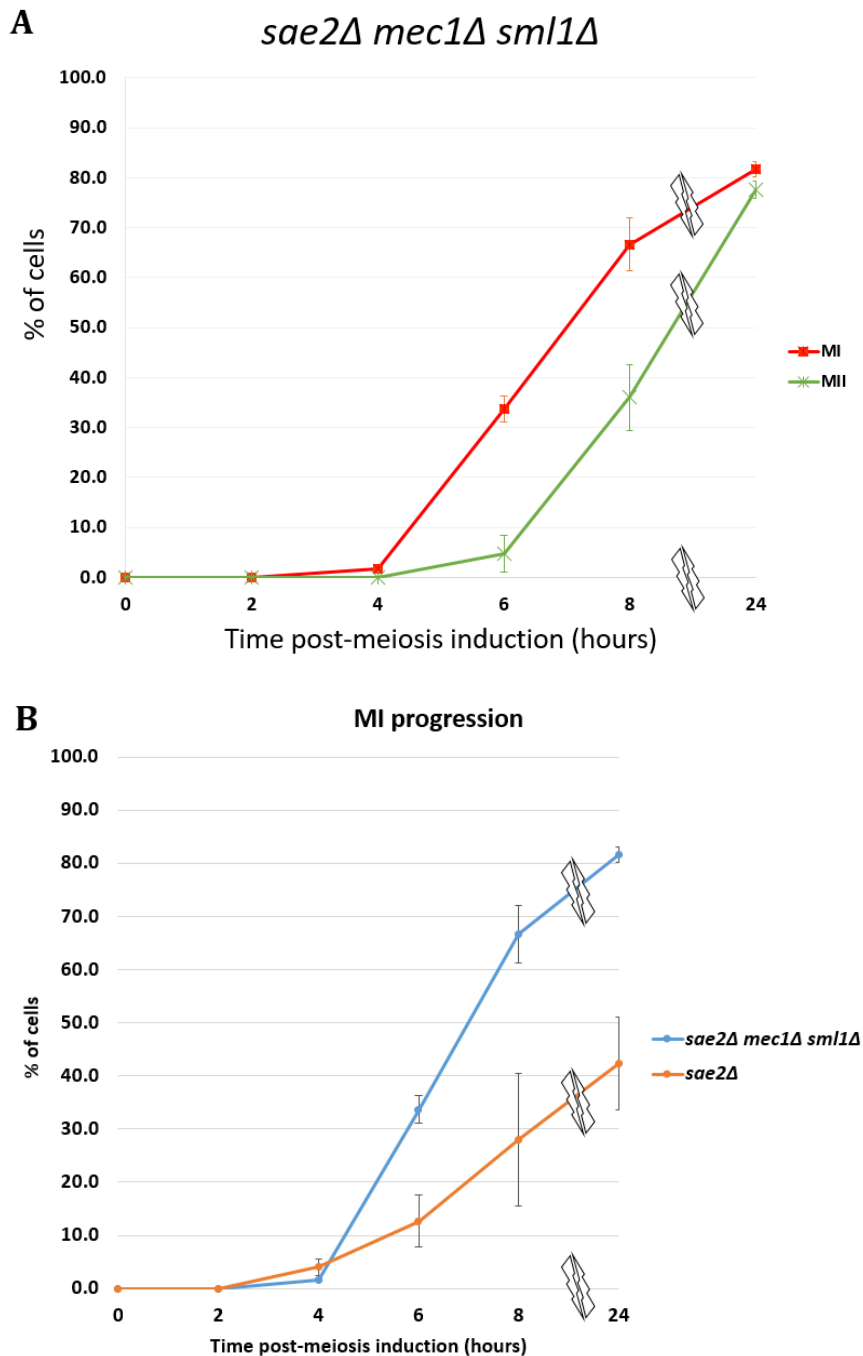


Figure 4.18 Analysis of the meiotic progression of *sae2Δ mec1Δ sml1Δ* and *sae2Δ* strains

- A) MI and MII progression of *sae2Δ mec1Δ sml1Δ* strain. $n = 3$, error bars represent the standard deviation from the mean. The meiotic progression of the mutant strain showed a slight delay. After six hours of meiosis induction, $33.7\% \pm 2.6$ of cells went through MI and $4.7\% \pm 3.7$ of cells went through MII. At the subsequent time-point, $66.7\% \pm 5.4$ of cells went through MI and $36.0\% \pm 6.6$ of cells went through MII. Eventually after 24-hours of meiosis induction, $81.7\% \pm 1.5$ of cells went through MI, and $77.7\% \pm 1.8$ went through MII.
- B) MI progression of *sae2Δ* and *sae2Δ mec1Δ sml1Δ* strains. The triple-mutant strain showed an earlier meiotic progression than *sae2Δ* strain. At the 24-hour time-point, most of the cells went through MI ($81.7\% \pm 1.5$).

4.7 **Exo1 phosphorylation is MRX complex dependent:**

The conserved MRX complex, formed by Mre11, Rad50, and Xrs2, has a crucial role in sensing and repairing DSBs (D'Amours and Jackson, 2002). The complex is required for the formation of Spo11-DSBs and plays an important role in removing covalently bound Spo11 from DSB ends (Usui et al., 1998; Moreau et al., 1999). This is achieved by utilising the nuclease activity of the MRX complex, allowing for further DSB ends resection (Moreau et al., 1999). Two mutants of Mre11 were employed to study the phosphorylation of Exo1 during meiosis. The *mre11-H125N* nuclease mutant which cannot remove covalently bound Spo11 from DSB ends (Krogh et al., 2005), and *mre11-58S* (H213Y) which cannot form the MRX complex and lacks the nuclease activity (Tsubouchi and Ogawa, 1998). The MRX complex and possibly Exo1 are both implicated in DSB ends bidirectional resection, first by 3' → 5' exonuclease activity by MRX, followed by 5' → 3' exonuclease activity (Garcia et al., 2011). As both proteins function in the resection process to produce a long tract of 3' ssDNA, the phosphorylation of Exo1 could be dependent on MRX functions.

The phosphorylation of Exo1 during *mre11-H125N* meiosis was analysed. Samples were taken at two-hour intervals for nuclear division and protein analysis. In the samples of the *mre11-H125N* nuclease mutant, the electrophoretic mobility-shift of Exo1 can be observed after four-hours of meiosis induction and persisted until the eight-hour time-point, Figure 4.19a. The phosphorylation proportion of Exo1 in *mre11-H125N* samples showed similar proportions to *MRE11*, and *sae2Δ* fourth-hour samples, Figure 4.19b. At the six and eight-hour *mre11-H125N* samples, Exo1 showed high phosphorylation proportions of $60.8\% \pm 11.7$, and $58.2\% \pm 11.4$ respectively. The six-hour sample had a similar phosphorylation proportion value to *sae2Δ* sample, but the proportion at the eight-hour sample was slightly higher. This result confirms the observation seen in *sae2Δ*, as Exo1 is hyper-phosphorylated when Spo11 cannot be removed from DSB sites, and the cell cycle checkpoint is continuously triggered. The meiotic progression of *mre11-H125N* was drastically impaired. As shown in Figures 4.20a and 4.20b, after eight hours of meiosis induction only 13.7% of cells went through MI. This might be because the majority of cells cannot proceed into meiosis due to a continuously active cell cycle checkpoint.

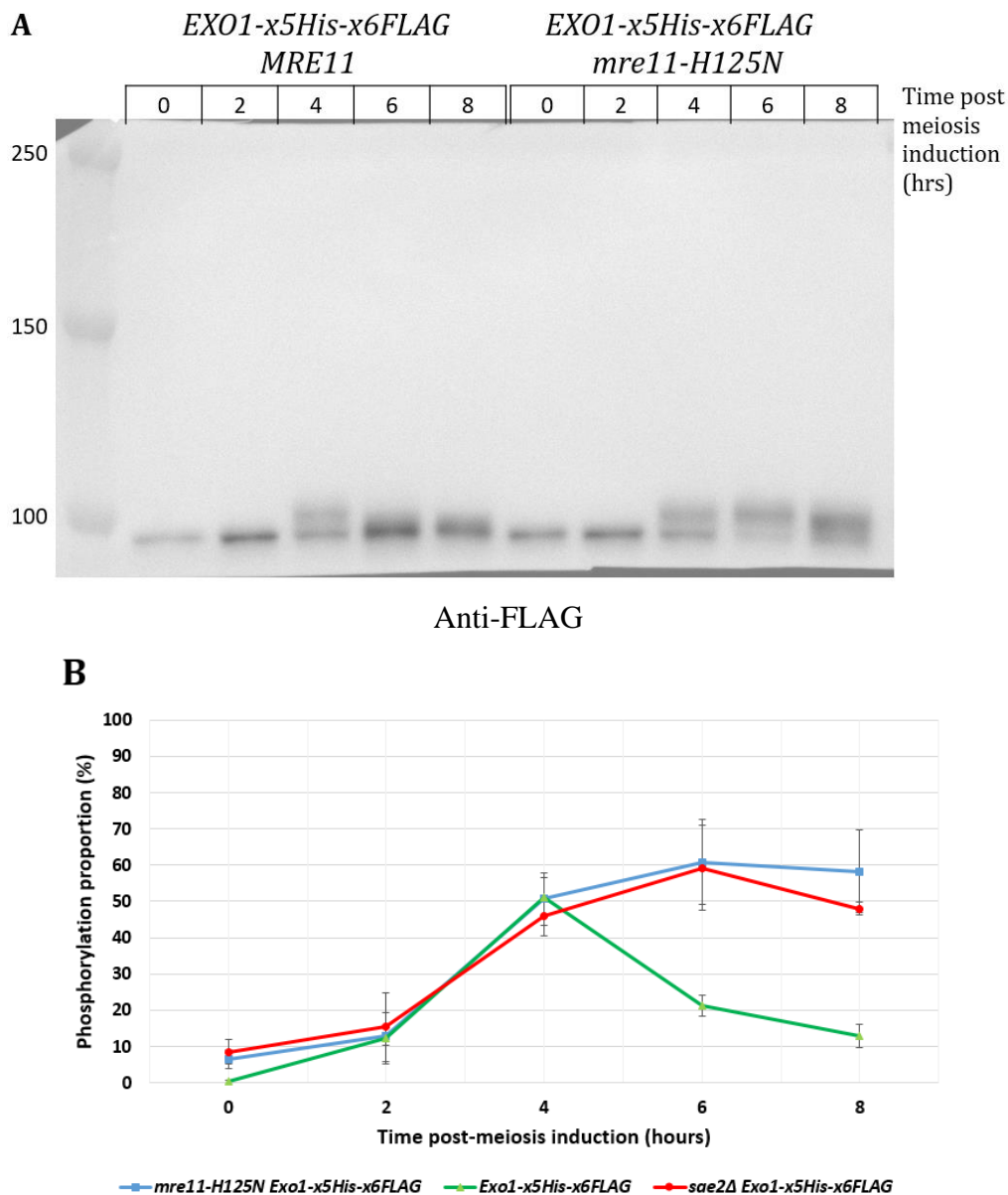


Figure 4.19 Analysis of Exo1 phosphorylation during the meiosis *mre11-H125N* mutant strain

- A) Western blot analysis of Exo1 showed an electrophoretic mobility shift after four hours of meiosis induction where it persisted and was not abolished as the cells progress through meiosis. In *MRE11* samples the upshifted band of Exo1 appeared at the four-hour time-point and was reduced to smear at the subsequent time-points.
- B) The phosphorylation proportion of Exo1 in *mre11-H125N* sample was at $50.7\% \pm 7.3$ after four hours of meiosis induction. This was followed by an increase to $60.9\% \pm 11.7$ at the six-hour time-point, and then a slight decrease at 58.2 ± 11.4 at the eight-hour time-point. $n = 3$, error bars represent the standard deviation from the mean. The phosphorylation proportion of Exo1 observed in *mre11-H125N* was similar to *sae2Δ* across all time-points except for eight-hours where in *sae2Δ* the phosphorylation proportion was slightly lower. $n = 3$, error bars represent the standard deviation from the mean.

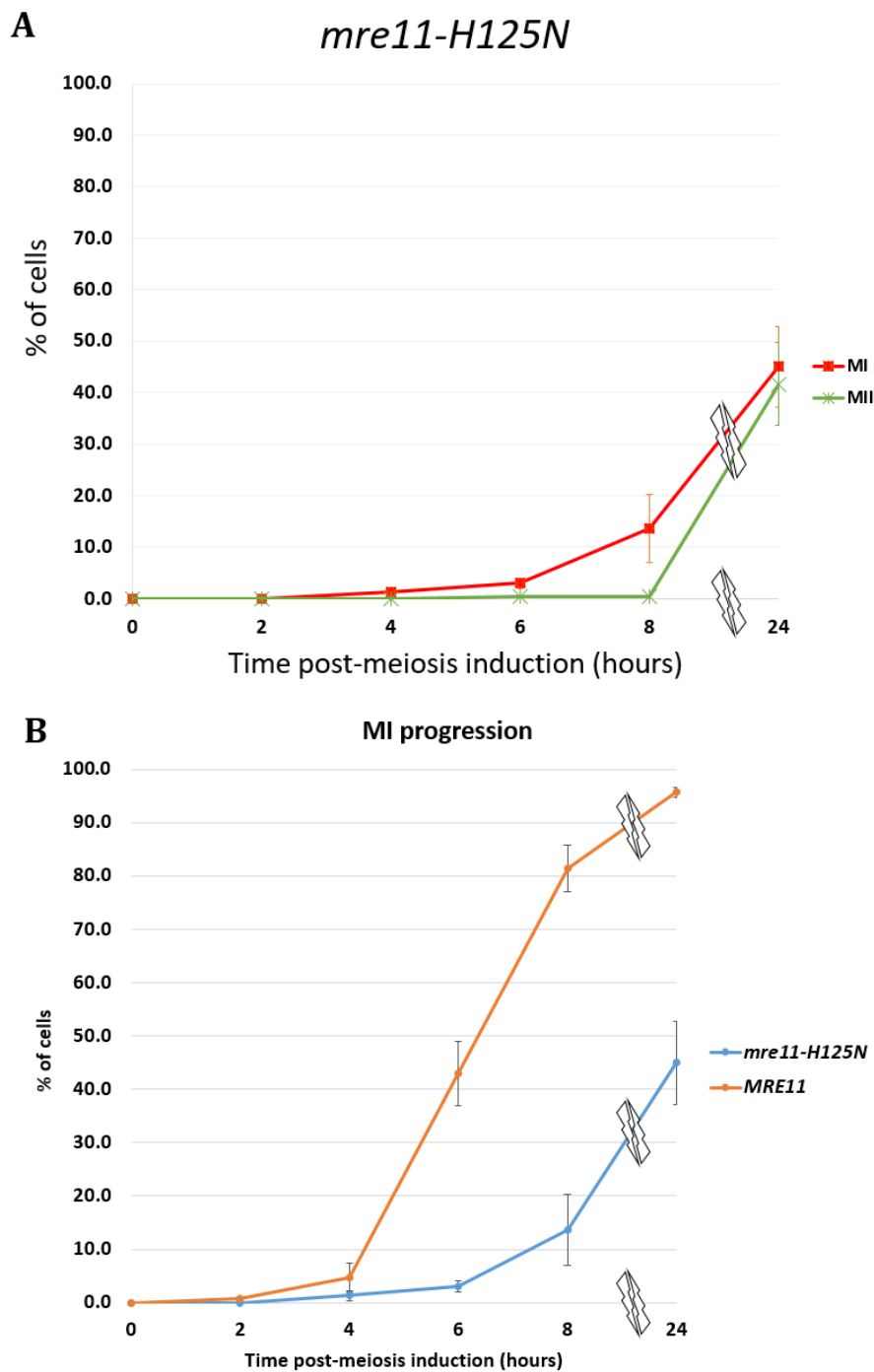


Figure 4.20 Analysis of the meiotic nuclear division of *mre11-H125N*

- A) The meiotic progression of the cells was severely impaired. $n = 3$, error bars represent the standard deviation from the mean. After eight hours of sporulation $13.7\% \pm 6.6$ of cells went through MI and $0.3\% \pm 0.3$ of cells went through MII. Eventually after 24-hours of sporulation, $41.7\% \pm 7.9$ of cells went through all stages of meiosis.
- B) MI progression of *MRE11*, and *mre11-H125N* strains. The mutant strain exhibited an extremely delayed and impaired meiotic program. Only $45\% \pm 7.7$ of cells went through MI after 24-hours of meiosis induction.

To test whether the phosphorylation of Exo1 is dependent on MRX complex, the phosphorylation was analysed during the sporulation of the MRX complex null mutant *mre11-58S*. Samples were taken every two hours for protein purification and nuclear division analysis. Upon western blot analysis, the electrophoretic mobility of Exo1 was not observed in *mre11-58S* samples, Figure 4.21a. A smear was observed in the six and eight-hour time-points. The phosphorylation proportions of the mutant samples were significantly lower than observed in wild type samples, Figure 4.21b. At the four-hour time-point, the phosphorylation proportion of Exo1 in *mre11-58S* was at 18.9 ± 2.7 , while the proportion was higher in *MRE11* at the same time-point, $51.2\% \pm 5.3$. The phosphorylation proportion of the mutant strain then increased at six and eight-hour samples, $22.7\% \pm 3.3$ and $20.2\% \pm 4.3$ respectively. This result suggest that the phosphorylation of Exo1 depends on the MRX complex formation. The meiotic progression of the *mre11-58S* strain was impaired and delayed, Figure 4.22a. At the six-hour time-point, only $17.0\% \pm 7.4$ of cells went through MI and $2.7\% \pm 7.4$ of cells went through MII. The majority of cells failed to go through all stages of meiosis, as after 24-hours of meiosis induction only 36.3% of cells went through MII. In comparison to *MRE11* MI progression, the *mre11-58S* strain shows that meiosis is drastically impaired, Figure 4.22b. This result suggest that faithful meiotic progression requires the MRX complex integrity.

Even though Spo11-DSBs cannot be repaired in *mre11* mutants, the phosphorylation proportion of both mutants was very different. The results here suggest that the over-phosphorylation observed when Spo11-DSBs are not repaired is dependent on the integrity of the MRX complex.

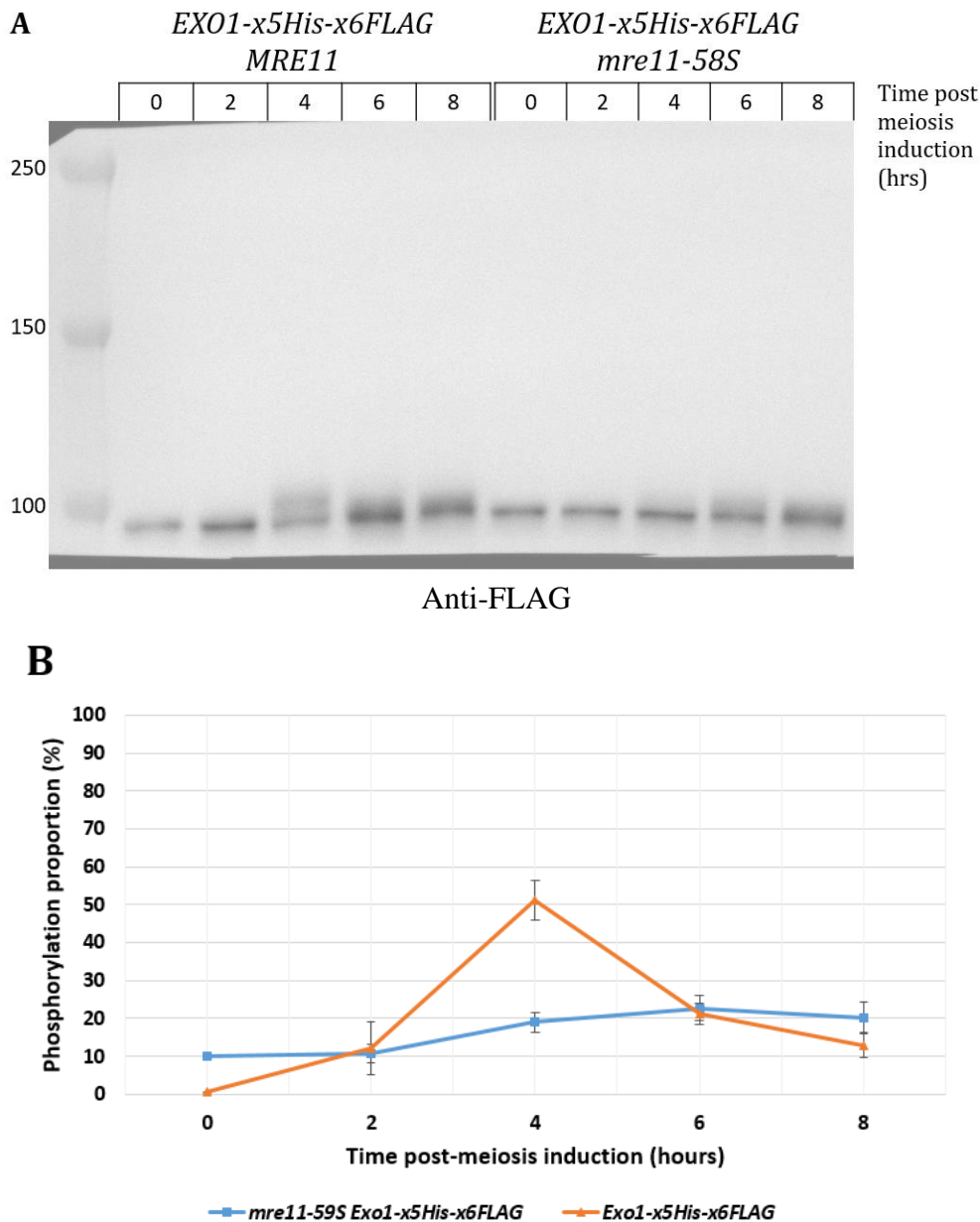


Figure 4.21 Analysis of Exo1 phosphorylation during the meiosis of *mre11-58S* mutant

- A)** Western blot analysis of Exo1 did not show an electrophoretic mobility shift in the mutant samples. A smear can be observed at six and eight hour time-points. The *MRE11* four hour time-point sample showed an upshift band of Exo1.
- B)** The phosphorylation proportion of Exo1 in *mre11-58S* samples was very low. $n = 3$, error bars represent the standard deviation from the mean. In the four-hour time-point, the phosphorylation proportion was $18.9\% \pm 2.7$. The phosphorylation proportion slightly increased to $22.7\% \pm 3.3$ at the six-hour time-point. This was followed by a slight decrease to $20.2\% \pm 4.3$ at the eight-hour time-point.

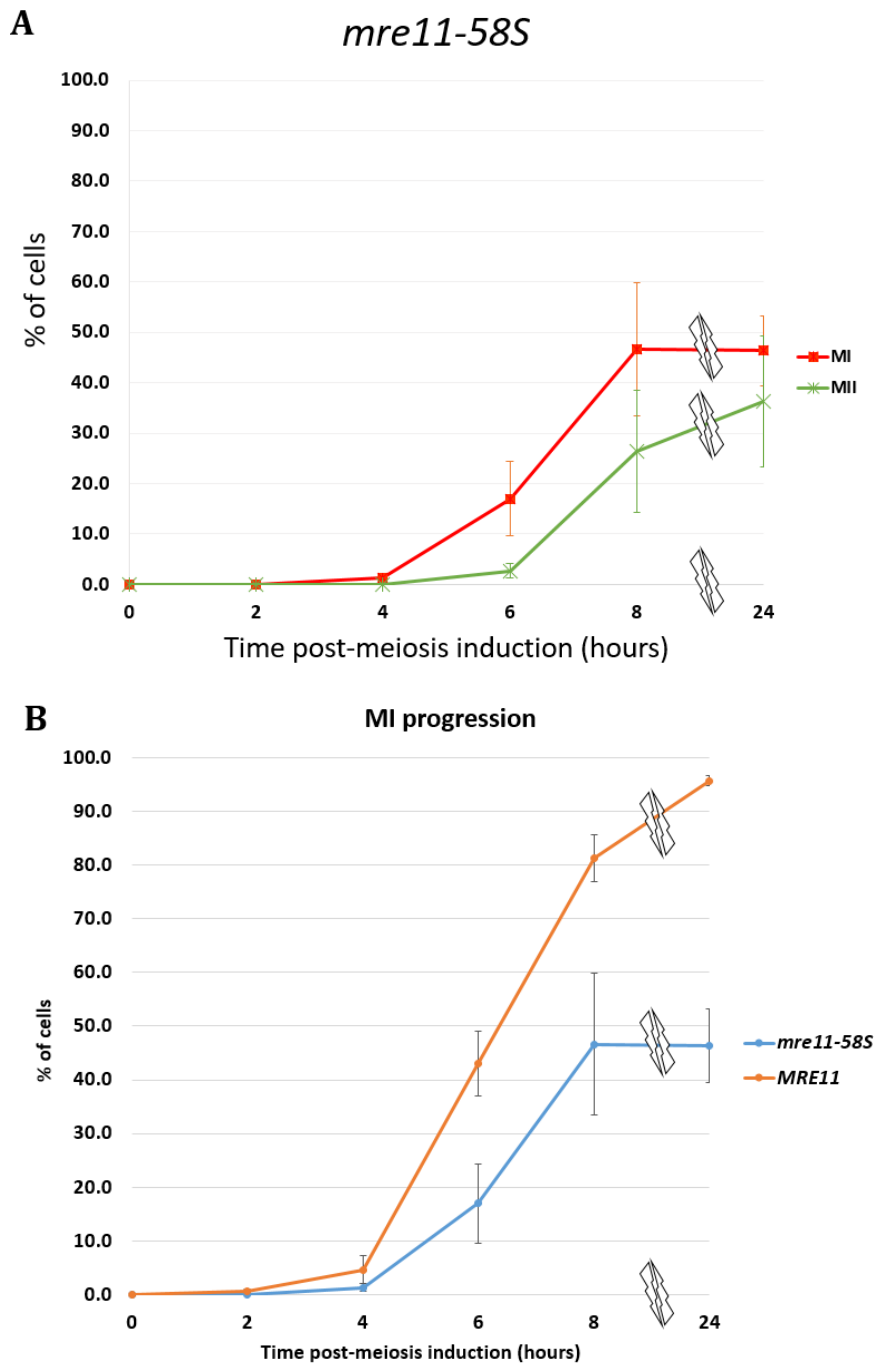


Figure 4.22 Analysis of the meiotic nuclear division of *mre11-58S*

- A) The meiotic progression of the cells was late and impaired. $n = 3$, error bars represent the standard deviation from the mean. After six hours of meiotic induction, $17.0\% \pm 7.4$ of cells went through MI, and $2.7\% \pm 7.4$ of cells went through MII. At the eight-hour time-point, $46.7\% \pm 13.2$ of cells went through MI, and $26.3\% \pm 12.1$ of cells went through MII. The standard deviation of the eight-hour time-point was high, which might correlate to difficulty in synchronisation the cells. After 24-hours of meiosis induction only $36.3\% \pm 13.0$ of cells managed to go through MII
- B) MI progression of *mre11-58S* and *MRE11* strains. The mutant strain showed a delayed meiosis and the majority of cells could not pass through MI.

Discussion:

As previous studies proposed, Exo1 is the nuclease responsible for exposing long tracts of 3'ssDNA during the homologous recombination pathway (Manfrini et al., 2010; Zakharyevich et al., 2010). Exo1 mitotic phosphorylation event was characterised to be in response to DNA damaging agents, and was proposed to be part of regulating Exo1 when 3'ssDNA are in abundance (Morin et al., 2008). In the absence of *DMC1* and *RAD51* during meiosis, 3'ssDNA are in abundance (Manfrini et al., 2010; Zakharyevich et al., 2010) and Exo1 is over-phosphorylated. Therefore, Exo1's phosphorylation event could be positively correlated to its resection activity that can expose long tracts of 3'ssDNA.

Although Exo1 functions in dHJs resolution (Zakharyevich et al., 2010), the phosphorylation event of Exo1 was normal in the absence of *NDT80* where dHJs stay intact with normal levels of DNA resection (Zakharyevich et al., 2010). This suggests that the phosphorylation event is not dependent on dHJ resolution, but rather depends on upstream events during the homologous recombination pathway. Interestingly, the phosphorylation and dephosphorylation of Exo1 in the absence of *NDT80* suggests that JM formation could correlate to the dephosphorylation of Exo1.

The kinases responsible for phosphorylating Exo1 during meiosis could be Cdc28, Tel1, Mec1, or Mek1. Exo1 phosphorylation was abolished when *mek1-as* was inhibited, which suggests that Exo1 phosphorylation is dependent on Mek1 function such as inter-homologue repair bias and crossover formation. Furthermore, when both kinases Tel1 and Mec1 were absent, Exo1 was not phosphorylated exhibiting the same bands observed during *spo11-Y135F* sporulation. During the meiosis of *tell1Δ* cells, Exo1 phosphorylation was normal. On the other hand, during the meiosis of *mec1Δ sml1Δ* strain, the phosphorylation signal was very weak. These results suggest that Mec1 plays a role in Exo1 phosphorylation but not Tel1. However, the absence of Mec1 function during meiosis impaired the synchronisation and the progression of the cells,

this may hinder the analysis of Exo1 phosphorylation as most cells are not in the same stage. The Cdc28 kinase is very essential for cell cycle and meiotic progression, inhibiting the kinase might cause multiple factors that could influence the phosphorylation of Exo1. However, since Sae2 phosphorylation by Cdc28 is essential to initiate DSB repair but not DSB formation, it is expected that Exo1 phosphorylation would be persistent in the absence of Cdc28 kinase function due to unrepaired DSBs i.e. similar to Exo1's phosphorylation in *sae2Δ* and *mre11-H125N*.

Interestingly, in the absence of *SAE2* during meiosis, Exo1 phosphorylation level was high and persisted until the eighth hour of meiotic induction. Unlike the over-phosphorylation observed in the absence of Dmc1 and Rad51, in the absence of Sae2, Spo11-DSBs are not repaired and resection cannot occur. Both observations suggest that Exo1 will be over-phosphorylated when the cell cycle checkpoint is active regardless of the processing of DSBs. In the absence of Sae2 and Tel1 kinase, the phosphorylation level was very low. This observation suggests that the hyper-phosphorylation event observed during *sae2Δ* meiosis was the result of Tel1-dependent checkpoint activation. Conversely, Exo1 phosphorylation during *sae2Δ mec1Δ* meiosis was similar to wild type meiosis. This shows that the over-phosphorylation of Exo1 during *sae2Δ* meiosis is caused by Tel1, while Mec1 is possibly required to persist the phosphorylation of Exo1. Moreover, during the meiosis of both strains *sae2Δ mec1Δ* and *sae2Δ tel1Δ*, spores were produced but were not viable, unlike *sae2Δ* meiosis where spores were not produced. This is possibly because in the absence of either kinases Tel1 or Mec1, Ndt80 is not inhibited. This would ultimately activate middle-sporulation genes that are required to produce spores, section 1.7. With this observation, the dephosphorylation of Exo1 could be correlated to the activation of middle-sporulation genes.

The dephosphorylation of Exo1 seems to be JM formation dependent since the phosphorylation was abolished in *ndt80Δ* mutant and persisted in *dmc1Δ rad51Δ* double mutant. Even though

JMs cannot be produced in *sae2Δ mec1Δ*, Exo1 was dephosphorylated. This could be explained by the fact that in this mutant, the cell-cycle is not arrested since Ndt80 is possibly active, which could allow the meiotic program to proceed. Hence, Exo1 dephosphorylation could either occur due to the activation of mid-sporulation genes or the production of JMs after the strand invasion step.

Exo1 was over-phosphorylated during the meiosis of *mre11-H125N* nuclease mutant. This event was similar to Exo1 phosphorylation observed during the sporulation of *sae2Δ* and *dmc1Δ rad51Δ* mutants. The over-phosphorylation observed in these mutants confirms that Exo1 phosphorylation was caused by a cell cycle checkpoint event. In the *mre11-58S* mutant, the cell-cycle checkpoint was expected to be continuously activated since Spo11-DSBs are not repaired such as in *sae2Δ* and *mre11-H125N* (Borde et al., 2004). Since Exo1 phosphorylation was reduced in this mutant, the cell-cycle checkpoint that causes Exo1 phosphorylation is dependent on the integrity of the MRX complex. The MRX complex, and specifically Xrs2 subunit was shown to be required for Tel1 recruitment to DSB sites (Nakada et al., 2003). The phosphorylation of Exo1 was not completely abolished during the meiosis of *mre11-58S*, this suggests that the Tel1-mediated cell cycle checkpoint was weak. The *mre11-58S* mutant can possibly interact with Rad50 and Xrs2, it also may be able to form a complex that is unstable. A co-immunoprecipitation experiment carried out by Hodgson et al., 2011 did not conclude that *mre11-58S* could not form a complex, and the fact that it can still associate to the DNA (Borde et al., 2004) suggests that that the *mre11-58S* interaction with Rad50 and Xrs2 is not completely lost.

The electrophoretic shift of Exo1 that was detected by western blots here is a good indication of phosphorylation but is not sensitive enough to detect minimally phosphorylated proteins. The upshifted bands detected in this chapter is the hyper-phosphorylation form of Exo1. Therefore, even if the exaggerated upshift is not detected, the possibility of Exo1 phosphorylation cannot be completely ruled out as it would be below the detection levels of western blot. However, the reduction of Exo1 phosphorylation is a big effect, and the dependency of the hyper-phosphorylation event is the way to start understanding Exo1 regulation during meiosis.

In conclusion, Exo1 phosphorylation coincides when most Spo11-DSBs are formed, and the event was narrowed down to the initial and long resection processes. These results suggest that Exo1 phosphorylation is dependent on the Tel1-mediated cell cycle checkpoint. The observations also suggest the role of Mek1 in phosphorylating Exo1 but does not uncover the function of Exo1 phosphorylation.

Chapter 5. Mass Spectrometry analysis of Exo1's phosphorylation residues

Introduction:

To fully understand Exo1 phosphorylation during meiosis, the phosphorylation sites on Exo1 must be isolated. Finding the phosphorylated residues on Exo1 will provide the means to generate strains by substituting them to a non-phosphorylatable residue such as alanine or to a phosphorylation-mimicking residue such as aspartic acid. Ultimately, the inability to phosphorylate Exo1 during meiosis and the phosphorylation mimicking mutant will be studied. To localise the phosphorylation sites on Exo1, the protein must be purified for mass-spectrometry (MS) analysis. Large-scale protein extraction under native conditions of Exo1 followed by immunoprecipitation was difficult as Exo1 was dephosphorylated and degraded.

A novel method was optimised to do large-scale protein extraction using guanidinium hydrochloride buffer (Buffer-G), followed by Ni-NTA purification. This is followed by protein elution, and immunoprecipitation by anti-FLAG magnetic beads, section 2.3.15. This method should eliminate other proteins that may overwhelm the MS instrument and produce highly purified sample of Exo1.

The aim of this chapter was to localise Exo1 meiosis-specific phosphorylation sites by MS. The purified Exo1 protein was treated with Trypsin while in SDS-PAGE gel (in-gel) and later with Trypsin while bound to anti-FLAG beads (in-beads). Trypsin digests proteins by cleaving the polypeptide sequence after arginine (R) or lysine (K), generating short peptides that can be analysed by MS. High-Pressure Liquid Chromatograph (HPLC) then separates the peptides according to their charge, followed by first MS (MS1) that separates the peptides by their mass-to-charge ration (m/z). Protonated peptides of a particular m/z -ratio coming from MS1 were selected and then made to split into smaller fragments.

During this study, two types of fragmentations were used, collision-induced dissociation (CID), and electron-transfer dissociation (ETD). The CID fragmentation method relies on accelerating protonated molecules by an electric potential increasing the molecule's kinetic energy and then colliding them to argon gas. The collision converts the kinetic energy into internal energy resulting in the fragmentation of the peptide by breaking their peptide bonds, as reviewed by Mitchell Wells and McLuckey, 2005. The ETD method fragments peptides by exposing them to fluoranthene, which transfers electrons to the peptide bonds causing the cleavage of the peptide backbone (Kim and Pandey, 2012). Both methods can be utilised to identify protein PTMs, however the ETD method allow peptides to retain the labile phosphorylation on serine or threonine residues helping in accurately localising the phosphorylation sites (Boersema et al., 2009). The CID and ETD method break different peptide bonds, as shown in Figure 5.1, the CID method breaks the y-b peptide bond while the ETD method breaks the c-z peptide bonds. Both methods produce different types of fragments, CID produces y and b fragments, while ETD produces c and z fragments.

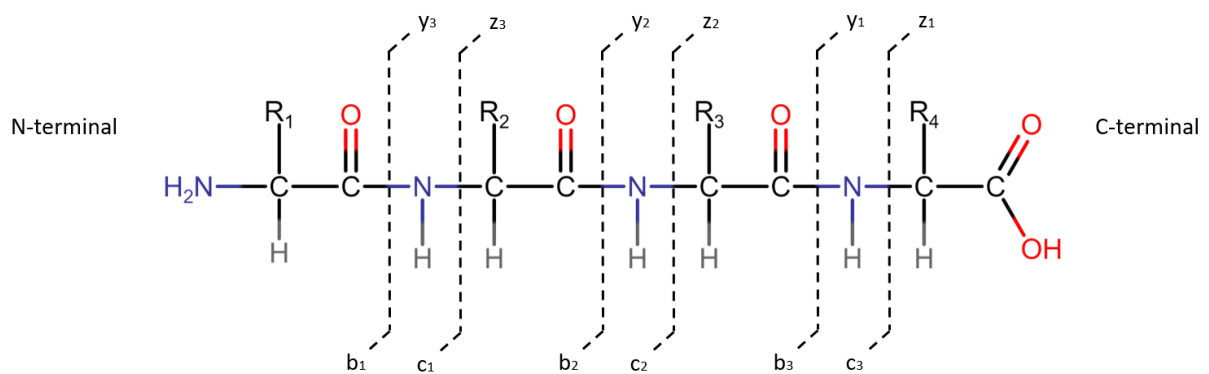


Figure 5.1 An example of peptide showing the peptide-backbone cleavage sites of CID and ETD methods.

CID cleaves y-b bonds producing y and b fragments. The y fragments are read from the C-terminal towards the N-terminal, while the b fragments are read from the N-terminal to the C-terminal. The ETD method cleaves c-z bonds producing c and z fragments. The z fragments are read from C- to N- terminal, and the c fragments are read from the N- to C-terminal.

The fragments produced then went into a second MS (MS2), which measures the m/z of each fragment, and their intensities. The dataset produced by MS1 and MS2 was then analysed by MaxQuant software. The software analyses the m/z and intensity of the full peptide and its respective fragments, then it compares them to a peptide database for all known yeast proteins. The peptide database was produced by *in silico* protease digestion of all known yeast proteins. Additionally, MaxQuant can determine the phosphorylation site on a peptide by analysing the fragments detected by MS2. If the fragments detected in MS2 cover most of the original peptide sequence and some of those fragments retain the phosphate group, then the phosphorylation site can be localised with high probability. Exo1 phosphorylated peptides and their respective fragmentation were analysed to localise the phosphorylated residue. The fragmentation of each phosphorylated peptide was manually checked using P-Label software, this was done because if the fragmentation was poor then manual analysis would help in localising the phosphorylation site. First, the MS was carried out for Exo1 extracted using the two-step method from the fourth time-point of meiosis induction. To test which peptide digestion method would generate more peptides, two methods of sample preparation were tested, peptide digestion while Exo1 is in-gel, and on-beads.

To investigate if Exo1 was phosphorylated before meiosis induction, MS was carried out for Exo1 extracted from synchronised cells grown in pre-sporulation media. MS was also done for Exo1 extracted from cells after four-hours of sporulation to localise Exo1's phosphorylation sites during meiosis. Finally, another MS was done for Exo1 in the absence of *SAE2* to study the hyper-phosphorylation event when the Tel1-mediated pathway is overactive. Having the phosphorylation profile of Exo1 in different states would help in accurately localising the phosphorylation sites on Exo1, which would greatly help in investigating the function of Exo1 phosphorylation.

Results:

5.1 Large-Scale Two-Step Purification of *Exo1-x5His-x6FLAG*:

To get a purified sample of Exo1, two-step purification was done for *Exo1-x5His-x6FLAG* to eliminate any other proteins that may overwhelm the MS instrument. The first purification step was done by Ni-NTA affinity-purification, and in order to perform the second purification step the purified protein must be eluted. Three elution steps were done using a buffer containing 150mM Imidazole and 5mM EDTA. Imidazole competes with histidine by binding to Ni ion, while EDTA chelates the Ni ions, using both in a buffer would elute any histidine containing proteins that are bound to Ni-NTA resin. Samples were taken from each step: The Ni-NTA resin, elution flow-through, and Ni-NTA resin after elution. The samples were then analysed by western blot using the FLAG antibody to assess the workflow. As shown in Figure 5.2, three rounds of Ni-NTA elution were enough to elute most of Ni-NTA bound Exo1. An intense Exo1 band was observed for the Ni-NTA sample, and an equally strong band from the first fraction (F1). In the subsequent two elutions; F2 and F3, Exo1 band intensity was reduced. Although some Exo1 was not eluted from the Ni-NTA resin, the amount of eluted Exo1 should be sufficient for the immunoprecipitation step. An additional band can be observed with a molecular weight of 80kDa, this band could be a cleaved version of Exo1 or a product of a non-specific binding of the FLAG antibody.

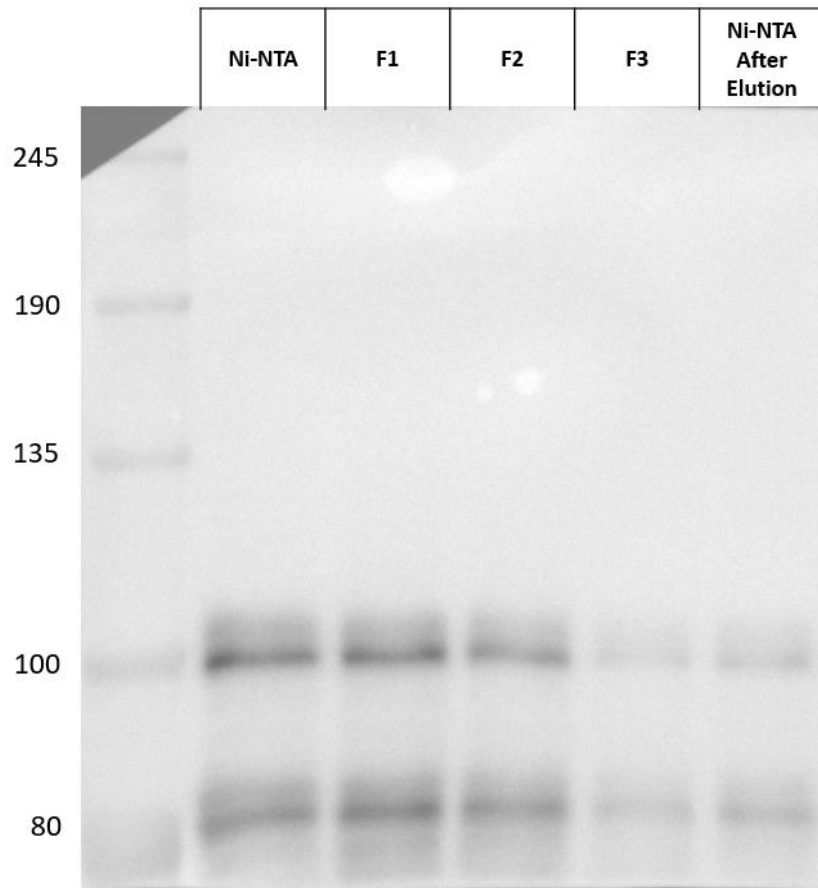


Figure 5.2 Testing *Exo1-x5His-x6FLAG* elution from Ni-NTA beads

Western blot to assess the methodology of Ni-NTA elution using an elution buffer containing 150mM imidazole, and 5mM EDTA. The Ni-NTA resin was eluted with protein loading buffer and loaded into the first lane, this constitutes to 1:20 of the Ni-NTA total volume. The Ni-NTA samples showed an Exo1 band with an electrophoretic shift and another band around 80kDa molecular weight. Fraction 1, fraction 2, and fraction 3 (F1, F2, and F3 respectively) are the eluted fractions from the Ni-NTA resin. Each elution step was carried out with five times the volume of Ni-NTA and 1:25 of each fraction was analysed by western blot, as shown in F1, F2, and F3 (second, third, and fourth lanes respectively). The F1 and F2 lanes showed a bright Exo1 band with an upshift above it, and all fractions showed another band around 80 kDa. The Exo1 band observed in F2 was slightly fainter than F1 and was very faint in F3. The last lane shows 1:20 of the Ni-NTA resin after elution where it the Exo1 signal was lower than the signal observed in Ni-NTA sample, suggesting that most of Exo1 protein have been eluted.

To test for the compatibility of the anti-FLAG beads with the elution buffer used. Ni-NTA purification was done for *Exo1-x5His-x6FLAG*. This was followed by elution and immunoprecipitation by anti-FLAG magnetic beads. Samples were taken from each step and western blot was done to assess the workflow. As shown in Figure 5.3, a bright Exo1 band was observed in the Ni-NTA sample. The 80kDa band is fainter in this sample because 5mM of Imidazole was added to the wash buffers and this might have helped in preventing low-affinity proteins from binding to Ni-NTA. A bright band can be observed in the anti-FLAG sample which corresponds to Exo1 molecular weight. Two bands were observed between 100kDa and 75kDa, these two bands could be the antibody that was bound on the beads. This is because when anti-FLAG purification was done to *EXO1*, bands of the same molecular weight can be observed, Figure A4, appendix IV. This shows that immunoprecipitation of Exo1 is efficient and this method could be utilised to purify Exo1 for MS analysis.

5.2 Mass-spectrometry of purified Exo1 and peptide generation by “in-gel” Trypsin treatment:

To localise Exo1 phosphorylation sites by MS, Exo1 was purified using the two-step purification method as described in 2.3.15. The purified Exo1 sample was run on SDS-PAGE to separate any other proteins in the sample i.e. FLAG antibody. The gel was then stained with Coomassie and no Exo1 band can be seen at the expected size as shown in Figure 5.4. The samples used in this gel were from the same samples for the western blot on Figure 5.3. The Coomassie stained gel was excised and prepared for Trypsin digestion; the excised area is annotated with a red rectangle. This area was chosen since it corresponds to the area where Exo1 was observed in the western blot. After the gel was treated with trypsin as described in section 2.4, the sample was run into HPLC for 60 minutes. Subsequently the samples were analysed by the first MS, followed by CID fragmentation and MS2 analysis.

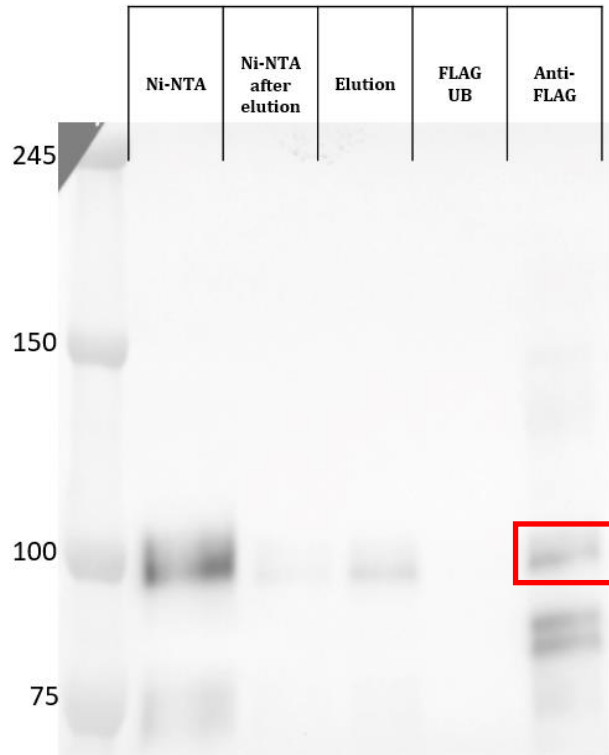


Figure 5.3 Immunoprecipitation of eluted *Exo1-x5His-x6FLAG* sample

Western blot done to test the efficiency of the immunoprecipitation of Exo1 after being eluted. The Ni-NTA resin was eluted with a buffer containing 150mM imidazole and 5mM EDTA. The second lane shows 1:20 of the Ni-NTA volume where an Exo1 band can be observed with an upshift. A faint band can be observed around the 75kDa molecular weight. The third lane shows 1:20 of the Ni-NTA volume after being eluted where a very faint Exo1 signal was observed. The Ni-NTA was eluted three times and the eluents were pooled, the fourth lane shows 1:25 of the total volume of the eluents where a faint band of Exo1 can be observed. Anti-FLAG immunoprecipitation was done for the eluents where 1:25 of the unbound fraction volume was loaded into the fifth lane where no signal can be observed. The last lane shows 1:25 volume of the anti-FLAG beads (100µl) where a bright Exo1 band can be observed and two bands can be observed between 100kDa and 75kDa. The 75kDa band observed in the Ni-NTA samples can be observed with a very low signal.

The red rectangle is the area that was excised for MS from the Coomassie stained gel.

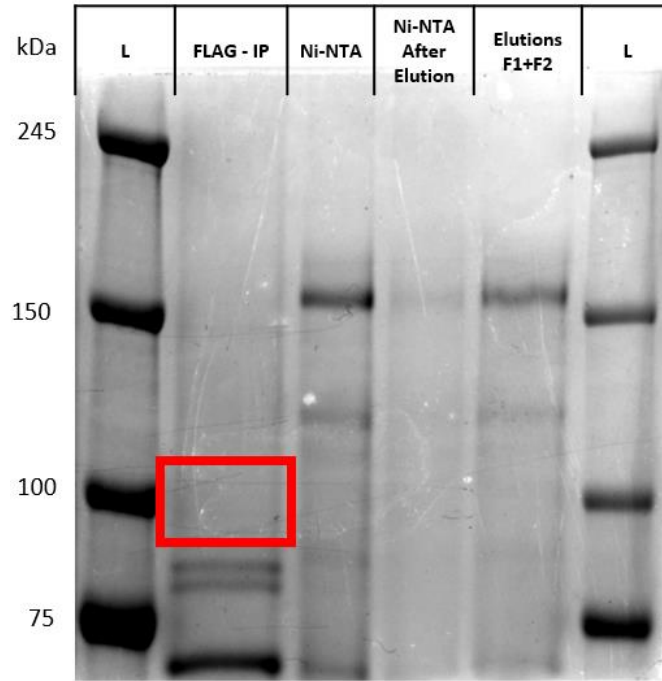


Figure 5.4 SDS-PAGE gel of *Exo1-x5His-x6FLAG* purified by two-step purification method.

Coomassie stained gel of *Exo1-x5His-x6FLAG* purification by Ni-NTA and then by FLAG immunoprecipitation. No bands around 100kDa were observed. The area annotated with the red box was excised out of the gel for Trypsin treatment followed by mass-spectrometry analysis.

Upon analysing the data produced by the MS, peptides from 256 proteins were detected, 229 from *S. cerevisiae* and 27 contaminants. The contaminant proteins were of human origins introduced during sample preparation. To investigate the abundance of Exo1 in the sample, the analysis software MaxQuant calculates the total intensity of each protein detected based on the sum of the intensity of its respective peptides. To normalise the intensities of the proteins detected, the intensity based absolute quantification of proteins (iBAQ) divides the sum of all the peptides intensities by the number of observable peptides of a protein. Based on the total intensity of each protein's respective peptides, Exo1 was the fourth most intense protein in the sample after Snf1, Hbt1, and an uncharacterised protein Ygr237c, Table 5.1. The absolute intensity iBAQ showed that Exo1 is the fifth most intense protein. This shows that Exo1 was purified in the sample but the purification did not eliminate other abundant proteins. From the 674 unique peptides detected 33 unique peptides were from Exo1 sequence, constituting of 39.3% of the total sequence of Exo1 protein, Figure 5.5. The total number of Exo1 peptides detected were 54, six of which were phosphorylated. In the six phosphorylated peptides, four different phosphorylation sites were detected, S431, S663, S664, and S692. As shown in Table 5.2, the serine residue S431 was shown to be phosphorylated in three of the six phosphorylated peptides, while the S664 residue was shown to be phosphorylated in two different phosphorylated peptides. The S664 residue in the fourth peptide was presented with a high phosphorylation probability. However in the fifth peptide, the phosphorylated residue cannot be determined if it is S663 or S664 and both were presented with an equal probability.

#	Protein name	Intensity
1	Snf1	7.79 x 10 ⁸
2	Hbt1	6.31 x 10 ⁸
3	Ygr237c	2.39 x 10 ⁸
4	Exo1	1.89 x 10 ⁸
5	Rom2	1.37 x 10 ⁸
6	Mhp1	1.37 x 10 ⁸
7	Hrk1	1.28 x 10 ⁸
8	Pbp1	7.12 x 10 ⁷
9	Aft1	5.08 x 10 ⁷
10	Yol087c	4.43 x 10 ⁷
#	Protein name	Absolute intensity (iBAQ)
1	Snf1	2.43 x 10 ⁷
2	Hbt1	9.86 x 10 ⁶
3	Ygr237c	6.13 x 10 ⁶
4	Ypr096c	5.98 x 10 ⁶
5	Exo1	5.11 x 10 ⁶
6	Hrk1	3.020 x 10 ⁶
7	Aft1	2.54 x 10 ⁶
8	Pbp1	2.15 x 10 ⁶
9	Mhp1	1.93 x 10 ⁶
10	Rom2	1.91 x 10 ⁶

Table 5.1 The ten most abundant proteins in Exo1 purified sample by “in-gel” preparation.

The top table shows the ten most abundant proteins detected by MS and their intensity based on the total intensity of their respective peptides. The bottom table shows the intensity based on absolute quantification of proteins (iBAQ) of the ten most abundant protein. iBAQ is calculated by dividing the total peptide intensity by the identified peptides of one protein.

MGIQGLLPQLKPIQNPVSLRRYEGEVLAIDGYAWLHRAACSCAY
 ELAMGKPTDKYLQFFIKRFSLLKTFKVEPYLVFDGDAIPVKK
 TESKRRDKRKENKAIAERLWACGEKKNAMDYFQKCVDITPEM
 AKCIICYCKLNGIRYIVAPFEADSQMVYLEQKNIVQGIISEDSD
 LLVFGCRRLITKLNDYGECEICRDNFIKLPKKFPLGSLTNEE
 IITMVCLSGCDYTNGIPKVGLITAMKLVRRFNTIERIILSIQRE
 GKLMIPDTYINEYEA AVLAFQFQRVFCPIRKKIVSLNEIPLYLK
 DTESKRRKLYACIGFVIHRETQKKQIVHFDDDDIDHHLHLKIAQ
 GDLNPYDFHQPLANREHKLQLASKSNIIEFGKTNTTNSEAKVKP
 IESFFQKMTKLDHNPKVANNIHSLRQAEDKLTMAIKRRKLSN
 ANVVQETLKDTRSKFFNKPSMTVVENFKKKGDSIQDFKEDTNS
 QSLEEPVSESQLSTQIPSSFITTNLEDDDDNLSEEVSEVSDIEED
 RKNSEGKTIGNEIYNTDDDDGDDTSEDYSETAESRVPTSSTTSF
 PGSSQRSISGCTKVLQKFRYS^SSFSGVNANRQPLFPRHVNQK
 SRGMVYVNQNRDDDCDDNDGKNQITQRPSLRKSLIGARSQRIV
 IDMKSVDERKSFNS^S^SPILHEESKKRDIETT^KSSQARPAVRS
 I^SLLSQFVYKGLKLRTGSHHHHHHG DYKDDDDKDYKDDDDKD
 YKDDDDKGDYKDDDDKDYKDDDDKDYKDDDDK*

Figure 5.5 Exo1 amino-acid sequence with the peptides sequences analysed by MS.
 The peptides detected by the MS are highlighted in grey. The Trypsin cleavage sites arginine (K) and lysine (R) are shown in purple. Morin et al. reported that underlined serine residues, S372, S587, S567, and S692 were phosphorylated in mitotically dividing cells. Four of those serine residues S567 and S692 were covered in this experiment. In this MS analysis, four possible phosphorylation sites were detected S431, S663, S664, and S692, shown in red and blue. The blue serine residue S692 was detected by Morin et al. The phosphorylation of S663 (annotated with “?”) was not confirmed in this experiment.

#	Exo1 phosphorylated peptide sequence	Phosphorylation site(s) probability	Phosphorylation site(s)
1	KL ^S P ^N NANVVQETLK	KLS (1) NANVVQETLK	S431
2	KL ^S P ^N NANVVQETLKDTR	KLS (1) NANVVQETLKDTR	S431
3	KL ^S P ^N NANVVQETLKDTR	KLS (1) NANVVQETLKDTR	S431
4	SFNS ^S P ^I PILHEESK	SFNS (0.001) S (0.999) PILHEESK	S664
5	SFNS ^S P ^S ? ^S P ^S ? ^I PILHEESKK	SFNS (0.463) S (0.463) PILHEES (0.074) KK	S663 or S664
6	SISLL ^S P ^I S ^Q FVYK	S (0.001) IS (0.999) LLSQFVYK	S692

Table 5.2 Table showing Exo1 phosphorylated peptides detected by MS for in-gel treated *Exo1-x5His-x6FLAG*.

The phosphorylation site S431 was detected in three peptides, each with a high probability. In the fourth peptide S664 was presented with a high phosphorylation probability, whereas in the fifth peptide the phosphorylated residue could not be determined whether it is S663 or S664. In the sixth peptide, the serine residue S692 was presented with a high phosphorylation probability.

The fragmentation of each peptide was manually assessed to confirm the data analysis given by MaxQuant, the fragmentation of all peptides are presented in Appendix V. The uncertainty of the phosphorylation S663 or S664 was because their peptide was not fully fragmented and the relative intensities of the fragments were low, Figure 5.6. The spectra of this peptide was analysed manually to investigate its fragmentation, where the phosphorylated residue was narrowed down to S663 or S664. If S664 is phosphorylated then an extra fragment (y9) can be observed but with a very low relative intensity. Since there are other readings with low relative intensity values that do not match the expected fragmentation, the y9 fragment observed here could be noise. This means that the phosphorylated residue in this peptide cannot be determined whether it is S663 or S664. However, since the phosphorylation of S664 was detected in another peptide with high probability, it is more likely that S664 was phosphorylated than S663. Additionally, the serine residue S692 was phosphorylated in one peptide only and more analysis is needed to confirm its phosphorylation. In conclusion, the MS done only covered 39.3% of Exo1 amino acid sequence, and after manually analysing the spectra of each phosphorylated fragment three phosphorylation sites were detected with high confidence, S431, S664, and S692, whereas the phosphorylation of S663 was uncertain. The phosphorylated residues detected in this experiment need to be confirmed by more MS analysis, and more coverage of Exo1 amino acid sequence may uncover missed phosphorylated residues.



Figure 5.6 P-label software showing the fragment ion spectra of the phosphorylated peptide SFNSSPILHEESK.

In this peptide, MaxQuant localised the phosphorylation to the serine residues between asparagine and proline. The fragments relative intensities are on the y-axis, and their m/z are on the x-axis. The peptide sequence is shown on the upper right corner with its charge (+2) and the y and b fragments detected in MS2. Both spectra presented are of the same reading (top and bottom) and show the real relative intensity of each fragment. The m/z of the spectra that match the expected peptide's fragment m/z are coloured in orange if it is a y-type fragment and green if it is a b-type fragment. The peaks shown in black do not belong to the expected fragmentation of the peptide. The top spectra highlights the peaks if the second suspected serine is phosphorylated and the bottom spectra if the first suspected serine is phosphorylated. The most intense fragment is the full peptide fragment without a phosphate group, shown in red. In both spectra, fragments y10, and b11 were detected with and without a phosphate group. If the second serine is phosphorylated one more fragment (y9) match one of the peaks. Since the fragmentation of the peptide is poor and the relative intensity the y9 fragment is low, the phosphorylation site cannot be determined with high confidence.

5.3 Mass-spectrometry of purified Exo1 and peptide generation by “on-beads” Trypsin treatment:

To get more sequence coverage of Exo1 and to make sure that all of the possible phosphorylatable residues were analysed. The MS analysis was carried out to trypsin treated Exo1 enriched on anti-FLAG beads (on-beads treatment). Presumably, this approach would give more coverage of Exo1's sequence as the in-gel preparation requires eluting the digested peptides from the gel pieces causing peptide loss. Additionally, the peptide digestion treatment is more efficient when done for proteins purified on-beads, producing more peptides in comparison to in-gel preparation. However, since proteins are not separated as in the in-gel method, the on-beads method would not eliminate proteins of other molecular weights. The MS analysis was carried out for Exo1 extracted from synchronised cells in pre-sporulation culture and from cells after four-hours of meiosis induction. This was done to compare the phosphorylation profile before meiosis and when the majority of Exo1 is phosphorylated during meiosis. To investigate the hyper-phosphorylation of Exo1, another MS analysis was carried out for Exo1 purified from cells that lack Sae2 and after four-hours of sporulation. In this experiment the cells arrest at the pachytene stage, which should allow for accurate localisation of phosphorylated residues since the cells cannot proceed into meiosis and most of Exo1 molecules were phosphorylated. In the MS analyses presented in this section, the generated peptides from the peptide digestions were run on HPLC for 90 minutes and subsequently analysed by MS1. ETD method was used for peptide fragmentation and the m/z of each fragment was measured by MS2. The longer time of HPLC would separate the peptides more allowing for higher MS resolution, while the ETD fragmentation method accurately localise phosphorylated residues, since using this method allow peptides to retain their labile phosphorylation site(s).

5.3.1 Mass spectrometry for Exo1 purified sample from pre-meiotic synchronised cells

The MS analysis carried out for Exo1 purified from pre-sporulation culture detected 535 unique peptides from yeast, and 33 peptides of human origin. The sum of peptides intensities showed that Exo1 was the third most intense protein in the sample, after Snf1, and Rpl28, Table 5.3. However, the absolute intensity iBAQ showed that Exo1 was the fourth most intense protein, suggesting that Exo1 was not purified well in the sample. The sum of Exo1 peptides intensities was significantly higher in this sample (1.07×10^{10}) than the sample analysed from in-gel (1.89×10^8). This suggest that the peptide generation method by on-beads digestion reduces the amount of proteins lost compared to in-gel treatment. Out of the peptides analysed, 57 where from Exo1 sequence with 30 unique peptides covering 42.6% of Exo1 amino acid sequence, Figure 5.7. Five peptides were phosphorylated uncovering four possible phosphorylated residues, S431, S654, S660, and S664, Table 5.4. All the phosphorylated residues detected had a high phosphorylation probability, Table 5.5. In the fourth phosphorylated peptide, there were two phosphorylated residues and they were narrowed down to S660, S663, and S664. The phosphorylation of S660 residue was presented with a high probability of phosphorylation, whereas the S663 residue had a phosphorylation probability of $p = 0.138$ and S664 was presented with a phosphorylation probability of $p = 0.863$. The slight uncertainty between S663 and S664 stems from the poor fragmentation of the peptide and high level of noise, Figure A5.10, appendix V. The phosphorylation frequency of each phosphorylated residue is shown in Table 5.5. Although the phosphorylation frequency appears to be high in this sample, only five phosphorylated peptides were detected out of fifty-seven in total meaning that most of Exo1 peptides were not phosphorylated. This could correlated to the lack of electrophoretic mobility shift in the 0-hour time-point sample. In addition, the phosphorylated peptides detected here could be of the few cells that may have prematurely started the meiotic program as they failed to synchronise.

Pre-sporulation culture		
#	Protein name	Intensity
1	Rpl28	3.23×10^{10}
2	Snf1	1.15×10^{10}
3	Exo1	1.07×10^{10}
4	Nma1	4.42×10^9
5	Bfr1	3.99×10^9
6	Adh1	3.58×10^9
7	Rgi1	2.32×10^9
8	Car2	2.11×10^9
9	Eno2	1.80×10^9
10	Pck1	1.74×10^9
#	Protein name	Absolute intensity (iBAQ)
1	Rpl28	1.69×10^9
2	Snf1	2.44×10^8
3	Rgi1	1.78×10^8
4	Exo1	1.48×10^8
5	Nma1	1.47×10^8
6	Adh1	1.44×10^8
7	Rsp31	8.45×10^7
8	Bfr1	8.31×10^7
9	Car2	6.60×10^7
10	Egd1	6.03×10^7

Table 5.3 The ten most abundant proteins detected by MS in the Exo1 purified sample from pre-sporulation culture.

Exo1 was the third most intense protein and the sum of Exo1 peptides intensity was 1.07×10^{10} . The absolute intensity of each proteins showed that Exo1 was the fourth protein with an absolute intensity of 1.48×10^8 .

MGIQGLLPQLKPIQNPVSLRRYEGEVL AIDGYAWLHRAACSCA
 YELAMGKPTDKYLQFFIKRFSLLKTFKVEPYLVFDGDAIPVK
 KSTESKRRDKRKENKAIAERLWACGEKKNAMDYFQKCVDI
 TPEMAKCIICYCKLNGIRYIVAPFEADSQMVYLEQKNIVQGI
 SEDSDLLVFGCRRLITKLN DYGECL EICRDNFIKLPKKFPLG
 SLTNEEIIITMVCLSGCDYTNGI PKVGLITAMKLVRRFNTIER
 IILSIQREGKLMIPDTYINEYEAAVLAFQFQRVFCPIRKKIV
 SLNEIPLYLKDTESKRRRLYACIGFVIHRETQKKQIVHFDD
 DIDHHLHLKIAQGD LN PYDFHQPLANREHKLQLASKSNIEFG
 KTNNTNSEAKVKPIESFFQKMTKLDHNPKVANNIHS LRQAED
 KLTMAIKRRKLSNANVVQETLKDTRSKFFNKPSMTVVENF
 KEKGDSIQDFKEDTNSQSLEEPVSESQ LSTQIPSSFITTNLED
 DDNLSEEVSEVVS DIEEDRKNSEGKTIGNEIYNTDDDGDGDT
 EDYSETAESRVPTSSTTSFPGSSQR S ISGCTKVLQKFRYSS
 FSGVNANRQPLFPRHVNQKSRGMVYVNQNRDDDCDDNDGKNQ
 ITQRPSLRKSLIGARSQRIVIDMKSVDE RKS FNS SPILHE
 ESKKRDIETT KSSQARPAVRSISLLSQFVYK GK LKLR TGSH
 HHHHHGDYKDDDDKDYKDDDDKDYKDDDDKGDYKDDDDKDY
 KDDDDKDYKDDDDK*|

Figure 5.7 Exo1 amino-acid sequence with the peptides sequences analysed by MS in the Exo1 purified sample from pre-sporulation culture.

The peptides detected by the MS are highlighted in grey. The MS covered 42.6% of Exo1 amino acid sequence. The Trypsin cleavage sites arginine (K) and lysine (R) are shown in purple. In this MS analysis, four possible phosphorylation sites were detected S431, S654, S660, and S664, shown in red.

#	Exo1 phosphorylated peptide sequence	Phosphorylation site(s) probability	Phosphorylation site(s)
1	KLS ^P NANVVQETLK	KLS (1) NANVVQETLK	S431
2	KLS ^P NANVVQETLKDTR	KLS (1) NANVVQETLKDTR	S431
3	IVIDMKS ^P VDER	IVIDMKS (1) VDER	S654
4	SVDERKS ^P FNSSPILHEESK	SVDERKS (0.872) FNS (0.078) S (0.049) PILHEESK	S660
5	SVDERKS ^P FNS ^S PILHEESK	S (0.002) VDERKS (0.998) FNS (0.138) S (0.863) PILHEESK	S660 and S664

Table 5.4 Exo1 phosphorylated peptides detected in Exo1 purified sample from pre-sporulation culture.

Five phosphorylated peptides were detected with four unique phosphorylation sites, S431, S654, S660, and S664. In the fifth peptide there is a small probability that S663 could be phosphorylated, however S664 was presented with a higher phosphorylation probability.

Phosphorylation site frequency			
Residue	Number of times detected	Phosphorylated	Not phosphorylated
S431	9	3	6
S663	8	1 or 0	7 or 8
S664	8	1 or 2	6 or 7
S692	3	1	2

Table 5.5 The frequency of each detected phosphorylated site in Exo1 purified sample from pre-sporulation culture.

The phosphorylated residues detected in this MS had low frequency, meaning that most peptides analysed were not phosphorylated.

5.3.2 Mass spectrometry for purified Exo1 from meiotic cell culture after four-hours of meiosis induction

MS analysis was carried out for Exo1 purified from sporulation culture after four hours of meiosis induction, this was when Exo1 phosphorylation peaked, as demonstrated in chapter 3. In this sample, Exo1 was the third most intense protein after Snf1, and Rpl28, Table 5.6. The total intensities of Exo1 peptides was 8.7×10^9 and the iBAQ intensity was 1.21×10^8 . The MS detected 375 yeast peptides, and 23 peptides of human origin. Out of the total number of peptides detected, 81 peptides were Exo1 peptides, with 52 unique peptides constituting of 51.4% of Exo1 amino acid sequence, Figure 5.8. The higher ratio of Exo1 peptides to the total number of peptides could be correlated to the increased expression of Exo1 observed at this time-point. The MS showed 20 phosphorylated Exo1 peptides with thirteen possible phosphorylation sites, S372, S431, T439, S585, S587, S654, S660, S663, S664, S681, S682, S692, and S695, Table 5.7. The increased number of phosphorylated residues correlates to the exaggerated electrophoretic mobility shift observed in the western blot of the four-hour sample. All phosphorylated residues were detected with high probability except for S663 and S681. The phosphorylation of the residue S663 in the thirteenth peptide had the same probability as S664, and it was phosphorylated with high probability along with S664 in two other peptides (peptide 14 and 15). Since S664 was presented by itself with a high phosphorylation probability in the sixteenth peptide, it is more likely that S664 was phosphorylated in peptide 13. The phosphorylated residue S681 on the seventeenth peptide could not be determined with high confidence. The analysis software gave S681 the highest probability from other possible residues, however in the eighteenth peptide, S682 had the highest probability with better fragmentation making S682 more likely to be phosphorylated. In conclusion, Exo1 phosphorylation sites were narrowed down to thirteen sites, and twelve residues S372, S431, T439, S585, S587, S654, S660, S663, S664, S682, S692, and S695 were the most likely phosphorylated residues during meiosis.

Four hours post-meiosis induction		
#	Protein name	Intensity
1	Snf1	1.07×10^{10}
2	Rpl28	9.67×10^9
3	Exo1	8.7×10^9
4	Car2	2.77×10^9
5	Bfr1	2.56×10^9
6	Nma1	1.43×10^9
7	Hrk1	1.35×10^9
8	Hbt1	1.25×10^9
9	Rgi1	9.75×10^8
10	Ygr237c	5.70×10^8
#	Protein name	Absolute intensity (iBAQ)
1	Rpl28	5.09×10^8
2	Snf1	2.27×10^8
3	Exo1	1.21×10^8
4	Car2	8.64×10^7
5	Rgi1	7.50×10^7
6	Bfr1	5.34×10^7
7	Nma1	4.75×10^7
8	Egd1	3.64×10^7
9	Hrk1	2.59×10^7
10	Rps31	2.26×10^7

Table 5.6 The intensity of the most abundant proteins detected in Exo1 purified sample from cells after four-hours of meiosis induction.

Exo1 was the third most intense protein based on the sum of peptides intensity (8.7×10^9) and when based on absolute intensity (1.21×10^8).

MGIQGLLPQL**K**PIQNPVSL**RR**YEGEVLAIDGYAWLH**RA**ACSCA
 YELAMG**K**PTD**K**YLQFFI**KR**FSL**LK**TF**K**VEPYLVFDGDAI**PVK**
KSTES**KRR**D**KR**KEN**K**AIAERLWACGE**KK**NAMDYFQ**K**CVDI
 TPEMA**K**CIICYC**K**LNGI**R**YIVAPFEADSQMVYLEQ**K**NIVQGI
 SEDSDLLVFGC**RR**LIT**K**LNDYGECELEIC**R**DNFI**KLP****KK**FPLG
 SLTNEEIIITMVCLSGCDYTNGI**P**KVGLITAM**KLV****RR**FNTIER
 IILSIQ**R**EG**K**LMIPTDYINEYEA AVLAFQFQ**R**VFCPI**RKK**IV
 SLNEIPLYL**K**DTES**KRKR**LYACIGFVIH**R**ETQ**KK**QIVHFDD
 DIDHHLHL**K**IAQGD LNPHYDFHQPLAN**R**EH**KL**QLASK**S**NIEFG
KTNTTNS**EAK**V**K**PIESFFQ**K**MT**K**LDHNP**K**VANNIHS**L**RQAED
KLTM**AIKRR**KL**S**NANVVQE**T**L**K**DT**R**S**K**FFN**K**PSMTVVENE
KE**K**GDSIQDF**K**EDTNSQSLEEPVSESQLSTQIPSSFITTNLED
 DDNLSEEVSEVVS DIEED**RK**NSEG**K**TIGNEIYNTDDDG DGDT
 EDYSETAES**R**VPTSSTTSFPGSSQ**R**SISGCT**KVL**Q**KFR**Y**S**
SFSGVNAN**R**QPLFP**R**HVNQ**K**S**R**GMVYVNQN**R**DDDCDDNDG**K**N
 QITQ**R**PSL**RK**SLIGARSQ**R**IVIDM**K**S**V**DER**K**S**FN**SS**P**ILH
 EES**KKR**DIETT**KSS**QARPAV**R**SI**S**LL**S**QFVY**K**G**K**L**K**LRT
 GSHHHHHHG DY**K**DDDD**K**DY**K**DDDD**K**DY**K**DDDD**K**GDY**K**DDDD
KDY**K**DDDD**K**DY**K**DDDD**K***|

Figure 5.8 Exo1 amino-acid sequence with the peptides sequences analysed by MS in Exo1 purified sample from cells after four-hours of meiosis induction.

The peptides detected by the MS are highlighted in grey. The Trypsin cleavage sites arginine (K) and lysine (R) are shown in purple. In this MS analysis, thirteen possible phosphorylation sites were detected and are shown in red: S372, S431, T439, S585, S587, S654, S660, S663, S664, S681, S682, S692, and S695.

#	Exo1 phosphorylated peptide sequence	Phosphorylation site(s) probability	Phosphorylation site(s)
1	LQLASKS ^P NIEFGK	LQLAS (0.004) KS (0.996) NIEFGK	S372
2	KLS ^P NANVVQETLK	KLS (1) NANVVQETLK	S431
3	KLS ^P NANVVQETLKDTR	KLS (1) NANVVQETLKDTR	S431
4	KLS ^P NANVVQETLKDTR	KLS (1) NANVVQETLKDTR	S431
5	KLS ^P NANVVQET ^P LKDTR	KLS (1) NANVVQET (1) LKDTR	S431 and T439
6	LSNANVVQET ^P LKDTR	LS (0.015) NANVVQET (0.985) LKDTR	T439
7	FRYS ^P SSFGVGNANRQPLFPR	FRY (0.071) S (0.913) S (0.013) S (0.003) FSGVGNANRQPLFPR	S585
8	FRYS ^P SS ^P FSGVGNANRQPLFPR	FRY (0.121) S (0.763) S (0.139) S (0.97) FS (0.007) GVNANRQPLFPR	S585 and S587
9	FRYSS ^P FSGVGNANR	FRYS (0.001) S (0.004) S (0.972) FS (0.023) GVNANR	S587
10	FRYSS ^P FSGVGNANRQPLFPR	FRYSS (0.001) S (0.999) FSGVGNANRQPLFPR	S587
11	IVIDMKS ^P VDER	IVIDMKS (1) VDER	S654
12	SVDERKS ^P FNSPILHEESK	SVDERKS (0.996) FNS (0.002) S (0.001) PILHEESK	S660
13	SVDERKS ^P FNS ^P S ^P PILHEESK	S (0.002) VDERKS (0.998) FNS (0.5) S (0.5) PILHEESK	S660 and (S663 or S664)
14	SFNS ^P S ^P PILHEESK	S (0.049) FNS (0.954) S (0.996) PILHEESK	S663 and S664
15	SFNS ^P S ^P PILHEESK	SFNS (1) S (1) PILHEESK	S663 and S664
16	KSFNS ^P PILHEESK	KSFNSS (1) PILHEESK	S664
17	DIETTKS ^P SQARPAVR	DIET (0.181) T (0.181) KS (0.559) S (0.08) QARPAVR	S681
18	DIETTKS ^P SQARPAVR	DIETTKS (0.012) S (0.988) QARPAVR	S682
19	SIS ^P LLSQFVYK	S (0.053) IS (0.947) LLSQFVYK	S692
20	SIS ^P LLS ^P QFVYK	S (0.075) IS (0.925) LLS (1) QFVYK	S692 and S695

Table 5.7 The twenty phosphorylated peptides detected by MS in Exo1 purified sample from a meiotic cell culture at fourth-hour time-point.

Thirteen phosphorylated residues were detected all were serine except T439. All phosphorylated residues had high phosphorylation probability except for S663 and S664 in the thirteenth peptide.

The frequency of each phosphorylated residue was analysed to confirm the phosphorylation of each site, ensuring that it was phosphorylated at multiple occurrences. As shown in Table 5.8, the phosphorylation sites S431, T439, S585, and S587 were covered in eight different peptides. The S431 residue was phosphorylated in four peptides, and the S587 residue was phosphorylated in three peptides making them one of the most phosphorylated residues detected. The T439 residue was phosphorylated in one peptide only, suggesting that this residue might not be always phosphorylated. In addition, both phosphorylation sites S663 and S664 were covered in seven peptides, and they were phosphorylated together in multiple cases. The low phosphorylation frequency of other residues does not mean that they were not phosphorylated. This may suggest that they were not phosphorylated in multiple species of Exo1, or those sites might have lost the phosphorylation during sample preparation as they may be more labile. Another possibility is that a phosphorylated peptide might not be in the detection range of the MS instrument, which is between 375 m/z to 1600 m/z . Nevertheless, the detection of any phosphorylated residue with high probability means that they are most probably phosphorylated *in vitro*.

5.3.3 Mass spectrometry analysis for Exo1 sample purified from *sae2Δ* strain after four-hours of meiosis induction

To investigate the over-phosphorylation of Exo1 when the Tel1-mediated pathway is overactive, MS was carried out for Exo1 purified from cells that lack the Sae2 protein and after four hours of meiosis induction. This was done to ensure that the Tel1-mediated pathway causes Exo1 phosphorylation in wild-type cells. Since the cells cannot proceed in the meiotic program in the absence of Sae2, more phosphorylation sites could potentially be detected. This is because Exo1 would not be dephosphorylated as most cells would stop at the same stage of the meiotic programme. This would allow more phosphorylation sites to be detected and validate the phosphorylation sites found during wild type meiosis.

Phosphorylation site frequency after four hours of meiosis induction			
Residue	Number of times detected	Phosphorylated	Not phosphorylated
S372	1	1	0
S431	8	4	4
T439	8	1	7
S585	8	2	6
S587	8	3	5
S654	6	1	5
S660	7	1	6
S663	7	2	5
S664	7	3	4
S681	3	1	2
S682	3	1	2
S692	7	2	5
S695	7	1	6

Table 5.8 The phosphorylation site frequency for the MS carried out for Exo1 purified from cells after four-hours of sporulation.

The residues with the highest frequency were S431, T439, S585, S587, and S664.

Exo1 was purified from *sae2Δ* cells after four hours of meiosis induction and MS was carried out for the purified sample. In this sample Exo1 was the third most intense protein based on the sum of peptides intensities, 1.82×10^9 , Table 5.9. The iBAQ intensity showed that Exo1 was the fifth most intense protein in the sample, 4.92×10^7 . Additionally, the MS uncovered 677 peptides, where 591 were yeast peptides and 86 were of human origins. Out of the yeast peptides analysed, 161 were from Exo1 sequence, with 54 unique Exo1 peptides covering 53.1% of Exo1 amino acid sequence, Figure 5.9. The MS showed 35 phosphorylated Exo1 peptides, and uncovered 14 phosphorylation sites: S372, S431, T439, S585, S587, S654, S660, S663, S664, S681, S682, S690, and S695, Table 5.10. All of the phosphorylation sites were presented with a high probability of phosphorylation. Only the 32nd peptide exhibited phosphorylation uncertainty between S690 and S692 as both were presented with an equal phosphorylation probability. However, both phosphorylation sites S690 and S692 were detected in other peptides with high probability of phosphorylation, meaning that both residues were phosphorylated in the analysed sample. The S664 residue showed the highest phosphorylation frequency out of all detected phosphorylation sites, Table 5.11. The residue with the second most phosphorylation frequency was S654. This suggests that S664 and S654 sites were phosphorylated in most of Exo1 phosphorylated species. The S682 residue was always phosphorylated and was never detected in its non-phosphorylated form, this suggest that this residue was possibly phosphorylated in all Exo1 peptides.

In conclusion, the MS for Exo1 purified from *sae2Δ* cells that were induced into meiosis showed fourteen phosphorylation sites, with one extra site (S690) when compared to wild type meiosis. This shows that the phosphorylation of Exo1 during wild-type meiosis and in the absence of *SAE2* are very similar, meaning that in both cases the phosphorylation of Exo1 occurs during the Tel1-mediated pathway.

Abundant proteins in <i>sae2Δ</i> MS sample		
#	Protein name	Intensity
1	Rpl28	9.93 x 10 ⁹
2	Car2	2.05 x 10 ⁹
3	Exo1	1.82 x 10 ⁹
4	Snf1	1.79 x 10 ⁹
5	Rpl32	9.30 x 10 ⁸
6	Hbt1	5.44 x 10 ⁸
7	Cdc24	5.13 x 10 ⁸
8	Rgi2	3.07 x 10 ⁸
9	Hrk1	2.61 x 10 ⁸
10	Gpd2	2.45 x 10 ⁸
#	Protein name	Absolute intensity (iBAQ)
1	Rpl28	1.10 x 10 ⁸
2	Rpl32	1.16 x 10 ⁸
3	Car2	8.54 x 10 ⁷
4	Snf1	5.60 x 10 ⁷
5	Exo1	4.92 x 10 ⁷
6	Rps31	3.33 x 10 ⁷
7	Rgi2	3.07 x 10 ⁷
8	Rgi1	3.03 x 10 ⁷
9	Cdc24	1.07 x 10 ⁷
10	Gpd2	9.82 x 10 ⁶

Table 5.9 The ten most intense proteins in the MS sample for Exo1 purified from *sae2Δ* cells.

The sum of Exo1 peptides intensities showed a value of 1.82×10^9 where Exo1 ranked as the third most intense protein. Upon analysing the absolute intensity of each protein, Exo1 ranked as the fifth protein with an iBAQ intensity of 4.92×10^7 .

MGIQGLLPQLKPIQNPVSLRRYEGEVLAIDGYAWLHRAACSCA
 YELAMGKPTDKYLQFFIKRFSLLKTFKVEPYLVFDGDAIPVK
 KSTESKRRDKRKENKAIAERLWACGEKKNAMDYFQKCVDI
 TPEMAKCIICYCKLNGIRYIVAPFEADSQMVYLEQKNIVQGI I
 SEDSDLLVFGCRRRLITKLN DYGECL EICRDNFIKLPKKFPLG
 SLTNEE IITMVCLSGCDYTNGI PKVGLITAMKLVRRFNTIER
 IILSIQREGKLMIPDTYINEYEAAVLAFQFQRVFCPIRKKIV
 SLNEIPLYLKDTESKRKRLYACIGFVIHRETQKKQIVHFDD
 DIDHHLHLKIAQGDLNPDYDFHQPLANREHKLQLASKSNIEFG
 KTNNTNSEAKVKPIESFFQKMTKLDHNPKVANNIHSLRQAED
 KLTMAIKRRKLSNANVVQETLKDTRSKFFNKPSMTVVENF
 KEKGDSIQDFKEDTNSQSLEEPVSESQ LSTQIPSSFITTNLED
 DDNLSEEVSEVVSDIEEDRKNSEGKTIGNEIYNTDDDGDGDT S
 EDYSETAESRVPTSSTTSFPGSSQRSISGCTKVLQKFRYS
 SFSGVNANRQPLFPRHVNQKSRGMVYVNQNRDDDCDDNDGKN
 QITQRPSLRKSLIGARSQRIVIDMKSVDERKSNSSPILH
 EESKKRDIETTSSQARPAVRSISLLSQFVYKGLKLR T
 GSHHHHHHG DYKDDDDKDYKDDDDKDYKDDDDKGDYKDDDD
 KDYKDDDDKDYKDDDDK*

Figure 5.9 Exo1 amino acid sequence showing the coverage of the MS analysis carried for Exo1 purified from meiotic cell that lack Sae2.

The sequences highlighted in grey were covered in the MS analysis, which constitute of 53.1% of Exo1's amino acid sequence. The fourteen-phosphorylation sites presented by the MaxQuant software are shown in red (S372, S431, T439, S585, S587, S654, S660, S663, S664, S681, S682, S690, and S695)

#	Exo1 phosphorylated peptide sequence	Phosphorylation site(s) probability	Phosphorylation site(s)
1	LQLASK ^S NIEFGK	LQLASKS (1) NIEFGK	S372
2	KLS ^P NANVVQETLK	KLS (1) NANVVQETLK	S431
3	KLS ^P NANVVQETLKDTR	KLS (1) NANVVQETLKDTR	S431
4	RKLS ^P NANVVQETLK	RKLS (1) NANVVQETLK	S431
5	KLS ^P NANVVQET ^P LKDTR	KLS (1) NANVVQET (1) LKDTR	S431 ; T439
6	KLSNANVVQET ^P LKDTR	KLSNANVVQET (1) LKDTR	T439
7	FRY ^S ^S ^S FSGV ^N ANRQPLFPR	FRY (0.064) S (0.932) S (0.068) S (0.936) FSGV ^N ANRQPLFPR	S585 ; S587
8	FRYSS ^S ^S ^S FSGV ^N ANRQPLFPR	FRYSS (0.001) S (0.999) FSGV ^N ANRQPLFPR	S587
9	YSS ^S ^S FSGV ^N ANR	YS (0.001) S (0.032) S (0.967) FSGV ^N ANR	S587
10	IVIDMK ^S VDER	IVIDMKS (1) VDER	S654
11	IVIDMK ^S VDER	IVIDMKS (1) VDER	S654
12	IVIDMK ^S VDER	IVIDMKS (1) VDER	S654
13	IVIDMK ^S VDERK	IVIDMKS (1) VDERK	S654
14	IVIDMK ^S VDERK	IVIDMKS (1) VDERK	S654
15	SVDERK ^S ^P FNSSPILHEESK	SVDERKS (0.997) FNS (0.003) SPILHEESK	S660
16	SVDERKSFNS ^S ^S ^P PILHEESK	KSFNS (1) S (1) PILHEESK	S663 ; S664
17	KSFNS ^S ^S ^P PILHEESK	KSFNS (1) S (1) PILHEESK	S663 ; S664
18	KSFNS ^S ^S ^P PILHEESK	KSFNS (1) S (1) PILHEESK	S663 ; S664
19	KSFNS ^S ^S ^P PILHEESK	RKSFNS (1) S (1) PILHEE	S663 ; S664
20	KSFNS ^S ^P PILHEESK	KSFNSS (1) PILHEESK	S664
21	KSFNS ^S ^P PILHEESK	KSFNSS (1) PILHEESK	S664
22	KSFNS ^S ^P PILHEESK	KSFNS (0.052) S (0.948) PILHEESK	S664
23	KSFNS ^S ^P PILHEESK	KSFNS (0.091) S (0.909) PILHEESK	S664
24	SFNS ^S ^S ^P PILHEESK	S (0.002) FNS (0.998) S (1) PILHEESK	S663 ; S664
25	SFNS ^S ^P PILHEESK	SFNSS (1) PILHEESK	S664
26	SFNS ^S ^P PILHEESK	SFNS (0.009) S (0.991) PILHEESK	S664
27	SFNS ^S ^P PILHEESK	SFNS (0.001) S (0.999) PILHEESK	S664
28	DIETTK ^S ^S ^P QARPAVR	DIETTKS (1) S (1) QARPAVR	S681 ; S682
29	DIETTK ^S ^S ^P QARPAVR	DIETTKS (1) S (1) QARPAVR	S681 ; S682
30	DIETTKS ^S ^P QARPAVR	DIETTKS (0.07) S (0.93) QARPAVR	S682
31	^S ^P ISLLSQFVYKGG	S (0.942) IS (0.058) LLSQFVYKGG	S690
32	^S ^P ^I ^S ^P LLS ^P QFVYK	S (0.5) IS (0.5) LLS (1) QFVYK	S690 or S692 ; S695
33	SI ^S ^P LLS ^P QFVYKGG	S (0.017) IS (0.984) LLS (0.999) QFVYKGG	S692 ; S695
34	SI ^S ^P LLSQFVYK	S (0.005) IS (0.995) LLSQFVYK	S692
35	SI ^S ^P LLSQFVYKGG	S (0.083) IS (0.912) LLS (0.005) QFVYKGG	S692

Table 5.10 The 35 phosphorylated peptides detected by MS with 14 unique phosphorylation sites for Exo1 purified from meiotic cell that lack Sae2. All of the phosphorylation sites were determined with high probability. The S690 in the 32nd peptide was presented with an equal phosphorylation probability to S692.

Phosphorylation site frequency of Exo1 in the absence of <i>SAE2</i>			
Residue	Number of times detected	Phosphorylated	Not phosphorylated
S372	2	1	1
S431	12	4	8
T439	15	2	13
S585	7	1	6
S587	7	3	4
S654	7	5	2
S660	19	1	18
S663	19	5	14
S664	19	12	7
S681	3	2	1
S682	3	3	0
S690	9	1 or 2	8 or 7
S692	9	3 or 4	5 or 6
S695	9	2	7

Table 5.11 Phosphorylation site frequency of Exo1 phosphorylated residues in meiotic cells that lack *Sae2*.

The most detected residues were S660, S663, and S664 where S664 was the residue with the highest phosphorylation frequency. The second two most detected sites were S431, and T439, where S431 showed a higher frequency than T439.

Discussion:

The two-step purification method developed in this study purified enough Exo1 to be analysed by MS. The purified Exo1 sample was run on SDS-PAGE and then the gel was stained with Coomassie. Although an Exo1 band was observed in the western blot of the same sample, the Coomassie stained gel did not show a band that corresponds to Exo1's molecular weight. Nevertheless, the area on the Coomassie stained gel that corresponds to the area where Exo1 signal was observed in the western blot was excised and treated for MS analysis. Using this method, the MS uncovered only 39.3% of Exo1 sequence. This maybe because trypsin treatment was not efficient, or Exo1 peptides were not fully eluted from the gel. Although Exo1 coverage was low and not many Exo1 peptides were detected (54 peptides), the MS uncovered four phosphorylation sites S431, S663, S664, and S692.

To get more Exo1 coverage and to preserve labile phosphorylated residues, on-beads peptide generation was carried out, and ETD fragmentation was used before MS2. Using on-beads trypsin digestion should be more efficient as the purified protein are more exposed to trypsin, and the peptides do not need to be eluted as in the previous treatment method. This method was used for purified Exo1 from two types of cell culture; pre-sporulation culture after synchronisation by starvation, and a meiotic cell culture after four-hours of sporulation. In the pre-sporulation culture, the cells were synchronised and ready to enter the meiotic program. In this cell culture, Exo1 expression was very low and the electrophoretic shift was not observed as shown in chapter 3. This experiment was done to investigate if Exo1 is phosphorylated before the cells enter meiosis and the data produced could serve as a control to the MS done for Exo1 extracted from cells induced into meiosis. In the Exo1 purified sample from pre-sporulation culture, the MS detected 57 Exo1 peptides uncovering 42.6% of Exo1 amino acid sequence. Whereas, the MS carried out of Exo1 purified from cells after four-hours of sporulation detected 81 peptides Exo1 peptides, covering 51.4% of Exo1 sequence. Even

though the sum of Exo1 peptides intensity was higher in the pre-sporulation sample, the coverage of Exo1 amino acid sequence was more in the meiotic sample. This was confirmed by the higher absolute intensity of Exo1 in the meiotic sample in comparison to the pre-sporulation sample meaning that Exo1 peptides detected in this sample covered more of Exo1's sequence. The methodology used to purify and analyse Exo1 cannot produce enough data to compare Exo1 content between samples. However, the intensity information produced by the MS can allow to analyse the abundance of Exo1 in comparison to other proteins in the same sample. Additionally, the MS instrument used has a range of $375m/z$ to $1600m/z$ so any Exo1 peptides that are not in range will not be detected which limits the comparison of protein intensities between samples.

The MS done for Exo1 purified from pre-sporulation culture uncovered five phosphorylation sites: S431, S654, S660, and S664. However, out of the 57 Exo1 peptides analysed in this MS only five peptides were phosphorylated. This result suggest that Exo1 is phosphorylated at low level before meiosis induction, even though the previous western blots done to analyse Exo1 did not show an electrophoretic mobility shift at the 0-hour time point. In the pre-sporulation culture, most of the cells are ready to enter meiosis and are synchronised at the G1-phase. However, a small number of cells (less than 10%) were budding, and some may have already started the meiotic program. This means in this culture, cells that are undergoing S-phase, or cells that may have already started the meiotic programme could be undergoing processes that may cause Exo1 phosphorylation i.e. DNA replication or Spo11-DSB. The phosphorylated residues detected in the pre-sporulation sample were also detected in the meiotic sample. This suggests that the phosphorylation of Exo1 detected in the pre-sporulation sample might be from cells that entered meiosis early. However, meiosis independent phosphorylation of Exo1 should be investigated; MS could be done for Exo1 purified from cells that are arrested at the

G1-phase mimicking the synchronised cells in the pre-sporulation culture, and cells that are synchronised into S-phase.

The MS done for Exo1 purified from cells after four-hours of sporulation detected 20 phosphorylated peptides, which uncovered 13 phosphorylated residues. The increase in phosphorylated residues detected in this MS correlates to the increased electrophoretic mobility shift observed at the fourth-hour time point. To confirm the phosphorylated residues detected during meiosis, MS was carried out for Exo1 purified from *sae2Δ* cells after four hours of sporulation. In this sample, there was a significant increase of detected phosphorylated peptides, 35 phosphorylated peptides in comparison to 20 phosphorylated peptides during wild type meiosis. Additionally, in the *sae2Δ* sample all of the previously detected phosphorylated residues were detected again with an additional phosphorylated residue S690. This confirms previously characterised phosphorylation sites and suggests that the phosphorylation of Exo1 at the fourth-hour time-point might be dependent on the Tel1-mediated pathway. The results produced here confirmed that Exo1 was phosphorylated during meiosis and uncovered fourteen phosphorylated residues. However, since some of Exo1 sequence was not covered in this study, more residues could possibly be phosphorylated that were not covered in the MS analyses.

All of the phosphorylated residues detected were towards the C-terminal of Exo1 which is consistent with mitotic specific phosphorylation of hEXO1 (Tomimatsu et al., 2014) and yeast Exo1 phosphorylation (Morin et al., 2008). Two of the four phosphorylation sites detected during meiosis S372 and S692 were previously reported in mitotically dividing cells and in response uncapped telomeres (Morin et al., 2008). The other two phosphorylation sites S567 and S587 characterised in uncapped telomeres mutants were not detected during this study. The S567 residue was not covered in the MS analyses during this study, and it could be phosphorylated during meiosis. While the S587 residue was covered in the MS analysis but was not detected to be phosphorylated. The different and additional phosphorylation sites

detected during meiosis confirms that the *exo1-4S::A* mutant can still be phosphorylated suggesting that the phosphorylation of Exo1 during meiosis is different than Exo1 phosphorylation during mitotically dividing cells.

To find the possible kinase or the different types of kinases that phosphorylate Exo1, the phosphorylated residues and their respective motifs were analysed. The three key kinases that may phosphorylate Exo1 and were previously implicated in meiotic DSB repair are Tel1, Mec1, Mek1, and Cdc28. Tel1 and Mec1 kinases phosphorylate serine or threonine residues that precede glutamate residues, also known as SQ/TQ (Traven and Heierhorst, 2005). Only two phosphorylated residues matched the Tel1/Mec1 motif sequence, S682 and S692. Mek1 phosphorylates RxxS or RxxT motifs, where “x” is represented with any amino acid residue (Suhandynata et al., 2016). Two phosphorylated residues matched Mek1 substrate consensus, S431 and S690. Additionally, the S664 phosphorylated residue matched the SP motif, which is a potential substrate of Cdc28 kinase (Holt et al., 2009). Other phosphorylated substrates did not match any known kinase consensus. Interestingly, some phosphorylated residues seemed to be dependent on the phosphorylation of a nearby residue. For example, the S663 residue that follow another serine residue S664, was only shown to be phosphorylated with high probability when S664 is phosphorylated. Similarly, the S681 residue was only detected with high probability when S682 is phosphorylated. This suggest that those two phosphorylation sites might be dependent on the phosphorylation of the serine residue that follows them.

To localise additional phosphorylation sites on Exo1, MS analysis could be done to Exo1 purified sample treated with a different protease or a combination of two. This is because the trypsin treatment used did not produce enough Exo1 peptides that are within the range of the MS. GluC enzyme could be used which cleaves after a glutamic acid (E) residue, or a mixture of two enzymes such as GluC and trypsin. Other enzymes could be used that can digest at other sites producing detectable peptides that trypsin cannot produce e.g. chymotrypsin. There are potential phosphorylated residues that were not covered in this study; some fit the potential kinases consensus or are in similar motifs where phosphorylated residues were detected. Therefore, additional MS analyses are needed to investigate whether they are phosphorylated during meiosis or not.

Chapter 6. General Discussion

To ensure faithful chromosome segregation during meiosis, the cell must make sure that the homologous recombination pathway can tether both homologues together by producing a CO. Failing to tether both homologues would cease the meiotic program by triggering the cell-cycle checkpoint or may produce aneuploid gametes due to chromosome nondisjunction. The main players in the pathway from proteins that function in Spo11-DSB induction until the resolution of JMs are tightly controlled by a cell-cycle checkpoint mechanism. This mechanism is thought to regulate the homologous recombination pathway by protein PTMs such as phosphorylation that can influence their function. During this study, Exo1 was shown to be phosphorylated during meiosis, which is different from the phosphorylation observed during mitotically dividing cells. This is because the phosphorylation mutant *exo1-4S::A* was found to be phosphorylated during meiosis, and additional phosphorylated residues were localised during meiosis. Thus far, Exo1 phosphorylation during meiosis has not been reported in the literature. Albeit, Exo1 meiotic functions were investigated where it was found to be the major nuclease that function during the resection process and during the resolution of dHJs (Zakharyevich et

al., 2010). The aim of this project was to study Exo1 phosphorylation further and find its relation to the putative meiotic functions of Exo1. This was done by investigating the phosphorylation of Exo1 during the meiotic pathway of different meiotic mutants, especially mutants in the homologous recombination pathway. To understand the biochemistry of Exo1 phosphorylation, the phosphorylation sites were investigated by MS analysis after the development of a novel large-scale protein extraction method. After localising fourteen phosphorylated residues on Exo1, the findings would ultimately lead to characterise the regulation of Exo1 during the meiotic homologous recombination pathway.

6.1 Exo1 phosphorylation is Tel1 kinase dependent

In the absence of *SAE2* Exo1 was over-phosphorylated during sporulation as demonstrated by western blot and MS analysis. In this strain, the meiotic progression was stalled because of the over-activation of a Tel1-mediated cell-cycle checkpoint event (Usui et al., 2001; Nakada et al., 2003). Under normal conditions, Tel1 is activated in response to DNA-DSBs (Lydall et al., 1996) which is followed by the phosphorylation of the MRX complex components (Usui et al., 2001), and Sae2 (Cartagena-Lirola et al., 2006), where both function in the processing of Spo11-DSBs (Keeney and Kleckner, 1995; Moreau et al., 1999). The activation of Tel1 causes a delayed entry into anaphase-I until that meiotic recombination is completed, which almost guarantee homologous chromosomes tethering avoiding nondisjunction events (Roeder and Bailis, 2000; Hochwagen and Amon, 2006). Mutants that fail to process Spo11-DSBs such as *sae2Δ* and *mre11-H125N* prolong MRX occupancy at DNA-DSBs (Borde et al., 2004) causing the continuous activation of Tel1 signalling as reviewed by Longhese et al., 2009.

Exo1 phosphorylation was prolonged in the absence of *SAE2* and in the Mre11 nuclease mutant *mre11-H125N* as demonstrated before. These observations suggest that the prolonged phosphorylation event might be correlated to the prolonged activation of Tel1. In addition, the phosphorylation of Exo1 was abolished in the double mutant *sae2Δ tell1Δ* but was normal in

sae2Δ mec1Δ, suggesting that the phosphorylation of Exo1 is Tel1 dependent and Mec1 independent, at least during the initial processing of Spo11-DSBs. The processing of Spo11-DSBs requires the function of Sae2 and MRX complex, and the long resection process requires the nuclease function of Exo1 (Zakharyevich et al., 2010; Mimitou et al., 2017). The cell-cycle dependent phosphorylation of Sae2 by Cdc28 initiate Spo11-DSB end-resection (Huertas et al., 2008), and the phosphorylation of Sae2 by Tel1/Mec1 promotes normal resection initiation (Cartagena-Lirola et al., 2006). *In vitro* studies showed that phosphorylated Sae2 promotes the endonuclease activity of the MRX complex (Cannavo and Cejka, 2014), and regulates its interaction with Rad50 (Cannavo et al., 2018). Additionally, Mimitou et al. showed that in the absence of Tel1 during meiosis, some DSBs were resected to wild type levels, but the majority of DSBs were hyporesected (Mimitou et al., 2017). This shows that Tel1 plays a role in promoting normal resection initiation, possibly via Sae2 phosphorylation. Similarly, it is possible that the Tel1 dependent phosphorylation of Exo1 could control Exo1's nuclease activity, perhaps by initiating Exo1's resection in concert with Sae2 and MRX complex.

The *mre11-58S* nuclease mutant (H213Y) is proficient in Spo11-DSB formation but is defected in DSB repair and MRX complex assembly (Usui et al., 1998; Tsubouchi and Ogawa, 1998). In this mutant, although DSBs are not repaired, the phosphorylation of Exo1 was drastically reduced suggesting that the Tel1-mediated cell-cycle checkpoint event was not continuously activated as observed in *sae2Δ* and *mre11-H125N* mutants. This suggests the role of the MRX complex integrity in recruiting Tel1 to Spo11-DSB sites. Indeed the MRX complex recruits Tel1 to DNA damage sites (Nakada et al., 2003), mediated by Xrs2 C-terminal interaction with Tel1 (Nakada et al., 2003; Oh et al., 2016). This could explain why the Tel1-mediated pathway is not over-active when the MRX complex integrity is compromised. Nevertheless, since the phosphorylation of Exo1 was not totally abolished, further investigations are required to

understand this phosphorylation event and the role of the MRX complex in Tel1 recruitment to DSB sites.

The Tel1-mediated phosphorylation of Exo1 that shortly occurs after Spo11-DSB formation could be the signal to commence the bidirectional resection activity of Sae2/MRX and Exo1. To explore this idea, a non-phosphorylatable Exo1 mutant would be tested if it still possesses the nuclease function that can produce long tracts of 3' ssDNA.

The prolonged over-phosphorylation of Exo1 during *sae2Δ* sporulation was abolished in the absence of Mec1 function. This suggests that the prolonged phosphorylation of Exo1 observed in *sae2Δ* is dependent on Mec1. However, Tel1 and Mec1 are required to arrest the cells meiotic progression in the absence of *SAE2*, via the inactivation of Ndt80 (Lydall et al., 1996; Carballo and Cha, 2007; Gray et al., 2013). Since Ndt80 cannot be inactivated in the double mutant *sae2Δ mec1Δ*, mid-sporulation genes are transcribed by Ndt80 (Hepworth et al., 1998), which may have caused the dephosphorylation of Exo1.

6.2 **Exo1 over-phosphorylation in the absence of DMC1 and RAD51**

During the meiosis of the double mutant *dmc1Δ rad51Δ*, Exo1 was over-phosphorylated. In this mutant, the DNA was over-resected and was thought to be due to Exo1 and Sgs1 nuclease activities (Manfrini et al., 2010). Hence, the hyperphosphorylation of Exo1 observed in this mutant could be correlated to Exo1 nuclease activity. In the absence of recombinases during meiosis, a cell-cycle checkpoint is triggered via Mec1 kinase function (Lydall et al., 1996). This is because in the absence of Mec1 kinase function in *dmc1Δ* strain the cell-cycle checkpoint is bypassed (Lydall et al., 1996). In the absence of *TEL1* and *DMC1* the cell-cycle checkpoint is triggered and a few number of cells undergo nuclear division (Usui et al., 2001), suggesting that Mec1 is more active than Tel1 at the later stages of the homologous recombination pathway. Since Mec1 is over activated in the absence of recombinases, the

persistent phosphorylation of Exo1 in this mutant could be correlated to Mec1 kinase activity. The phosphorylation of Exo1 was normal in the absence of Tel1 during meiosis and was drastically reduced in the absence of Mec1. These observations suggest the role of Mec1 in Exo1 phosphorylation, especially when Spo11-DSBs are processed. Additionally, Mek1 is over active in the absence of *DMC1* during meiosis via Hop1 hyperphosphorylation (Carballo et al., 2008). Since Mek1 is overactive in this mutant, Exo1 over phosphorylation could be dependent on Mek1 activity.

Sae2 was also hyper-phosphorylated in the absence of Dmc1 during meiosis (Cartagena-Lirola et al., 2006). This comes as striking since Sae2 function is upstream of Dmc1 activity and Sae2 phosphorylation (Cartagena-Lirola et al., 2006; Huertas et al., 2008). Therefore, the hyper-phosphorylation of Exo1 in the absence of recombinases could be a sporadic event due to a cell-cycle checkpoint in a similar way to Sae2 hyperphosphorylation. To investigate this further, Exo1 phosphorylation in the absence of recombinases should be tested in the absence of Mec1 or Mek1 activity. Additionally, the non-phosphorylatable form of Exo1 must be investigated in the absence of *DMC1* and *RAD51* to test if DNA resection is affected.

6.3 Exo1 phosphorylation residues during meiosis

To understand Exo1 function during meiosis and the mode of regulating DNA resection, the phosphorylation sites on Exo1 must be identified. This was done by utilising MS analysis on Exo1 purified from meiotic cells and pre-meiotic cells to serve as control. The MS analysis done for Exo1 purified from pre-meiotic cells revealed four phosphorylated residues: S431, S654, S660, and S664. The S431 residue matched Mek1 substrate consensus RxxS (Suhandynata et al., 2016), and S664 matched Cdc28 substrate consensus SP (Holt et al., 2009). The residues S654 and S660 did not match any known kinase substrate consensus. The phosphorylation of Exo1 at this stage was surprising since at this time-point, western blots did not show an Exo1 electrophoretic mobility shift, and the cells were not sporulating yet.

However, there is a possibility that some cells may have started meiosis early, or some are still undergoing mitotic cell division. This means that the pre-meiotic phosphorylation residues detected might be due to other cellular mechanisms that not related to meiosis and further investigation is needed to understand why some residues were phosphorylated at this stage. The MS analysis done for Exo1 purified from cell induced into meiosis revealed thirteen phosphorylation sites in wild type meiosis and fourteen phosphorylation sites in *sae2Δ* strain meiosis. Five of the localised phosphorylation sites match known kinases substrate consensus. S431 and S690 matched Mek1 substrate consensus (RxxS), while S682 and S692 matched Tel1/Mec1 substrate consensus (SQ), and S664 matched Cdc28 substrate consensus (SP). This result suggest that Exo1 is phosphorylated by Cdc28, Tel1/Mec1, and Mek1. The phosphorylation site S664 is the only site with Cdc28 motif consensus (SP) in Exo1's amino acid sequence. During meiosis, it has been shown that Cdc28 dependent phosphorylation of Sae2 (Huertas et al., 2008) is required to initiate meiotic DSB resection (Manfrini et al., 2010). Since Exo1's S664 phosphorylation is a possible target of Cdc28, the phosphorylation of this site could influence Exo1 resection activity when phosphorylated Sae2 initiate meiotic DSB processing.

Some serine and threonine residues were never covered in the MS analyses in this study. These sites could potentially be phosphorylated since they lie in amino acid sequences that follow Mek1 or Tel1/Mec1 substrate consensus. These sites need to be considered if a non-phosphorylatable form of Exo1 is made. For instance, the serine rich motif 566-GSSQRSISG-574 could potentially be phosphorylated since it contains 567-SSQ-569 and 570-RSIS-573 motifs, which are similar to phosphorylated motifs 680-SSQ-683, and 689-RSIS-692 respectively. All of the localised phosphorylation sites were towards the C-terminal of Exo1's amino acid sequence. Similarly, the mitotic significant phosphorylation sites were also localised at the C-terminal of Exo1 (Morin et al., 2008). In addition, a conserved region in

Exo1's C-terminal is implicated in protein-protein interaction with Mlh1 (Tran et al., 2007). Mlh1 and Mlh3 form the MutL γ nuclease complex which has been implicated in resolving ZMM-stabilised JMs (Zakharyevich et al., 2010, 2012). Mutating Mlh1 interaction region on Exo1 C-terminal domain abolishes the interaction between Exo1 and Mlh1 (Tran et al., 2007), and significantly reduced COs but not DSB resection (Zakharyevich et al., 2010). Deleting Exo1's C-terminal domain reduced CO formation (Zakharyevich et al., 2010) and it is unknown whether this truncated version of Exo1 influenced its nuclease function. Therefore, since most of the phosphorylated residues were towards the C-terminal of Exo1, the phosphorylation of Exo1 could influence Exo1-Mlh1 interaction and CO formation. The nuclease domains of Exo1 XPG-N and XPG-I are towards the N-terminal of Exo1 sequence, section 1.8. In human and yeast studies, the phosphorylation of hEXO1/Exo1 was towards its C-terminal domain, which influenced Exo1's nuclease activity (Morin et al., 2008; Tomimatsu et al., 2014, 2017). The CDK mediated phosphorylation of human EXO1 protein promoted its nuclease activity (Tomimatsu et al., 2014). This suggest that the phosphorylation of Exo1 during meiosis might also promote its nuclease activity. However, during mitotically dividing cells, the Mek1 mitotic paralogue Rad53 can phosphorylate yeast Exo1 when ssDNA are in abundance, inhibiting Exo1's nuclease activity (Morin et al., 2008). Additionally, the phosphorylation of the human EXO1 protein by ATR (Mec1 homologue in yeast) signals hEXO1's degradation preventing pathological resection (Tomimatsu et al., 2017). These observations and the meiotic specific phosphorylation of Exo1 by multiple kinases suggest that Exo1 is possibly phosphorylated sequentially, first to promote Exo1's nuclease function perhaps via Cdc28 or Tel1, and phosphorylated again to inhibit Exo1's resection activity via Mec1 or Mek1.

6.4 **Future Directions:**

In this study, it was demonstrated that Exo1 phosphorylation was dependent on Tel1 function when Spo11-DSB ends were not repaired and blocked i.e. *sae2Δ*. However, during this study the hyperphosphorylation of Exo1 in the absence of recombinases was not investigated. To understand the dependency of Exo1 phosphorylation in the absence of recombinases, the phosphorylation event should be studied in the absence of Mec1 or Mek1. This will give more insight into the correlation of increased resection length in the absence of recombinases and the hyperphosphorylation of Exo1. Since the Rad53 dependent phosphorylation of Exo1 inhibits its nuclease function (Morin et al., 2008), it is expected that the Mek1 dependent phosphorylation of Exo1 could potentially limit Exo1's nuclease activity as well.

The MRX complex and Exo1 may co-localise since Exo1 phosphorylation was shown to be Tel1-dependent especially when DSB ends were blocked. This is also supported by the reduced phosphorylation of Exo1 during the meiosis of the MRX complex mutant *mre11-58S*. If Exo1 can co-localise with MRX complex, then the MRX complex loading onto Spo11-DSB sites may act as a platform for Tel1 and Exo1 recruitment. The Xrs2 C-terminal has been shown to function in Tel1 recruitment to DNA-DSB sites in mitotically dividing cells (Ma and Greider, 2009), and this may also occur during meiosis for Spo11-DSBs. Once Tel1 is activated by the presence of DSBs and recruited by MRX complex, Tel1 would promote the bidirectional resection of MRX/Sae2 and Exo1 which would expose long tracts of 3' ssDNA allowing for efficient homologous repair. This idea is supported by the hyporesection observed during *tell1Δ* strain meiosis (Mimitou et al., 2017). To test if Tel1 is co-localised with MRX and Exo1, chromatin-immunoprecipitation (ChIP) should be done for Exo1, Tel1, and MRX complex components followed by qPCR to test for each protein's DNA occupancy. Additionally, an Xrs2 C-terminal mutant (K846A/F847A) has been proposed fail in recruiting Tel1 to DSB sites

during mitosis (Ma and Greider, 2009). This mutant should be tested if it can recruit Tel1 during meiosis, investigate if Exo1 can be phosphorylated, and test the resection length of this mutant.

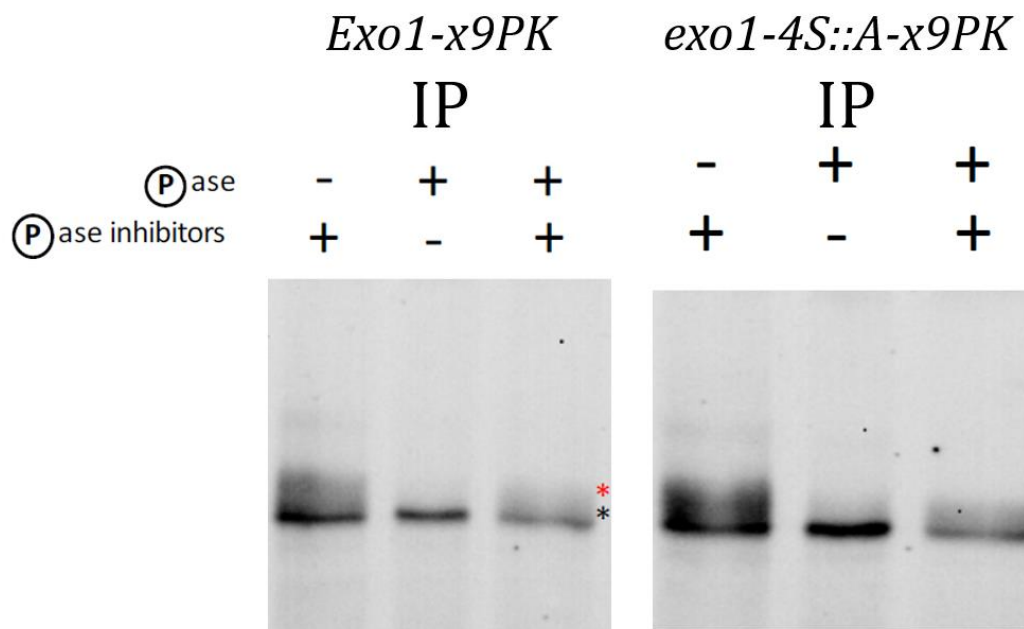
To investigate the regulation of Exo1 activities during meiosis, two phosphorylation mutants will be constructed; a non-phosphorylatable form where all phosphorylated sites are mutated to alanine, and a phosphorylation mimicking form where all phosphorylated site are mutated to aspartic acid. Since there are additional possible phosphorylation sites that were not covered during this study, more MS analyses will be done to investigate if additional residues can be phosphorylated during meiosis. Exo1 MS coverage could potentially be increased by treating purified Exo1 sample with GluC which cleaves after glutamic acid or Chymotrypsin which can cleave after phenylalanine/tyrosine/tryptophan. Using these two different enzymes would generate different peptides that trypsin cannot produce and within the range of the MS instrument. After localising all of the possible phosphorylation sites on Exo1 and producing Exo1 phosphorylated mutants, the phenotypes of both mutants such as meiotic progression, spore viability, and resection length will be investigated. Finally, Exo1 meiotic-phosphorylation mutants should also be tested if they can bind to the DNA, and if they can co-localised with Mre11 and Tel1.

The dephosphorylation of Exo1 must be studied to fully understand Exo1 meiotic functions. Since Exo1 was phosphorylated and dephosphorylated in the absence of NDT80, the production of JMs in the absence of NDT80 might play a role in the dephosphorylation of Exo1. As all of the phosphorylation sites of Exo1 were towards its C-terminal and in close proximity to the binding site of Mlh1. The dephosphorylation of Exo1 could potentially influence Mlh1 binding which might be correlated to Exo1 JMs resolution activity. This can be studied by investigating the phosphorylation of Exo1's Mlh1 binding mutant (*exo1-FF477AA*). Additionally, to test if phosphorylation can influence CO formation, the phosphorylation mutants binding to Mlh1 should be tested and their efficiency in producing COs.

Appendix:

Appendix I:

A1: Phosphatase assay for *Exo1-x9PK* and *exo1-4S::A-x9PK* by Strong, 2017



Anti-PK immunoprecipitation and Anti-PK immunoblotting

Figure A1 *Exo1-X9PK* and the phosphorylation mutant *exo1-4S::A-X9PK* are phosphorylated during meiosis.

Western blots of 7.5% SDS-PAGE gel using anti-PK to identify *Exo1-X9PK* (left) and *exo1-4S::A-X9PK* (right). The anti-PK immunoprecipitated samples were from cells after 4 hours of meiosis induction, isolated by native extraction. The purified samples were treated with various combination of Lambda phosphatase and phosphatase inhibitors, indicated by + or -. On the left and right western blots, the first and third lanes show an electrophoretic mobility shift manifested as a smear (red asterisk). This smear is reduced in the second lane of each western blot, in which the samples has been treated with Lambda phosphatase only and in the absence of phosphatase inhibitors. The reduction of this smear after treatment suggests the removal of phosphorylation, confirming that the smear is phosphorylated version of the non-modified protein.

A2: pBH368 plasmid map



Figure A2 pBH368, x6FLAG::KanMX plasmid map.

The plasmid contains a DNA sequence that encodes for x5His and two x3FLAG repeats (x6FLAG). This is followed by the *KanMX* cassette, which contains the eukaryotic *KanR* gene with TEF promoter and terminator regions. The plasmid also contains a bacterial origin of replication locus so that plasmid can be amplified in *E.coli* and a prokaryotic *AmpR* gene. The *KanMX* is used to select for yeast transformants while the *AmpR* is used to select for the plasmid transformants in *E.coli*. This plasmid map also shows the primers used to amplify the tagging cassette of Exo1.

A3: Tagging of *EXO1-4S::A* allele with x5His-x6FLAG using the CRISPR-Cas9 system:

A strain previously made in our group had the phosphorylation mutant *EXO1-4S::A* allele tagged with the PK epitope tag. Because Exo1 PK tagged strains were not producing reliable results the tag was changed to x5His-x6FLAG. This was done using the Cas9-KanMX system that was produced in our group, where it can introduce a DNA-DSB at the *KanMX* locus that was originally used to select for the PK tagged *Exo1-4S::A*. If a repair template was provided with a complementary DNA sequence, then the cells would repair the DSB made by the Cas9 protein using the transformed template.

The CRISPR/Cas9 system is a prokaryotic acquired immune system, it recognises foreign DNA such as phage DNA and destroys it by cleavage. This is done by recognising specific DNA sequences by matching the guide RNA (gRNA) sequence to a complementary DNA sequence. Cas9 is an endonuclease and causes a DNA double-strand break at the gRNA-DNA complementary site. This system has been well studied and utilised for efficient genetic manipulation of yeast (DiCarlo et al., 2015). The Cas9-KanMX RNA-protein complex can bind to the *KanMX* gene at the genomic DNA locus and introduce a DSB 300bp downstream of the *KanMX* promoter. A repair template was transformed containing x5His-x6FLAG::*NatMX* sequence flanked by complementary sequences. The repair template can be used for repairing the Cas9 induced DSB, eventually incorporating the tag cassette to *EXO1-4S::A*. The Cas9-*KanMX* was provided by Dr Bin Hu in a 2micron plasmid (pBH261). This plasmid contains the *LEU2* yeast selection marker and can express the Cas9 protein with the *KanMX*-gRNA recognition scaffold. Plasmid pBH261 and the PCR amplified cassette x5His-x6FLAG-*NatMX* were co-transformed into *Exo1-4S::A-x9PK::KanMX* haploid strain. The transformation was carried out as described in 2.3.10. The transformed haploids were selected on Leu- drop-out plates and colonies were observed after five overnights at 30°C. The Cas9-*KanMX* plasmid was selected out by growing the transformants in YPAD plates for two overnights, and strains that cannot grow on Leu- and YPAD-G418 plates but can grow on YPAD-CloNat were selected. The strain produced was mated with a wild-type *MAT α* strain to produce two opposite mating type strains that can then be mated to produce the desired homozygous diploid strain.

A4: Western blot for large scale two-step purification for *EXO1* and *EXO1-x5His-x6FLAG* strains

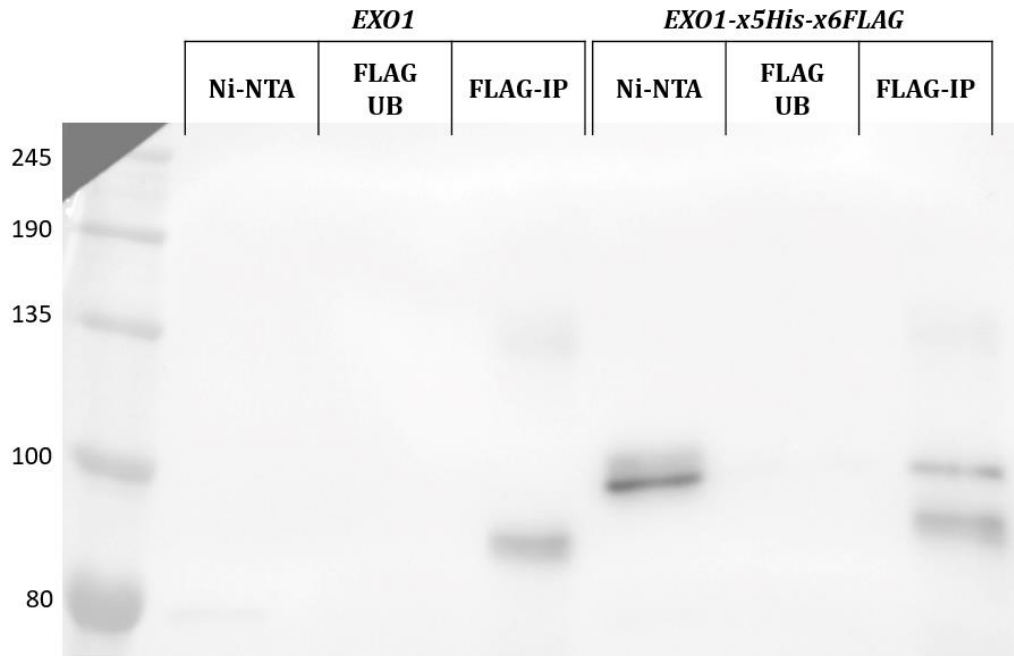


Figure A4 Western blot for Ni-NTA purified sample for *EXO1* and *Exo1-x5His-x6FLAG* meiotic samples followed by anti-FLAG immunoprecipitation.

The samples shown in this western were ran on 7.5% SDS-PAGE, which did not separate the proteins properly. In the *EXO1* Ni-NTA sample, a very faint band can be observed around 80kDa. In the second lane, no signal was observed in the FLAG unbound sample. In the third lane, the FLAG-IP sample of the non-tagged wild-type showed a smear between 135kDa and ~90kDa. The Ni-NTA purification from *Exo1-x5His-x6FLAG* sample showed an Exo1 band around 100kDa with a smear preceding it, this band was not shown across the *EXO1* samples. A faint Exo1 signal can be observed in FLAG unbound (FLAG UB) sample. The anti-FLAG immunoprecipitation sample showed an Exo1 band but no upshift can be observed. The Exo1 band was followed by a smear between 135kDa and ~90kDa, similar to the smear observed in FLAG-IP *EXO1* sample.

A5: The spectra of fragmented Exo1 phosphorylated peptides showing the relative intensity and the m/z of each fragment detected:

The figures in this section show all of Exo1 phosphorylated peptides and the fragments detected by MS2. The MS measures the m/z and the relative intensity of each fragment. The relative intensity is measured based on the most intense peak, which is usually the whole fragment m/z with or without the phosphate group that has been measured by MS1. The spectra of each peptide was visualised by p-Label software that can show the fragmentation of each peptide by entering the peptide scan number and the peptide sequence. The scan number of each peptide and its corresponding sequence were automatically analysed by MaxQuant. After entering the scan number and the peptide sequence, the expected phosphorylation site was manually entered, after the site was determined by the analysis given by MaxQuant phosphorylation probability algorithm. Once all of the parameters were entered the p-Label software will show the fragmentation of the peptide scan, and the fragments that corresponds to the y and b fragments if the peptide was fragmented by CID, or the c and z fragments if the peptide was fragmented by ETD. The fragments produced were read either from the C-terminal of the peptide or from the N-terminal. Fragments that were produced from the middle of the peptide due to multiple fragmentation were ignored since their m/z is unknown. In most cases, not all of the peptide's fragments will match the detected m/z , because the relative intensity of the fragment was very low or the fragment was not produced. Additionally, some m/z reading will not match any of corresponding expected fragments of a given peptide. Those peaks are noise produced during fragmentation, and could be fragments of the same peptides but cannot be determined since they were fragmented in the middle of the peptide. The p-Label software highlights the m/z of the measured fragments that match the m/z of the theoretical fragments of the peptide sequence. The matching threshold can be set to remove any noise that have very low relative intensity. Usually the threshold is set above the average relative intensity of the noise peaks. To determine the phosphorylation site in a peptide, the fragmentation of the peptide was analysed. The phosphorylated residue was determined based on the fragments that lost the phosphate group and the fragments that retained the phosphate group with a single serine or threonine residue. If serine or threonine residues were close to each other and the bonds between them were not broken i.e. they were not identified in two different fragments, then the phosphorylated residue cannot be determined with high probability.

Appendix V (cont'd):

A5.1 MS spectra of Exo1 peptides detected in Exo1 purified sample from cells after four hours of meiosis induction: In-gel trypsin treatment and CID fragmentation

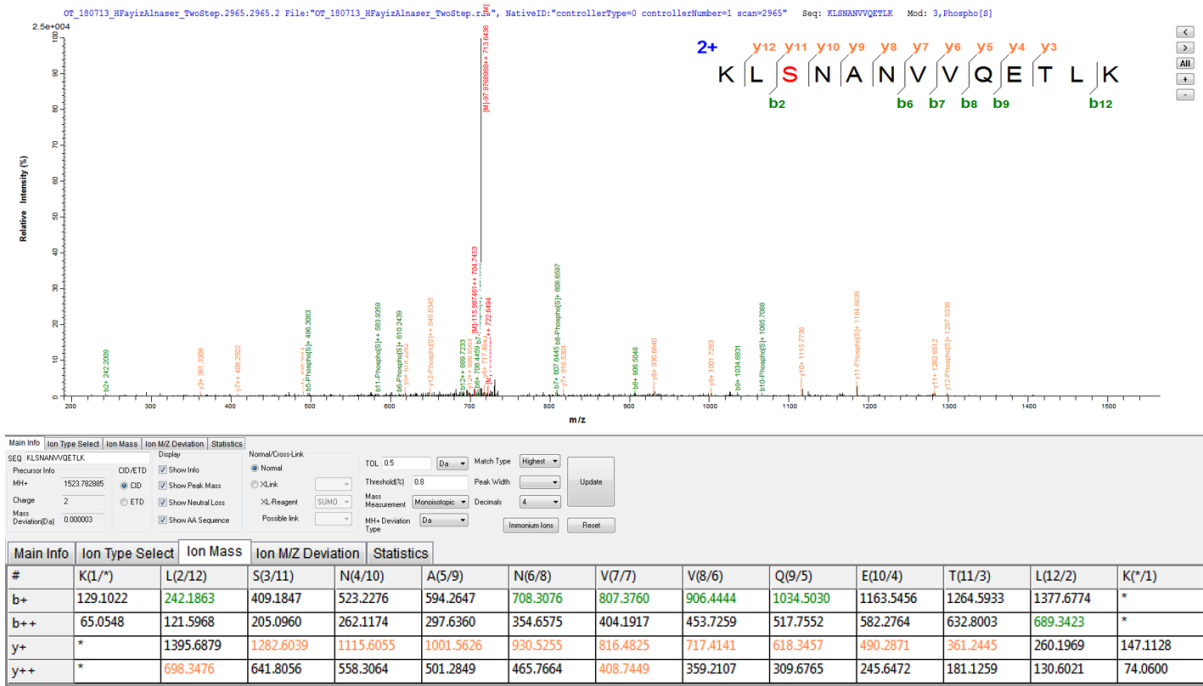


Figure A5.1 MS spectra for KLS^PNANVVQETLK with S431 phosphorylation.

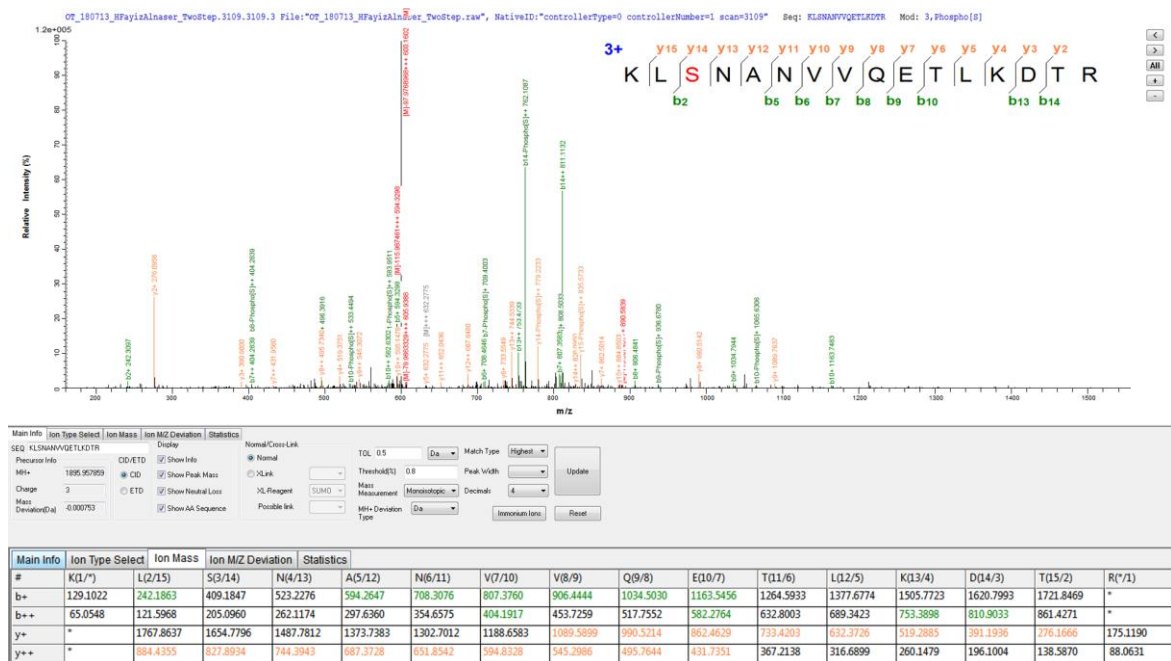


Figure A5.2 MS spectra for KLS^PNANVVQETLKDTR with S431 phosphorylation.

Appendix V (cont'd):

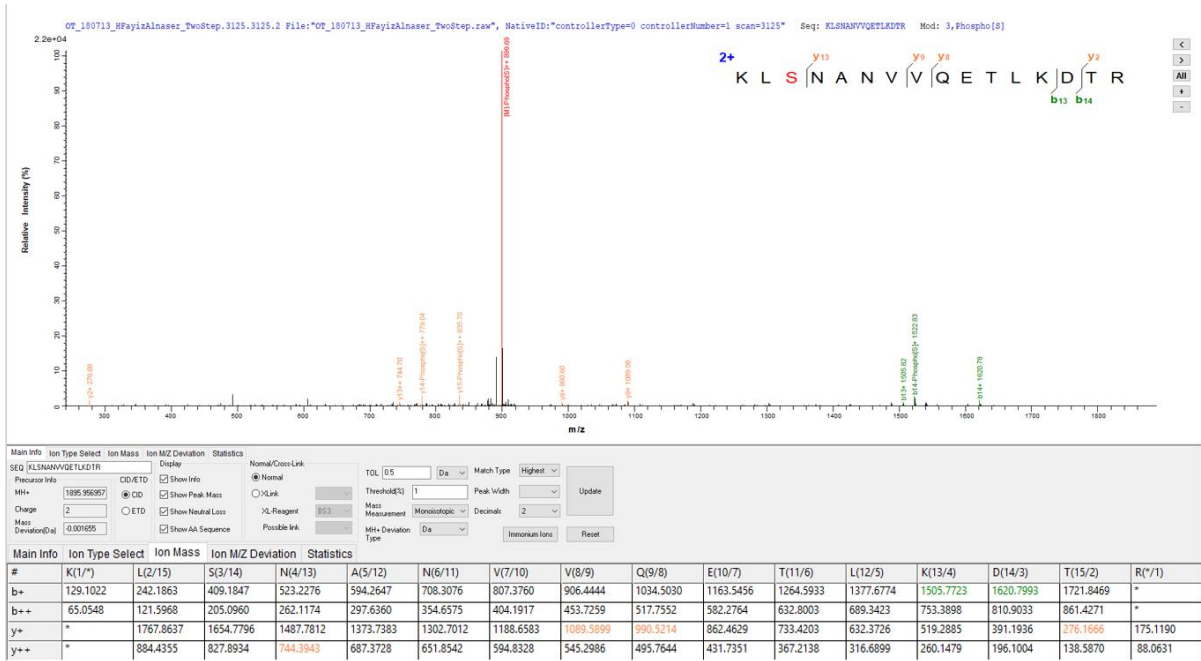


Figure A5.3 MS spectra for KLS^PNANVVQETLKDTR with S431 phosphorylation.

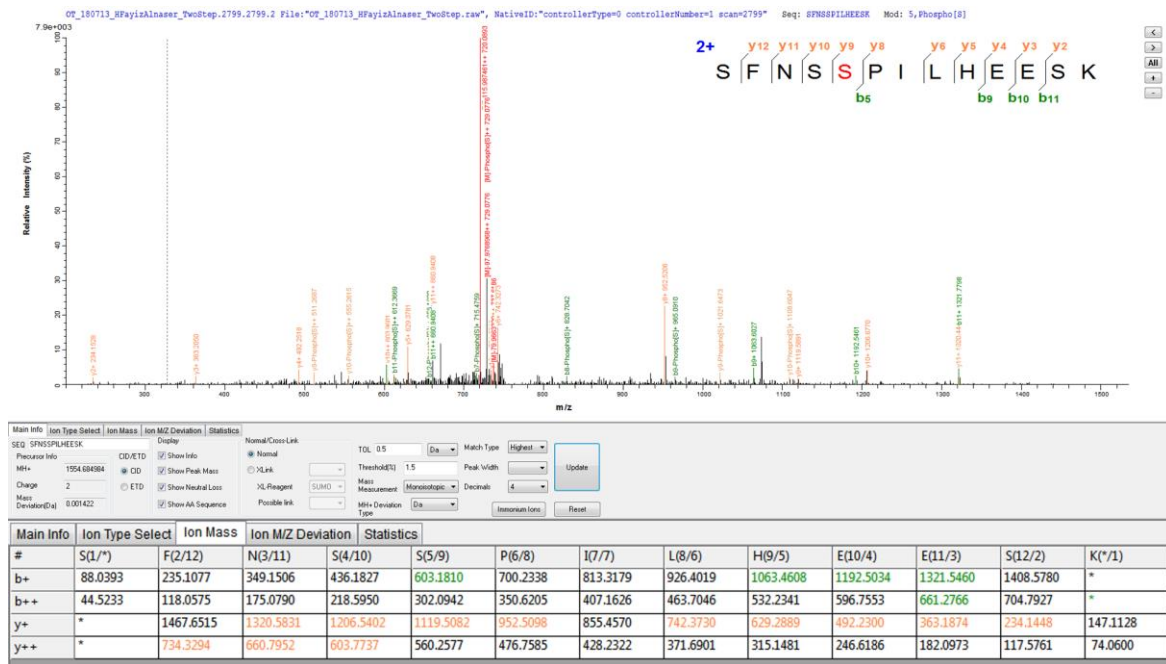


Figure A5.4 MS spectra for SFNSS^PPILHEESK with S664 phosphorylation

Appendix V (cont'd):

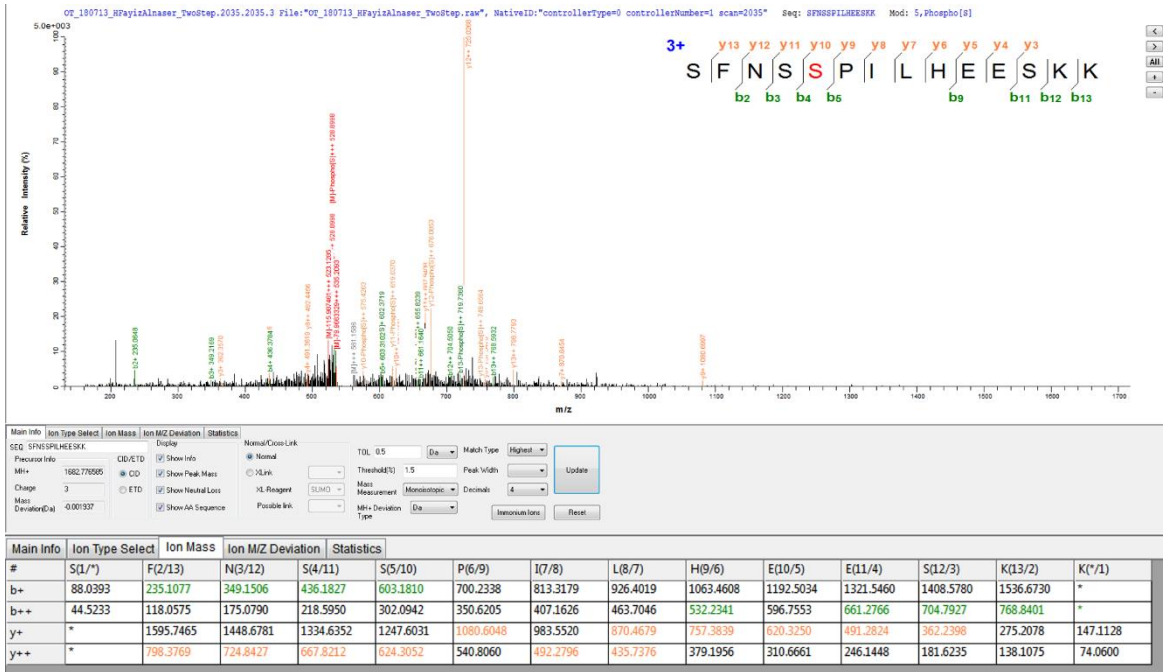


Figure A5.5 MS spectra for SFNS^PS^PPILHEESK where S663 and S663 residues were both had the same probability of being phosphorylated.

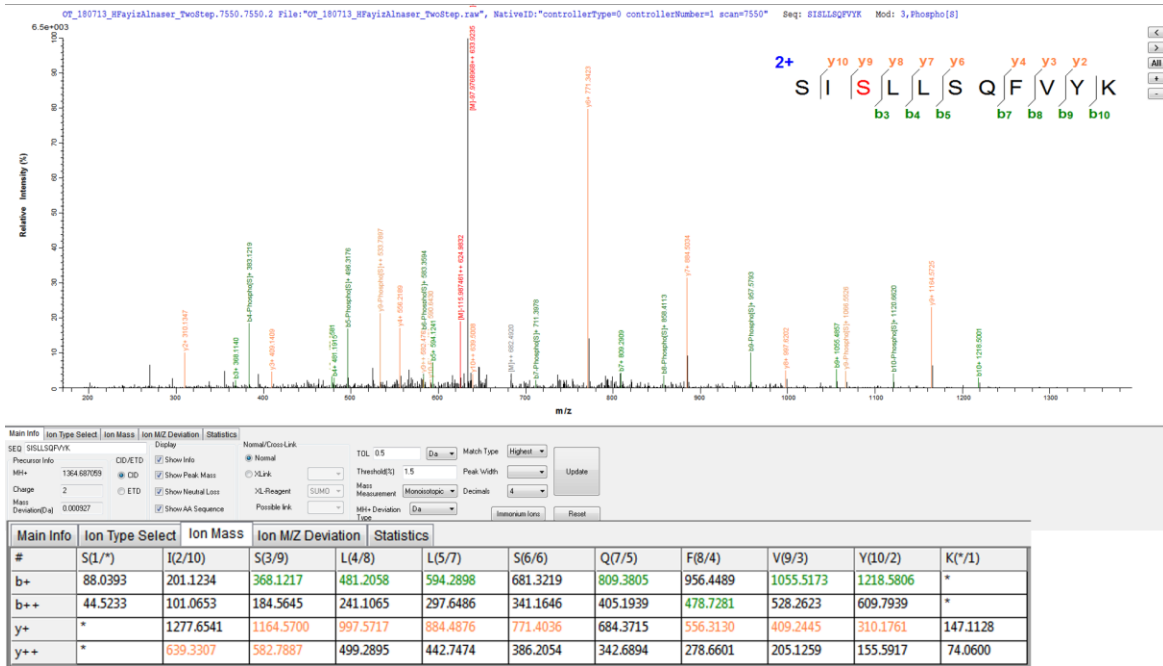


Figure A5.6 MS spectra for SIS^PLLSQVYK with S692 phosphorylation.

Appendix V (cont'd):

A5.2 MS spectra of Exo1 peptides detected in Exo1 purified sample from synchronised cells at the pre-sporulation stage: on-beads trypsin treatment and ETD fragmentation

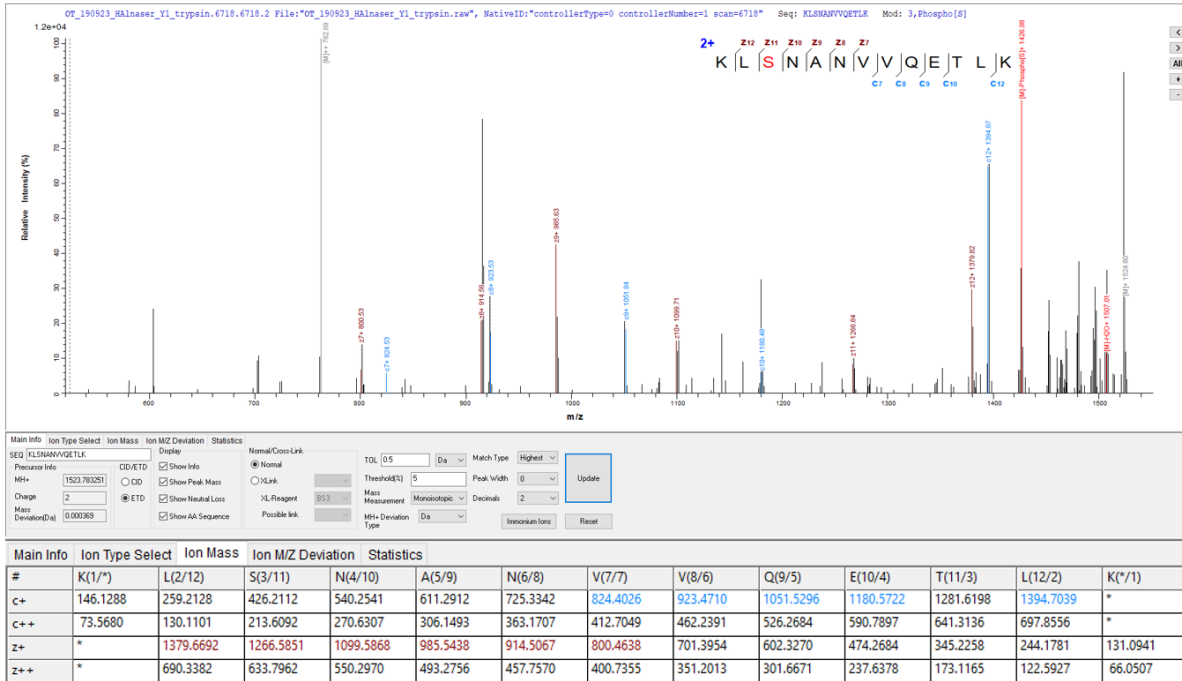


Figure A5.7 MS spectra for KLS^PNANVVQETLK with S431 phosphorylation

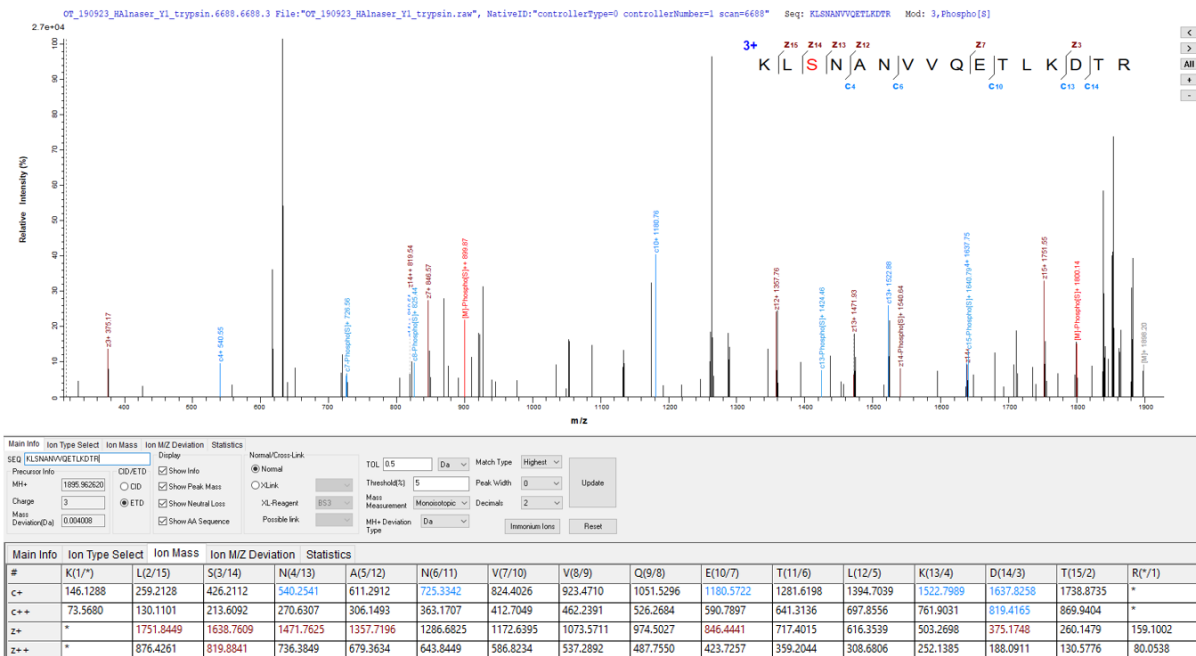


Figure A5.8 MS spectra for KLS^PNANVVQETLKDTR with S431 phosphorylation

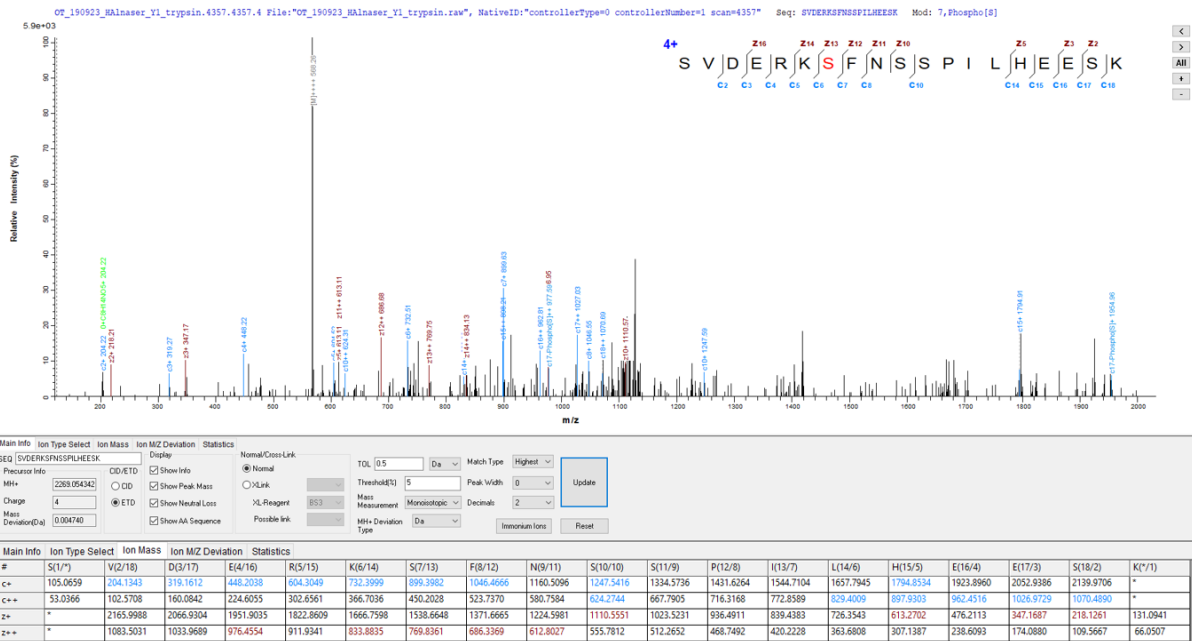


Figure A5.9 MS spectra for SVDERKSPFNSSPILHEESK with S660 phosphorylation

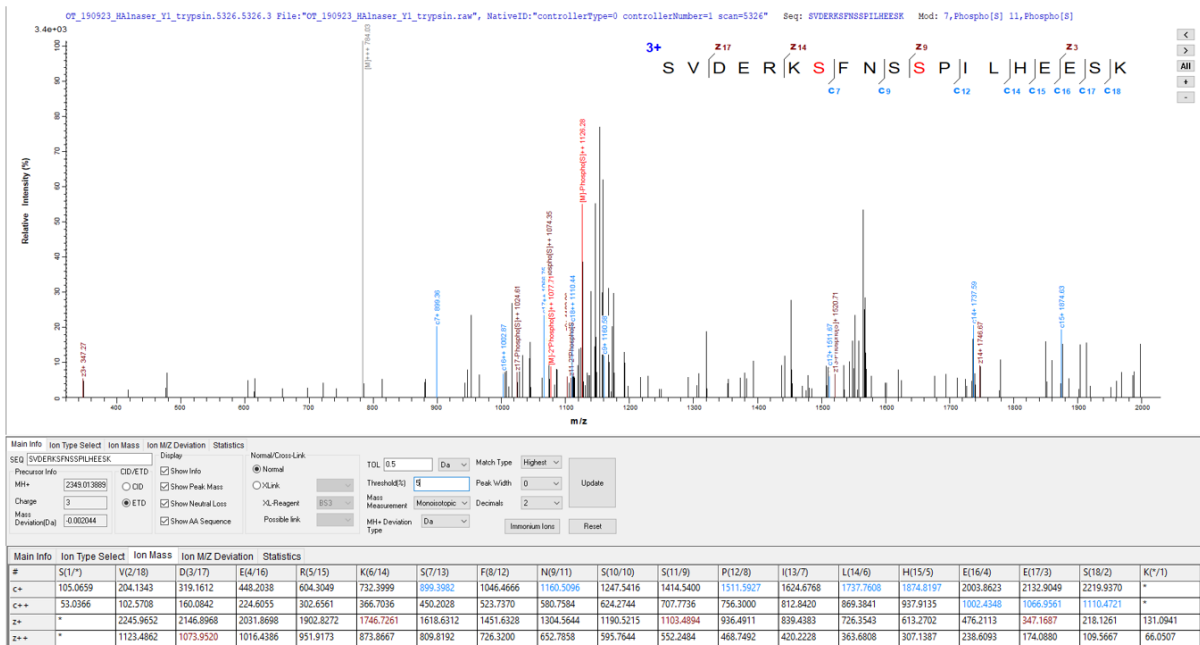


Figure A5.10 MS spectra for SVDERKSPFNSSPILHEESK with S660 and S663 phosphorylation

Appendix V (cont'd):

A5.3 MS spectra of Exo1 peptides detected in Exo1 purified sample from cells after four hours of meiosis induction: on-beads trypsin treatment and ETD fragmentation

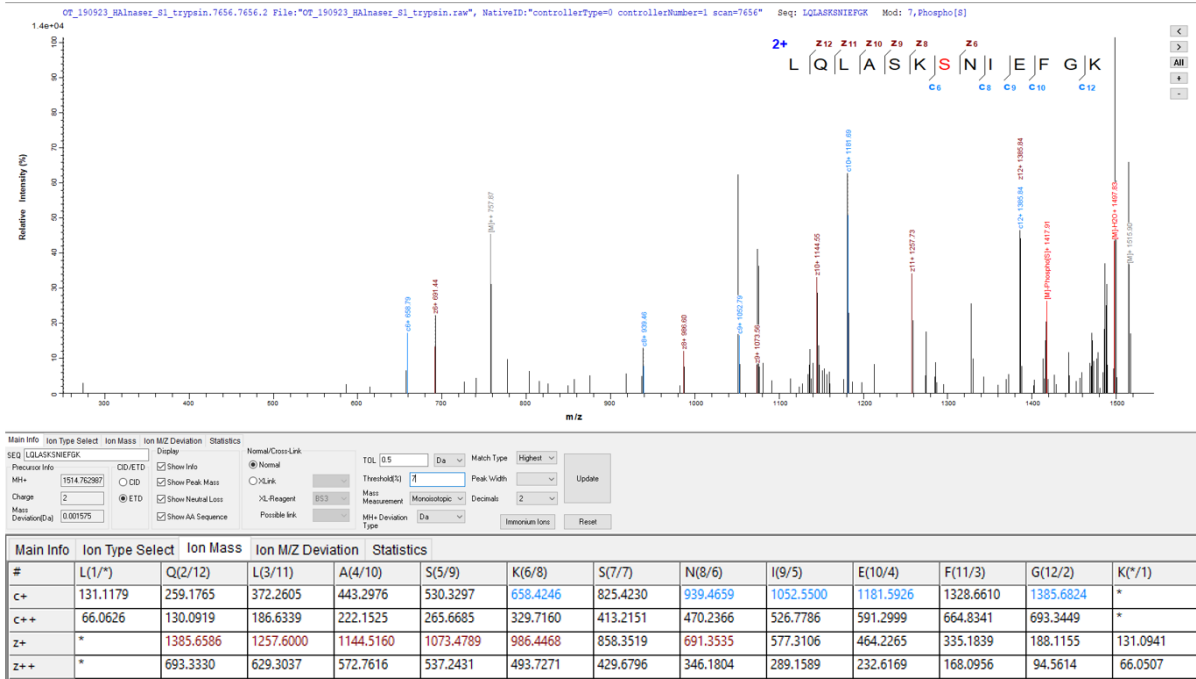


Figure A5.11 MS spectra for LQLASK^SPNIEGK with S372 phosphorylation

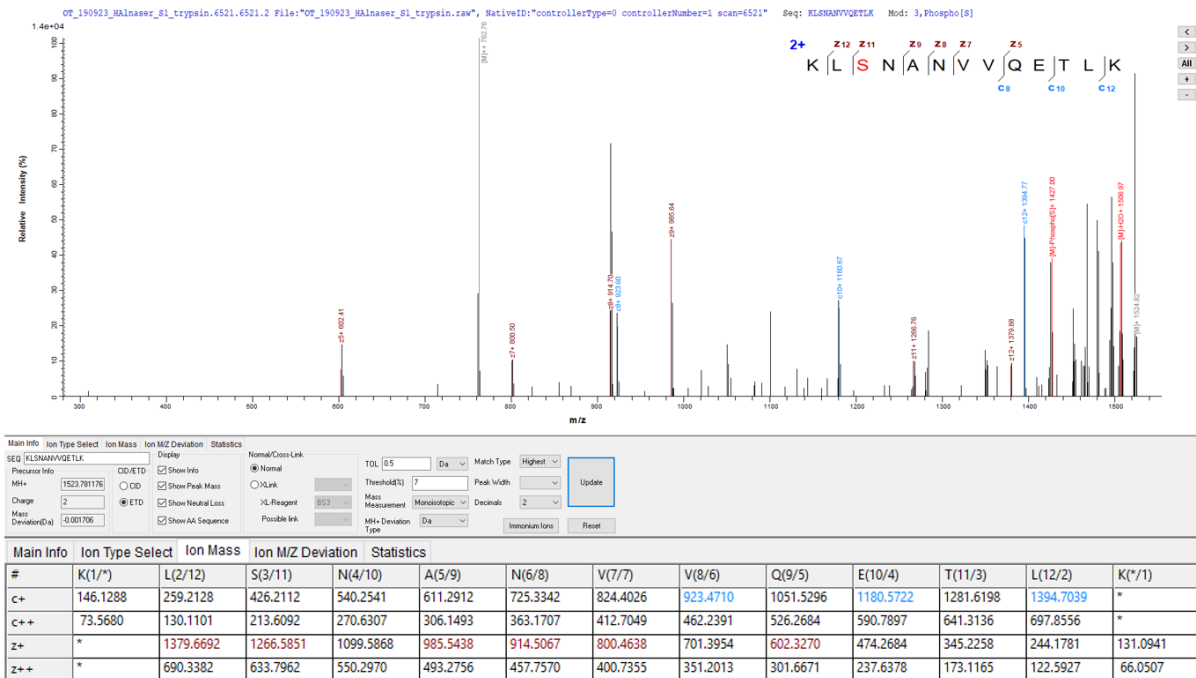


Figure A5.12 MS spectra for KLS^SNANVVQETLK with S431 phosphorylation

Appendix V (cont'd):

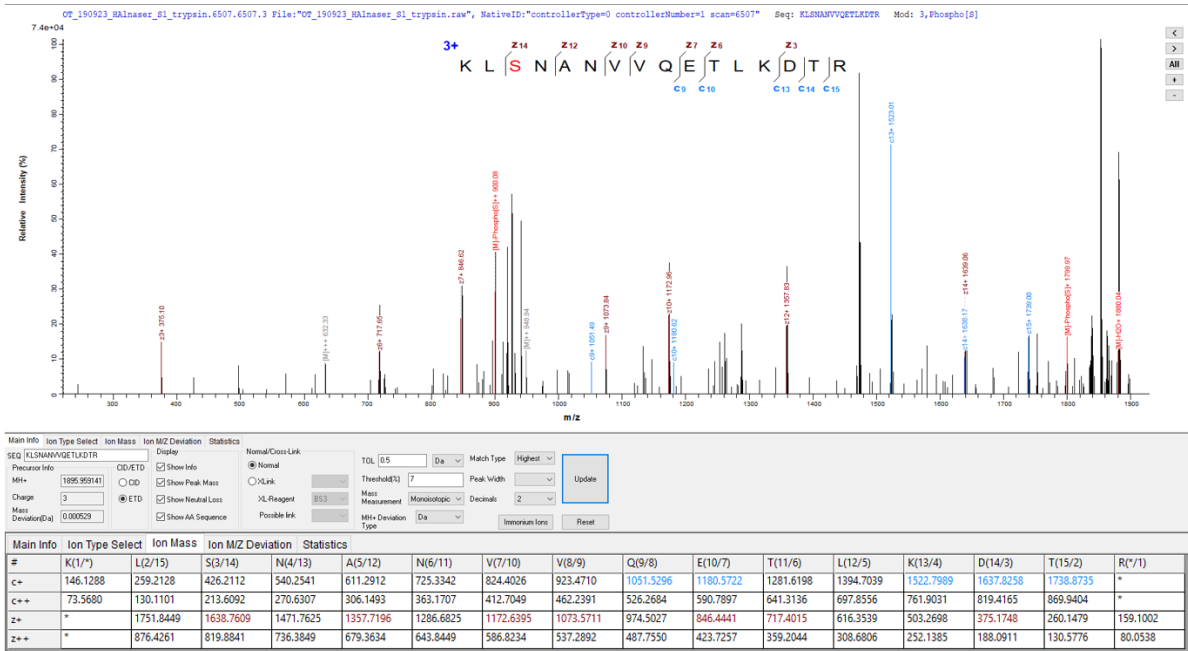


Figure A5.13 MS spectra for KLS^PNANVVQETLKDTR with S431 phosphorylation

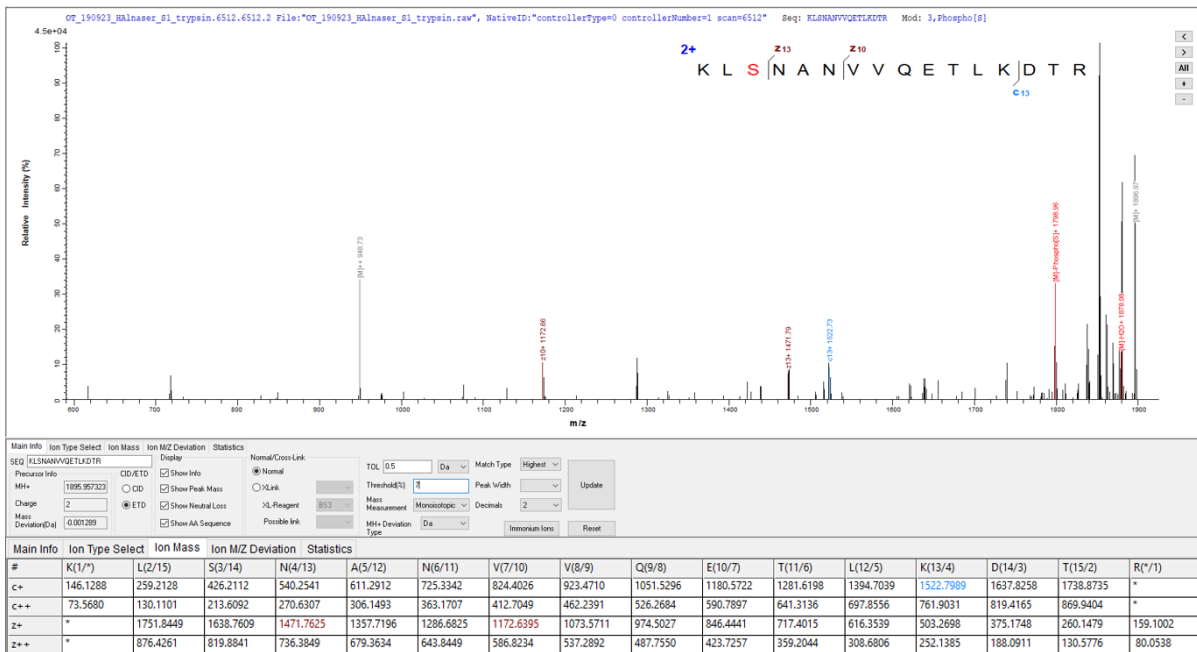


Figure A5.14 MS spectra for KLS^PNANVVQETLKDTR with S431 phosphorylation

Appendix V (cont'd):

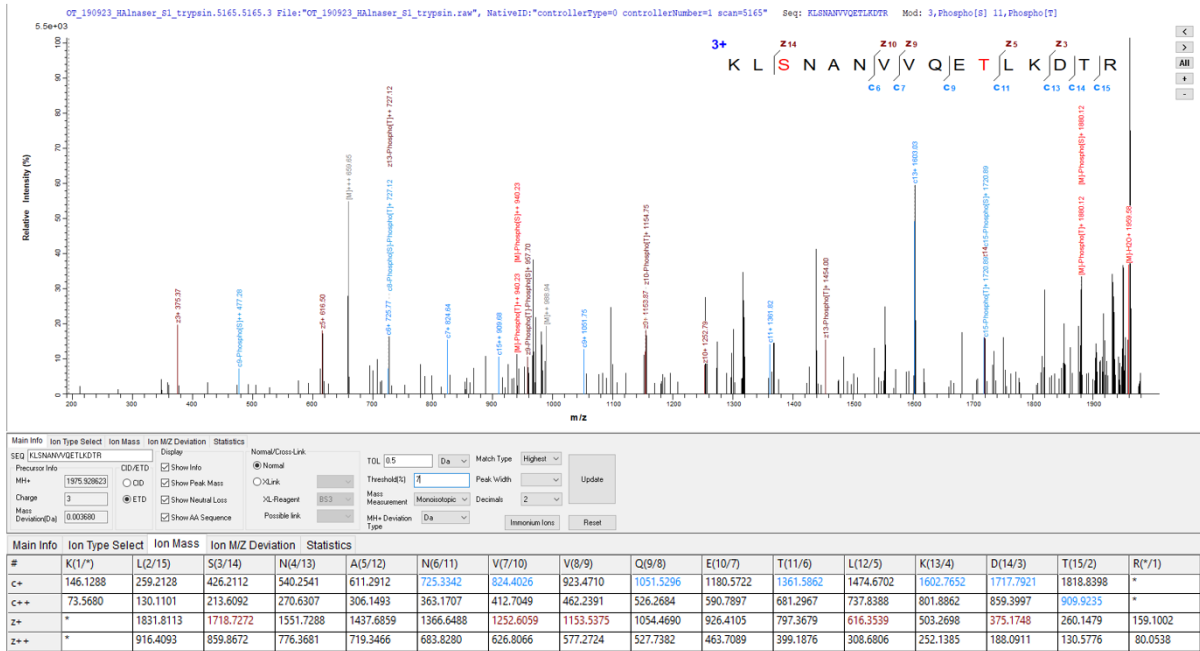


Figure A5.15 MS spectra for $KLS^P N A N V V Q E T^P L K D T R$ with S431 and T439 phosphorylation

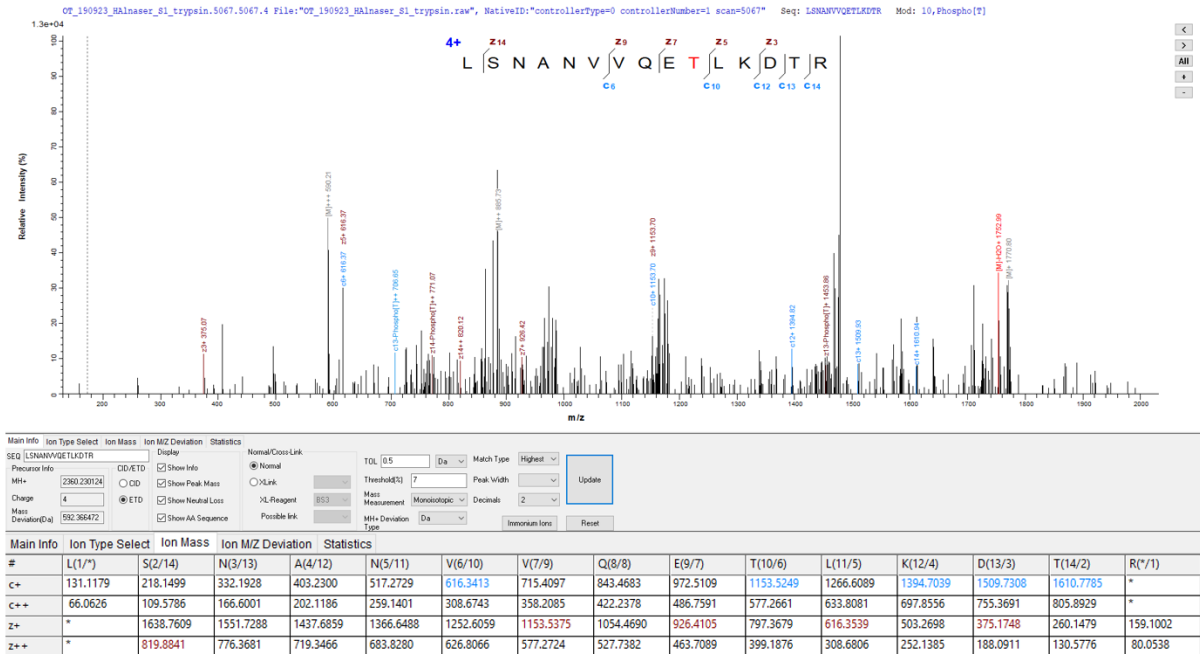


Figure A5.16 MS spectra for $LSNANVVQET^P L K D T R$ with T439 phosphorylation

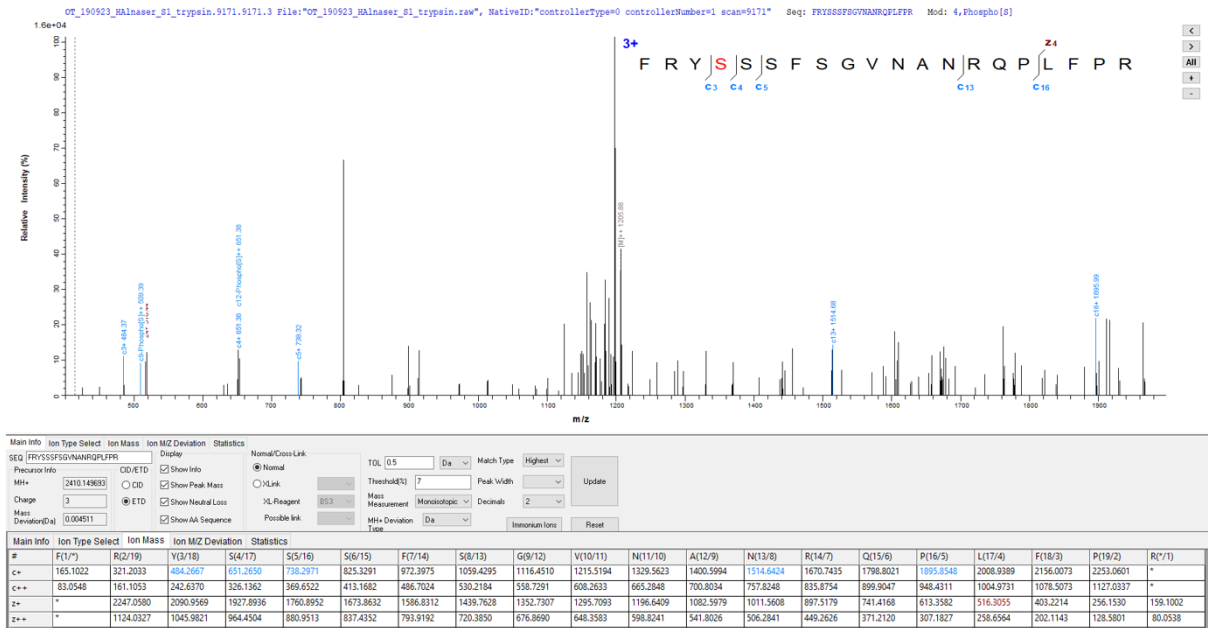


Figure A5.17 MS spectra for FRYSPSSFSGVNNRQLFPR with S585 phosphorylation

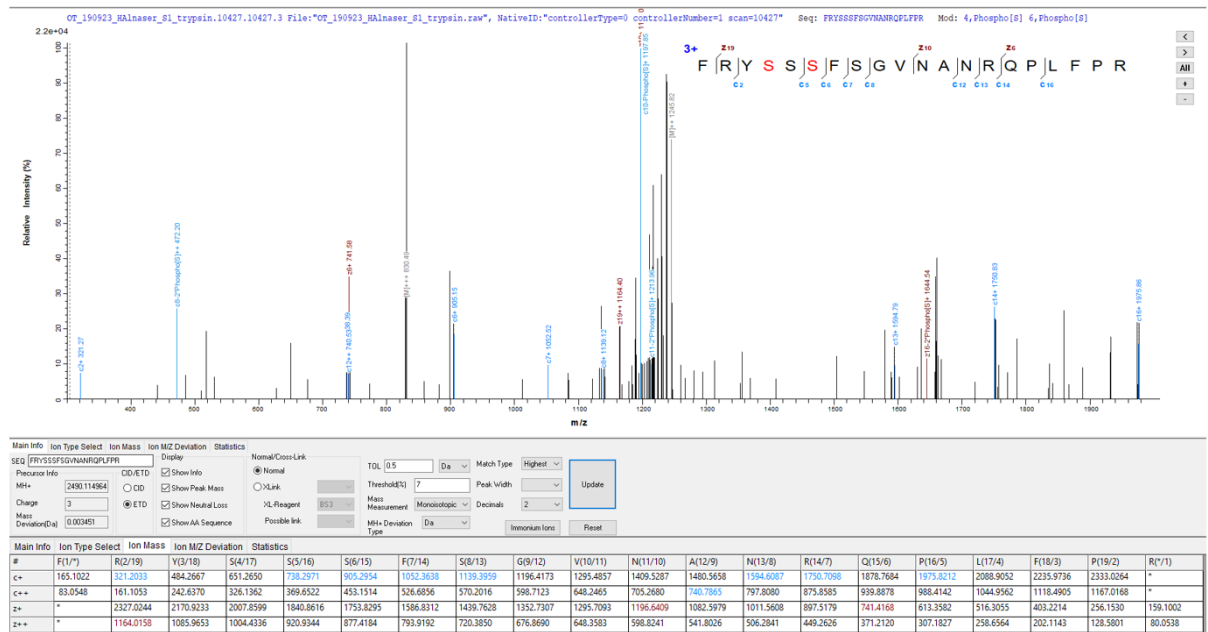


Figure A5.18 MS spectra for FRYSPSSPSSFSGVNNRQLFPR with S585 and S587 phosphorylation

Appendix V (cont'd):

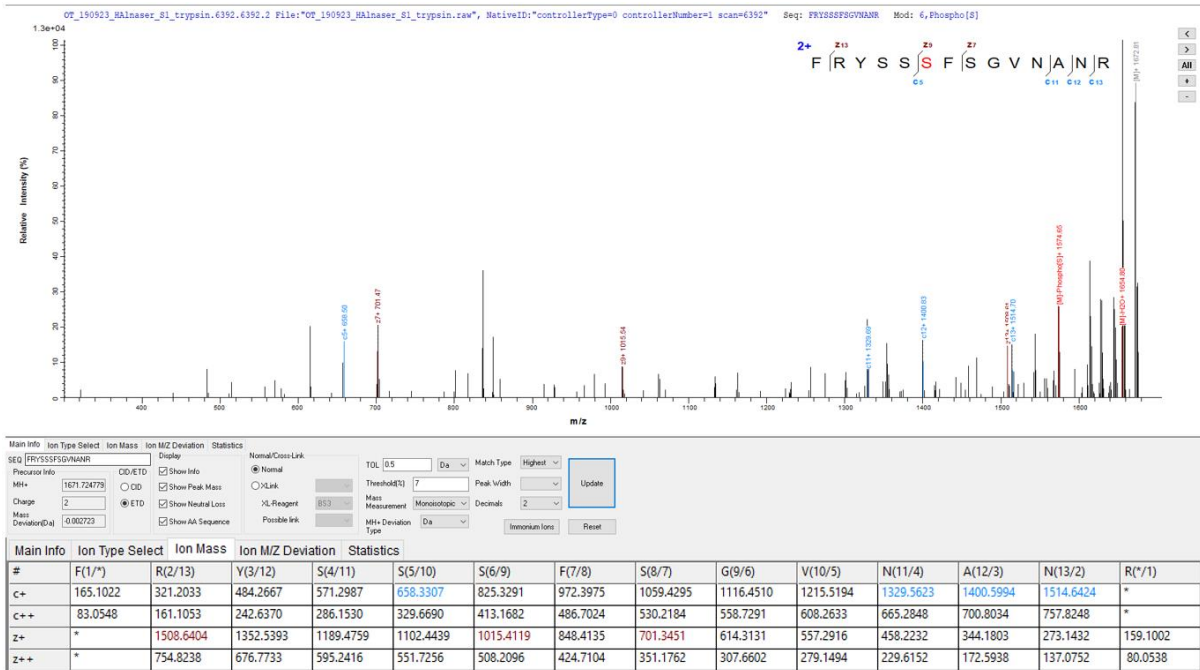


Figure A5.19 MS spectra for FRYSS^PFSGV N A N R with S587 phosphorylation

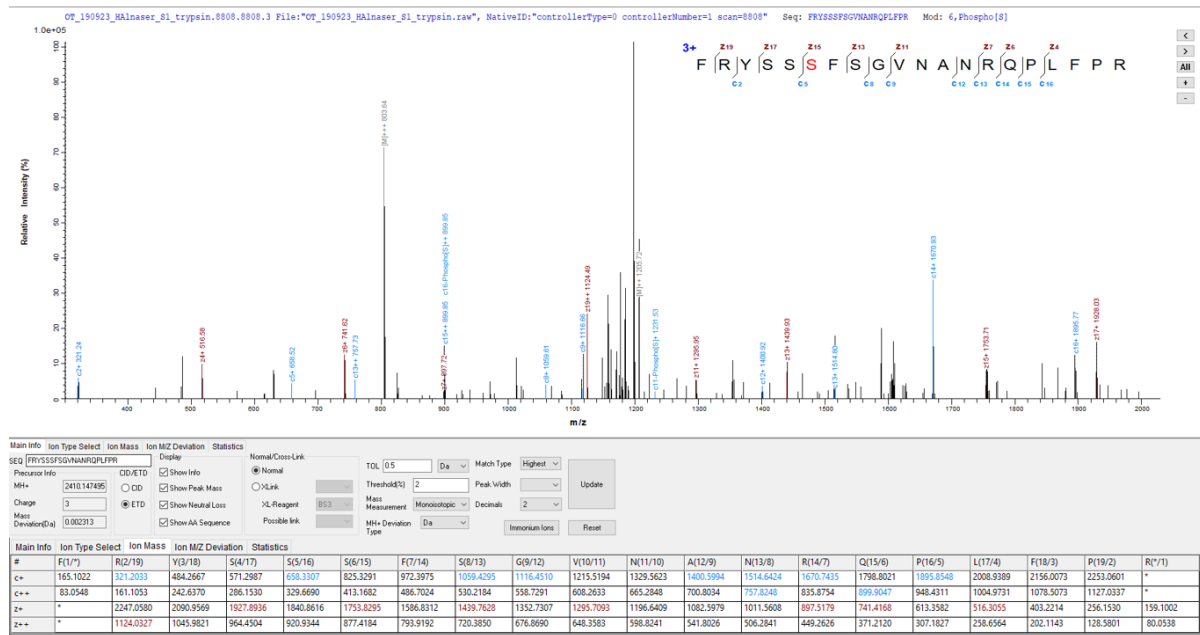


Figure A5.20 MS spectra for FRYSS^PFSGV N A N R Q P L F P R with S587 phosphorylation

Appendix V (cont'd):

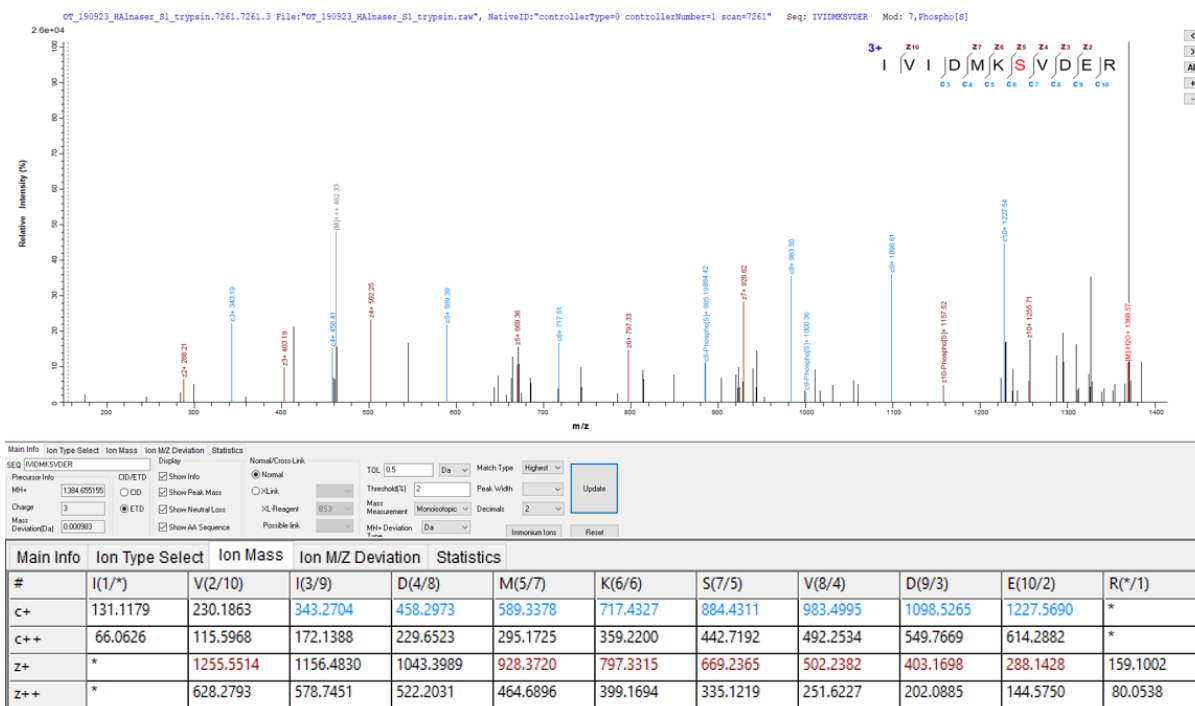


Figure A5.21 MS spectra for IVIDMKSPVSEIR with S654 phosphorylation

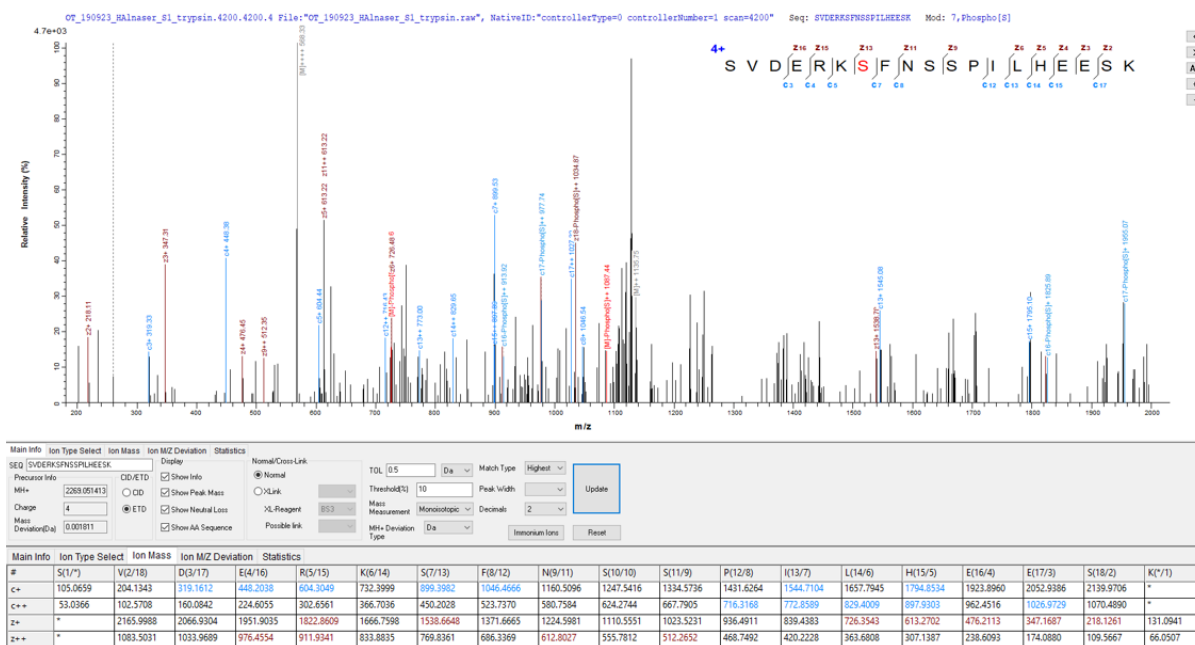


Figure A5.22 MS spectra for SVDERKSPFNSSPILHEESK with S660 phosphorylation

Appendix V (cont'd):

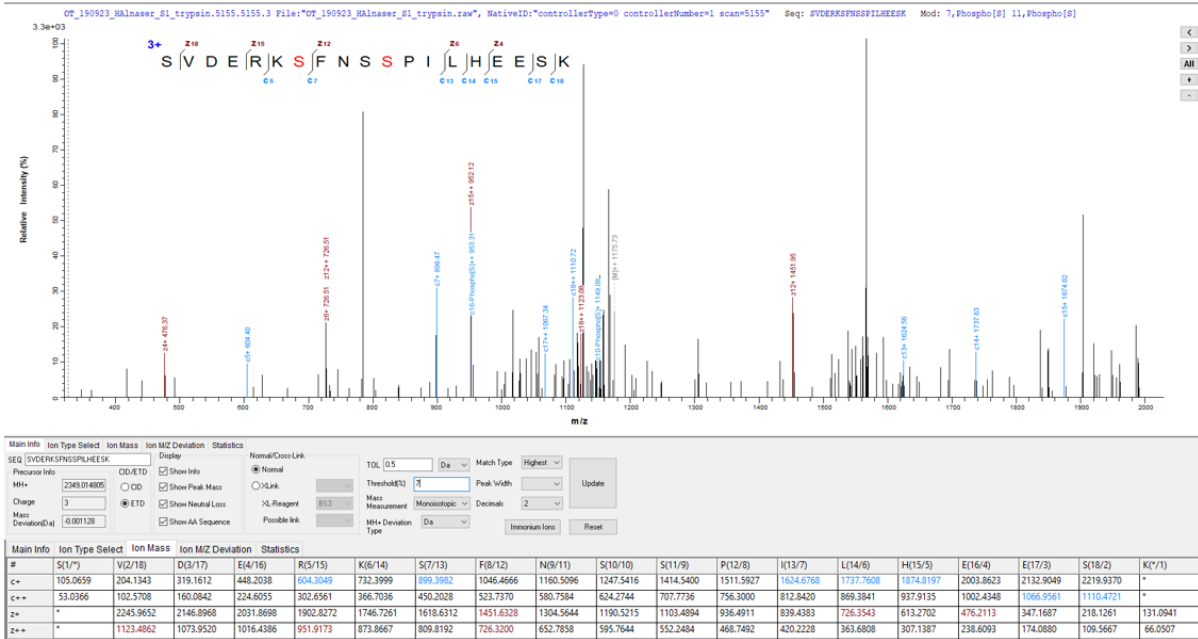


Figure A5.23 MS spectra for SVDERKSPFNSSPILHEESK with S660 and S664 or S663 phosphorylation

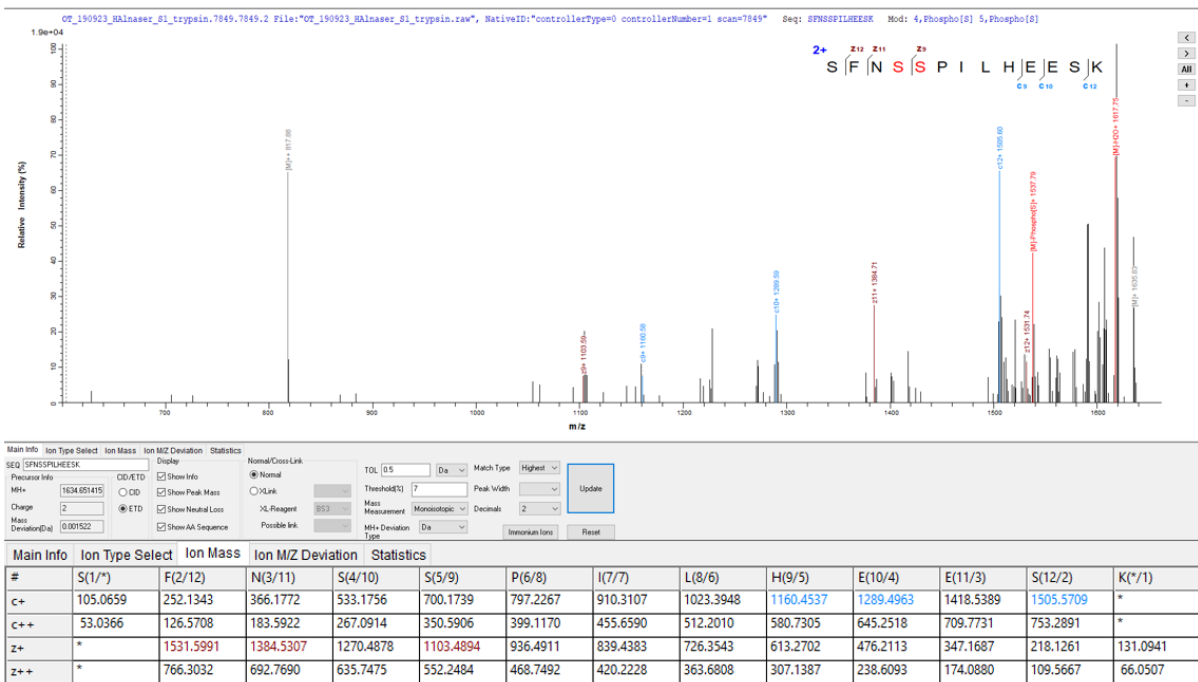


Figure A5.24 MS spectra for SFNSPSPILHEESK with S663 and S664 phosphorylation

Appendix V (cont'd):

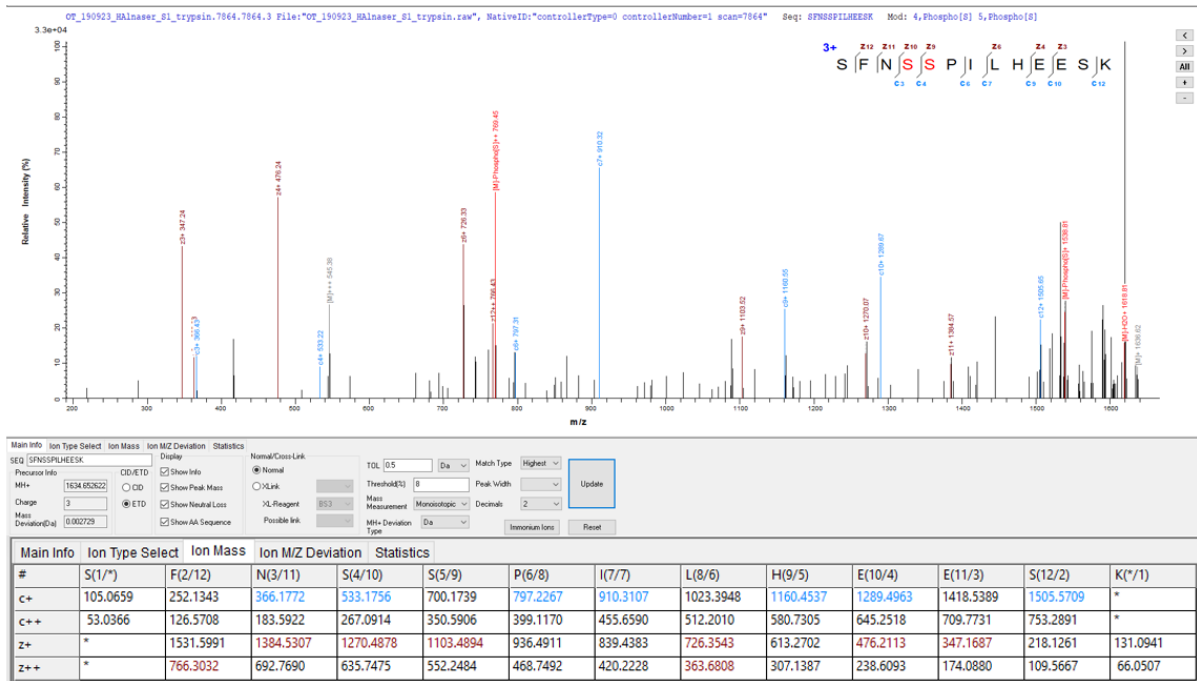


Figure A5.25 MS spectra for SFNS^SPILHEESK with S663 and S664 phosphorylation

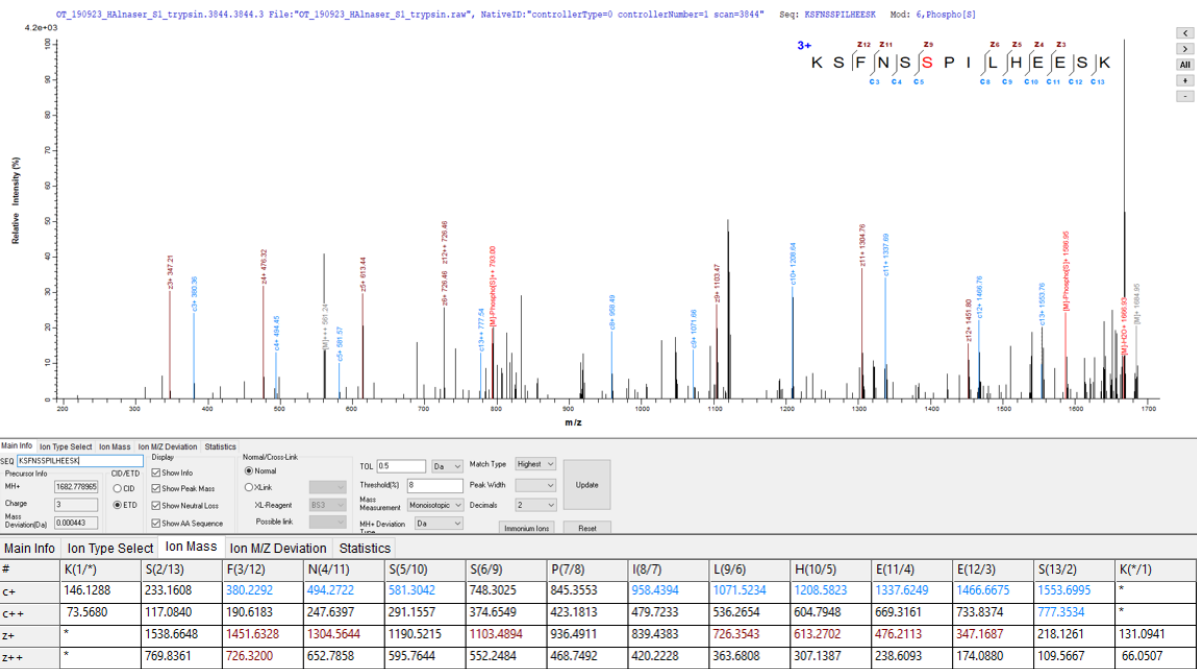


Figure A5.26 MS spectra for KSFNS^SPILHEESK with S664 phosphorylation

Appendix V (cont'd):

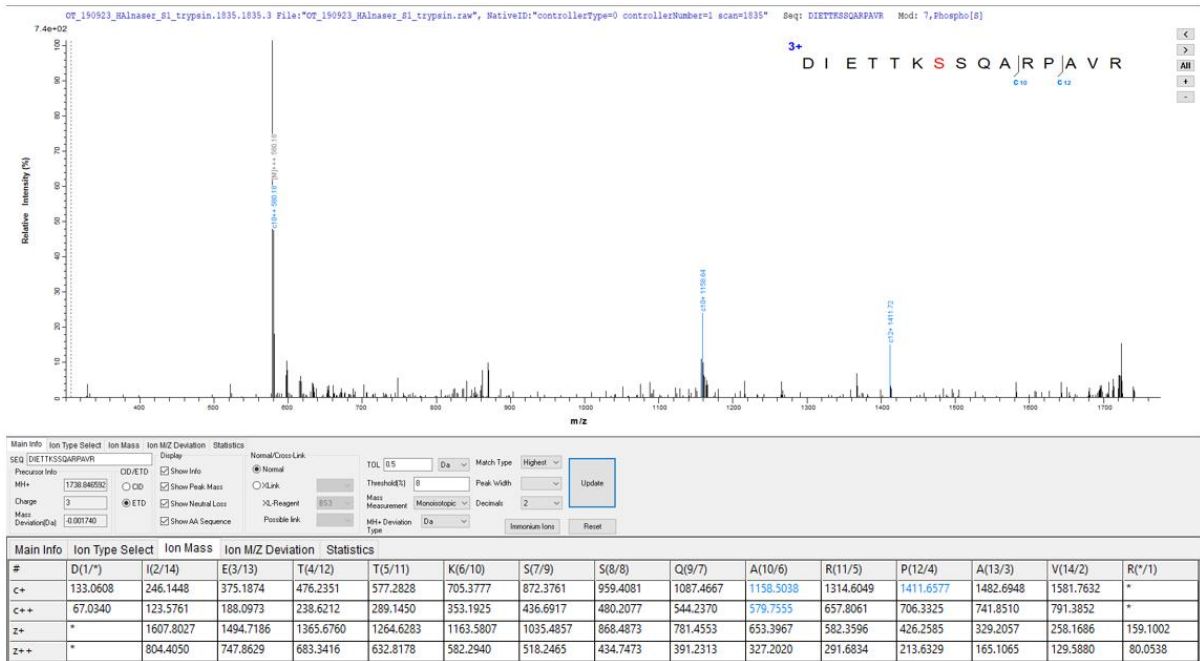


Figure A5.27 MS spectra for DIETTKS^PSQARPAVR with S681 showing low phosphorylation probability

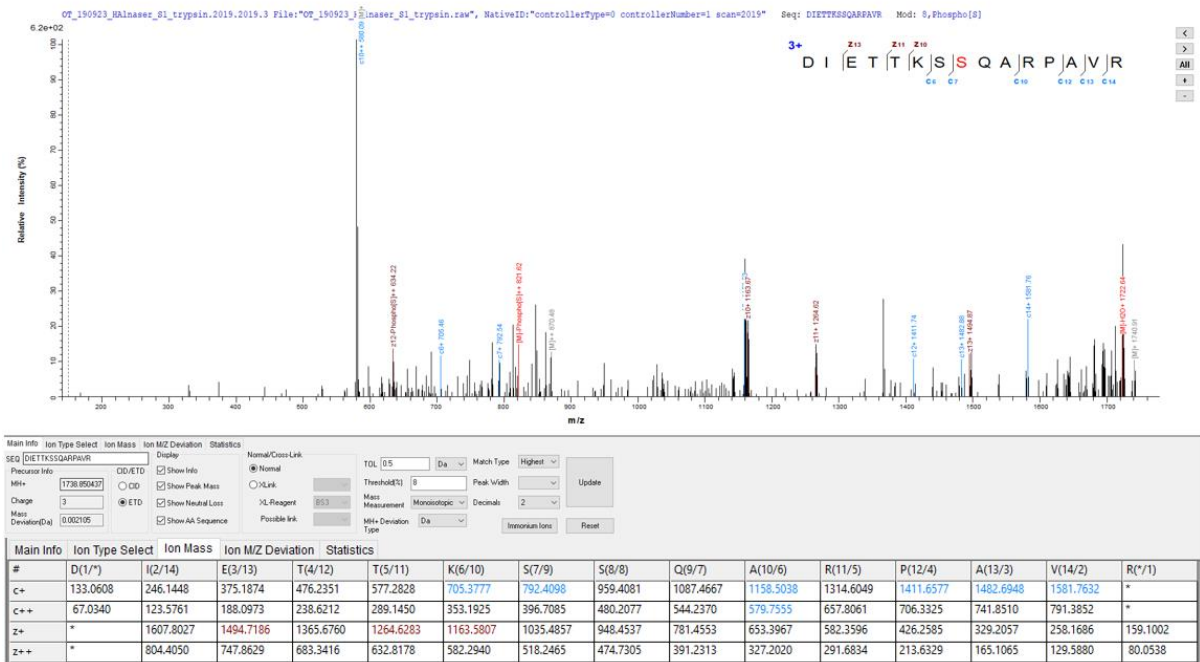


Figure A5.28 MS spectra for DIETTKS^PSQARPAVR with S682 phosphorylation

Appendix V (cont'd):

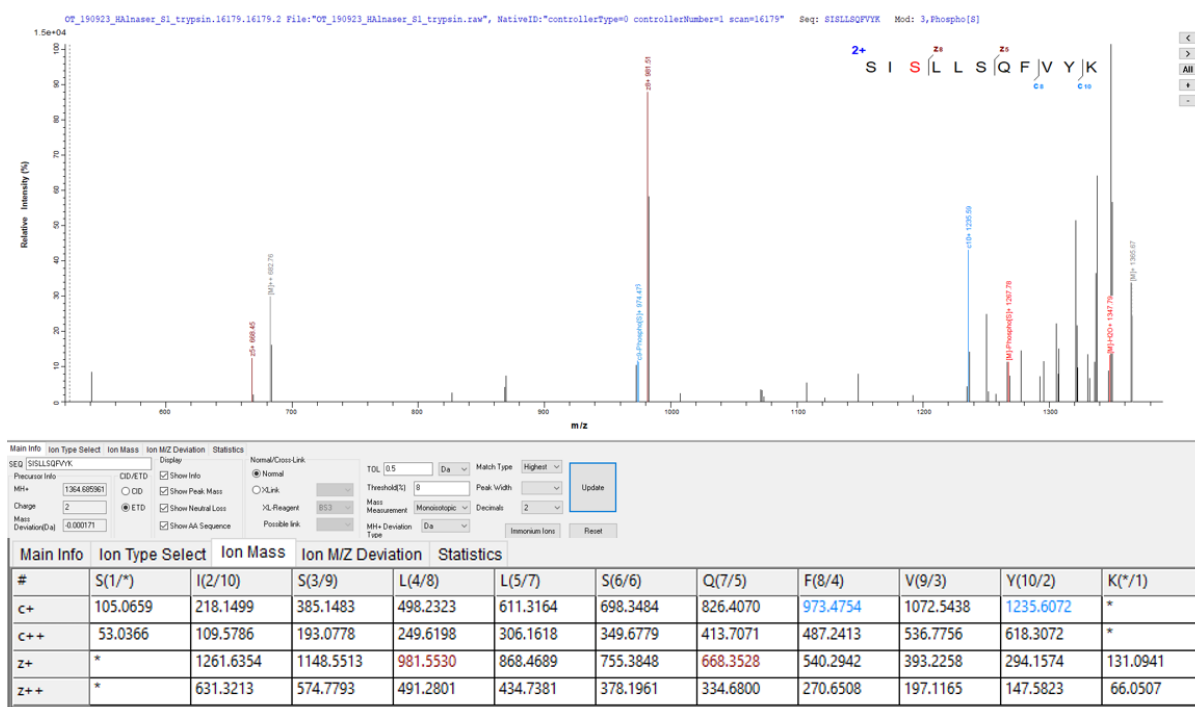


Figure A5.29 MS spectra for SIS^PLLSQFVYK with S692 phosphorylation

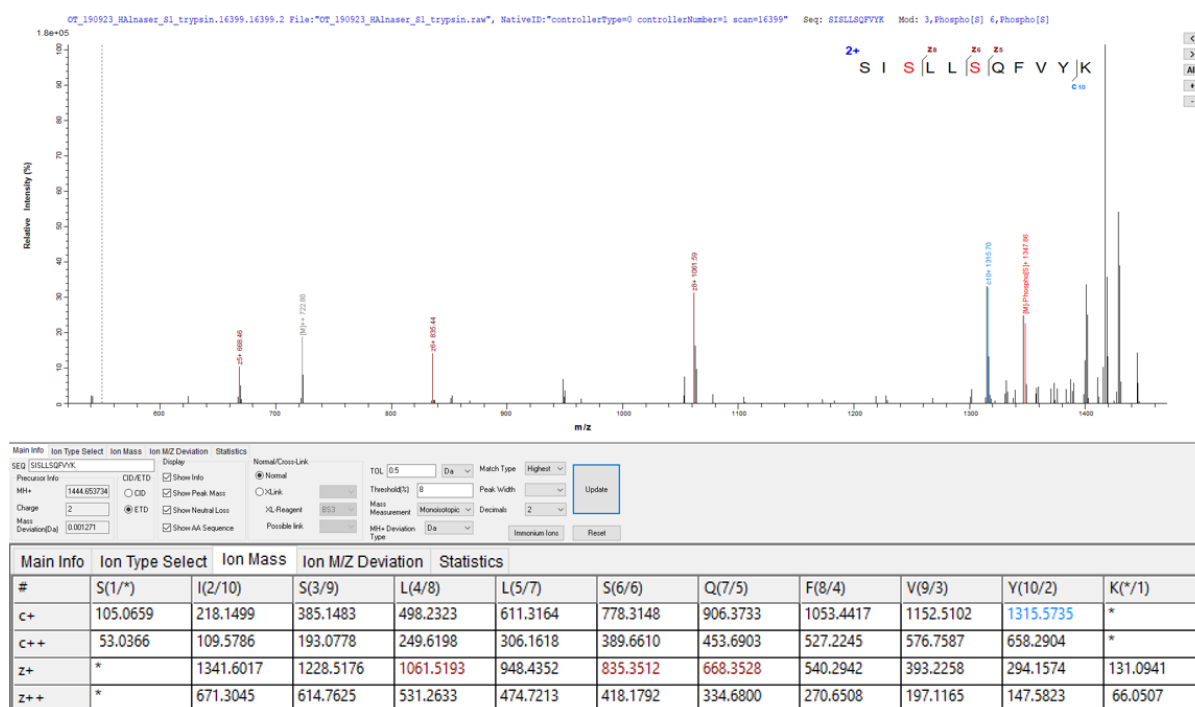


Figure A5.30 MS spectra for SIS^PLLS^PQFVYK with S692 and S695 phosphorylation

Appendix V (cont'd):

A5.4 MS spectra of Exo1 peptides detected in Exo1 purified sample from *sae2Δ* cells after four hours of meiosis induction: on-beads trypsin treatment and ETD fragmentation

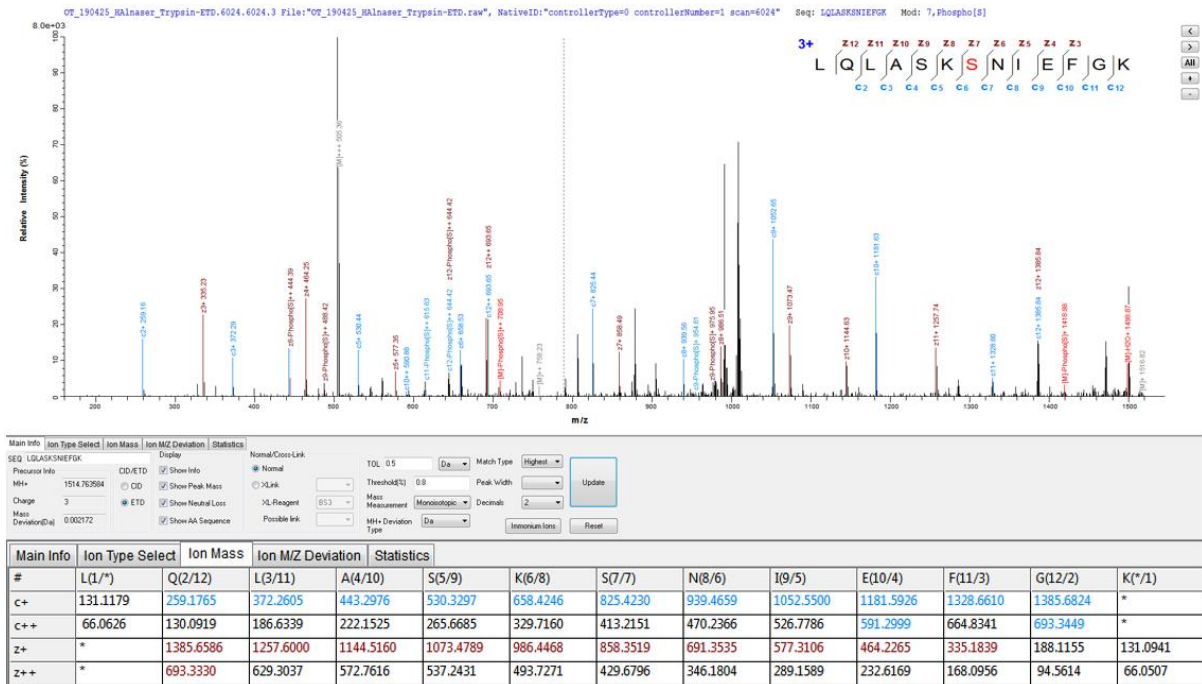


Figure A5.31 MS spectra for LQLASKS^PNIEGK with S372 phosphorylation

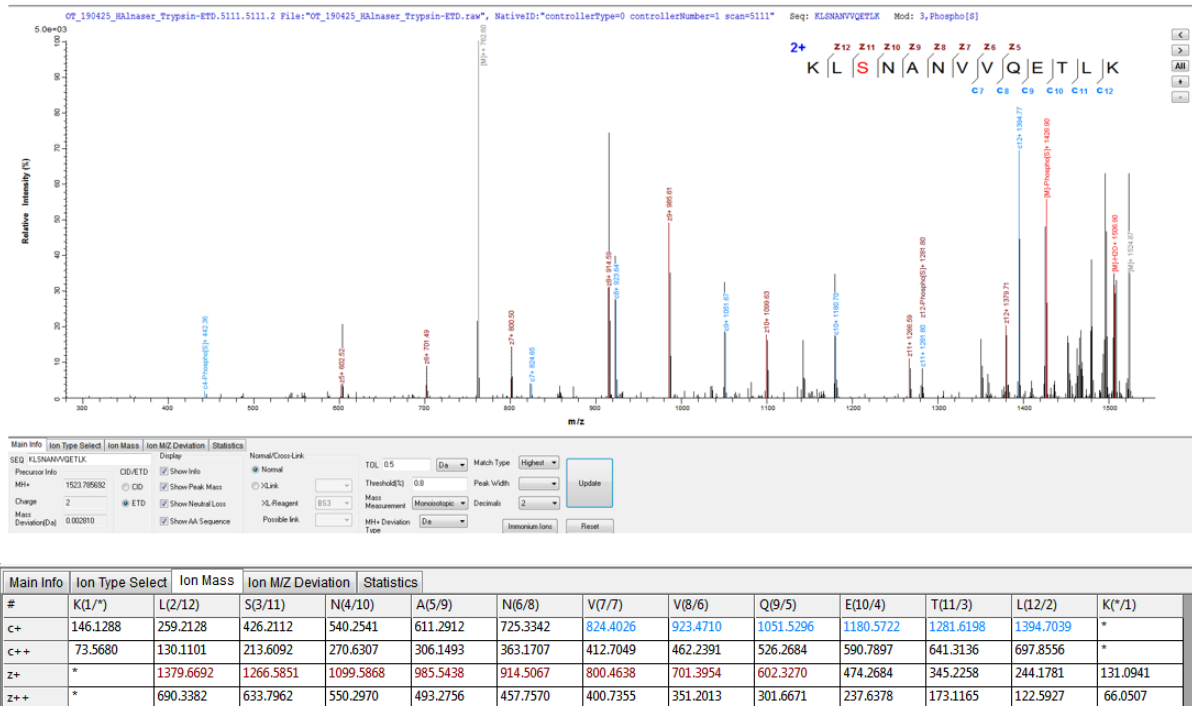


Figure A5.32 MS spectra for KLS^PNANVVQETLK with S431 phosphorylation

Appendix V (cont'd):

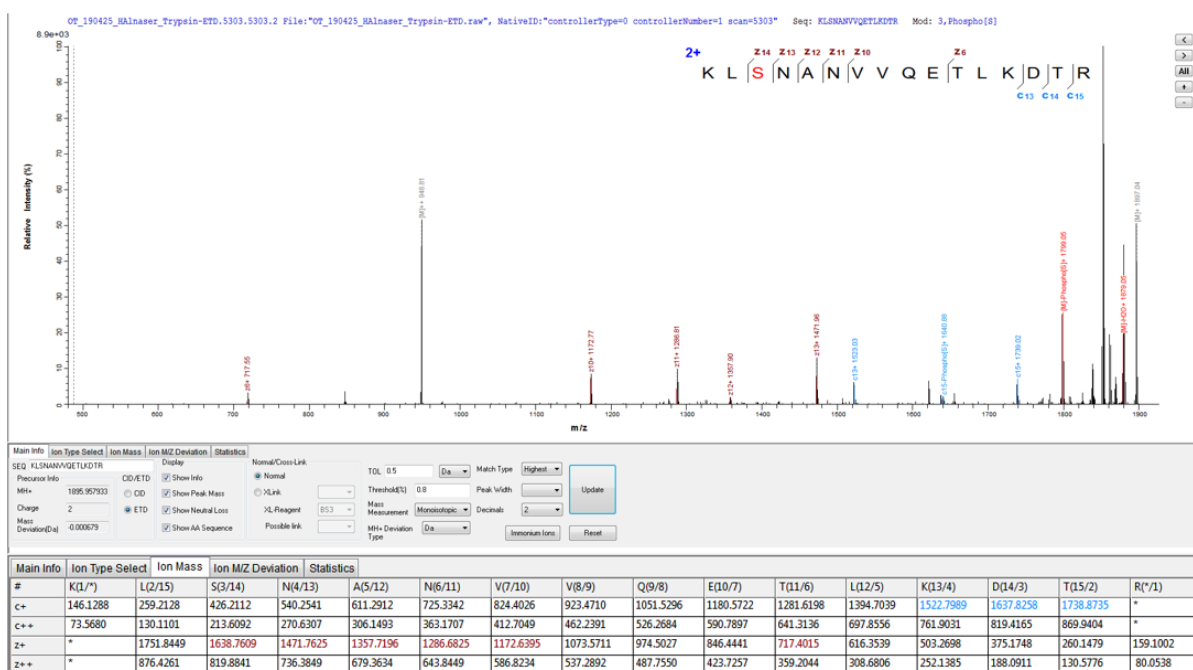


Figure A5.33 MS spectra for KLS^PNANVVQETLKDTR with S431 phosphorylation

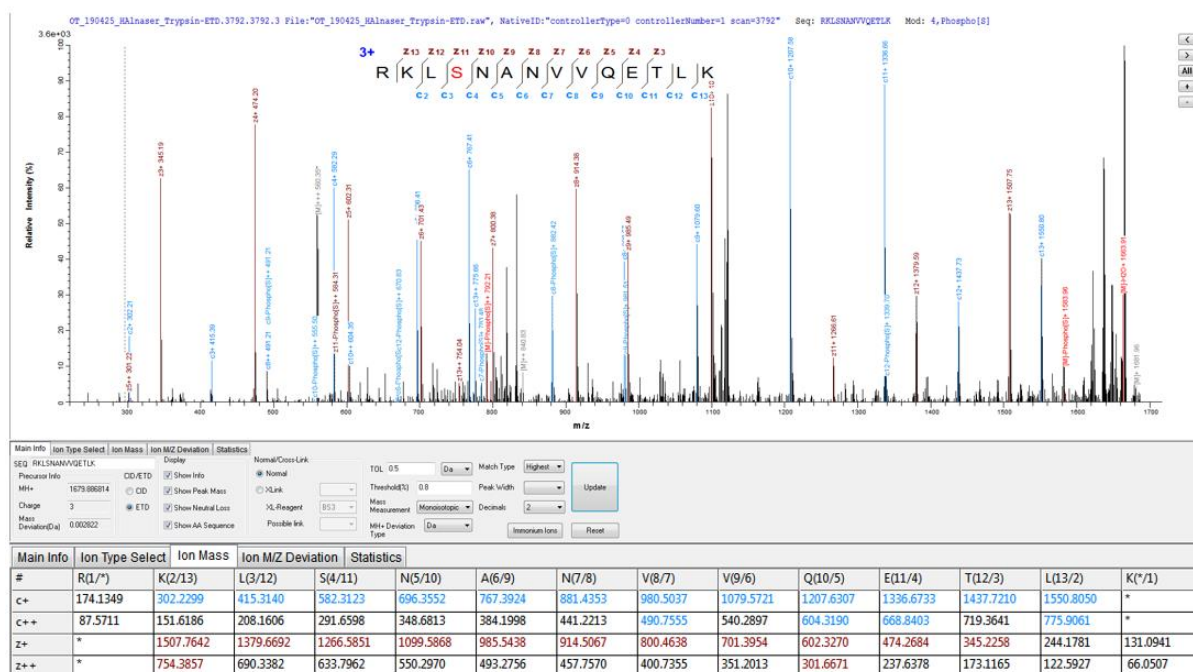


Figure A5.34 MS spectra for RKLS^PNANVVQETLK with S431 phosphorylation

Appendix V (cont'd):

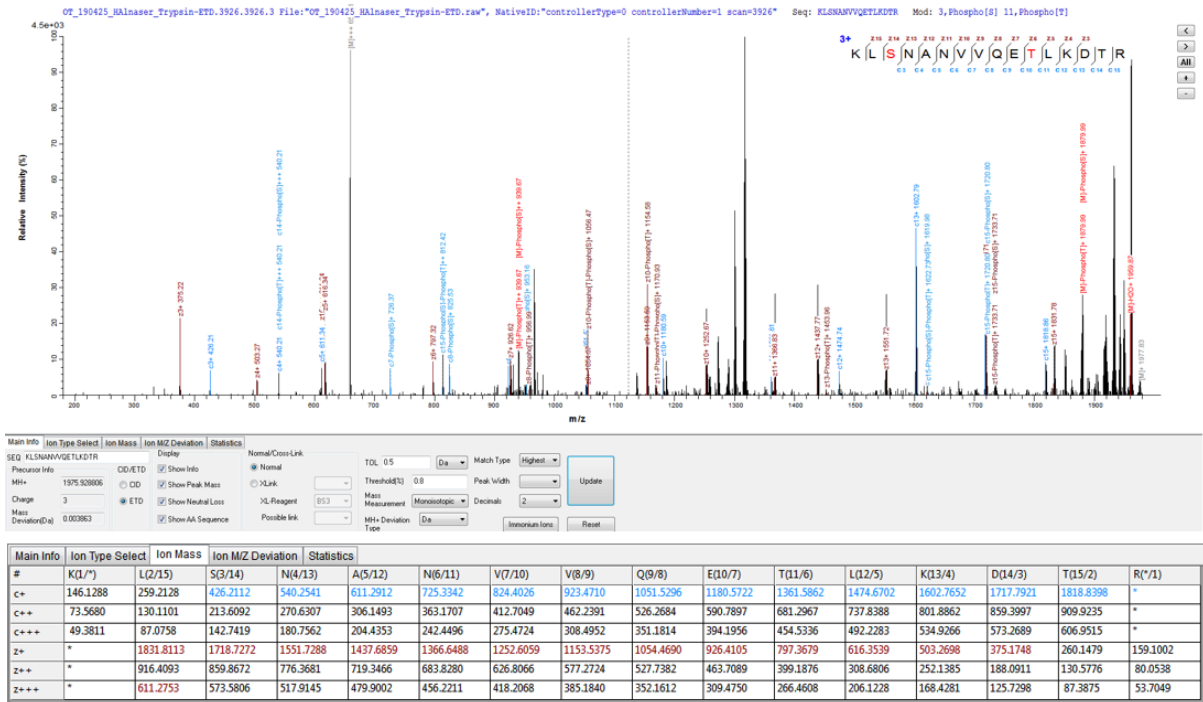


Figure A5.35 MS spectra for RKLSPNANVVQETPLK with S431 and S439 phosphorylation

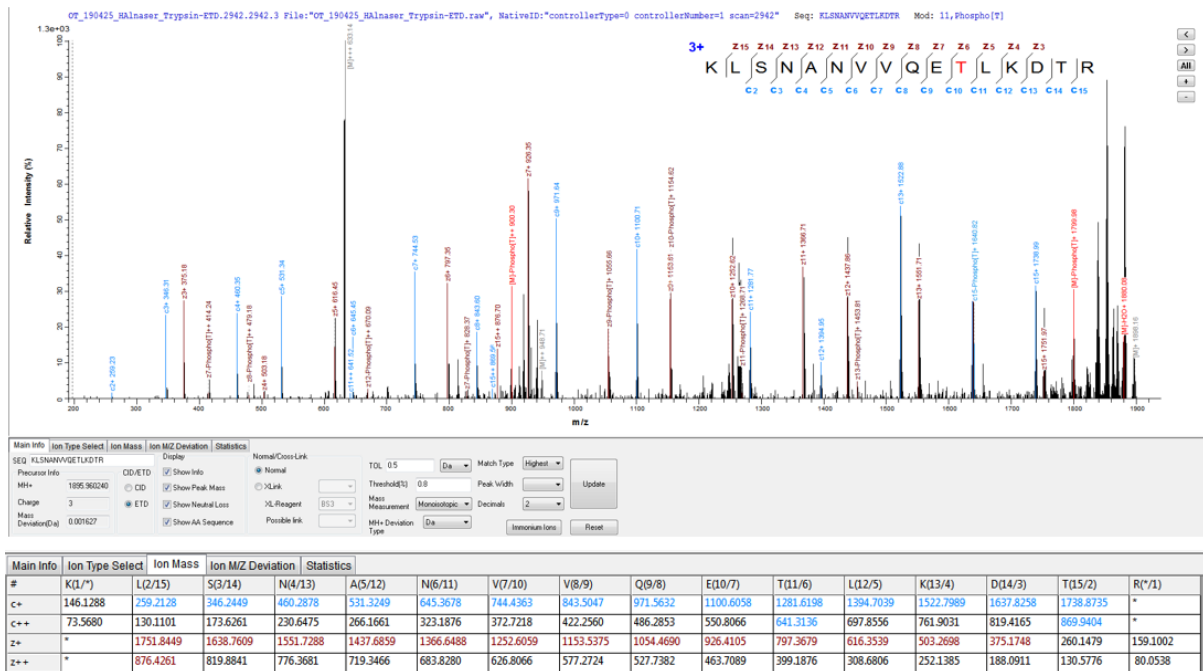


Figure A5.36 MS spectra for RKLSNANVVQETPLK with S439 phosphorylation

Appendix V (cont'd):

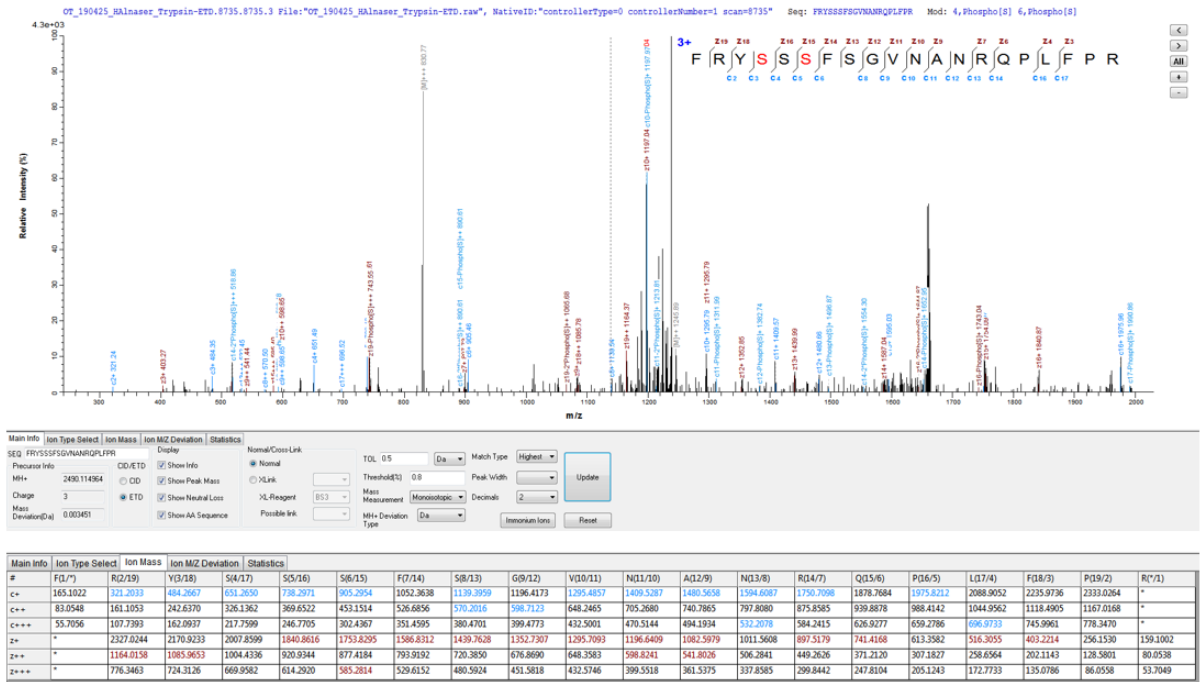


Figure A5.37 MS spectra for FRYSSPSSP FSGVNANRQPLFPR with S585 and S587 phosphorylation

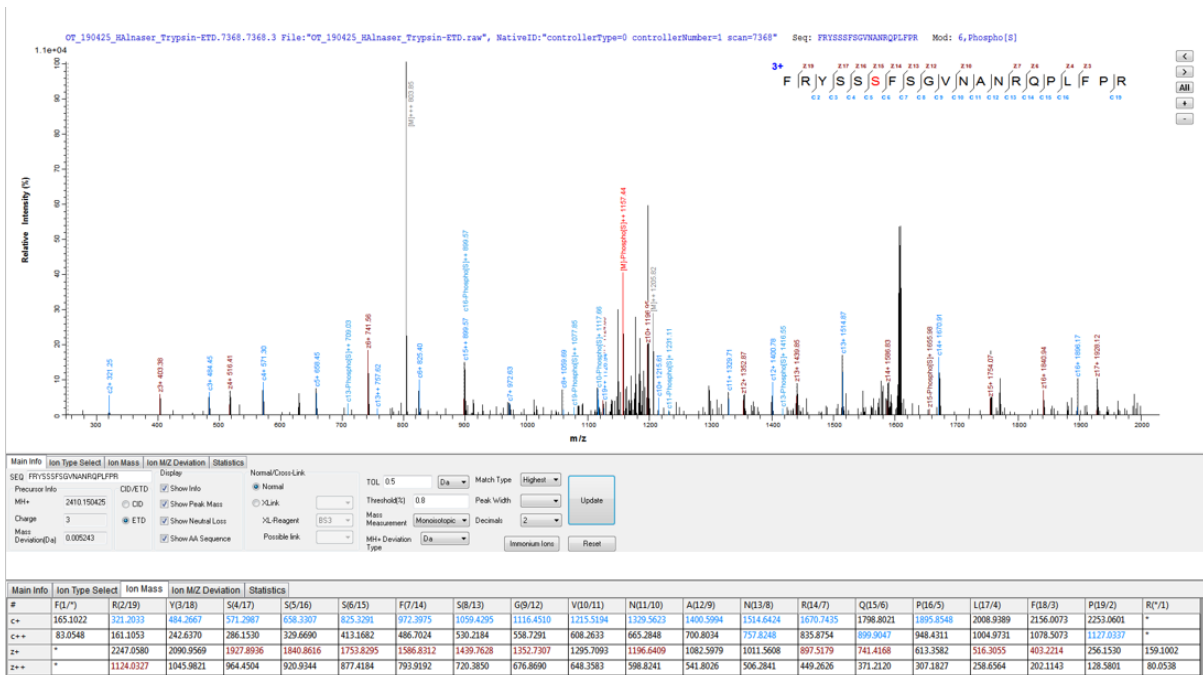


Figure A5.38 MS spectra for FRYSSPSSP FSGVNANRQPLFPR with S587 phosphorylation

Appendix V (cont'd):

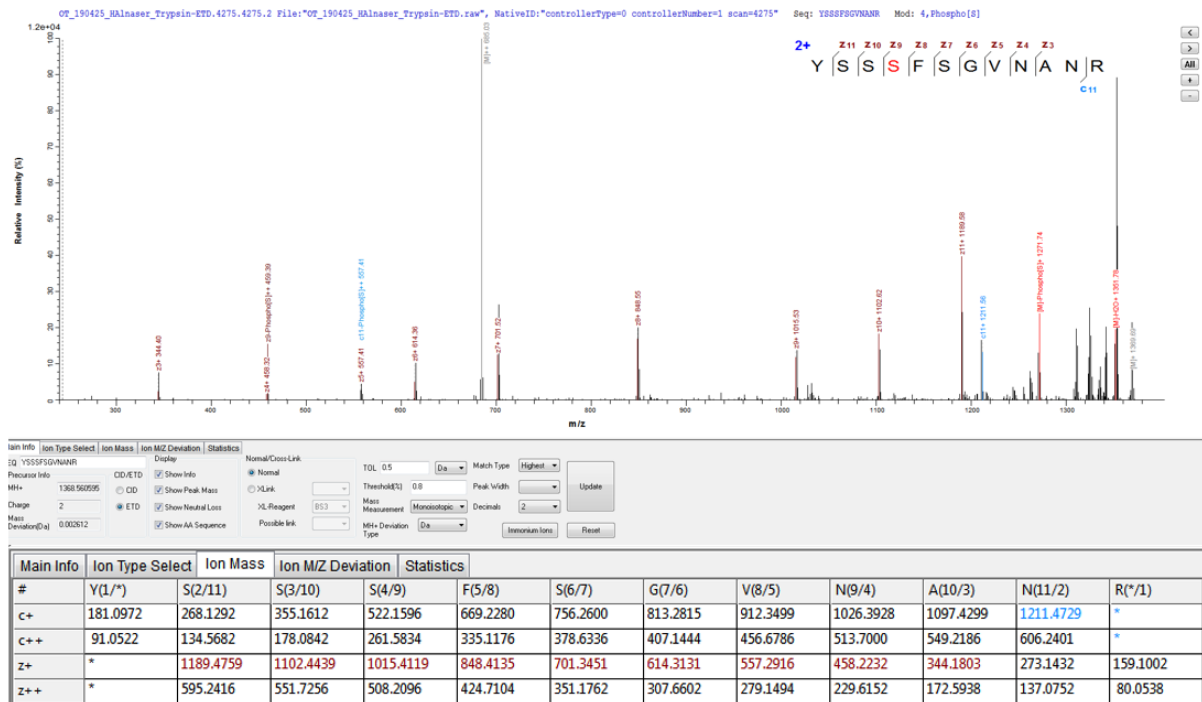


Figure A5.39 MS spectra for YSSP^SFSGVNR with S587 phosphorylation

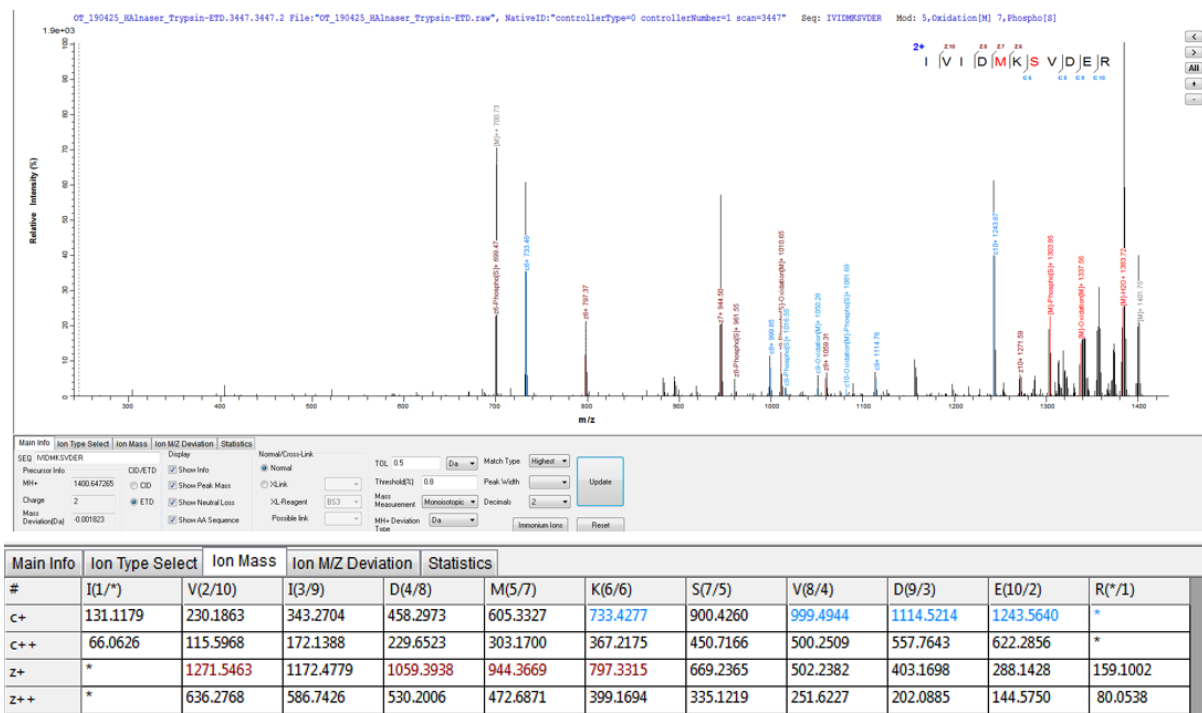


Figure A5.40 MS spectra for IVIDMKSPVDER with S654 phosphorylation. The methionine residue was oxidised.

Appendix V (cont'd):

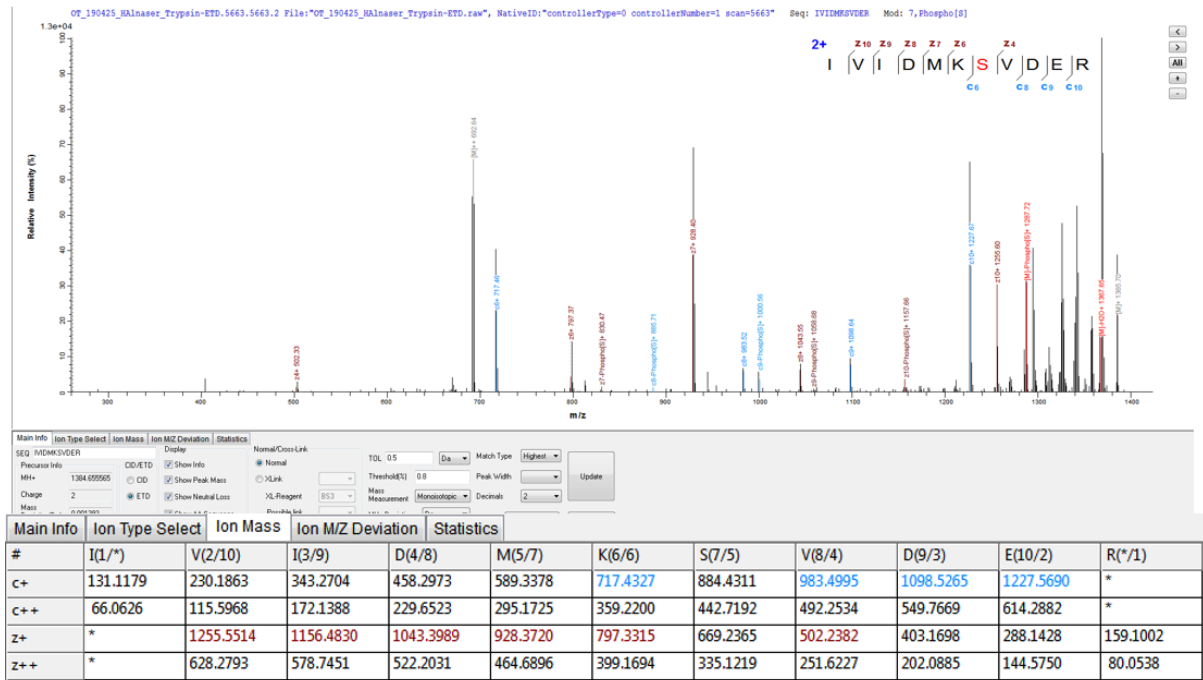


Figure A5.41 MS spectra for IVIDMK^SPVDER with S654 phosphorylation.

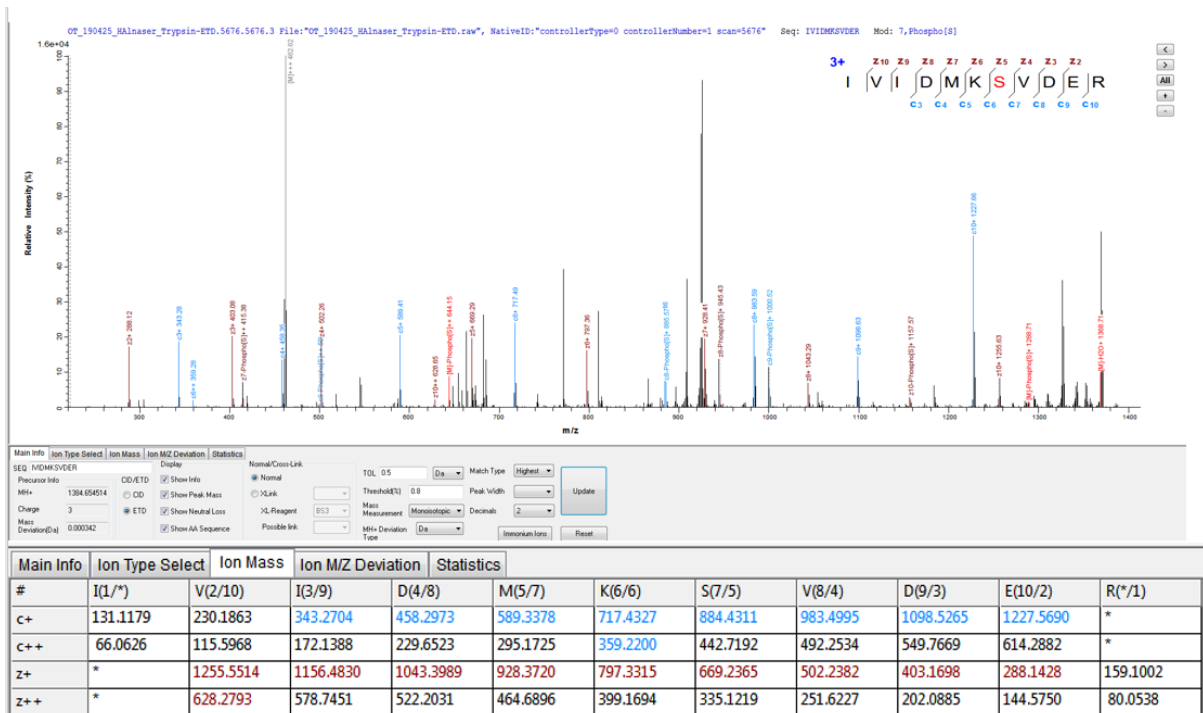


Figure A5.42 MS spectra for IVIDMK^SPVDER with S654 phosphorylation.

Appendix V (cont'd):

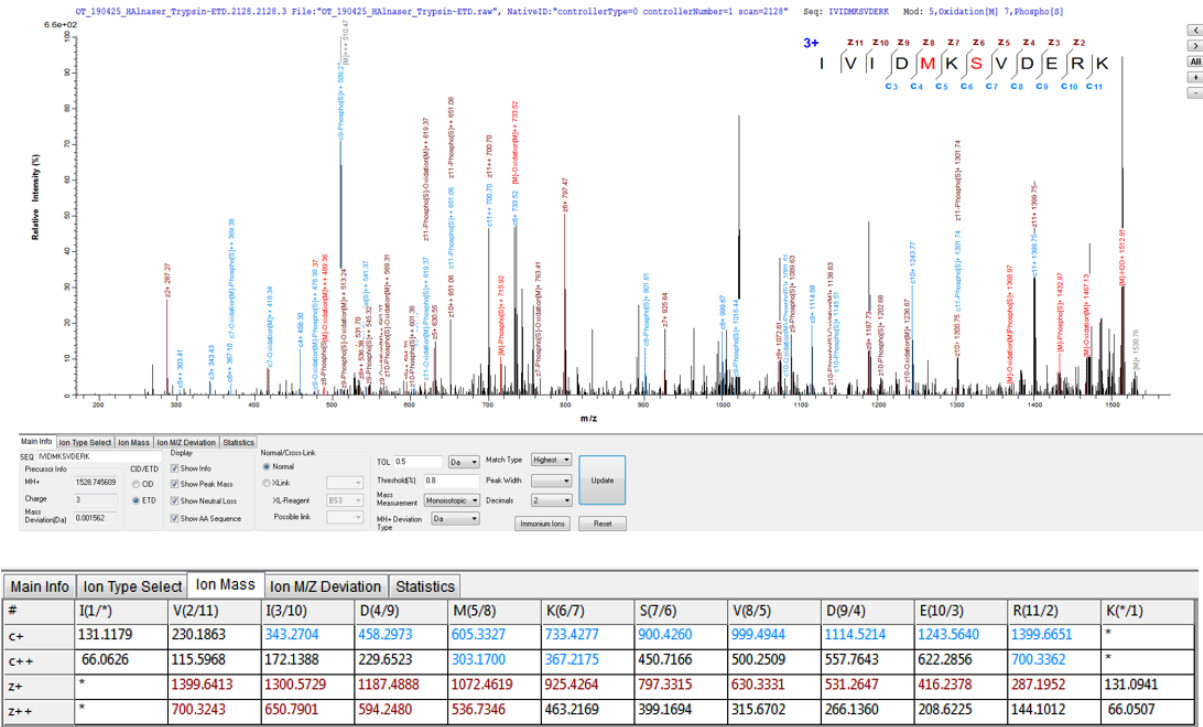


Figure A5.43 MS spectra for IVIDMK^SPVDERK with S654 phosphorylation. The methionine residue was oxidised.

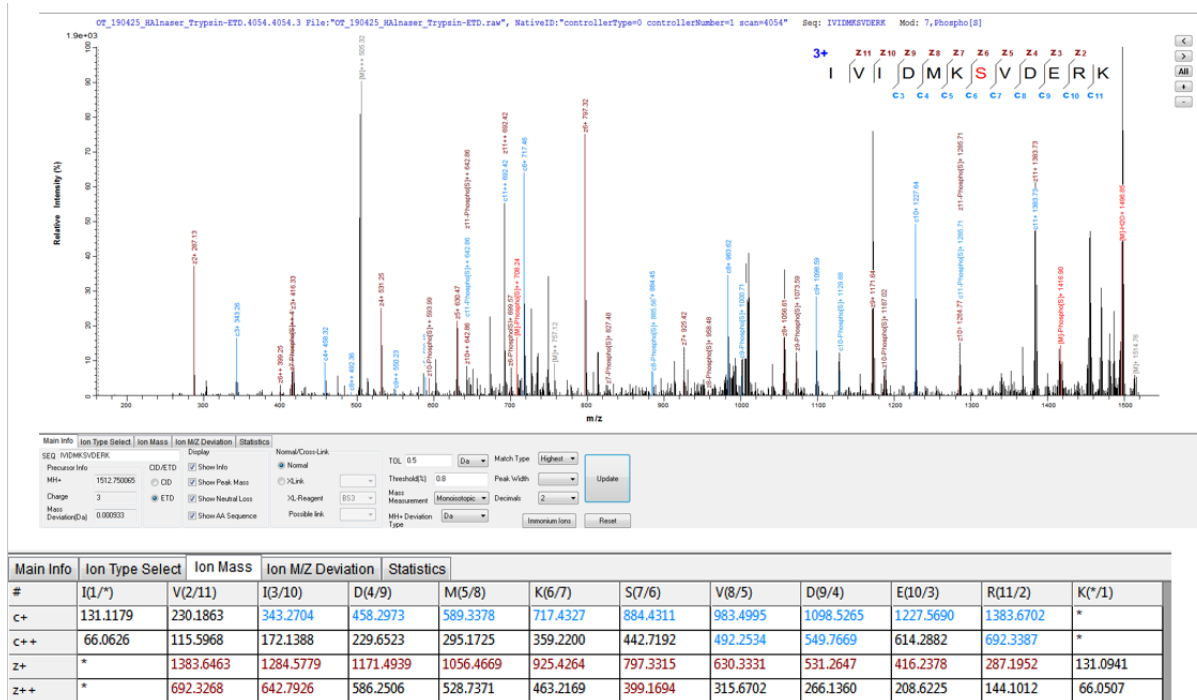


Figure A5.44 MS spectra for IVIDMK^SPVDERK with S654 phosphorylation.

Appendix V (cont'd):

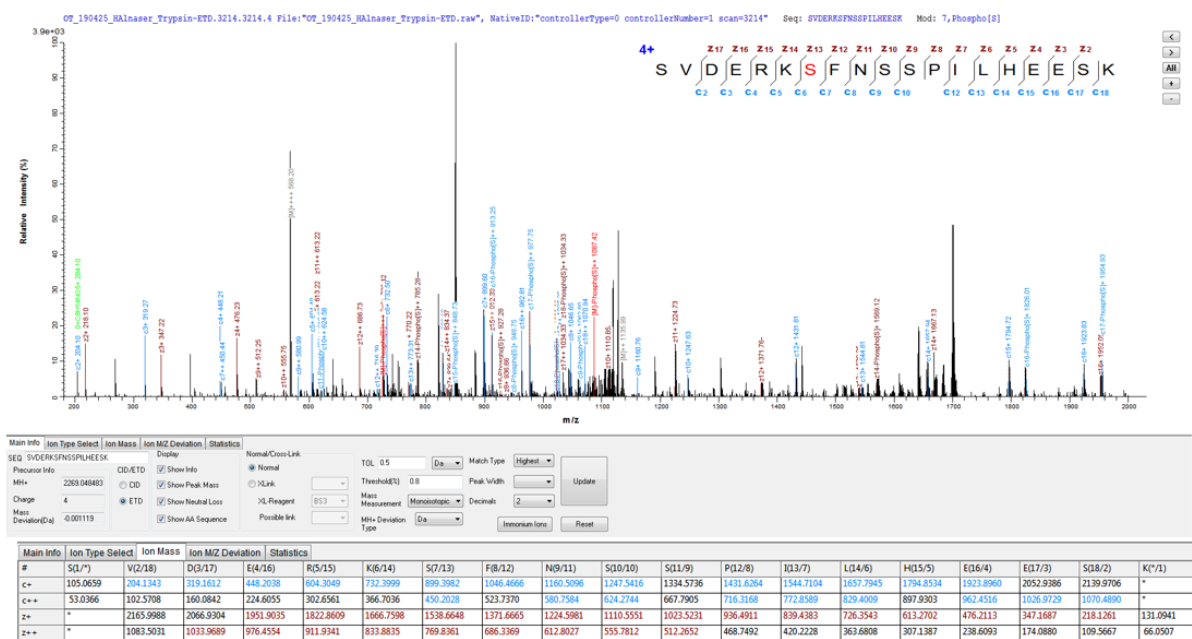


Figure A5.45 MS spectra for SVDERKSFNSSLPIHEESK with S660 phosphorylation.

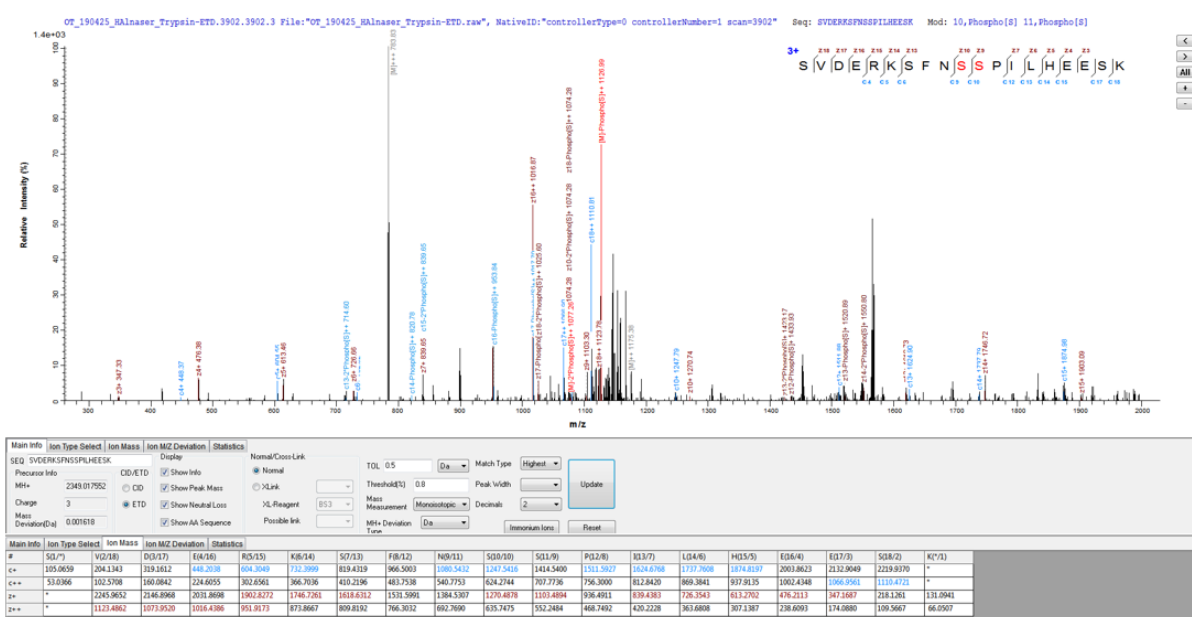


Figure A5.46 MS spectra for SVDERKSFNSSLPIHEESK with S663 and S664 phosphorylation.

Appendix V (cont'd):

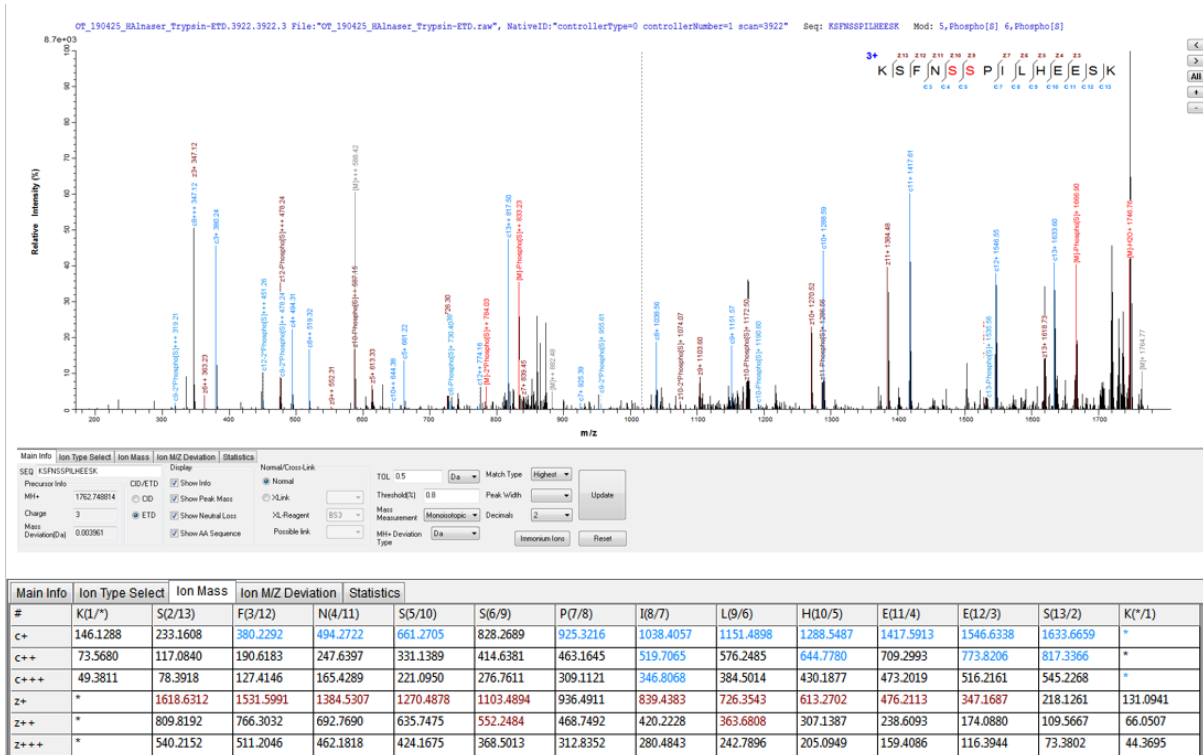


Figure A5.47 MS spectra for KSFNS^PS^PPILHEESK with S663 and S664 phosphorylation.

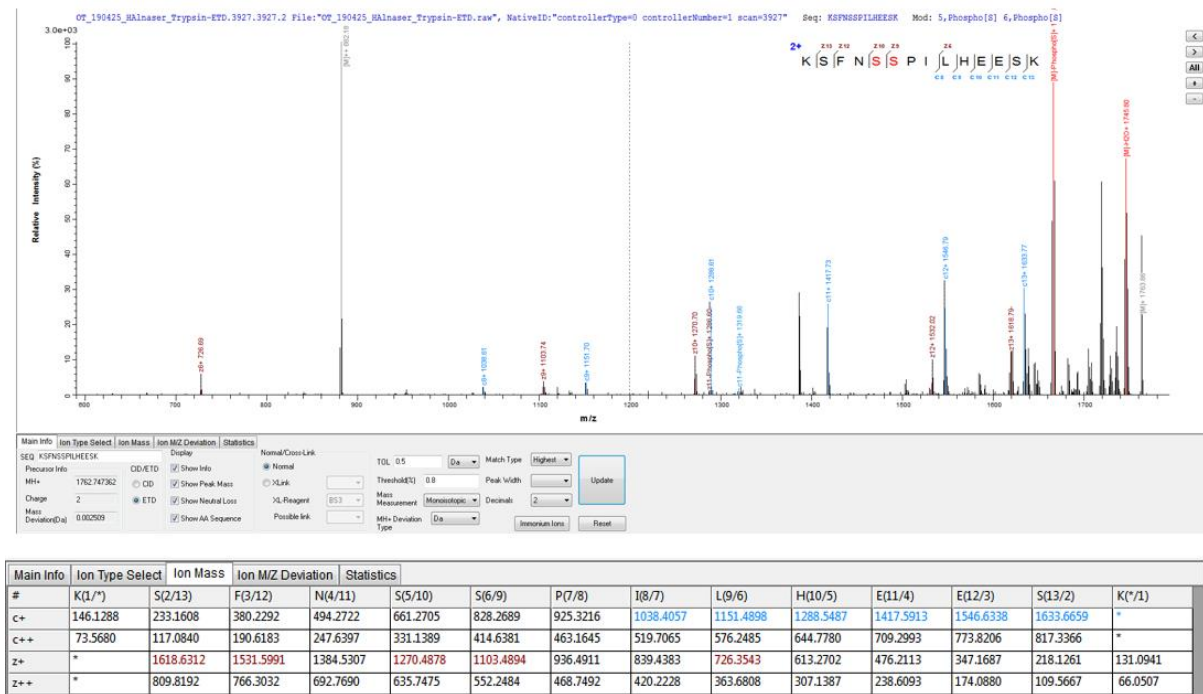


Figure A5.48 MS spectra for KSFNS^PS^PPILHEESK with S663 and S664 phosphorylation.

Appendix V (cont'd):

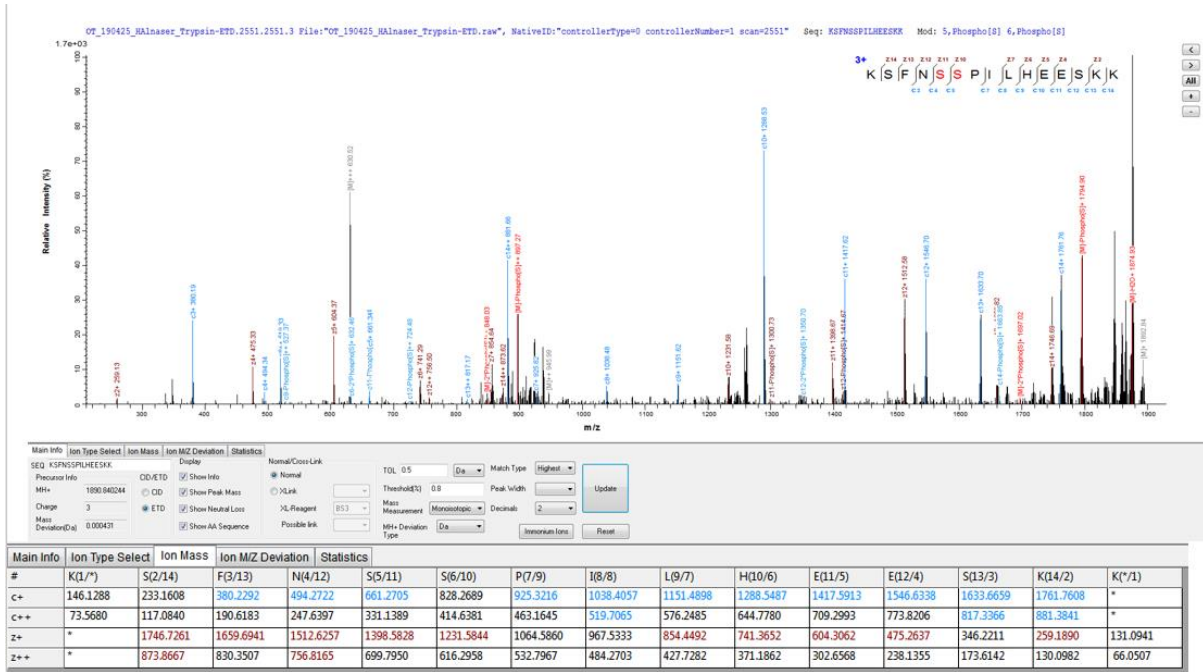


Figure A5.49 MS spectra for KSFNS^PS^PPILHEESK with S663 and S664 phosphorylation.

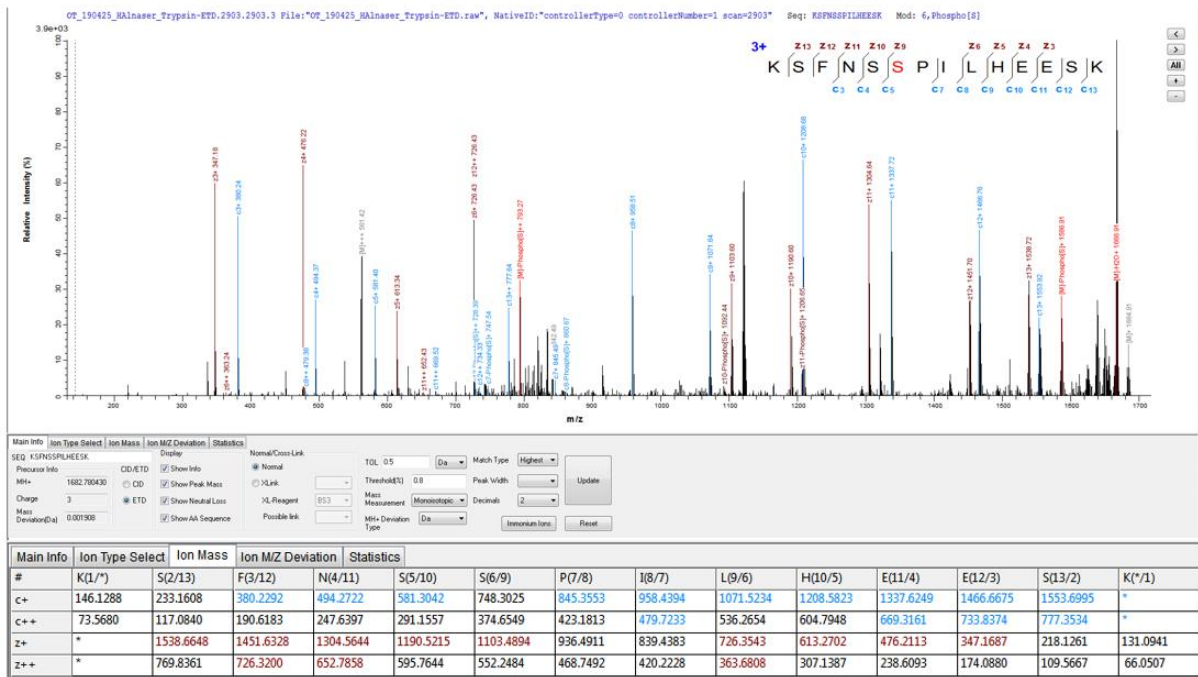


Figure A5.50 MS spectra for KSFNS^SPILHEESK with S664 phosphorylation.

Appendix V (cont'd):

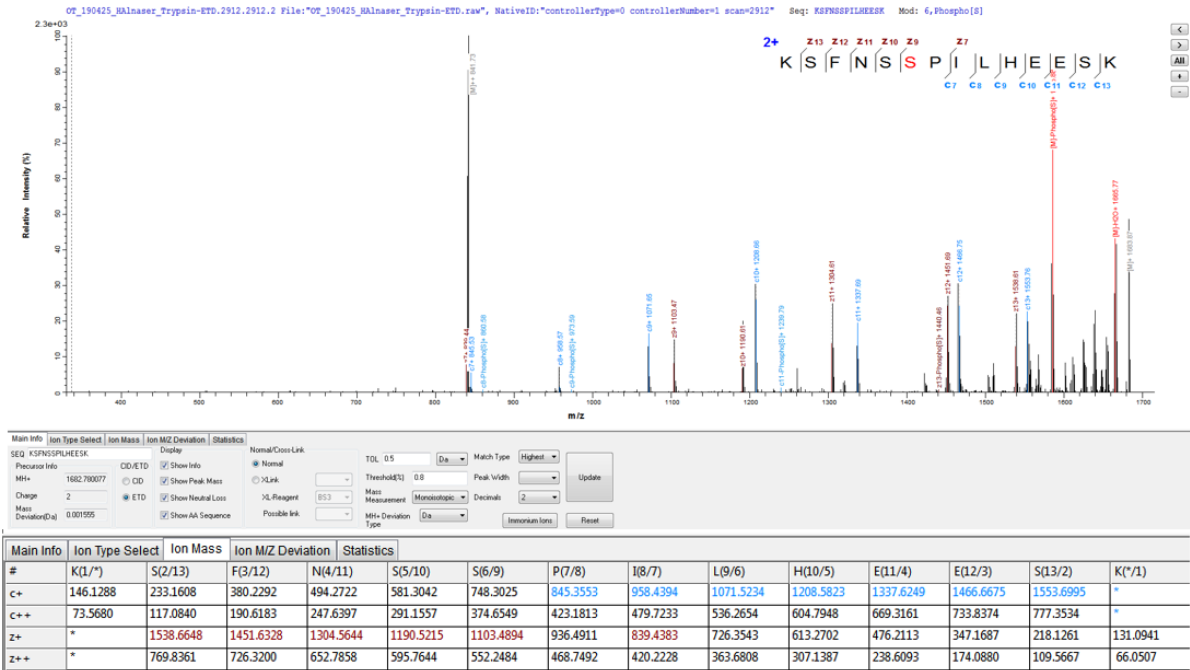


Figure A5.51 MS spectra for KSFNS^PPILHEESK with S664 phosphorylation.

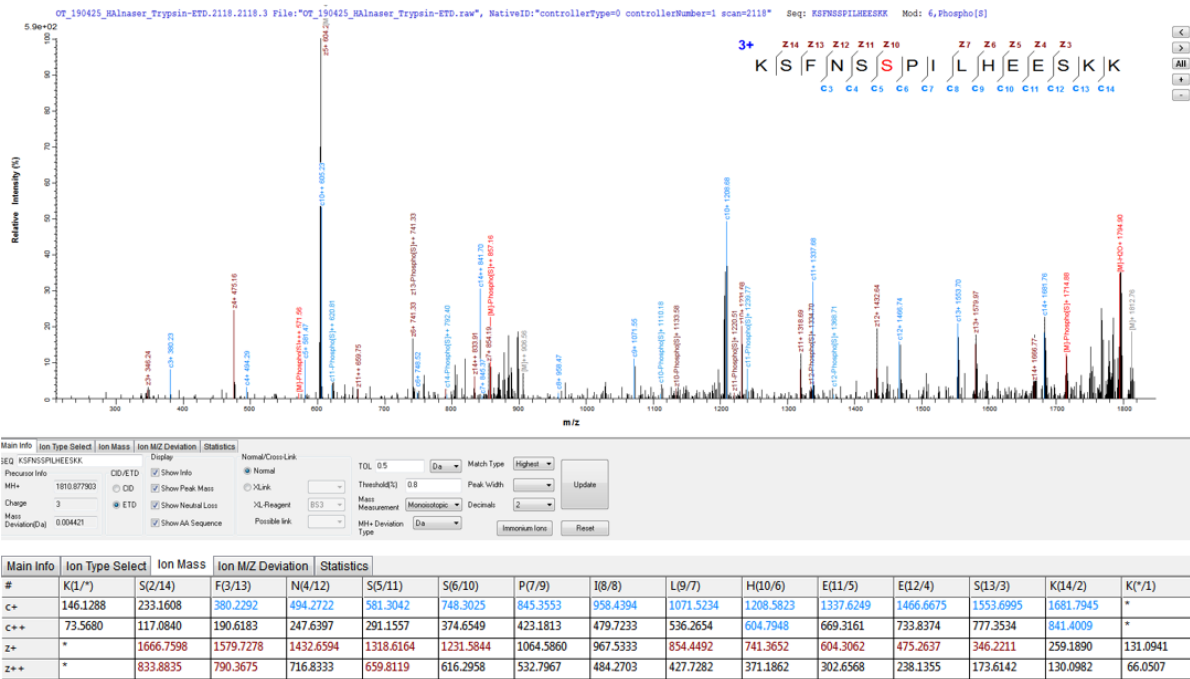


Figure A5.52 MS spectra for KSFNS^PPILHEESKK with S664 phosphorylation.

Appendix V (cont'd):

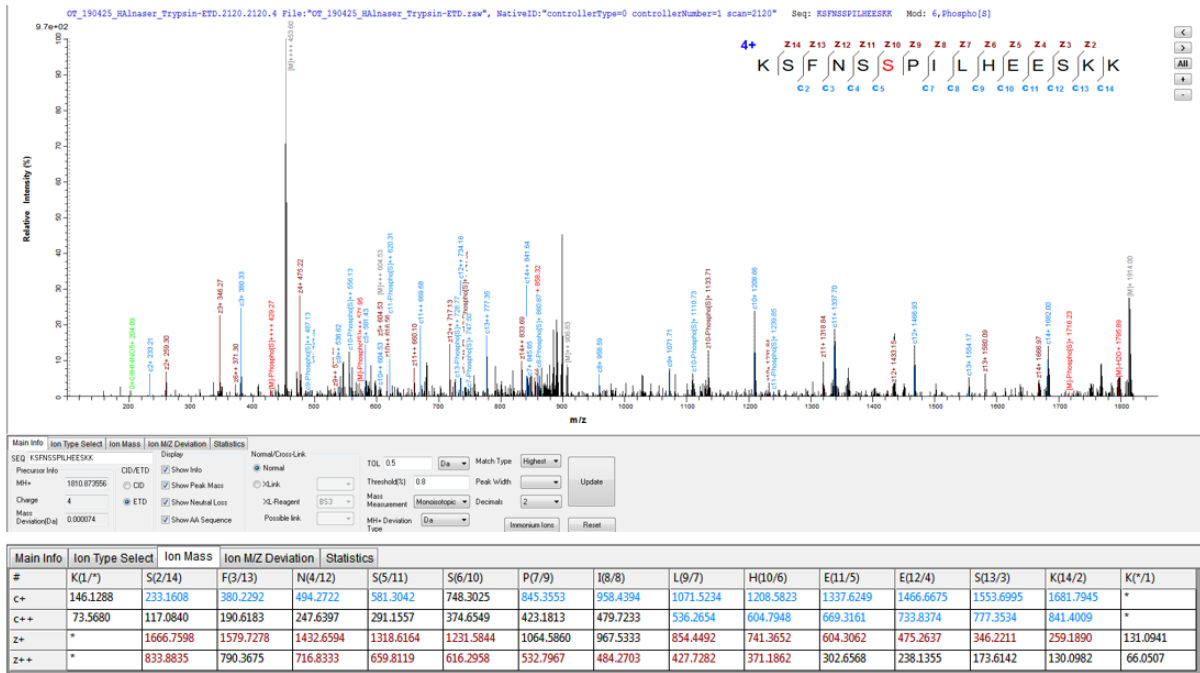


Figure A5.53 MS spectra for KSFNS^SPILHEESKK with S664 phosphorylation.

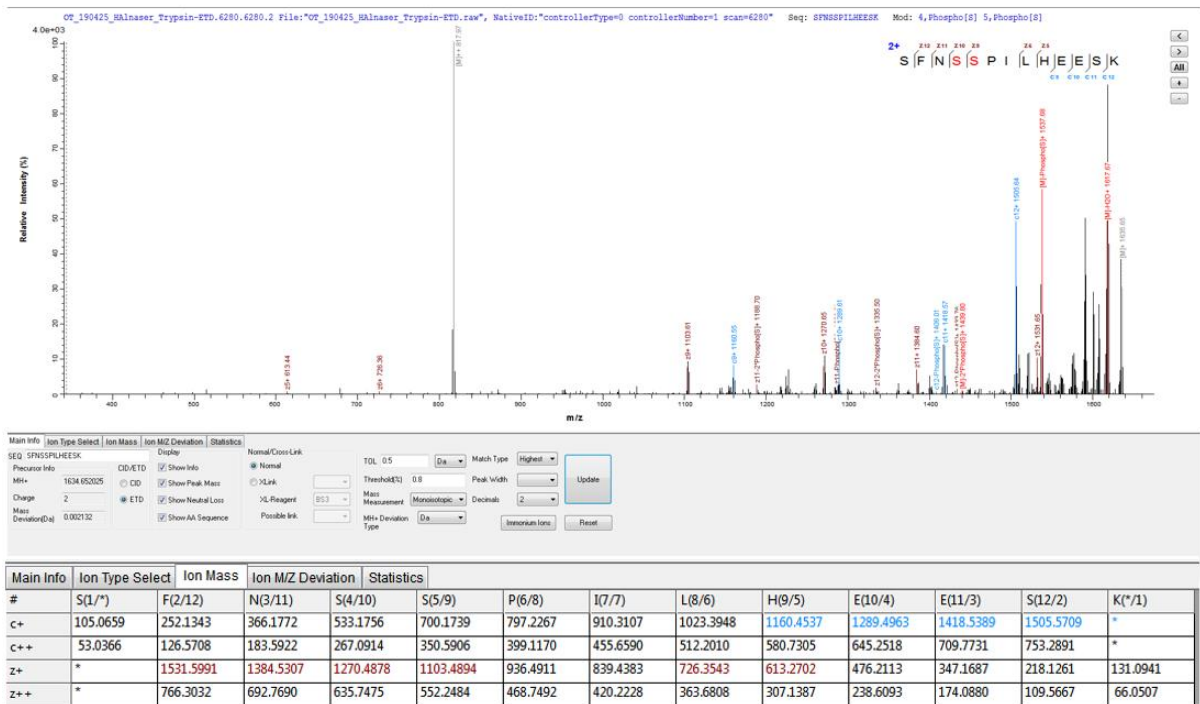


Figure A5.54 MS spectra for SFNS^SPILHEESKK with S663 and S664 phosphorylation.

Appendix V (cont'd):

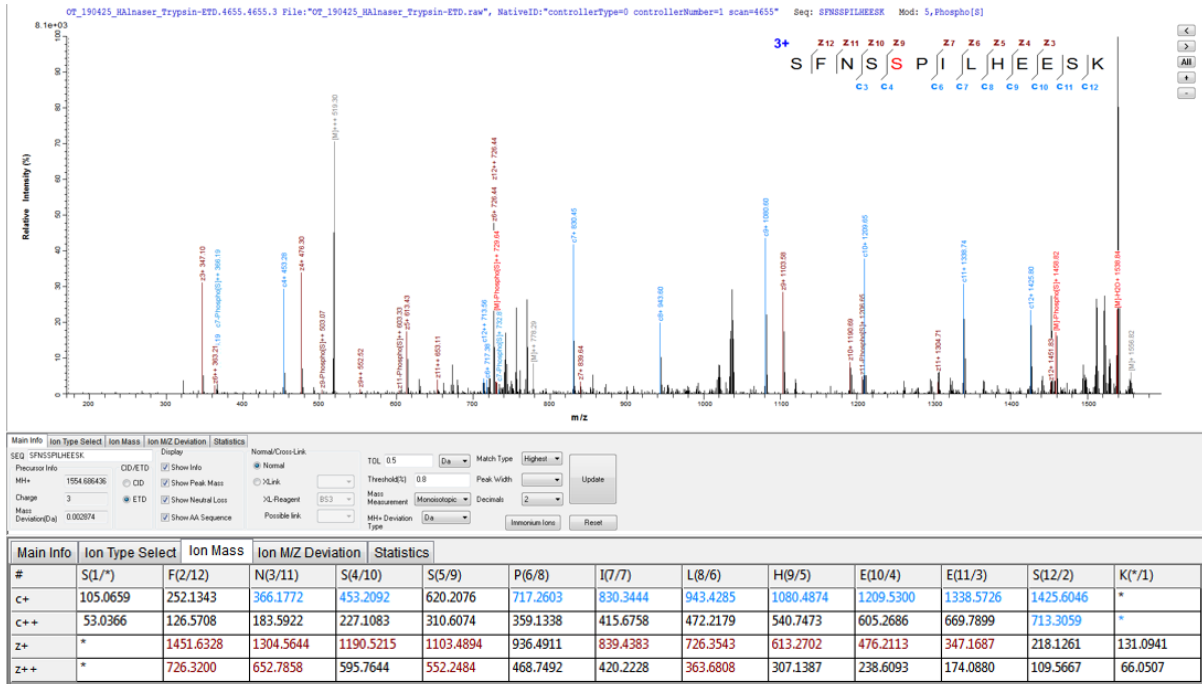


Figure A5.55 MS spectra for SFNSS^PPILHEESK with S664 phosphorylation.

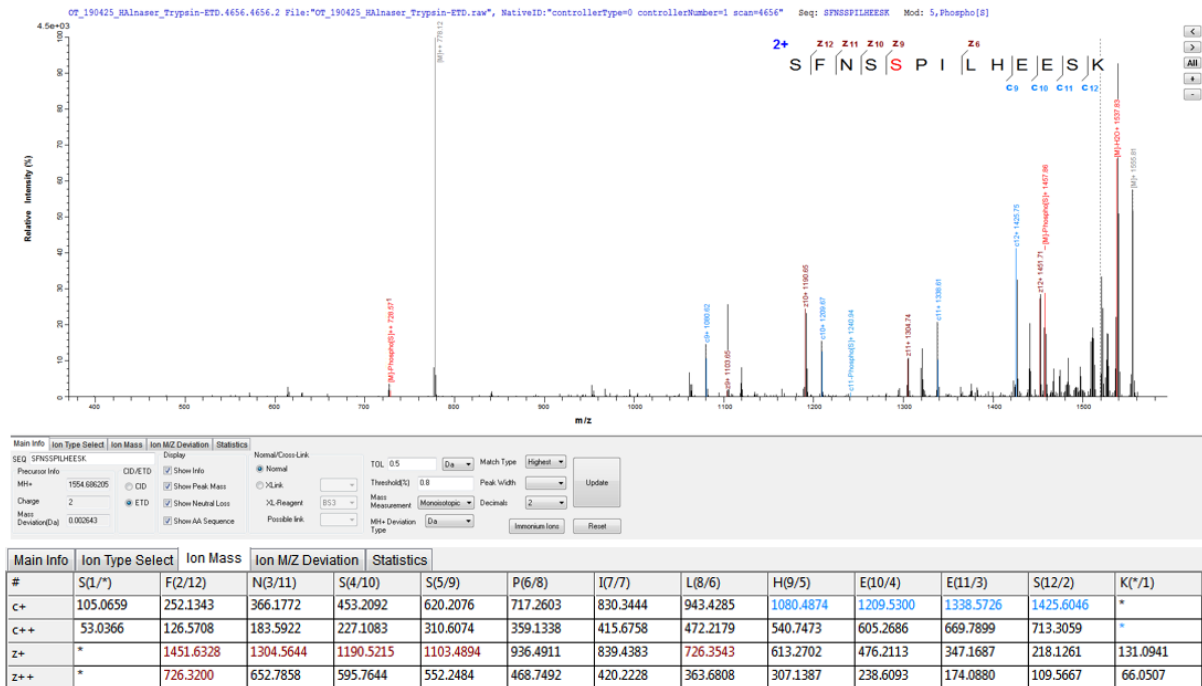


Figure A5.56 MS spectra for SFNSS^PPILHEESK with S664 phosphorylation.

Appendix V (cont'd):

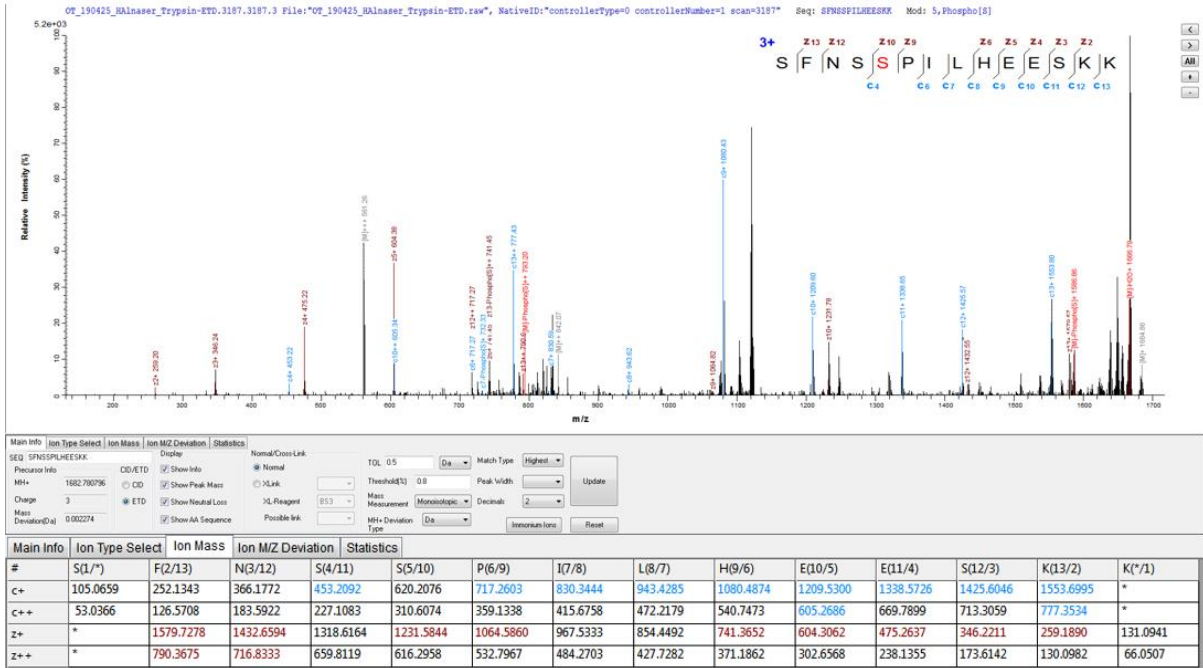


Figure A5.7 MS spectra for SFNNS^PPILHEESKK with S664 phosphorylation.

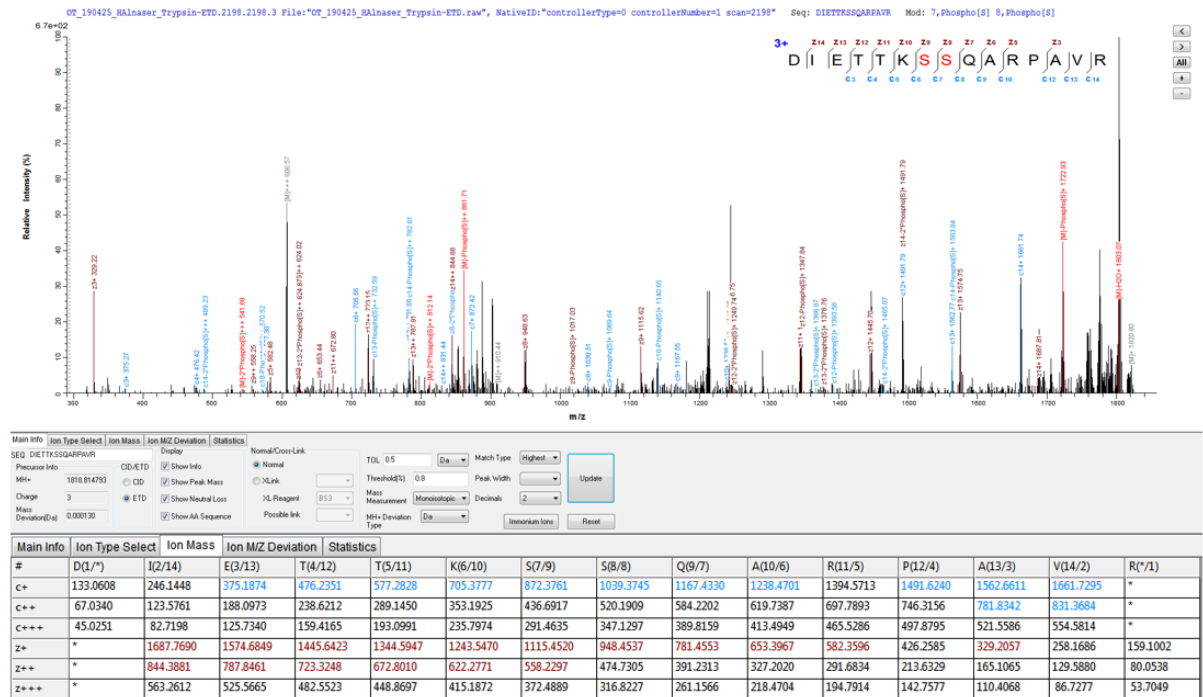


Figure A5.8 MS spectra for DIETTKS^PPQARPAVR with S681 and S682 phosphorylation.

Appendix V (cont'd):

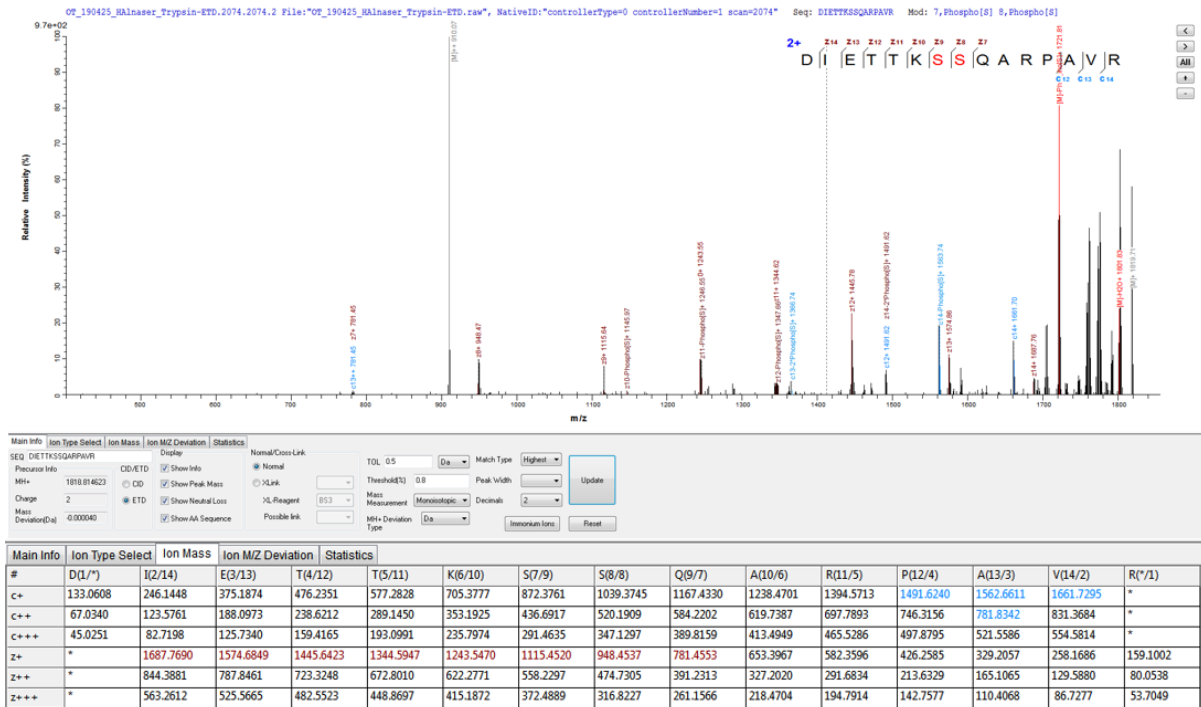


Figure A5.59 MS spectra for DIETTKS^P^PQARPAVR with S681 and S682 phosphorylation.

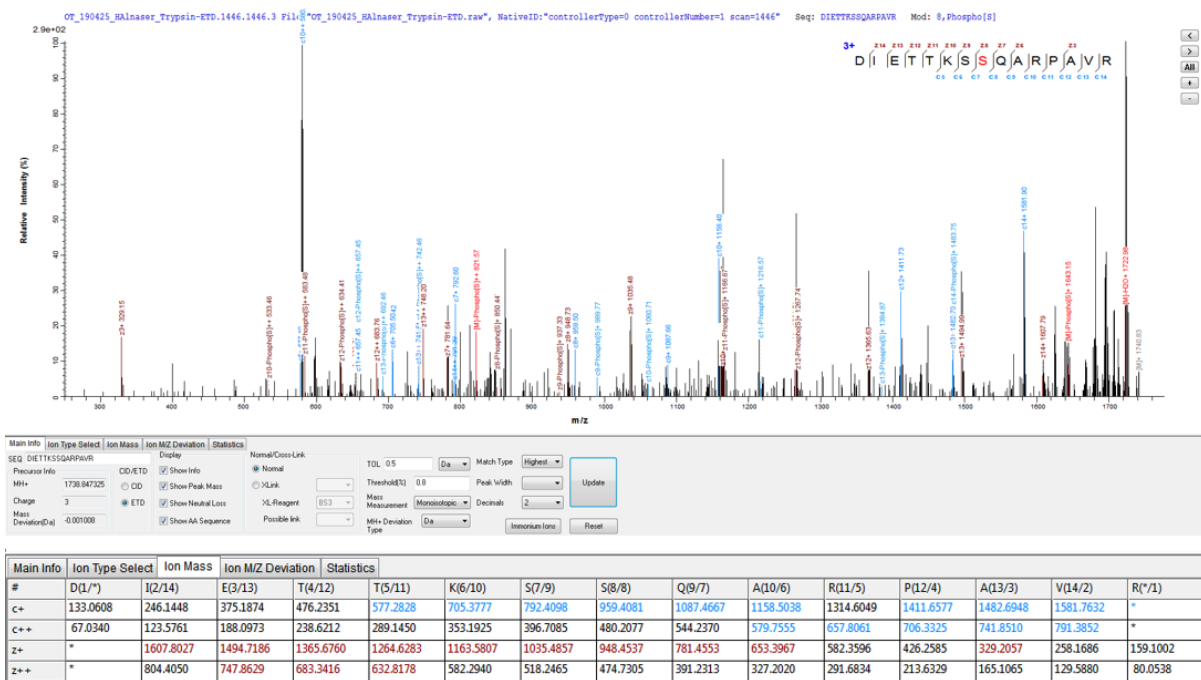


Figure A5.60 MS spectra for DIETTKS^PQARPAVR with S682 phosphorylation.

Appendix V (cont'd):

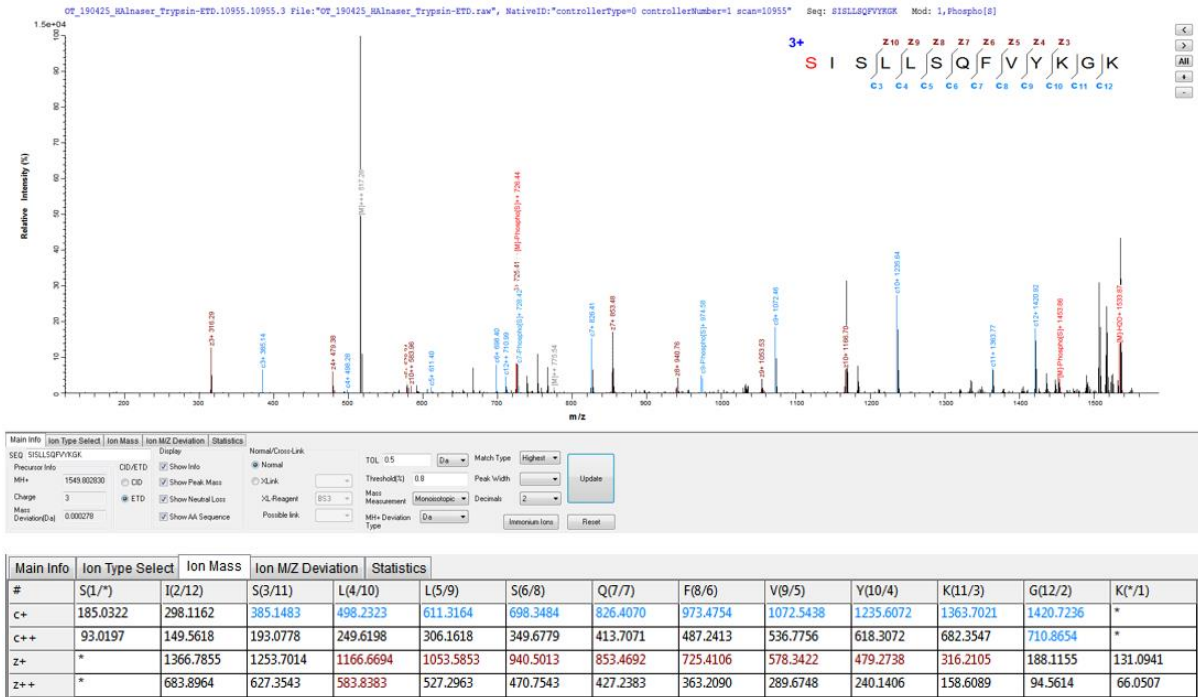


Figure A5.61 MS spectra for **S^PI**SLLSQFVYKKGK with S690 phosphorylation.

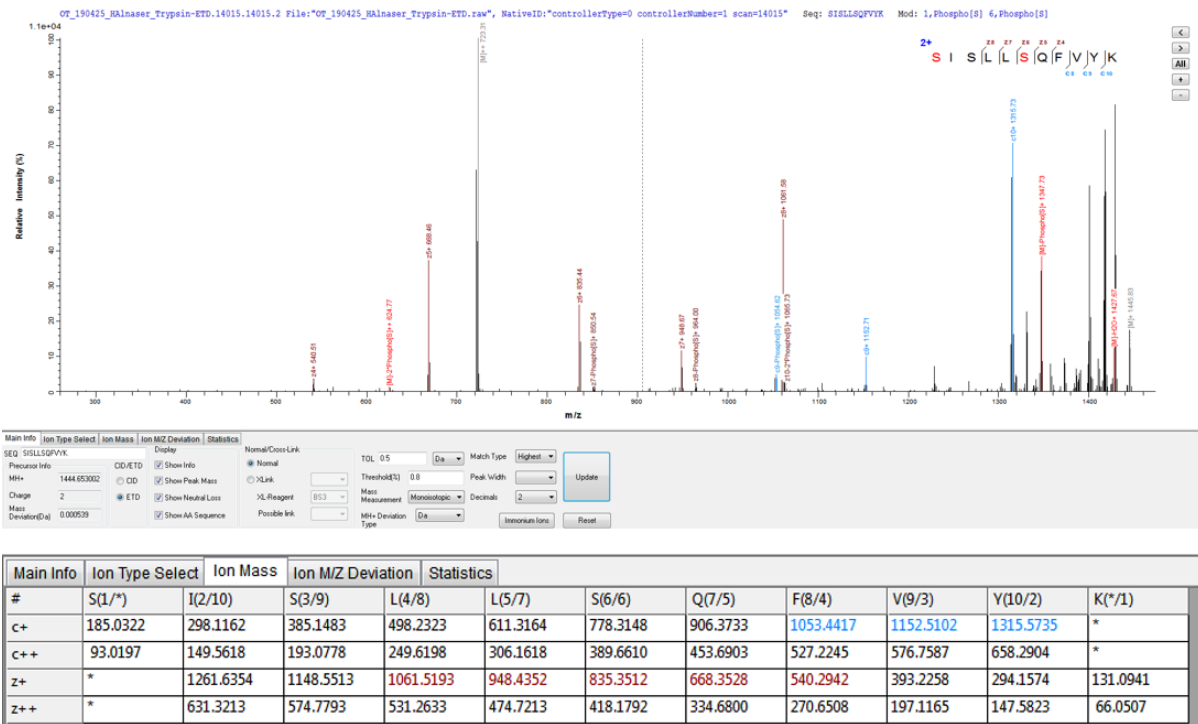


Figure A5.62 MS spectra for **S^{P^2}I S^{P^2}LLS^PQFVYK** with S690 or S692, and S695 phosphorylation.

Appendix V (cont'd):

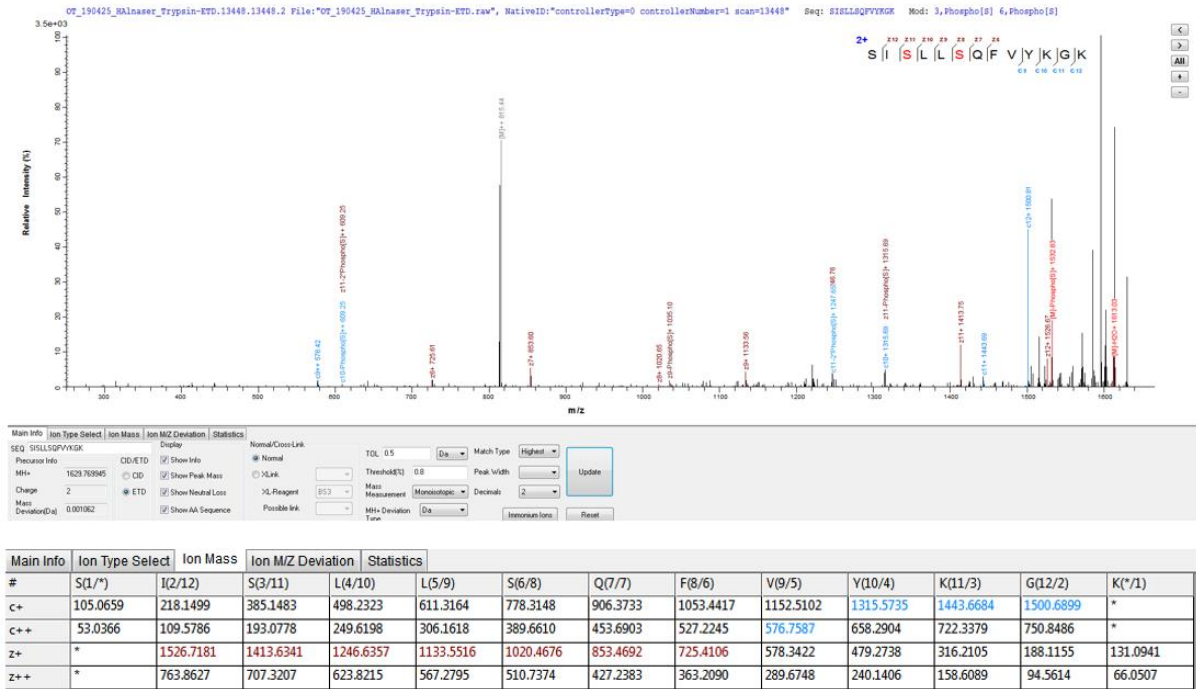


Figure A5.63 MS spectra for SIS^PLLS^PQFVYK GK with S692 and S695 phosphorylation.

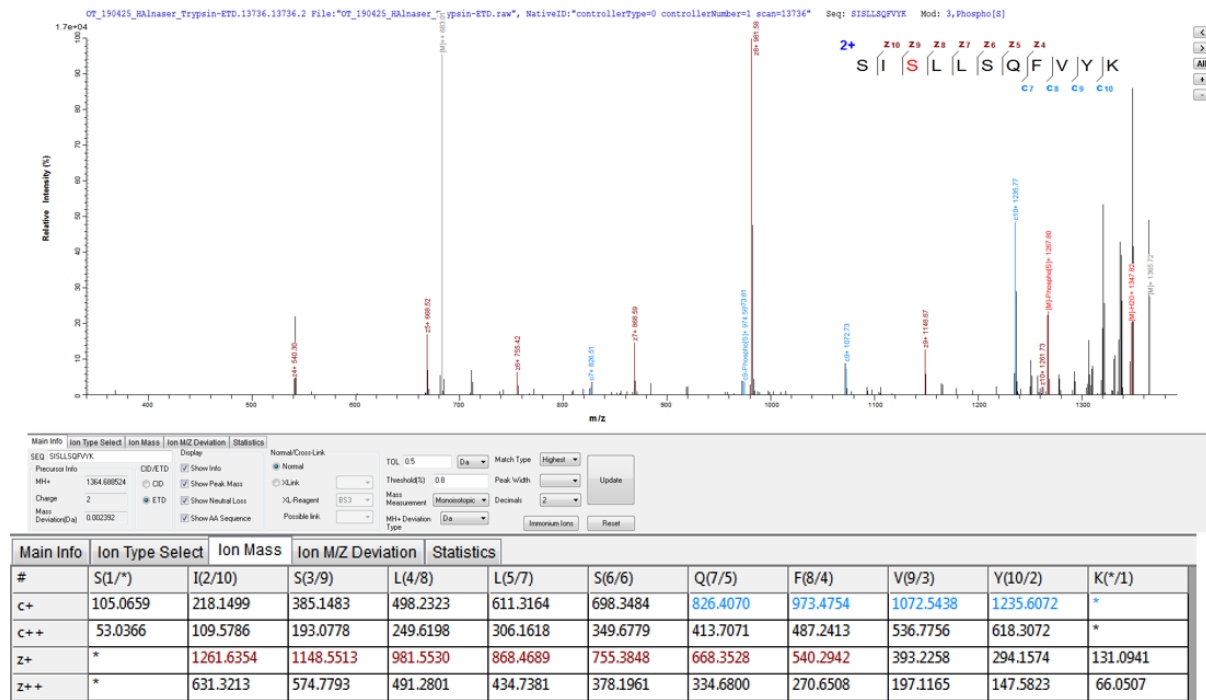


Figure A5.64 MS spectra for SIS^PLLS QFVYK with S692 phosphorylation.

A6 The cohesin subunit Scc3 is phosphorylated during meiosis and in response to Spo11-DSBs

Introduction:

During meiosis two rounds of chromosome segregation occur; MI and MII, producing gametes with half the ploidy of the progenitor cells. During MI, homologous chromosomes are segregated, whereas during MII, sister chromatids are separated, which is similar to mitosis where sister chromatids segregate. Chromosome disjunction relies on the tethering of homologous chromosomes as a result of Spo11-DSB repair. This is because when COs are produced by repairing Spo11-DSBs, homologous chromosomes are attached together by sister-chromatid cohesion (SCC). SCC acts as the physical link between sister-chromatids, where it provides the resistance to pulling forces exerted by microtubules during chromosomes segregation. In addition, SCC ensures sister chromatid segregation to opposite poles of the cells during MI, and is retained until its destruction in MII where sister chromatids segregate.

SCC is maintained by cohesin, a ring-protein complex which holds both sister chromatids together (Gruber et al., 2003). The main components of budding yeast cohesin are composed of two structure-maintenance complex (SMC) ATPase Smc1 and Smc3 (Haering et al., 2002). The non-SMC subunits that are essential for cohesin complex are the α -kleisin subunit Scc1 and Scc3 (Haering et al., 2002). During meiosis, cohesin complex is formed with Rec8, a meiotic specific α -kleisin subunit (Buonomo et al., 2000).

The cohesin interaction with chromosomes is modulated by the cell cycle progression. During G1-phase, cohesin complex is loaded onto the chromatid fibres by cohesin loading complex Scc2-Scc4 (Ciosk et al., 2000). Subsequently, the DNA replication process during S-phase establishes cohesin complex on sister chromatids (Uhlmann and Nasmyth, 1998) mediated by the acetylation of the Smc3 subunit by Eco1 (Zhang et al., 2008; Rowland et al., 2009). Non-

established cohesin complexes are removed by Wapl1 with help of Pds5 and Scc3 subunits, inhibiting cohesin entrapment of sister chromatids (Rowland et al., 2009). The cohesin complex remains associated with chromosomes tethering both sister chromatids together until anaphase (Uhlmann et al., 2000). SCC is essential for chromosomes alignment on the mitotic spindle during metaphase which is important for chromosome biorientation. In yeast, the Scc1 subunit is cleaved during anaphase by Esp1 (separase) protein, also known as separase, which dissociates cohesin from chromosomes (Uhlmann et al., 2000). In higher eukaryotes, the cohesin complex is dissociated in at least two steps, first arms cohesin is dissociated, and then centromeric cohesin is cleaved. The bulk of cohesin is dissociated from chromosomes by separase independent pathways (Sumara et al., 2000). Minor amounts of cohesin complexes remain on the centromeres and a similar small amount are cleaved by separase activity (Waizenegger et al., 2000). The centromeric cohesin is protected from cleavage by the recruitment of protein phosphatase-2 to the centromeric region by SGO1 (Watanabe et al., 2005; Kitajima et al., 2006).

During meiosis, the alignment, pairing, and synapsis of homologous chromosomes (section 1.4) critically depend on the cohesin complex. The cohesin complex is loaded into the DNA during pre-meiotic S-phase. Spo11-DSBs can occur when cohesin complex cannot be formed in *rec8Δ* strains (Klein et al., 1999), however the distribution of Spo11-DSBs on chromosome arms is reduced suggesting that cohesin can influence the distribution of Spo11 (Kugou et al., 2009). Additionally, the formation of the axial elements of the synaptonemal complex, and recombination depend on cohesin (Klein et al., 1999; Brar et al., 2009). At the onset of anaphase-I, the phosphorylation of Rec8 by three kinases, Cdc5, Cdc7, and Hrr25 promotes its cleavage by separase (Brar et al., 2006; Katis et al., 2010). This phosphorylation event is restricted to Rec8 on chromosomes arms, while Rec8 at the kinetochores is protected from phosphorylation by the recruitment of protein phosphatase-2 mediated by Sgo1 (Kitajima et

al., 2004, 2006). The protection of centromeric cohesin from cleavage is essential for faithful sister chromatids segregation in MII.

The cohesin complex is required for DNA repair in cells after DNA replication as it brings both sisters chromatids in close proximity allowing for efficient recombination (Sjögren and Nasmyth, 2001). In addition, the cohesin complex is enriched at DSB sites (Ünal et al., 2004) and is established by Eco1, similar to cohesin establishment during S-phase (Ström and Sjögren, 2005). It is unknown if cohesin is recruited to DSB sites induced by Spo11 during meiosis as it is in mitotic cells.

The *SCC3* gene is essential for the viability of cells (Tóth et al., 1999). This is because Scc3 protein is an essential subunit of the cohesin complex (Haering et al., 2002) and the *scc3-1* temperature sensitive allele induced major cohesion defects (Tóth et al., 1999). The role of Scc3 in the cohesin complex is not well understood and it was the primary subject in few studies. *In vivo* studies showed that Scc3 contributes to cohesin loading by binding to Scc1 subunit (Haering et al., 2002; Hu et al., 2011), and *in vitro* studies showed that Scc3 enhances the topological DNA entrapment by cohesin (Murayama and Uhlmann, 2014). A recent *in vitro* study demonstrated the crystal structure of Scc3-Scc1 sub-complex bound to DNA (Li et al., 2018), suggesting that Scc3 may act as a DNA anchoring point for cohesin loading or maintenance. Additionally, Scc3 regulates the anti-establishment of cohesin via Pds5, and Wpl1 (Rowland et al., 2009).

In higher eukaryotes, the separase independent pathway that releases cohesin complex from chromosomes depends on two mitosis-specific kinases PLK1 and Aurora-B (Sumara et al., 2002; Giménez-Abián et al., 2004). These two kinases were implicated in the phosphorylation of SCC1 and SA2 (Scc3 homologue in yeast), where the phosphorylation of SCC1 enhanced the cleavability of SCC1 by separase, and the phosphorylation of SA2 was essential for cohesin dissociation (Hauf et al., 2005). During yeast meiosis and at the onset of anaphase-I, arms cohesin is exclusively dissociated by separase activity, unlike the separase independent dissociation in higher eukaryotes mitosis. This is because chromosomes were not segregated in the *rec8N* non-cleavable mutant (Buonomo et al., 2000). In addition, the cleavage of Rec8 by separase is dependent on its phosphorylation by Hrr25 and Cdc7 kinases (Katis et al., 2010). Since the phosphorylation of the cohesin subunit Rec8 is essential for cohesin activity, this raise the possibility of the phosphorylation another subunit which may regulate cohesin's activities. Here the phosphorylation of the Scc3 subunit was characterised in response to DNA damage, and during yeast meiosis in response to Spo11-DSB by an antibody that binds to phosphorylated SQ/TQ motifs. These motifs are mostly phosphorylated by Tel1 and Mec1 kinases (see section 1.7). The aim was to understand the function of this phosphorylation event and its dependency during meiosis. Two Scc3 mutant were produced, a non-phosphorylatable and a phosphomimicking mutant where the phosphomimicking form caused synthetic lethality and the non-phosphorylatable mutant was normal. The few results presented here suggest a role of Scc3 phosphorylation in response to Spo11-DSBs.

Results:

A6.1 Scc3 is phosphorylated during meiosis:

To investigate whether Scc3 is phosphorylated during meiosis. A strain that expresses a x6PK epitope tagged Scc3 was induced into meiosis and samples were taken at hourly intervals. Immunoprecipitation was carried out using anti-PK antibody which targets the x6PK tag on

Scc3. Western blot was carried out for Scc3 purified samples using anti-PK antibody and using anti-phosphorylated SQ/TQ antibody (anti P-SQ/TQ). Due to the low specificity of the anti P-SQ/TQ antibody, the western blot using the anti-phosphorylated SQ/TQ had ten times the amount of the purified sample to the sample loaded for anti-PK western blot and was exposed for at least 10 minutes. A band that corresponds to Scc3 can be observed across all samples in the anti-PK western blot, Figure A5.1. In the 0, 2, 3, and 4 hour samples an extra band can be observed below Scc3 intense band, which could correspond to cleavage product or PTM such as phosphorylation. At later time points the lower band's intensity was decreased till it was barely detected. In the anti P-SQ/TQ western blot a very faint band can be observed at the 0-hour time point, where the intensity of the band peaked at the fourth-hour time point, and then decreased at later time points. This result suggests that SQ/TQ motifs on Scc3 can be phosphorylated during meiosis.

To confirm that Scc3 is phosphorylated during meiosis, phosphatase treatment was carried out for Exo1 purified sample from cells after four-hours of meiosis induction. This time point was chosen since it was when the anti P-SQ/TQ western blot showed the most intense band. The purified protein extracts were treated with three combinations of Lambda phosphatase and phosphatase inhibitors. As shown in Figure A5.2, the (IP) sample was treated with phosphatase inhibitor, the (+/-) sample was treated with Lambda phosphatase in the absence of phosphatase inhibitors, and the (++) sample was treated with both phosphatase and phosphatase inhibitor. The anti P-SQ/TQ western blot showed a band in the (IP) and (++) samples, first and third lanes respectively, whereas no signal can be observed in the phosphatase treated sample (+/-). This result suggest that the SQ/TQ motifs on Scc3 are phosphorylated during meiosis due to loss of phosphorylation when the protein was treated with phosphatase.

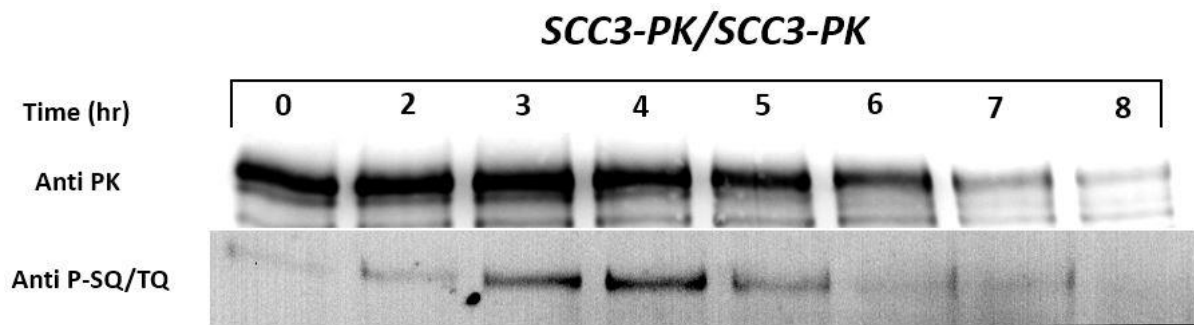
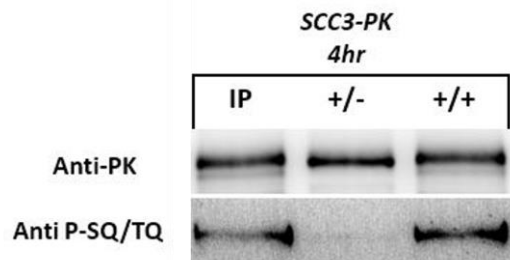


Figure A6.1 Scc3 is phosphorylated during meiosis

Western blot using anti-PK (top) and anti-phosphorylated SQ/TQ bottom for immunoprecipitated Scc3-PK samples from cells induced into meiosis. The anti-PK western blot shows Scc3 bands and anti P-SQ/TQ showed a weak signal in the 0-hour time point where the signal peaked at the four-hour sample. At the subsequent time points the anti P-SQ/TQ signal decreased.



+/- Lambda phosphatase treatment with no inhibitors

+/+ Lambda phosphatase treatment with phosphatase inhibitors

Figure A6.2 Phosphatase treatment for *Scc3-PK* purified after four-hours of meiosis induction

Western blot using anti-PK (top) and anti P-SQ/TQ (bottom) for immunoprecipitated Scc3-PK from cells at 4-hours of meiosis induction. The immunoprecipitated samples were treated with various combinations of Lambda phosphatase and phosphatase inhibitors indicated by + or -. The first and third lane showed a band in the anti P-SQ/TQ western blot, suggestive of phosphorylated Scc3-PK. In the second lane the anti P-SQ/TQ signal was absent, in which the sample was treated with phosphatase in the absence of inhibitors, suggestive of a removal of phosphorylation. This confirms that the bands detected in the anti P-SQ/TQ western blot for Scc3-PK purified meiotic samples are of phosphorylated Scc3-PK.

Appendix VI (cont'd):

A6.2 The phosphorylation of Scc3 is cohesin complex dependent:

The phosphorylation of Scc3 was examined in the absence of Rec8 to investigate whether this phosphorylation event is dependent on cohesin complex formation. In *rec8Δ* strain, meiotic SCC is lost, Spo11-DSB are induced at normal levels without being repaired (Klein et al., 1999), and SC cannot be formed (Brar et al., 2009). A *SCC3-PK* strain that lacks Rec8 was induced into meiosis and samples were taken when meiosis was induced, after three, and four hours of meiosis induction. Western blot was carried out for the immunoprecipitated Scc3-PK samples with anti-PK and anti P-SQ/TQ. Scc3 band can be observed across all tested time points in the anti-PK western blot, but no signal was detected in the anti P-SQ/TQ blot. This shows that Scc3 was not phosphorylated in the absence of Rec8, suggesting that this phosphorylation event is dependent on cohesin complex formation.

A6.3 Scc3 phosphorylation is Spo11-DSB dependent and in the Tel1-mediated pathway

The Tel1/Mec1 kinases that phosphorylate SQ/TQ motifs are mostly activated in response to DNA-DSBs, section 1.7. Since SQ/TQ motifs on Scc3 can be phosphorylated, the phosphorylation event could be correlated to Spo11-DSBs that occurs during meiosis where Tel1 and Mec1 are activated. Additionally, the phosphorylation of Scc3 was investigated when the Tel1-mediated pathway is continuously activated by unrepaired Spo11-DSBs i.e. during *sae2Δ* strain meiosis. The phosphorylation of Scc3 was not detected in the *spo11-Y135F* DSB hydrolysis mutant, and persisted during the sporulation of the *sae2Δ* strain, where Spo11-DSBs are formed but cannot be repaired, Figure A5.4. This shows that the phosphorylation of SQ/TQ motifs on Scc3 is dependent on the formation of Spo11-DSBs, and persisted when the Tel1-mediated pathway was continuously activated in *sae2Δ*.

Appendix VI (cont'd):

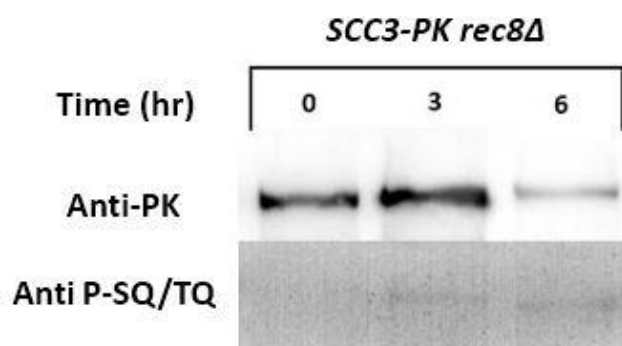


Figure A6.3 Scc3 phosphorylation is Rec8 dependent

Western blot using anti-PK (top) and anti P-SQ/TQ (bottom) for immunoprecipitated Scc3-PK from *rec8Δ* strain induced into meiosis. Anti-PK western showed a band that corresponds to Scc3 across all samples. The sixth-hour time point showed a faint band. No signal was detected in the anti P-SQ/TQ western blot.

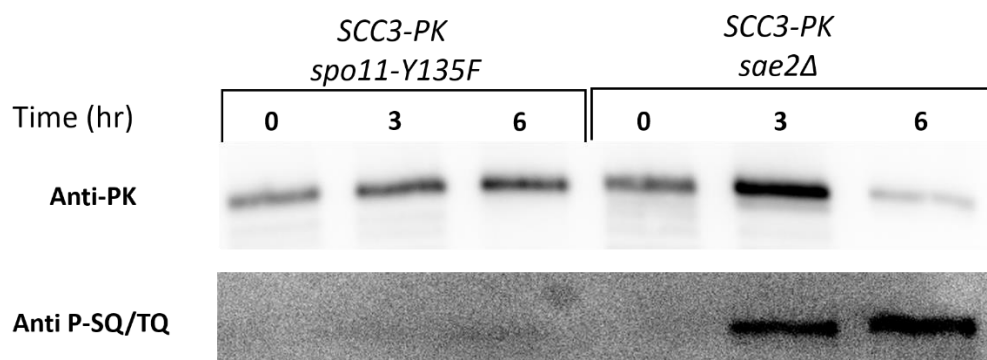


Figure A6.4 Scc3 phosphorylation is Spo11-DSB dependent and Scc3 phosphorylation persisted in *sae2Δ* strain meiosis.

Western blot using anti-PK (top) and anti P-SQ/TQ (bottom) for immunoprecipitated Scc3-PK from *spo11-Y135F* and *sae2Δ* strains induced into meiosis. The anti-PK western blot showed a band across all samples in both strains. The anti P-SQ/TQ western blot did not show any signal across *spo11-Y135F* samples, suggesting that Scc3 was not phosphorylated. The *sae2Δ* showed a signal at three- and six-hour time points suggesting that Scc3 is phosphorylated in the absence of *sae2Δ*.

Appendix VI (cont'd):

A6.4 The *scc3-9DQ* phosphorylation mimicking mutant is synthetically lethal:

To investigate the phosphorylation of Scc3, all of the serine or threonines that precede a glutamic acid residue were mutated to a non-phosphorylatable residue (alanine) or to a phosphorylation mimicking residue (aspartic acid). Scc3 protein has nine residues that are either SQ or TQ which are phosphorylated during meiosis. The *scc3-9AQ* non-phosphorylatable mutant was induced into meiosis and samples were taken at hourly intervals for western blot. As shown in Figure 5.5, the anti P-SQ/TQ cannot bind to any phosphorylation SQ/TQ residues as they have been mutated to alanine. The *scc3-9DQ* phosphorylation mimicking mutant was lethal. Therefore, the mutant was made using a wild type diploid cell to get the mutated allele integrated into the genome at one locus, producing a heterozygous diploid at the Scc3 allele. Tetrad dissection was done for a heterozygous mutant *SCC3/scc3-9DQ*, where spores with Scc3 phosphorylation mimicking allele did not grow, showing that this allele causes lethality, Figure A5.6. To investigate why the phosphorylation mimicking form causes lethality, four different phosphorylation mimicking mutants were made. Each phosphorylation mimicking mutant had a region where serine or threonine in SQ/TQ motifs mutated to aspartic acid, Scc3 protein map in Figure A5.7. The aspartic acid mutations in the middle region of Scc3 that is proximal to Scc3's N-terminal region was lethal. The function of this region is unknown but it is structurally known as the "nose region" and it is essential for cell viability (Roig et al., 2014).

Appendix VI (cont'd):

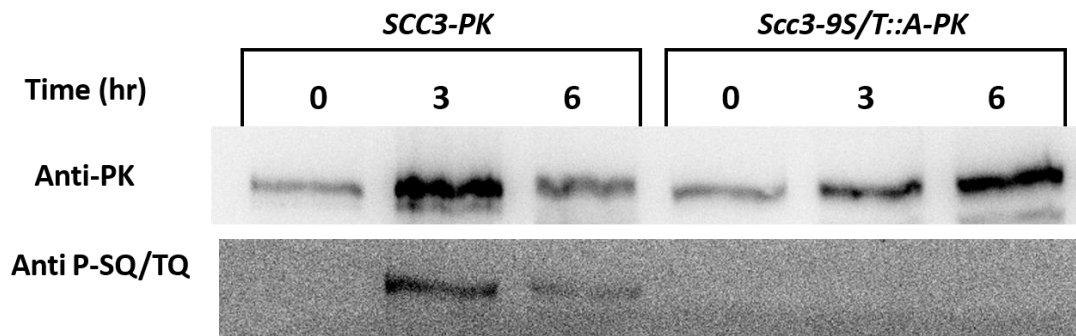


Figure A6.5 The phosphorylation mutant *Scc3-9S/T::A-PK* is not phosphorylated during meiosis.

Upon mutating all of the SQ and TQ residues to AQ in *Scc3*, the phosphorylation was abolished. The meiotic progression and spore viability of the mutant was not affected (data not shown)

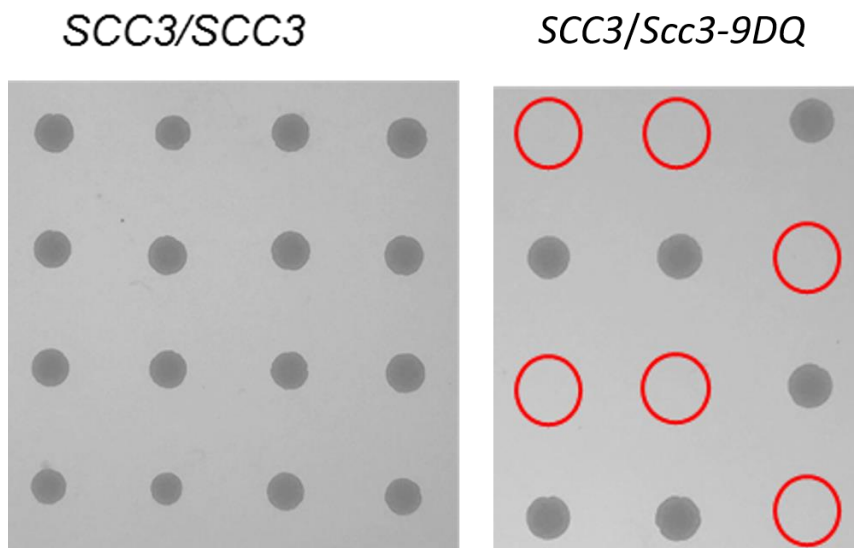


Figure A6.6 The phosphorylation mimicking mutant *Scc3-9S/T::D-PK* (*Scc3-9DQ*) is synthetically lethal

Left – yeast tetrad dissection of *SCC3* strain. Right – Tetrad dissection of *SCC3/Scc3-9DQ* revealed that the phosphorylation mimicking mutant is synthetically lethal.

Appendix VI (cont'd):

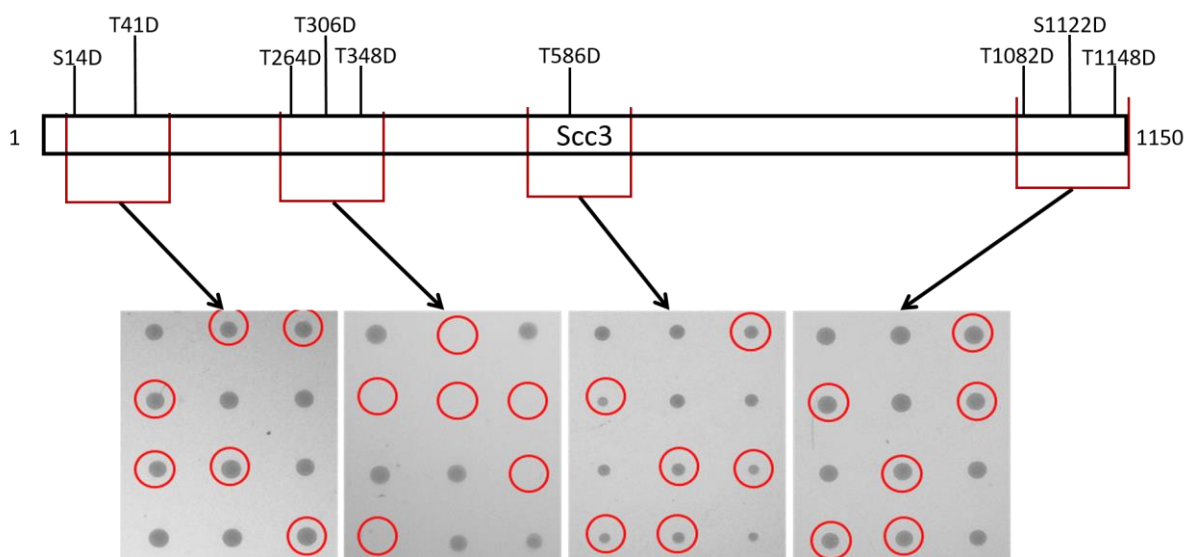


Figure A6.7 The *scc3-3DQ* mutant (T264D, T306D, T348D) is synthetically lethal
The synthetic lethality of the *Scc3-9DQ* mutant was isolated to T264, T306, and T348 residues. The other mutants were viable, albeit the *scc3-T586D* mutant showed stunt growth.

Appendix VI (cont'd):

A6.5 Scc3 is phosphorylation in response to DNA damage is mediated by Tel1 and Mec1 kinases:

To investigate whether Scc3 is phosphorylated in response to DNA damage, the wild type tagged Scc3-PK, the non-phosphorylatable mutant *scc3-9AQ*, and mutant that lacks Tel1 and Mec1 were grown with 0.01% of methyl methanesulfonate (MMS) or in the absence of MMS. Immunoprecipitation was carried out for Scc3-PK, followed by western blot using anti-PK and anti P-SQ/TQ antibodies. The anti P-SQ/TQ western blot showed a band in the Scc3-PK sample that was treated in MMS, suggestive of phosphorylation. No signal was observed in the non-phosphorylatable *scc3-9AQ* strain, and the strain that lacks Tel1/Mec1 kinases, suggesting that Scc3 is not phosphorylated. This results suggests that the SQ/TQ motifs in Scc3 are phosphorylated in response to DNA damage, where this phosphorylation event depends on Tel1 and Mec1 kinases.

A6.6 Discussion:

The dissociation of cohesin in yeast largely depends on the cleavage of Scc1 (mitotic cohesin) or Rec8 (meiotic cohesin) mediated by separase activity. In higher eukaryotes, most of cohesin dissociation is independent of separase activity, especially in unprotected cohesin that are associated at chromosome arms. The phosphorylation of Scc3's human homologue SA2 was shown to be essential for arms cohesin dissociation during prophase (Hauf et al., 2005). The phosphorylation of Scc3 could potentially release cohesin from chromosomes in response to DNA damage, possibly to allow for the recruitment of DNA repair proteins and efficient CO production. To test this idea, the non-phosphorylatable mutant should be tested for COs production by utilising the heteroduplex analysis at *HIS4LEU2* locus (Storlazzi et al., 1995).

Appendix VI (cont'd):

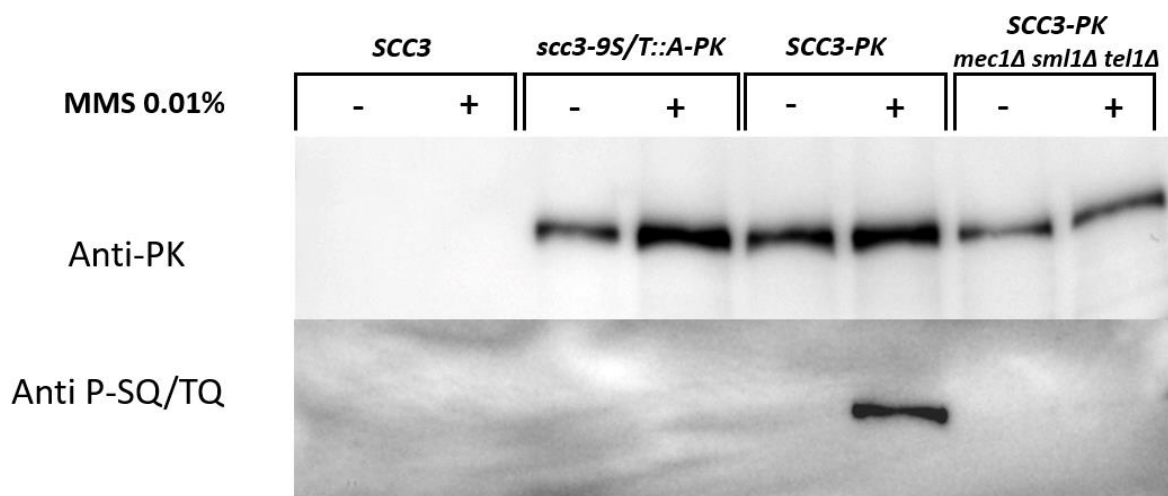


Figure A6.8 Scc3 is phosphorylated in response to DNA damaging agent MMS

Western blot using anti-PK (top) and anti P-SQ/TQ (bottom) for immunoprecipitated Scc3 mutants after being with 0.01% MMS (+) or without MMS (-). In the anti-PK western blot, bands that corresponds to Scc3 were observed across all samples except for wild type non-tagged *SCC3* strain. In the anti P-SQ/TQ western blot a band was observed in the wild type tagged *Scc3-PK* strain only, suggestive of phosphorylation. No bands were observed in the non-phosphorylatable mutant sample and the mutant that lacks Mec1 and Tel1, suggesting that Scc3 is not phosphorylated.

The phosphorylation mimicking form lethality should be investigated and the function of the so-called nose-region. The structure of the nose-region could have changed due to the aspartic acid residues that were introduced to it. Since cells cannot survive due to the absence of this region (Roig et al., 2014) or in the *scc3-3DQ* mutant, the nose-region's roll could be essential for SCC and could function in cohesin loading or cohesin dissociation. To test the function of this region, chromatin immunoprecipitation followed by real-time PCR could be carried out to *scc3-3DQ* mutant to investigate their occupancy on the chromatids. This will show if the mutant protein can be loaded into the chromosomes. Additionally, co-immunoprecipitation should be carried out to *scc3-3DQ* mutant and Rec8/Scc1 test if cohesin complex can be formed. To test if phosphorylation of the three TQ motifs at the nose-region could release cohesin from chromatin. *In vitro* experiment could be done by phosphorylating Scc3 nose-region by Tel1/Mec1 kinases while cohesin is bound to a minichromosome (Ivanov and Nasmyth, 2007). The nose-region could be selectively phosphorylated by mutating all of the serine and threonine residues in SQ/TQ motifs to alanine except for the nose-region then phosphorylated *in vitro* by the addition of Tel1 and Mec1 kinases.

Since the phosphorylation of Scc3 was only detected by anti P-SQ/TQ antibody, other residues could be phosphorylated that the antibody cannot bind to. To investigate Scc3 phosphorylation during meiosis, mass spectrometry for Scc3 could be done to isolate Scc3's phosphorylation sites. Once Scc3's phosphorylation sites are characterised, they could be mutated to alanine to prevent phosphorylation or aspartic acid to mimic phosphorylation. The DNA occupancy and CO formation of both phosphorylation mutants could be investigated during meiosis to test if cohesin complex can influence homologous recombination during meiosis via Scc3 phosphorylation.

The work on Scc3 phosphorylation was halted because the work on Exo1 phosphorylation advanced more and was more practical. For instance, detecting the phosphorylation of Scc3 using the anti P-SQ/TQ antibody required a purified sample of Scc3 that is ten-times more in volume than the volume used to detect *Scc3-PK* by the anti-PK antibody. Additionally, the phosphorylation null mutant *scc3-9AQ* did not show any significant phenotype. This led to the conclusion that Scc3 phosphorylation level might be low, and the function of this phosphorylation event might not be crucial for meiosis. Other reason is that work on Exo1 and Scc3 at the same time was not efficient as both projects will not progress in a time given for a PhD. Therefore, most of the time during my PhD was invested in studying the meiotic specific phosphorylation of Exo1. Nevertheless, future work will be considered to reveal the function of Scc3 phosphorylation and will be left for future students and researchers in our lab.

Bibliography:

- Acquaviva, L., J. Drogat, P.M. Dehé, C. de la R. Saint-André, and V. Géli. 2013. Spp1 at the crossroads of H3K4me3 regulation and meiotic recombination. *Epigenetics*. 8. doi:10.4161/epi.24295.
- Alani, E., R. Padmore, and N. Kleckner. 1990. Analysis of wild-type and rad50 mutants of yeast suggests an intimate relationship between meiotic chromosome synapsis and recombination. *Cell*. 61:419–436. doi:10.1016/0092-8674(90)90524-I.
- Allers, T., and M. Lichten. 2001. Differential timing and control of noncrossover and crossover recombination during meiosis. *Cell*. 106:47–57. doi:10.1016/S0092-8674(01)00416-0.
- Argueso, J.L., J. Wanat, Z. Gemici, and E. Alani. 2004. Competing crossover pathways act during meiosis in *Saccharomyces cerevisiae*. *Genetics*. 168:1805–1816. doi:10.1534/genetics.104.032912.
- Baudat, F., and A. Nicolas. 1997. Clustering of meiotic double-strand breaks on yeast chromosome III. *Proc. Natl. Acad. Sci. U. S. A.* 94:5213–8. doi:10.1073/pnas.94.10.5213.
- Baumann, P., and S.C. West. 1998. Role of the human RAD51 protein in homologous recombination and double-stranded-break repair. *Trends Biochem. Sci.* 23:247–251. doi:10.1016/S0968-0004(98)01232-8.
- Bergerat, A., B. De Massy, D. Gadelle, P.C. Varoutas, A. Nicolas, and P. Forterre. 1997. An atypical topoisomerase II from archaea with implications for meiotic recombination. *Nature*. 386:414–417. doi:10.1038/386414a0.
- Bishop, D.K., D. Park, L. Xu, and N. Kleckner. 1992. DMC1: A meiosis-specific yeast homolog of *E. coli* recA required for recombination, synaptonemal complex formation, and cell cycle progression. *Cell*. 69:439–456. doi:10.1016/0092-8674(92)90446-J.
- Blitzblau, H.G., and A. Hochwagen. 2013. ATR/Mec1 prevents lethal meiotic recombination initiation on partially replicated chromosomes in budding yeast. *Elife*. 2013. doi:10.7554/eLife.00844.001.
- Boersema, P.J., S. Mohammed, and A.J.R. Heck. 2009. Phosphopeptide fragmentation and analysis by mass spectrometry. *J. Mass Spectrom.* 44:861–878. doi:10.1002/jms.1599.
- Bologna, S., V. Altmannova, E. Valtorta, C. Koenig, P. Liberali, C. Gentili, D. Anrather, G. Ammerer, L. Pelkmans, L. Krejci, and S. Ferrari. 2015. Sumoylation regulates EXO1 stability and processing of DNA damage. *Cell Cycle*. 14:2439–2450. doi:10.1080/15384101.2015.1060381.
- Borde, V. 2007. The multiple roles of the Mre11 complex for meiotic recombination. *Chromosom. Res.* 15:551–563. doi:10.1007/s10577-007-1147-9.
- Borde, V., W. Lin, E. Novikov, J.H. Petrini, M. Lichten, and A. Nicolas. 2004. Association of Mre11p with Double-Strand Break Sites during Yeast Meiosis. *Mol. Cell*. 13:389–401. doi:10.1016/S1097-2765(04)00034-6.
- Brar, G.A., A. Hochwagen, L.S. Ee, and A. Amon. 2009. The Multiple Roles of Cohesin in Meiotic Chromosome Morphogenesis and Pairing. *Mol. Biol. Cell*. 20:1030–1047. doi:10.1091/mbc.e08-06-0637.

- Brar, G.A., B.M. Kiburz, Y. Zhang, J.E. Kim, F. White, and A. Amon. 2006. Rec8 phosphorylation and recombination promote the step-wise loss of cohesins in meiosis. *Nature*. 441:532–536. doi:10.1038/nature04794.
- Buonomo, S.B., R.K. Clyne, J. Fuchs, J. Loidl, F. Uhlmann, and K. Nasmyth. 2000. Disjunction of Homologous Chromosomes in Meiosis I Depends on Proteolytic Cleavage of the Meiotic Cohesin Rec8 by Separin combination (or cross over) of the DNA strands and axes of homologous chromatids. Another is the monoorientation of sister kinetochore. 103. 387–398 pp.
- Busygina, V., M.G. Sehorn, I.Y. Shi, H. Tsubouchi, G.S. Roeder, and P. Sung. 2008. Hed1 regulates Rad51-mediated recombination via a novel mechanism. *Genes Dev.* 22:786–795. doi:10.1101/gad.1638708.
- Cannavo, E., and P. Cejka. 2014. Sae2 promotes dsDNA endonuclease activity within Mre11-Rad50-Xrs2 to resect DNA breaks. *Nature*. 514:122–125. doi:10.1038/nature13771.
- Cannavo, E., D. Johnson, S.N. Andres, V.M. Kissling, J.K. Reinert, V. Garcia, D.A. Erie, D. Hess, N.H. Thomä, R.I. Enchev, M. Peter, R.S. Williams, M.J. Neale, and P. Cejka. 2018. Regulatory control of DNA end resection by Sae2 phosphorylation. *Nat. Commun.* 9:4016. doi:10.1038/s41467-018-06417-5.
- Carballo, J.A., and R.S. Cha. 2007. Meiotic roles of Mec1, a budding yeast homolog of mammalian ATR/ATM. *Chromosom. Res.* 15:539–550. doi:10.1007/s10577-007-1145-y.
- Carballo, J.A., A.L. Johnson, S.G. Sedgwick, and R.S. Cha. 2008. Phosphorylation of the Axial Element Protein Hop1 by Mec1/Tel1 Ensures Meiotic Interhomolog Recombination. *Cell*. 132:758–770. doi:10.1016/j.cell.2008.01.035.
- Carlile, T.M., and A. Amon. 2008. Meiosis I Is Established through Division-Specific Translational Control of a Cyclin. *Cell*. 133:280–291. doi:10.1016/j.cell.2008.02.032.
- Cartagena-Lirola, H., I. Guerini, V. Viscardi, G. Lucchini, and M.P. Longhese. 2006. Budding yeast Sae2 is an in vivo target of the Mec1 and Tel1 checkpoint kinases during meiosis. *Cell Cycle*. 5:1549–1559. doi:10.4161/cc.5.14.2916.
- Cha, R.S., B.M. Weiner, S. Keeney, J. Dekker, and N. Kleckner. 2000. Progression of meiotic DNA replication is modulated by interchromosomal interaction proteins, negatively by Spo11p and positively by Rec8p. *Genes Dev.* 14:493–503. doi:10.1101/gad.14.4.493.
- Chan, Y.-L., A. Zhang, B.P. Weissman, and D.K. Bishop. 2018. RPA resolves conflicting activities of accessory proteins during reconstitution of Dmc1-mediated meiotic recombination. *Nucleic Acids Res.* doi:10.1101/356592.
- Chen, H., M. Lisby, and L. Symington. 2013. RPA Coordinates DNA End Resection and Prevents Formation of DNA Hairpins. *Mol. Cell*. 50:589–600. doi:10.1016/j.molcel.2013.04.032.
- Cheng, Y.-H., C.-N. Chuang, H.-J. Shen, F.-M. Lin, and T.-F. Wang. 2013. Three Distinct Modes of Mec1/ATR and Tel1/ATM Activation Illustrate Differential Checkpoint Targeting during Budding Yeast Early Meiosis. *Mol. Cell Biol.* 33:3365–3376. doi:10.1128/MCB.00438-13.

- Chikashige, Y., D.Q. Ding, Y. Imai, M. Yamamoto, T. Haraguchi, and Y. Hiraoka. 1997. Meiotic nuclear reorganization: Switching the position of centromeres and telomeres in the fission yeast *Schizosaccharomyces pombe*. *EMBO J.* 16:193–202. doi:10.1093/emboj/16.1.193.
- Ciosk, R., M. Shirayama, A. Shevchenko, T. Tanaka, A. Toth, A. Shevchenko, and K. Nasmyth. 2000. Cohesin's binding to chromosomes depends on a separate complex consisting of Scc2 and Scc4 proteins. *Mol. Cell.* 5:243–254. doi:10.1016/S1097-2765(00)80420-7.
- Cloud, V., Y.L. Chan, J. Grubb, B. Budke, and D.K. Bishop. 2012. Rad51 is an accessory factor for Dmc1-mediated joint molecule formation during meiosis. *Science (80-.).* 337:1222–1225. doi:10.1126/science.1219379.
- Cotta-Ramusino, C., D. Fachinetti, C. Lucca, Y. Doksani, M. Lopes, J. Sogo, and M. Foiani. 2005. Exo1 processes stalled replication forks and counteracts fork reversal in checkpoint-defective cells. *Mol. Cell.* 17:153–159. doi:10.1016/j.molcel.2004.11.032.
- D'Amours, D., and S.P. Jackson. 2002. The Mre11 complex: At the crossroads of DNA repair and checkpoint signalling. *Nat. Rev. Mol. Cell Biol.* 3:317–327. doi:10.1038/nrm805.
- Diaz, R.L., A.D. Alcid, J.M. Berger, and S. Keeney. 2002. Identification of residues in yeast Spo11p critical for meiotic DNA double-strand break formation. *Mol. Cell. Biol.* 22:1106–15. doi:10.1128/MCB.22.4.1106.
- DiCarlo, J.E., A. Chavez, S.L. Dietz, K.M. Esvelt, and G.M. Church. 2015. Safeguarding CRISPR-Cas9 gene drives in yeast. *Nat. Biotechnol.* 33:1250–1255. doi:10.1038/nbt.3412.
- Dirick, L., L. Goetsch, G. Ammerer, and B. Byers. 1998. Regulation of meiotic S phase by Ime2 and a Clb5,6-associated kinase in *Saccharomyces cerevisiae*. *Science (80-.).* 281:1854–1857. doi:10.1126/science.281.5384.1854.
- Farmer, S., E.J.E. Hong, W.K. Leung, B. Argunhan, Y. Terentyev, N. Humphries, H. Toyozumi, and H. Tsubouchi. 2012. Budding yeast Pch2, a widely conserved meiotic protein, is involved in the initiation of meiotic recombination. *PLoS One.* 7:39724. doi:10.1371/journal.pone.0039724.
- Fledel-Alon, A., D.J. Wilson, K. Broman, X. Wen, C. Ober, G. Coop, and M. Przeworski. 2009. Broad-scale recombination patterns underlying proper disjunction in humans. *PLoS Genet.* 5:1000658. doi:10.1371/journal.pgen.1000658.
- Foiani, M., E. Nadjar-Boger, R. Capone, S. Sagee, T. Hashimshoni, and Y. Kassir. 1996. A meiosis-specific protein kinase, Ime2, is required for the correct timing of DNA replication and for spore formation in yeast meiosis. *Mol. Gen. Genet.* 253:278–288. doi:10.1007/s004380050323.
- Garcia, V., S. Gray, R.M. Allison, T.J. Cooper, and M.J. Neale. 2015. Tel1 ATM-mediated interference suppresses clustered meiotic double-strand-break formation. *Nature.* 520:114–118. doi:10.1038/nature13993.
- Garcia, V., S.E.L. Phelps, S. Gray, and M.J. Neale. 2011. Bidirectional resection of DNA double-strand breaks by Mre11 and Exo1. *Nature.* 479:241–244. doi:10.1038/nature10515.

- Garvik, B., M. Carson, and L. Hartwell. 1995. Single-stranded DNA arising at telomeres in *cdc13* mutants may constitute a specific signal for the RAD9 checkpoint. *Mol. Cell. Biol.* 15:6128–6138. doi:10.1128/mcb.15.11.6128.
- Giménez-Abián, J.F., I. Sumara, T. Hirota, S. Hauf, D. Gerlich, C. De La Torre, J. Ellenberg, and J.M. Peters. 2004. Regulation of sister chromatid cohesion between chromosome arms. *Curr. Biol.* 14:1187–1193. doi:10.1016/j.cub.2004.06.052.
- Goldfarb, T., and M. Lichten. 2010. Frequent and efficient use of the sister chromatid for DNA double-strand break repair during budding yeast meiosis. *PLoS Biol.* 8. doi:10.1371/journal.pbio.1000520.
- Gray, S., R.M. Allison, V. Garcia, A.S.H. Goldman, and M.J. Neale. 2013. Positive regulation of meiotic DNA double-strand break formation by activation of the DNA damage checkpoint kinase Mec1(ATR). *Open Biol.* 3. doi:10.1098/rsob.130019.
- Gruber, S., C.H. Haering, and K. Nasmyth. 2003. Chromosomal cohesin forms a ring. *Cell.* 112:765–777. doi:10.1016/S0092-8674(03)00162-4.
- Haering, C.H., J. Löwe, A. Hochwagen, and K. Nasmyth. 2002. Molecular architecture of SMC proteins and the yeast cohesin complex. *Mol. Cell.* 9:773–788. doi:10.1016/S1097-2765(02)00515-4.
- Harper, L., I. Golubovskaya, and W.Z. Cande. 2004. A bouquet of chromosomes. *J. Cell Sci.* 117:4025–4032. doi:10.1242/jcs.01363.
- Hartwell, L.H. 1974. *Saccharomyces cerevisiae* cell cycle. *Bacteriol. Rev.* 38:164–198. doi:38(2): 164–198.
- Hassold, T., H. Hall, and P. Hunt. 2007. The origin of human aneuploidy: Where we have been, where we are going. *Hum. Mol. Genet.* 16. doi:10.1093/hmg/ddm243.
- Hassold, T., and P. Hunt. 2001. To err (meiotically) is human: The genesis of human aneuploidy. *Nat. Rev. Genet.* 2:280–291. doi:10.1038/35066065.
- Hauf, S., E. Roitinger, B. Koch, C.M. Dittrich, K. Mechtler, and J.M. Peters. 2005. Dissociation of cohesin from chromosome arms and loss of arm cohesion during early mitosis depends on phosphorylation of SA2. In *PLoS Biology*. R.S. Hawley, editor. Public Library of Science. 0419–0432.
- Hayase, A., M. Takagi, T. Miyazaki, H. Oshiumi, M. Shinohara, and A. Shinohara. 2004. A protein complex containing Mei5 and Sae3 promotes the assembly of the meiosis-specific RecA homolog Dmc1. *Cell.* 119:927–940. doi:10.1016/j.cell.2004.10.031.
- Henderson, K.A., K. Kee, S. Maleki, P.A. Santini, and S. Keeney. 2006. Cyclin-Dependent Kinase Directly Regulates Initiation of Meiotic Recombination. *Cell.* 125:1321–1332. doi:10.1016/j.cell.2006.04.039.
- Henry, J.M., R. Camahort, D.A. Rice, L. Florens, S.K. Swanson, M.P. Washburn, and J.L. Gerton. 2006. Mnd1/Hop2 Facilitates Dmc1-Dependent Interhomolog Crossover Formation in Meiosis of Budding Yeast. *Mol. Cell. Biol.* 26:2913–2923. doi:10.1128/MCB.26.8.2913-2923.2006.
- Hepworth, S.R., H. Friesen, and J. Segall. 1998. NDT80 and the Meiotic Recombination Checkpoint Regulate Expression of Middle Sporulation-Specific Genes in *Saccharomyces cerevisiae*. *Mol. Cell. Biol.* 18:5750–5761. doi:10.1128/mcb.18.10.5750.

- Hinshaw, S.M., V. Makrantoni, S.C. Harrison, and A.L. Marston. 2017. The Kinetochore Receptor for the Cohesin Loading Complex. *Cell*. 171:72-84.e13. doi:10.1016/j.cell.2017.08.017.
- Hochwagen, A., and A. Amon. 2006. Checking your breaks: Surveillance mechanisms of meiotic recombination. *Curr. Biol.* 16. doi:10.1016/j.cub.2006.03.009.
- Hodgson, A., Y. Terentyev, R.A. Johnson, A. Bishop-Bailey, T. Angevin, A. Croucher, and A.S.H. Goldman. 2011. Mre11 and Exo1 contribute to the initiation and processivity of resection at meiotic double-strand breaks made independently of Spo11. *DNA Repair (Amst)*. 10:138–148. doi:10.1016/j.dnarep.2010.11.008.
- Hollingsworth, N.M. 2016. Mek1/Mre4 is a master regulator of meiotic recombination in budding yeast. *Microb. Cell*. 3:129–131. doi:10.15698/mic2016.03.487.
- Hollingsworth, N.M., L. Goetsch, and B. Byers. 1990. The HOP1 gene encodes a meiosis-specific component of yeast chromosomes. *Cell*. 61:73–84. doi:10.1016/0092-8674(90)90216-2.
- Holt, L.J., B.B. Tuch, J. Villen, A.D. Johnson, S.P. Gygi, and D.O. Morgan. 2009. Global analysis of cdk1 substrate phosphorylation sites provides insights into evolution. *Science (80-.)*. 325:1682–1686. doi:10.1126/science.1172867.
- Hopfner, K.P., A. Karcher, L. Craig, T.T. Woo, J.P. Carney, and J.A. Tainer. 2001. Structural biochemistry and interaction architecture of the DNA double-strand break repair Mre11 nuclease and Rad50-ATPase. *Cell*. 105:473–485. doi:10.1016/S0092-8674(01)00335-X.
- Hopp, T., and K.S. Prickett. 1988. A short ptypeptide marker sequence useful for recombinant protein identification and purification. *Nat. Biotechnol.* 1542:33–36. doi:10.1017/CBO9781107415324.004.
- Hu, B., T. Itoh, A. Mishra, Y. Katoh, K.L. Chan, W. Upcher, C. Godlee, M.B. Roig, K. Shirahige, and K. Nasmyth. 2011. ATP hydrolysis is required for relocating cohesin from sites occupied by its Scc2/4 loading complex. *Curr. Biol.* 21:12–24. doi:10.1016/j.cub.2010.12.004.
- Huertas, P., F. Cortés-Ledesma, A.A. Sartori, A. Aguilera, and S.P. Jackson. 2008. CDK targets Sae2 to control DNA-end resection and homologous recombination. *Nature*. 455:689–692. doi:10.1038/nature07215.
- Humphries, N., W.K. Leung, B. Argunhan, Y. Terentyev, M. Dvorackova, and H. Tsubouchi. 2013. The Ecm11-Gmc2 Complex Promotes Synaptonemal Complex Formation through Assembly of Transverse Filaments in Budding Yeast. *PLoS Genet*. 9:1003194. doi:10.1371/journal.pgen.1003194.
- Hunter, N., and N. Kleckner. 2001. The single end invasion: an asymmetric intermediate at the double-strand-break to double-holiday junction transition of meiotic recombination. *Cell*. 106:59–70.
- Inbar, O., B. Liefshitz, G. Bitan, and M. Kupiec. 2000. The relationship between homology length and crossing over during the repair of a broken chromosome. *J. Biol. Chem.* 275:30833–30838. doi:10.1074/jbc.C000133200.
- Ivanov, D., and K. Nasmyth. 2007. A Physical Assay for Sister Chromatid Cohesion In Vitro. *Mol. Cell*. 27:300–310. doi:10.1016/j.molcel.2007.07.002.

- Jessberger, R. 2012. Age-related aneuploidy through cohesion exhaustion. *EMBO Rep.* 13:539–546. doi:10.1038/embor.2012.54.
- Jinks-Robertson, S., M. Michelitch, and S. Ramcharan. 1993. Substrate length requirements for efficient mitotic recombination in *Saccharomyces cerevisiae*. *Mol. Cell. Biol.* 13:3937–3950. doi:10.1128/mcb.13.7.3937.
- Jordan, P., A. Copsey, L. Newnham, E. Kolar, M. Lichten, and E. Hoffmann. 2009. Ipl1/Aurora B kinase coordinates synaptonemal complex disassembly with cell cycle progression and crossover formation in budding yeast meiosis. *Genes Dev.* 23:2237–2251. doi:10.1101/gad.536109.
- Kane, S.M., and R. Roth. 1974. Carbohydrate metabolism during ascospore development in yeast. *J. Bacteriol.* 118:8–14.
- Kassir, Y., D. Granot, and S. Giora. 1988. IME1, a Positive Regulator Gene of Meiosis in *S. cerevisiae*. *Cell.* 52:853–862.
- Katis, V.L., J.J. Lipp, R. Imre, A. Bogdanova, E. Okaz, B. Habermann, K. Mechtler, K. Nasmyth, and W. Zachariae. 2010. Rec8 phosphorylation by casein kinase 1 and Cdc7-Dbf4 kinase regulates cohesin cleavage by separase during meiosis. *Dev. Cell.* 18:397–409. doi:10.1016/j.devcel.2010.01.014.
- Keelagher, R.E., V.E. Cotton, A.S.H. Goldman, and R.H. Borts. 2011. Separable roles for Exonuclease I in meiotic DNA double-strand break repair. *DNA Repair (Amst).* 10:126–137. doi:10.1016/j.dnarep.2010.09.024.
- Keeney, S. 2001. Mechanism and Control of Meiotic Recombination Initiation. *Curr. Top. Dev. Biol.* 52.
- Keeney, S. 2008. Spo11 and the formation of DNA double-strand breaks in meiosis. *Genome Dyn. Stab.* 2:81–123. doi:10.1007/7050_2007_026.
- Keeney, S., C.N. Giroux, and N. Kleckner. 1997. Meiosis-specific DNA double-strand breaks are catalyzed by Spo11, a member of a widely conserved protein family. *Cell.* 88:375–384. doi:10.1016/S0092-8674(00)81876-0.
- Keeney, S., and N. Kleckner. 1995. Covalent protein-DNA complexes at the 5' strand termini of meiosis-specific double-strand breaks in yeast. 92. 11274–11278 pp.
- Khazanehdari, K.A., and R.H. Borts. 2000. EXO1 and MSH4 differentially affect crossing-over and segregation. *Chromosoma.* 109:94–102. doi:10.1007/s004120050416.
- Kim, M.S., and A. Pandey. 2012. Electron transfer dissociation mass spectrometry in proteomics. *Proteomics.* 12:530–542. doi:10.1002/pmic.201100517.
- Kirmizis, A., H. Santos-Rosa, C.J. Penkett, M.A. Singer, M. Vermeulen, M. Mann, J. Bähler, R.D. Green, and T. Kouzarides. 2007. Arginine methylation at histone H3R2 controls deposition of H3K4 trimethylation. *Nature.* 449:928–932. doi:10.1038/nature06160.
- Kitajima, T.S., S.A. Kawashima, and Y. Watanabe. 2004. The conserved kinetochore protein shugoshin protects centromeric cohesion during meiosis. *Nature.* 427:510–517. doi:10.1038/nature02312.
- Kitajima, T.S., T. Sakuno, K.I. Ishiguro, S.I. Iemura, T. Natsume, S.A. Kawashima, and Y. Watanabe. 2006. Shugoshin collaborates with protein phosphatase 2A to protect

- cohesin. *Nature*. 441:46–52. doi:10.1038/nature04663.
- Klein, F., P. Mahr, M. Galova, S.B.C.C. Buonomo, C. Michaelis, K. Nairz, and K. Nasmyth. 1999. A central role for cohesins in sister chromatid cohesion, formation of axial elements, and recombination during yeast meiosis. 98. *Cell Press*. 91–103 pp.
- Kocer, A., J. Reichmann, D. Best, and I.R. Adams. 2009. Germ cell sex determination in mammals. *Mol. Hum. Reprod.* 15:205–213. doi:10.1093/molehr/gap008.
- Krejci, L., V. Altmannova, M. Spirek, and X. Zhao. 2012. Homologous recombination and its regulation. *Nucleic Acids Res.* 40:5795–5818. doi:10.1093/nar/gks270.
- Krogh, B.O., B. Llorente, A. Lam, and L.S. Symington. 2005. Mutations in Mre11 phosphoesterase motif I that impair *Saccharomyces cerevisiae* Mre11-Rad50-Xrs2 complex stability in addition to nuclease activity. *Genetics*. 171:1561–1570. doi:10.1534/genetics.105.049478.
- Kugou, K., T. Fukuda, S. Yamada, M. Ito, H. Sasanuma, S. Mori, Y. Katou, T. Itoh, K. Matsumoto, T. Shibata, K. Shirahige, and K. Ohta. 2009. Rec8 Guides Canonical Spo11 Distribution along Yeast Meiotic Chromosomes. *Mol. Biol. Cell*. 20:3064–3076. doi:10.1091/mbc.E08-12-1223.
- Lamb, N.E., S.L. Sherman, and T.J. Hassold. 2005. Effect of meiotic recombination on the production of aneuploid gametes in humans. *Cytogenet. Genome Res.* 111:250–255. doi:10.1159/000086896.
- Lengsfeld, B.M., A.J. Rattray, V. Bhaskara, R. Ghirlando, and T.T. Paull. 2007. Sae2 Is an Endonuclease that Processes Hairpin DNA Cooperatively with the Mre11/Rad50/Xrs2 Complex. *Mol. Cell*. 28:638–651. doi:10.1016/j.molcel.2007.11.001.
- Li, Y., K.W. Muir, M.W. Bowler, J. Metz, C.H. Haering, and D. Panne. 2018. Structural basis for scc3-dependent cohesin recruitment to chromatin. *Elife*. 7. doi:10.7554/eLife.38356.
- Lieber, M.R. 1997. The FEN-1 family of structure-specific nucleases in eukaryotic DNA replication, recombination and repair. *BioEssays*. 19:233–240. doi:10.1002/bies.950190309.
- Longhese, M.P., D. Bonetti, I. Guerini, N. Manfrini, and M. Clerici. 2009. DNA double-strand breaks in meiosis: Checking their formation, processing and repair. *DNA Repair (Amst)*. 8:1127–1138. doi:10.1016/j.dnarep.2009.04.005.
- De los Santos, T., N. Hunter, C. Lee, B. Larkin, J. Loidl, and N.M. Hollingsworth. 2003. The MUS81/MMS4 endonuclease acts independently of double-holliday junction resolution to promote a distinct subset of crossovers during meiosis in budding yeast. *Genetics*. 164:81–94.
- Lydall, D., Y. Nikolsky, D.K. Bishop, and T. Weinert. 1996. A meiotic recombination checkpoint controlled by mitotic checkpoint genes. *Nature*. 383:840–843. doi:10.1038/383840a0.
- Lynn, A., R. Soucek, and G.V. Börner. 2007. ZMM proteins during meiosis: Crossover artists at work. *Chromosom. Res.* 15:591–605. doi:10.1007/s10577-007-1150-1.
- Ma, Y., and C.W. Greider. 2009. Kinase-Independent Functions of TEL1 in Telomere Maintenance. *Mol. Cell. Biol.* 29:5193–5202. doi:10.1128/MCB.01896-08.

- MacQueen, A.J., and G.S. Roeder. 2009. Fpr3 and Zip3 Ensure that Initiation of Meiotic Recombination Precedes Chromosome Synapsis in Budding Yeast. *Curr. Biol.* 19:1519–1526. doi:10.1016/j.cub.2009.08.048.
- Mallory, J.C., and T.D. Petes. 2000. Protein kinase activity of Tel1p and Mec1p, two *Saccharomyces cerevisiae* proteins related to the human ATM protein kinase. *Proc. Natl. Acad. Sci. U. S. A.* 97:13749–13754. doi:10.1073/pnas.250475697.
- Manfrini, N., I. Guerini, A. Citterio, G. Lucchini, and M.P. Longhese. 2010. Processing of meiotic DNA double strand breaks requires cyclin-dependent kinase and multiple nucleases. *J. Biol. Chem.* 285:11628–11637. doi:10.1074/jbc.M110.104083.
- Maringele, L., and D. Lydall. 2002. EXO1-dependent single-stranded DNA at telomeres activates subsets of DNA damage and spindle checkpoint pathways in budding yeast *yku70Δ* mutants. *Genes Dev.* 16:1919–1933. doi:10.1101/gad.225102.
- Masson, J.Y., and S.C. West. 2001. The Rad51 and Dmc1 recombinases: A non-identical twin relationship. 26. Elsevier Current Trends.
- de Massy, B., V. Rocco, and A. Nicolas. 1995. The nucleotide mapping of DNA double-strand breaks at the CYS3 initiation site of meiotic recombination in *Saccharomyces cerevisiae*. 14. 4589–4598 pp.
- Matos, J., M.G. Blanco, S. Maslen, J.M. Skehel, and S.C. West. 2011. Regulatory control of the resolution of DNA recombination intermediates during meiosis and mitosis. *Cell.* 147:158–172. doi:10.1016/j.cell.2011.08.032.
- McKee, A.H.Z., and N. Kleckner. 1997a. A general method for identifying recessive diploid-specific mutations in *Saccharomyces cerevisiae*, its application to the isolation of mutants blocked at intermediate stages of meiotic prophase and characterization of a new gene SAE2. *Genetics.* 146:797–816.
- McKee, A.H.Z., and N. Kleckner. 1997b. Mutations in *Saccharomyces cerevisiae* that block meiotic prophase chromosome metabolism and confer cell cycle arrest at pachytene identify two new meiosis-specific genes SAE1 and SAE3. *Genetics.* 146:817–834.
- McKee, B.D. 2004. Homologous pairing and chromosome dynamics in meiosis and mitosis. *Biochim. Biophys. Acta - Gene Struct. Expr.* 1677:165–180. doi:10.1016/j.bbaexp.2003.11.017.
- Merlini, L., O. Dudin, and S.G. Martin. 2013. Mate and fuse: How yeast cells do it. *Open Biol.* 3. doi:10.1098/rsob.130008.
- Mimitou, E.P., and L.S. Symington. 2009. DNA end resection: Many nucleases make light work. *DNA Repair (Amst).* 8:983–995. doi:10.1016/j.dnarep.2009.04.017.
- Mimitou, E.P., S. Yamada, and S. Keeney. 2017. A global view of meiotic double-strand break end resection. *Science (80-).* 355. doi:10.1126/science.aak9704.
- Mitchell, A.P. 1994. Control of Meiotic Gene Expression in *Saccharomyces cerevisiae*. *Microbiol. Rev.* 58:56–70.
- Mitchell, A.P., S.E. Driscoll, and H.E. Smith. 1990. Positive control of sporulation-specific genes by the IME1 and IME2 products in *Saccharomyces cerevisiae*. *Mol. Cell. Biol.* 10:2104–2110. doi:10.1128/mcb.10.5.2104.

- Mitchell Wells, J., and S.A. McLuckey. 2005. Collision-induced dissociation (CID) of peptides and proteins. *Methods Enzymol.* 402:148–185. doi:10.1016/S0076-6879(05)02005-7.
- Montano, S.P., M.L. Coté, I. Fingerman, M. Pierce, A.K. Vershon, and M.M. Georgiadis. 2002. Crystal structure of the DNA-binding domain from Ndt80, a transcriptional activator required for meiosis in yeast. *Proc. Natl. Acad. Sci. U. S. A.* 99:14041–14046. doi:10.1073/pnas.222312199.
- Moreau, S., J.R. Ferguson, and L.S. Symington. 1999. The Nuclease Activity of Mre11 Is Required for Meiosis but Not for Mating Type Switching, End Joining, or Telomere Maintenance. *Mol. Cell. Biol.* 19:556–566. doi:10.1128/MCB.19.1.556.
- Morin, I., H.-P.P. Ngo, A. Greenall, M.K. Zubko, N. Morrice, and D. Lydall. 2008. Checkpoint-dependent phosphorylation of Exo1 modulates the DNA damage response. *EMBO J.* 27:2400–2410. doi:10.1038/emboj.2008.171.
- Murakami, H., and S. Keeney. 2014. Temporospatial Coordination of Meiotic DNA Replication and Recombination via DDK Recruitment to Replisomes. *Cell.* 158:861–873. doi:10.1016/j.cell.2014.06.028.
- Murayama, Y., and F. Uhlmann. 2014. Biochemical reconstitution of topological DNA binding by the cohesin ring. *Nature.* 505:367–371. doi:10.1038/nature12867.
- Nakada, D., K. Matsumoto, and K. Sugimoto. 2003. ATM-related Tel1 associates with double-strand breaks through an Xrs2-dependent mechanism. *Genes Dev.* 17:1957–1962. doi:10.1101/gad.1099003.
- Nakagawa, T., and H. Ogawa. 1999. The *Saccharomyces cerevisiae* MER3 gene, encoding a novel helicase-like protein, is required for crossover control in meiosis. *EMBO J.* 18:5714–5723. doi:10.1093/emboj/18.20.5714.
- Neale, M.J., J. Pan, and S. Keeney. 2005. Endonucleolytic processing of covalent protein-linked DNA double-strand breaks. *Nature.* 436:1053–1057. doi:10.1038/nature03872.
- Nielsen, F.C., A.C. Jäger, A. Lützen, J.R. Bundgaard, and L.J. Rasmussen. 2004. Characterization of human exonuclease 1 in complex with mismatch repair proteins, subcellular localization and association with PCNA. *Oncogene.* 23:1457–1468. doi:10.1038/sj.onc.1207265.
- Nimonkar, A. V., C.C. Dombrowski, J.S. Siino, A.Z. Stasiak, A. Stasiak, and S.C. Kowalczykowski. 2012. *Saccharomyces cerevisiae* Dmc1 and Rad51 proteins preferentially function with Tid1 and Rad54 proteins, respectively, to promote DNA strand invasion during genetic recombination. *J. Biol. Chem.* 287:28727–28737. doi:10.1074/jbc.M112.373290.
- Niu, H., X. Li, E. Job, C. Park, D. Moazed, S.P. Gygi, and N.M. Hollingsworth. 2007. Mek1 Kinase Is Regulated To Suppress Double-Strand Break Repair between Sister Chromatids during Budding Yeast Meiosis. *Mol. Cell. Biol.* 27:5456–5467. doi:10.1128/MCB.00416-07.
- Oh, J., A. Al-Zain, E. Cannavo, P. Cejka, and L.S. Symington. 2016. Xrs2 Dependent and Independent Functions of the Mre11-Rad50 Complex. *Mol. Cell.* 64:405–415. doi:10.1016/j.molcel.2016.09.011.
- Padmore, R., L. Cao, and N. Kleckner. 1991. Temporal comparison of recombination and

- synaptonemal complex formation during meiosis in *S. cerevisiae*. *Cell*. 66:1239–1256. doi:10.1016/0092-8674(91)90046-2.
- Panizza, S., M.A. Mendoza, M. Berlinger, L. Huang, A. Nicolas, K. Shirahige, and F. Klein. 2011. Spo11-accessory proteins link double-strand break sites to the chromosome axis in early meiotic recombination. *Cell*. 146:372–383. doi:10.1016/j.cell.2011.07.003.
- Paull, T.T., and M. Gellert. 1998. The 3' to 5' exonuclease activity of Mre11 facilitates repair of DNA double-strand breaks. *Mol. Cell*. 1:969–979. doi:10.1016/S1097-2765(00)80097-0.
- Petes, T.D. 2001. Meiotic recombination hot spots and cold spots. *Nat. Rev. Genet.* 2:360–369. doi:10.1038/35072078.
- Primig, M., R.M. Williams, E.A. Winzeler, G.G. Tevzadze, A.R. Conway, S.Y. Hwang, R.W. Davis, and R.E. Esposito. 2000. The Core Meiotic Transcriptome in Budding Yeasts. *Nat. Genet.* 26:415–423.
- Prinz, S., A. Amon, and F. Klein. 1997. Isolation of COM1, a new gene required to complete meiotic double-strand break-induced recombination in *Saccharomyces cerevisiae*. *Genetics*. 146:781–795.
- Prugar, E., C. Burnett, X. Chen, and N.M. Hollingsworth. 2017. Coordination of double strand break repair and meiotic progression in yeast by a Mek1-Ndt80 negative feedback loop. *Genetics*. 206:497–512. doi:10.1534/genetics.117.199703.
- Roeder, G.S., and J.M. Bailis. 2000. The pachytene checkpoint. *Trends Genet.* 16:395–403. doi:10.1016/S0168-9525(00)02080-1.
- Rogacheva, M. V, C.M. Manhart, G. Chen, A. Guarne, J. Surtees, and E. Alani. 2014. Mlh1-Mlh3, a meiotic crossover and DNA mismatch repair factor, is a Msh2-Msh3-stimulated endonuclease. *J. Biol. Chem.* 289:5664–5673. doi:10.1074/jbc.M113.534644.
- Roig, M.B., J. Löwe, K.L. Chan, F. Beckouët, J. Metson, and K. Nasmyth. 2014. Structure and function of cohesin's Scc3/SA regulatory subunit. *FEBS Lett.* 588:3692–3702. doi:10.1016/j.febslet.2014.08.015.
- Rowland, B.D., M.B. Roig, T. Nishino, A. Kurze, P. Uluocak, A. Mishra, F. Beckouët, P. Underwood, J. Metson, R. Imre, K. Mechtler, V.L. Katis, and K. Nasmyth. 2009. Building Sister Chromatid Cohesion: Smc3 Acetylation Counteracts an Antiestablishment Activity. *Mol. Cell*. 33:763–774. doi:10.1016/j.molcel.2009.02.028.
- Rubin-Bejerano, I., S. Sagee, O. Friedman, L. Pnueli, and Y. Kassir. 2004. The In Vivo Activity of Ime1, the Key Transcriptional Activator of Meiosis-Specific Genes in *Saccharomyces cerevisiae*, Is Inhibited by the Cyclic AMP/Protein Kinase A Signal Pathway through the Glycogen Synthase Kinase 3- Homolog Rim11. *Mol. Cell. Biol.* 24:6967–6979. doi:10.1128/mcb.24.16.6967-6979.2004.
- Sansam, C.L., and R.J. Pezza. 2015. Connecting by breaking and repairing: Mechanisms of DNA strand exchange in meiotic recombination. *FEBS J.* 282:2431–2444. doi:10.1111/febs.13317.
- Sasanuma, H., Y. Furihata, M. Shinohara, and A. Shinohara. 2013. Remodeling of the Rad51 DNA strand-exchange protein by the Srs2 helicase. *Genetics*. 194:859–872. doi:10.1534/genetics.113.150615.

- Sasanuma, H., H. Murakami, T. Fukuda, T. Shibata, A. Nicolas, and K. Ohta. 2007. Meiotic association between Spo11 regulated by Rec102, Rec104 and Rec114. *Nucleic Acids Res.* 35:1119–1133. doi:10.1093/nar/gkl1162.
- Schmekel, K., J. Wahrman, U. Skoglund, and B. Daneholt. 1993. The central region of the synaptonemal complex in *Blaps cribrosa* studied by electron microscope tomography. *Chromosoma.* 102:669–681. doi:10.1007/BF00650893.
- Schwacha, A., and N. Kleckner. 1997. Interhomolog bias during meiotic recombination: Meiotic functions promote a highly differentiated interhomolog-only pathway. *Cell.* 90:1123–1135. doi:10.1016/S0092-8674(00)80378-5.
- Serrentino, M.E., E. Chaplais, V. Sommermeyer, and V. Borde. 2013. Differential Association of the Conserved SUMO Ligase Zip3 with Meiotic Double-Strand Break Sites Reveals Regional Variations in the Outcome of Meiotic Recombination. *PLoS Genet.* 9. doi:10.1371/journal.pgen.1003416.
- Shinohara, A., H. Ogawa, and T. Ogawa. 1992. Rad51 protein involved in repair and recombination in *S. cerevisiae* is a RecA-like protein. *Cell.* 69:457–470. doi:10.1016/0092-8674(92)90447-K.
- Shinohara, M., S.L. Gasior, D.K. Bishop, and A. Shinohara. 2000. Tid1/Rdh54 promotes colocalization of Rad51 and Dmc1 during meiotic recombination. *Proc. Natl. Acad. Sci.* 97:10814–10819. doi:10.1073/pnas.97.20.10814.
- Shuster, E.D., and B. Byers. 1989. Pachytene arrest and other meiotic effects of the start mutations in *Saccharomyces cerevisiae*. *Genetics.* 123:29–43. doi:10.1016/0168-9525(90)90039-9.
- Simoneau, A., X. Robellet, A.M. Ladouceur, and D. D'Amours. 2014. Cdk1-dependent regulation of the Mre11 complex couples DNA repair pathways to cell cycle progression. *Cell Cycle.* 13:1078–1090. doi:10.4161/cc.27946.
- Sjögren, C., and K. Nasmyth. 2001. Sister chromatid cohesion is required for postreplicative double-strand break repair in *Saccharomyces cerevisiae*. *Curr. Biol.* 11:991–995. doi:10.1016/S0960-9822(01)00271-8.
- Smith, A. V, and G.S. Roeder. 1997. The yeast Red1 protein localizes to the cores of meiotic chromosomes. *J. Cell Biol.* 136:957–967. doi:10.1083/jcb.136.5.957.
- Snowden, T., S. Acharya, C. Butz, M. Berardini, and R. Fishel. 2004. hMSH4-hMSH5 recognizes holliday junctions and forms a meiosis-specific sliding clamp that embraces homologous chromosomes. *Mol. Cell.* 15:437–451. doi:10.1016/j.molcel.2004.06.040.
- Sourirajan, A., and M. Lichten. 2008. Polo-like kinase Cdc5 drives exit from pachytene during budding yeast meiosis. *Genes Dev.* 22:2627–2632. doi:10.1101/gad.1711408.
- Stahl, F. 1996. Meiotic recombination in yeast: Coronation of the double-strand-break repair model. *Cell.* 87:965–968. doi:10.1016/S0092-8674(00)81791-2.
- Storlazzi, A., L. Xu, L. Cao, and N. Kleckner. 1995. Crossover and noncrossover recombination during meiosis: timing and pathway relationships. *Proc. Natl. Acad. Sci.* 92:8512–8516. doi:10.1073/pnas.92.18.8512.
- Ström, L., and C. Sjögren. 2005. DNA damage-induced cohesion. *Cell Cycle.* 4:536–539. doi:10.4161/cc.4.4.1613.

- Strong, E. 2017. Post translational modification of Exo1 in *Saccharomyces cerevisiae*. The University of Sheffield.
- Subramanian, V. V, and A. Hochwagen. 2014. The meiotic checkpoint network: Step-by-step through meiotic prophase. *Cold Spring Harb. Perspect. Biol.* 6:a016675. doi:10.1101/cshperspect.a016675.
- Suhandynata, R.T., L. Wan, H. Zhou, and N.M. Hollingsworth. 2016. Identification of putative Mek1 substrates during meiosis in *Saccharomyces cerevisiae* using quantitative phosphoproteomics. *PLoS One.* 11:e0155931. doi:10.1371/journal.pone.0155931.
- Sumara, I., E. Vorlaufer, C. Gieffers, B.H. Peters, and J.M. Peters. 2000. Characterization of vertebrate cohesin complexes and their regulation in prophase. *J. Cell Biol.* 151:749–761. doi:10.1083/jcb.151.4.749.
- Sumara, I., E. Vorlaufer, P.T. Stukenberg, O. Kelm, N. Redemann, E.A. Nigg, and J.M. Peters. 2002. The dissociation of cohesin from chromosomes in prophase is regulated by polo-like kinase. *Mol. Cell.* 9:515–525. doi:10.1016/S1097-2765(02)00473-2.
- Sun, H., D. Treco, N.P. Schultes, and J.W. Szostak. 1989. Double-strand breaks at an initiation site for meiotic gene conversion. *Nature.* 338:87–90. doi:10.1038/338087a0.
- Sym, M., M. Sym, J. a Engebrecht, J. Engebrecht, G.S. Roeder, G.S. Roeder, and N. Haven. 1993. ZIP1 is a synaptonemal complex protein required for meiotic chromosome synapsis. *Cell.* 72:365–78.
- Szankasi, P., and G.R. Smith. 1992. A DNA exonuclease induced during meiosis of *Schizosaccharomyces pombe*. *J. Biol. Chem.* 267:3014–3023.
- Szankasi, P., and G.R. Smith. 1995. A Role for Exonuclease I from *S. pombe* in Mutation Avoidance and Mismatch. *Trends Genet.* 267:1166–1169.
- Terasawa, M., T. Ogawa, Y. Tsukamoto, and H. Ogawa. 2008. Sae2p phosphorylation is crucial for cooperation with Mre11p for resection of DNA double-strand break ends during meiotic recombination in *Saccharomyces cerevisiae*. *Genes Genet. Syst.* 83:209–217. doi:10.1266/ggs.83.209.
- Terentyev, Y., R. Johnson, M.J. Neale, M. Khisroon, A. Bishop-Bailey, and A.S.H. Goldman. 2010. Evidence that MEK1 positively promotes interhomologue double-strand break repair. *Nucleic Acids Res.* 38:4349–4360. doi:10.1093/nar/gkq137.
- Terret, M.E., and P. V Jallepalli. 2006. Meiosis: Separase strikes twice. *Nat. Cell Biol.* 8:910–911. doi:10.1038/ncb0906-910.
- Tomimatsu, N., B. Mukherjee, M. Catherine Hardebeck, M. Ilcheva, C. Vanessa Camacho, J. Louise Harris, M. Porteus, B. Llorente, K.K. um Khanna, and S. Burma. 2014. Phosphorylation of EXO1 by CDKs 1 and 2 regulates DNA end resection and repair pathway choice. *Nat. Commun.* 5:3561. doi:10.1038/ncomms4561.
- Tomimatsu, N., B. Mukherjee, J.L. Harris, F.L. Boffo, M.C. Hardebeck, P.R. Potts, K.K. Khanna, and S. Burma. 2017. DNA-damage-induced degradation of EXO1 exonuclease limits DNA end resection to ensure accurate DNA repair. *J. Biol. Chem.* 292:10779–10790. doi:10.1074/jbc.M116.772475.
- Tóth, A., R. Ciosk, F. Uhlmann, M. Galova, A. Schleiffer, and K. Nasmyth. 1999. Yeast cohesin complex requires a conserved protein, Eco1p(Ctf7), to establish cohesion

- between sister chromatids during DNA replication. *Genes Dev.* 13:320–333. doi:10.1101/gad.13.3.320.
- Tran, P.T., N. Erdeniz, S. Dudley, and R.M. Liskay. 2002. Characterization of nuclease-dependent functions of Exo1p in *Saccharomyces cerevisiae*. *DNA Repair (Amst)*. 1:895–912. doi:10.1016/S1568-7864(02)00114-3.
- Tran, P.T., N. Erdeniz, L.S. Symington, and R.M. Liskay. 2004. EXO1-A multi-tasking eukaryotic nuclease. *DNA Repair (Amst)*. 3:1549–1559. doi:10.1016/j.dnarep.2004.05.015.
- Tran, P.T., J.P. Fey, N. Erdeniz, L. Gellon, S. Boiteux, and R.M. Liskay. 2007. A mutation in EXO1 defines separable roles in DNA mismatch repair and post-replication repair. *DNA Repair (Amst)*. 6:1572–1583. doi:10.1016/j.dnarep.2007.05.004.
- Traven, A., and J. Heierhorst. 2005. SQ/TQ cluster domains: Concentrated ATM/ATR kinase phosphorylation site regions in DNA-damage-response proteins. *BioEssays*. 27:397–407. doi:10.1002/bies.20204.
- Tsubouchi, H., and H. Ogawa. 1998. A novel mre11 mutation impairs processing of double-strand breaks of DNA during both mitosis and meiosis. *Mol. Cell. Biol.* 18:260–268. doi:10.1128/MCB.18.1.260.
- Tsubouchi, H., and H. Ogawa. 2000. Exo1 roles for repair of DNA double-strand breaks and meiotic crossing over in *Saccharomyces cerevisiae*. *Mol Biol Cell*. 11:2221–2233. doi:10.1091/mbc.11.7.2221.
- Tsukamoto, Y., C. Mitsuoka, M. Terasawa, H. Ogawa, and T. Ogawa. 2005. Xrs2p Regulates Mre11p Translocation to the Nucleus and Plays a Role in Telomere Elongation and Meiotic Recombination. *Mol. Biol. Cell*. 16:849–860. doi:10.1091/mbc.
- Uhlmann, F., and K. Nasmyth. 1998. Cohesion between sister chromatids must be established during DNA replication. *Curr. Biol.* 8:1095–1102. doi:10.1016/s0960-9822(98)70463-4.
- Uhlmann, F., D. Wernic, M.A. Poupard, E. V Koonin, and K. Nasmyth. 2000. Cleavage of cohesin by the CD clan protease separin triggers anaphase in yeast. *Cell*. 103:375–386. doi:10.1016/S0092-8674(00)00130-6.
- Ünal, E., A. Arbel-Eden, U. Sattler, R. Shroff, M. Lichten, J.E. Haber, and D. Koshland. 2004. DNA damage response pathway uses histone modification to assemble a double-strand break-specific cohesin domain. *Mol. Cell*. 16:991–1002. doi:10.1016/j.molcel.2004.11.027.
- Usui, T., H. Ogawa, and J.H. Petrini. 2001. A DNA damage response pathway controlled by Tel1 and the Mre11 complex. *Mol. Cell*. 7:1255–1266. doi:10.1016/S1097-2765(01)00270-2.
- Usui, T., T. Ohta, H. Oshiumi, J.I. Tomizawa, H. Ogawa, and T. Ogawa. 1998. Complex formation and functional versatility of Mre11 of budding yeast in recombination. *Cell*. 95:705–716. doi:10.1016/S0092-8674(00)81640-2.
- Waizenegger, I.C., S. Hauf, A. Meinke, and J.M. Peters. 2000. Two distinct pathways remove mammalian cohesin from chromosome arms in prophase and from centromeres in anaphase. *Cell*. 103:399–410. doi:10.1016/S0092-8674(00)00132-X.
- Wan, L., T. de los Santos, C. Zhang, K. Shokat, and N.M. Hollingsworth. 2004. Mek1 kinase

- activity functions downstream of RED1 in the regulation of meiotic double strand break repair in budding yeast. *Mol. Biol. Cell.* 15:11–23. doi:10.1091/mbc.E03-07-0499.
- Watanabe, Y., T.S. Kitajima, T. Hyman, M. Yanagida, and T. Hirano. 2005. Shugoshin protects cohesin complexes at centromeres. *In Philosophical Transactions of the Royal Society B: Biological Sciences.* 515–521.
- Wu, T.C., and M. Lichten. 1994. Meiosis-induced double-strand break sites determined by yeast chromatin structure. *Science (80-)*. 263:515–518. doi:10.1126/science.8290959.
- Xu, L., M. Ajimura, R. Padmore, C. Klein, and N. Kleckner. 1995. NDT80, a meiosis-specific gene required for exit from pachytene in *Saccharomyces cerevisiae*. *Mol. Cell. Biol.* 15:6572–6581. doi:10.1128/MCB.15.12.6572.
- Zakharyevich, K., Y. Ma, S. Tang, P.Y.H. Hwang, S. Boiteux, and N. Hunter. 2010. Temporally and Biochemically Distinct Activities of Exo1 during Meiosis: Double-Strand Break Resection and Resolution of Double Holliday Junctions. *Mol. Cell.* 40:1001–1015. doi:10.1016/j.molcel.2010.11.032.
- Zakharyevich, K., S. Tang, Y. Ma, and N. Hunter. 2012. Delineation of joint molecule resolution pathways in meiosis identifies a crossover-specific resolvase. *Cell.* 149:334–347. doi:10.1016/j.cell.2012.03.023.
- Zeng, X., K. Li, R. Yuan, H. Gao, J. Luo, F. Liu, Y. Wu, G. Wu, and X. Yan. 2018. Nuclear Envelope-Associated Chromosome Dynamics during Meiotic Prophase I. *Front. Cell Dev. Biol.* 5:121. doi:10.3389/fcell.2017.00121.
- Zhang, J., X. Shi, Y. Li, B.J. Kim, J. Jia, Z. Huang, T. Yang, X. Fu, S.Y. Jung, Y. Wang, P. Zhang, S.T. Kim, X. Pan, and J. Qin. 2008. Acetylation of Smc3 by Eco1 Is Required for S Phase Sister Chromatid Cohesion in Both Human and Yeast. *Mol. Cell.* 31:143–151. doi:10.1016/j.molcel.2008.06.006.
- Zhao, X., A. Chabes, V. Domkin, L. Thelander, and R. Rothstein. 2001. The ribonucleotide reductase inhibitor Sml1 is a new target of the Mec1/Rad53 kinase cascade during growth and in response to DNA damage. *EMBO J.* 20:3544–3553. doi:10.1093/emboj/20.13.3544.
- Zickler, D., and N. Kleckner. 1998. THE LEPTOTENE-ZYGOTENE TRANSITION OF MEIOSIS. *Annu. Rev. Genet.* 32:619–697. doi:10.1146/annurev.genet.32.1.619.
- Zickler, D., and N. Kleckner. 1999. Meiotic Chromosomes: Integrating Structure and Function. *Annu. Rev. Genet.* 33:603–754. doi:10.1146/annurev.genet.33.1.603.
- Zickler, D., and N. Kleckner. 2016. A few of our favorite things: Pairing, the bouquet, crossover interference and evolution of meiosis. *Semin. Cell Dev. Biol.* 54:135–148. doi:10.1016/j.semcdb.2016.02.024.